Monitoring the effects of tropospheric ozone exposure on forests, a spectroscopic approach.



Anna Lee Jones

Wolfson College

University of Oxford

A thesis submitted for the degree of

Doctor of Philosophy

Trinity 2025

Abstract

Near the Earth's surface, tropospheric ozone (O_3) is a highly oxidising and toxic pollutant. Tropospheric O_3 concentrations have reached dangerously high concentrations around the world and are predicted to continue to increase. O_3 pollution reduces the growth, productivity, and resilience of vegetation due to oxidative stress. Broadleaf trees are vulnerable to O_3 damage, but the extent of O_3 damage to forests is not well understood. O_3 stress causes visible foliar symptoms which are currently used to monitor the impact of O_3 on forests, but a high-throughput and remote technology would allow large-scale, accurate assessments of O_3 damage to forests. O_3 has been shown to affect the leaf reflectance profile of sensitive crops and some conifers, but the reflectance signature of O_3 damage in broadleaf trees has not been explored. In this thesis I have used hyperspectral leaf reflectance to first identify the spectral signature of O_3 damage in broadleaf saplings under controlled experimental conditions, and then to expand this to mature trees under natural conditions. I have found a consistent and robust signal of O_3 damage in the hyperspectral leaf reflectance of broadleaf trees, using both vegetation indices and whole-spectra, machine learning approaches. O_3 affected the width and intensity of the green reflectance peak of sapling and mature trees, and the vegetation index MCARI consistently responded to O_3 exposure. In saplings there were also clear changes in the short-wavelength infrared reflectance proportional to O_3 dosage. I also investigated the effect of future CO_2 concentrations on leaf reflectance and found elevated CO_2 broadly did not impact leaf reflectance, although one index linked to senescence did increase. Therefore elevated CO_2 concentrations in the future should not affect the ability to detect O_3 damage via leaf reflectance because the spectral signature of O_3 damage is stronger and affects a distinct region of the spectra. Finally, I explored how the O_3 damage signal could be scaled up to a remote sensing application, and trialled a simple satellite analysis using vegetation indices. As O_3 concentrations continue to rise globally, understanding the extent of O_3 damage to forests is crucial to effectively harness the carbon sequestration potential of forests. I demonstrate the exciting potential of spectral monitoring of O_3 damage in broadleaf temperate forests.

Acknowledgements

I would like to thank the many supervisors, co-supervisors, project partners, and otherwise supporters of my research. Firstly, Lizzy Jeffers thank you for your guidance and support throughout my PhD, particularly for allowing me the freedom to shape the project myself. I would like to thank Felicity Hayes, for agreeing initially to let me use the solardomes which culminated in becoming an official supervisor and vital source of wisdom, knowledge, and feedback. I have very happy memories of my time at CEH Bangor, and also thank Mike Perring for his input.

None of my fieldwork would have been possible without the support of the NERC Field Spectroscopy Facility, and in particular the patience, guidance, and enthusiasm of Robbie Ramsay over several field campaigns. I would also like to thank the BIFoR FACE team for responding to my cold calling and allowing me to conduct research in their experiment, in particular Christian Pfrang, Rob MacKenzie, Kris Hart, Peter Miles, Sami Ullah, and Anna Gardner.

For the inspiration behind this research and their ozone expertise I would like to thank Brian Kerridge, Gary Hayman, Barry Latter, and Chris Huntingford. Thank you also to Hugh Mortimer who demonstrated how exciting interdisciplinary research can be, and encouraged me to pursue research beyond my PhD. I would also like to thank those who made my research in Wytham Woods possible: Alex Black, Nigel Fisher, and Yadvinder Mahli. I am grateful for the support from afar given by Howard Griffiths, who inspired me to specialise in plant sciences and along with Wanne Kromdijk kindly lent me a PAM fluorometer in exchange for a bottle of Tequila (the finest CAM photosynthesis based spirit).

I'm grateful to Kathy Willis and the Oxford Long Term Ecology Lab for supporting, encouraging, and guiding me through the PhD process. Our discussions and lab meetings never failed to broaden my perspective and make me think about my work in new ways. Thank you to David, Eva, Keiran, Nancy, Timmy, and Gus for your friendship and for being listening ears during the PhD journey. Thank you to James Borrell and his research group at Kew for taking me on as an internship student and providing a welcome shift of focus.

This thesis may never have been written without the endless love and support of my boyfriend David, who has rescued me from late nights in the office and lured me away from my laptop with delicious food more times than I can count. Thank you David for helping me to believe in myself.

Thank you to Mum, Dad, Erin, Nanny, and Grampy for encouraging me, praying for me, and being a solid foundation. I'd like to think my love of nature has been heavily influenced by generations of avid gardeners and plant enthusiasts. "But ask the animals, and they will teach you; the birds of the air, and they will tell you; ask the plants of the earth, and they will teach you; and the fish of the sea will declare to you. Who among all these does not know that the hand of the Lord has done this? In his hand is the life of every living thing and the breath of every human being." Job 12:7-10.

I will be forever grateful to have lived with the best housemates and friends a PhD student could wish for. Thank you Alice, Joe, Sophie, and Luke for making my time in Oxford full of laughter, trash, and fun as well as always being ready to bemoan the frustrations of being PhD students. Thank you to everyone at Wolfson Boat club for keeping me sane, providing some of my favourite times in Oxford, and for many river based adventures.

Thank you to all the friends who have supported from afar: the Queens' gang, and my home friends who have provided much needed escapes from 'the bubble'.

Contents

List of Figures viii

List of Tables x

List of Abbreviations xi

1 Introduction 1

1.1 Thesis Introduction . . . 1

1.1.1 Thesis Structure . . . 2

1.2 Literature Review . . . 2

1.2.1 Introduction to Tropospheric O_3 . . . 2

1.2.2 The Effect of O_3 on Plants . . . 8

1.2.3 Monitoring O_3 Damage to Vegetation . . . 15

1.3 Thesis Aims . . . 20

References . . . 22

2 Reflections of stress: Ozone damage in broadleaf saplings can be identified from hyperspectral leaf reflectance. 42

2.1 Commentary . . . 42

2.2 Manuscript . . . 43

2.2.1 Abstract . . . 45

2.2.2 Introduction . . . 46

2.2.3 Material and Methods . . . 48

2.2.4 Results . . . 53

2.2.5 Discussion . . . 71

2.2.6 Conclusions . . . 75

2.2.7 Acknowledgements . . . 75

2.2.8 CRediT authorship contribution statement . . . 75

References . . . 76

3 On mature reflection: Ozone damage can be detected in oak trees by hyperspectral reflectance. 82
3.1 Commentary . . . 82
3.2 Manuscript . . . 83
3.2.1 Highlights . . . 85
3.2.2 Abstract . . . 85
3.2.3 Introduction . . . 85
3.2.4 Methods . . . 89
3.2.5 Results . . . 93
3.2.6 Discussion . . . 105
3.2.7 Conclusions . . . 109
3.2.8 Acknowledgements . . . 110
3.2.9 CRediT authorship contribution statement . . . 111
References . . . 112

4 The effect of elevated CO_2 on hyperspectral leaf reflectance in mature trees 121
4.1 Commentary . . . 121
4.2 Manuscript . . . 123
4.2.1 Abstract . . . 124
4.2.2 Introduction . . . 125
4.2.3 Methods . . . 130
4.2.4 Results . . . 135
4.2.5 Discussion . . . 147
4.2.6 Conclusion . . . 150
4.2.7 Acknowledgements . . . 151
4.2.8 Funding . . . 151
4.2.9 Data Availability . . . 151
4.2.10 Declarations . . . 152
References . . . 152

5 An exploration of remote sensing ozone damage to forests 162
5.1 Abstract . . . 162
5.2 Introduction . . . 163
5.3 Methods . . . 165
5.3.1 O_3 Input Data . . . 165
5.3.2 Vegetation Indices . . . 166
5.3.3 Forest Cover . . . 167
5.3.4 Data Processing . . . 167
5.3.5 Data Visualisation and Analysis . . . 167

5.4 Results . . . 168
5.5 Discussion . . . 172
References . . . 176

6 Conclusion **179**
6.1 Introduction . . . 179
6.2 Key Findings . . . 180
6.3 Discussion . . . 182
6.4 Contribution and Impact . . . 184
6.5 Limitations and Future Directions . . . 185
6.6 Synthesis . . . 188
References . . . 189

Appendices

A Appendix to Chapter 1 **192**
A.1 Author Contributions . . . 192

B Appendix to Chapter 2 **194**
B.1 Additional Methods . . . 194
B.1.1 O_3 Damage Score Examples . . . 194
B.1.2 Formulae of Vegetation Indices . . . 196
B.1.3 Destructive Harvest . . . 197
B.1.4 Gas Exchange . . . 197
B.1.5 Fluorometry . . . 197
B.1.6 Biochemical Extractions . . . 198
B.2 Additional Results . . . 200
B.2.1 Growth . . . 200
B.2.2 Destructive Harvest . . . 202
B.2.3 Gas Exchange . . . 203
B.2.4 Fluorometry . . . 206
B.2.5 Biochemical Extractions . . . 207
B.2.6 PCA . . . 211
B.2.7 PLSDA . . . 213
B.2.8 Vegetation Indices . . . 216
References . . . 221

C Appendix to Chapter 3 **222**

D Appendix to Chapter 5 **226**
D.1 GRVI . . . 227
D.2 NDVI . . . 230

List of Figures

1.1 Scan of an O_3 damaged beech leaf. 16

2.1 Chapter 2 graphical abstract. 43
2.2 O_3 experiment damage scores. 55
2.3 O_3 experiment leaf spectra. 58
2.4 O_3 experiment principal component analysis 60
2.5 O_3 experiment vegetation indices. 62
2.6 O_3 experiment NDSI heat map. 65
2.7 OZDI by species and month in O_3 experiment. 67

3.1 Chapter 2 graphical abstract. 83
3.2 O_3 monitoring results. 94
3.3 BIFoR and Wytham reflectance spectra. 96
3.4 BIFoR and Wytham PCA. 99
3.5 Partial Least Squares Regression Analysis 100
3.6 Heat map of NSDI correlation to O_3 concentration. 102
3.7 Vegetation indices against O_3 concentration. 104

4.1 Average spectra. 137
4.2 Principal component analysis. 139
4.3 Principal component distributions. 140
4.4 PLSDA model tuning. 142
4.5 Spectra of wavelength importance for PLSDA. 143
4.6 Distributions of vegetation indices. 146

5.1 Remote sensing input layers. 165
5.2 AOT40 of UK forests, time series. 168
5.3 MCARI of UK forests, time series. 169
5.4 MCARI and AOT40 correlation plots. 170
5.5 MCARI and AOT40 bivariate maps. 171

B.1 Intra-seasonal sapling growth. 200
B.2 Sapling growth 2022-2023. 201
B.3 Destructive harvest results. 202

B.4 LICOR results. 204
B.5 Chlorophyll index. 205
B.6 PAM results. 206
B.7 Pigment extractions by species. 207
B.8 Chlorophyll A extraction results. 208
B.9 Chlorophyll B extraction results 208
B.10 Carotenoid extraction results 209
B.11 Xanthophyll extraction results 209
B.12 Phenol extraction results 210
B.13 Seasonal extraction results 210
B.14 Spectra PCA,by species 211
B.15 Spectra PCA, by O_3 treatment 212
B.16 Alder PLSDA. 213
B.17 Beech PLSDA. 214
B.18 Birch PLSDA. 214
B.19 Crab apple PLSDA. 215
B.20 Oak PLSDA. 215
B.21 MCARI results. 216
B.22 PRI results. 217
B.23 PSRI results. 218
B.24 NDVI results. 219
B.25 RENDVI results. 220

C.1 Stippling photos. 222
C.2 Average O_3 concentration per month. 223
C.3 Principal component scree plot. 223
C.4 PCA by O_3 concentration. 224
C.5 PCA by date of measurement. 225
C.6 Vegetation indices against cumulative O_3. 225

D.1 GRVI of UK forests, time series. 227
D.2 GRVI and AOT40 correlation plots. 228
D.3 GRVI and AOT40 bivariate maps. 229
D.4 NDVI of UK forests, time series. 230
D.5 NDVI and AOT40 correlation plots. 231
D.6 NDVI and AOT40 bivariate maps. 232

List of Tables

2.1 Solardome O_3 treatments. 50
2.2 O_3 experiment OzDI PERMANOVA results. 70

3.1 Vegetation indices formulae. 93
3.2 Pearson correlation analysis of vegetation indices to O_3 concentration. 104

4.1 Vegetation indices formulae. 134
4.2 Summary of linear mixed effect model results for vegetation indices of leaves exposed to ambient (aCO_2) or elevated CO_2 (eCO_2). In all model the degrees of freedom were 5.97, using Satterthwaite's method. P values marked with * indicate a statistically significant effect ($\alpha = 0.05$). All values are given to two significant figures in standard form. 145

B.1 O_3 damage scoring criteria. 195
B.2 Vegetation indices formulae. 196
B.3 Reflectance PERMANOVA results. 211

C.1 BIFoR and Wytham sampling dates. 222
C.2 Vegetation index Pearson correlations to cumulative O_3. 223

List of Abbreviations

aCO_2 . . . . . Ambient carbon dioxide.

AURN . . . . Automatic urban and rural air quality monitoring network, UK.

BVOC . . . . . Biogenic volatile organic compound.

BUV . . . . . Backscatter ultraviolet.

CCD . . . . . Convective cloud differential, a method of calculating the tropospheric O_3 column.

CSA . . . . . Cloud slicing algorithm, a method of calculating the tropospheric O_3 column.

DEFRA . . . . Department for environment food and rural affairs, UK.

eCO_2 . . . . . Elevated carbon dioxide.

EDU . . . . . Ethylenediurea.

EMEP . . . . . The cooperative programme for monitoring and evaluation of the long-range transmission of air pollutants in Europe, linked to the Convention on Long-range Transboundary Air Pollution.

EPA . . . . . Environmental protection agency, US.

ETR . . . . . Electron transport rate.

FACE . . . . . Free-air concentration enrichment.

GOME . . . . Global O_3 monitoring experiment.

HIRAS . . . . Hyperspectral infrared atmospheric sounder, satellite series.

HO_x . . . . . Hydroxyl radicals.

ICP Forests . International co-operative programme on assessment and monitoring of air pollution effects on forests.

IPCC . . . . . Intergovernmental panel on climate change.

LIDAR . . . . Light detection and ranging, a remote sensing technology.

LMA . . . . . Leaf mass per unit area.

MDA . . . . . Malondialdehyde.

NASA . . . . . National aeronautics and space administration, US.

NDSI . . . . . Normalised difference spectral index.

NDVI . . . . . Normalised difference vegetation index.

NIR . . . . . Near-infrared radiation.

NO_x . . . . . Nitrogen oxides.

NOAA . . . . . National oceanic and atmospheric administration, US.

NPQ . . . . . Non-photochemical quenching.

O_3 . . . . . Ozone.

OMI . . . . . O_3 monitoring instrument.

PAM . . . . . Pulse-amplitude modulated (fluorometer).

PC . . . . . Principal component.

PgC . . . . . Petagrams of carbon.

PLSR . . . . . Partial least squares regression.

PODY . . . . . Phytotoxic ozone dose.

ppb . . . . . Parts per billion by volume.

PRI . . . . . Photochemical reflective index.

RCP . . . . . Representative concentration pathways.

RMSEP . . . . Root mean square error of prediction.

ROS . . . . . Reactive oxygen species.

RTM . . . . . Radiative transfer model.

Rubisco . . . . Reduced Ribulose-1,5-bisphosphate carboxylase/oxygenase.

SHADOZ . . . Southern hemisphere additional ozonesondes, an archive of sub/tropical and remote ozonesonde data.

SIF . . . . . Solar induced fluorescence.

SSP . . . . . Shared socioeconomic pathway.

TIR . . . . . Thermal infrared radiation.

TOLNet . . . . Tropospheric ozone LIDAR network.

TOR . . . . . Tropospheric O_3 residual, a method of calculating the tropospheric O_3 column.

TOAR . . . . . Tropospheric O_3 assessment report.

TROPOMI . . Tropospheric monitoring instrument, on board the Copernicus Sentinel-5 Precursor satellite.

UAV . . . . . Unmanned aerial vehicle, also commonly known as a drone.

UNECE . . . . United Nations Economic Commission for Europe.

UV . . . . . Ultraviolet.

VIS . . . . . Visible light radiation.

VOCs . . . . . Volatile organic compounds.

WOUDC . . . World ozone and ultraviolet radiation data centre.

WUE . . . . . Water use efficiency.

Y . . . . . Effective quantum yield.

1 Introduction

Contents

1.1 Thesis Introduction 1
1.1.1 Thesis Structure 2
1.2 Literature Review 2
1.2.1 Introduction to Tropospheric O_3 2
1.2.2 The Effect of O_3 on Plants 8
1.2.3 Monitoring O_3 Damage to Vegetation 15
1.3 Thesis Aims 20
References 22

1.1 Thesis Introduction

This thesis examines the spectral signature of O_3 damage in temperate broadleaf trees and explores the potential of spectral monitoring of the effects of O_3 stress on temperate broadleaf forests under current and future atmospheric conditions. This is an integrated thesis comprised of six chapters: an introduction, four data chapters, and a conclusion. The references for each chapter (or appendix) are listed at the end of the chapter (or appendix). This first chapter outlines the structure of the thesis and reviews the background literature relating to O_3 pollution and its effect on trees, before laying out the aims of the thesis. Data Chapters 2-4 are journal papers, preceded by a short commentary setting them within the context

of the thesis. Chapter 5 is a further data chapter, not yet submitted to a journal. Chapter 6 discusses the previous chapters and concludes the thesis.

1.1.1 Thesis Structure

Chapter 1: Thesis Introduction and literature review.

Chapter 2: Reflections of stress: Ozone damage in broadleaf saplings can be identified from hyperspectral leaf reflectance, published in Environmental Pollution, 2024.

Chapter 3: On mature reflection: Ozone damage can be detected in oak trees by hyperspectral reflectance, published in Ecological Indicators, 2025.

Chapter 4: The effect of elevated CO_2 on hyperspectral leaf reflectance in mature trees, under review in Trees: Structure and Function, 2025.

Chapter 5: An exploration of remote sensing ozone damage to forests.

Chapter 6: Thesis conclusions, and future directions.

The author contributions for each chapter are given in Appendix A.

1.2 Literature Review

1.2.1 Introduction to Tropospheric O_3

Ozone (O_3) is a polar molecule comprised of three oxygen atoms. Ozone (from the Greek "ozein", to smell) was discovered by Christian Schönbein in 1839 and its molecular structure confirmed by Jacques-Louis Soret in 1865 [1–3]. It is highly reactive and strongly oxidising. O_3 occurs throughout the Earth's atmosphere, and is found at highest concentrations in the "ozone layer" of the stratosphere which absorbs most of the sun's ultraviolet (UV) radiation [4]. In the troposphere (from the Earth's surface to a height of 6-10km) O_3 is a greenhouse gas which contributes to positive radiative forcing [5]. Near the surface O_3 causes oxidative damage at the molecular and cellular level to lipids, proteins, and nucleic acids in living organisms [6]. At the ground level, the annual average O_3 concentration is around 30 parts per billion by volume (ppb), O_3 concentrations are regularly over 60 ppb in polluted areas [7].

Most O_3 in the troposphere is produced in situ by sunlight-induced, free radical reactions between precursor gases including nitrogen oxides (NO_x), volatile organic compounds (VOCs), methane (CH_4), and carbon monoxide (CO) [8]. The other source of tropospheric O_3 is stratosphere-troposphere exchange [9, 10], but this contribution is significantly smaller than photochemical production in the troposphere [11–13]. O_3 forms in the troposphere by photolysis of NO_2 and subsequent reaction of the photoproduct with O_2, conversely when NO_x concentrations are low (e.g. in the remote atmosphere) hydroxyl radicals (HO_x) can react with hydroperoxyl (HO2), to destroy O_3 [8]. The balance between photochemical O_3 production and loss in the troposphere is dependent on the relative concentrations of HO_x and NO_x [8].

Variations in Tropospheric O_3 through Time and Space

Tropospheric O_3 concentrations vary across the globe, due to meteorological conditions, precursor concentrations, and atmospheric transport processes. These pathways to O_3 production and loss will be affected differently by climate change, but Lu et al argue that the interactions between O_3 and vegetation in terms of dry deposition and biogenic VOC emissions will largely affect the surface O_3 response to climate change [14].

Broadly, the northern hemisphere experiences a peak in O_3 in the spring and summer due to photochemical production, whereas the southern hemisphere O_3 peak occurs in winter [15, 16]. Regional variation, for example O_3 minima during monsoon season [17], also affects seasonal variation in ground level O_3.

Surface level O_3 measurements are available from networks of monitoring sites, ozonesondes, satellite retrievals, as well as atmospheric models which may combine these data sources. The first tropospheric O_3 assessment report (TOAR) brought together a global database of O_3 monitoring stations across the world, with data from 1970-2015 covering urban and remote sites [18]. However, monitoring stations are unevenly distributed across the world and public access to data is variable.

Measuring Tropospheric O_3

Statistical and machine learning methods are employed to create continuous and global maps of surface level O_3 based on ground-based monitoring data. Influences such as meteorological conditions, radiation, and pollution emission may feed into these analyses, for example in Zhan et al's model of O_3 concentration across China in 2015 at $0.1 \circ \times 0.1 \circ$ resolution [19]. Betancourt et al used explainable machine learning methods to produce a global map of tropospheric O_3 at $0.1 \circ \times 0.1 \circ$ spatial resolution for 2010-2014 [20].

Ozonesondes are balloon-borne instruments used to monitor the vertical O_3 profile from the troposphere to the mid-stratosphere [21]. According the major ozonesondes data networks SHADOZ and WOUDC, there are around 60 active ozonesondes stations globally [22, 23]. In their recent review of tropospheric O_3 monitoring, Xu et al present a map of global distributions of ozonesondes sites which shows significant bias towards North America and Europe [24]. In situ data from ozonesondes is used to "ground truth" remotely sensed O_3 concentrations, without the effects of the radiative properties of the atmospheric.

Light detection and ranging (LIDAR) is an active remote sensing technique which can be deployed on the ground, on UAV, or on aircraft. The Tropospheric Ozone LIDAR Network (TOLNet) is an inter-agency collaboration between NASA, NOAA, and the EPA which brings together static and mobile LIDAR retrievals of tropospheric O_3. TOLNet provides high spatio-temporal resolution observations of tropospheric ozone to better understand physical processes driving O_3 dynamics and validate the tropospheric O_3 measurements from space borne missions, [25]. Active measurement techniques such as LIDAR are a key part of future missions planned for remote sensing of O_3 concentrations from space [24].

Current tropospheric measurements of O_3 from satellites rely on passive remote sensing techniques. Passive sensors generally use ultraviolet (UV) wavelengths of interest around 250 to 350 nm, and thermal infrared (TIR) radiation between 9.6 and 4.7 µm to detect O_3 concentrations [24]. There are also significant O_3 absorbing features in the Chappuis visible bands [26] and terahertz regime [27]. The backscatter

ultraviolet (BUV) technique is the dominant UV/VIS passive sensor technique used for O_3 retrievals, for example in the Global O_3 Monitoring Experiment (GOME) series [28, 29] and the O_3 Monitoring Instrument (OMI) [30]. TIR sensors for monitoring tropospheric O_3 quantify the variation in thermal radiation emitted by O_3 molecules, for example in the Chinese HIRAS series of instruments [31].

Retrieval algorithms have been developed to estimate tropospheric O_3 below the stratospheric O_3 layer from satellite measurements. Direct retrieval algorithms are the simplest type, and rely on specific O_3 signatures such as the Huggins bands [32]. For each satellite instrument, there are several different direct retrieval algorithms, with different mean biases. The algorithms generally seek to minimise the sum of squares of the residuals between measured and modelled spectral measurements, and there are many different approaches to this such as optimal estimation [33], Tikhonov regularization [34], and neural networks [35].

Tropospheric O_3 can also be retrieved indirectly from spectral measurements. The tropospheric column can be calculated by subtracting the stratospheric column from the total O_3 column, this is the basis of the Tropospheric O_3 Residual (TOR) method first proposed by Fishman and Larsen [36]. The TOR method works well in regions with lower spatial and temporal variability in stratospheric O_3 concentration [24]. The Convective Cloud Differential (CCD) method uses pixels containing highly reflective clouds with cloud tops at the tropopause level to determine stratospheric O_3 in the tropical Pacific, and from this derives the tropospheric column [37]. The official TROPOMI O_3 product uses a CCD method [38]. Alternatively, the Cloud Slicing Algorithm (CSA) uses the upper-cloud O_3 column to indicate the intra-cloud O_3 volume mixing ration and derive upper tropospheric O_3 [39]. The limb-nadir matching method uses stratospheric O_3 data from limb-viewing measurements and then derives tropospheric O_3 profiles [40].

Retrievals from different satellite instruments can be compared and combined to give longer time series of tropospheric O_3 trends [41] and to investigate spatial and temporal variability [42]. Sentinel 5A, due to launch in October 2025, aims to provide measurements for global O_3 retrievals at a few kilometres resolution [43].

Another approach is to use atmospheric models to predict tropospheric O_3 concentrations at high spatio-temporal resolution. The EMEP MSC-W model has underpinned the development of European air quality policies since the late 1970s, and produces produce daily maps of ground level O_3 at 3 km resolution [44, 45]. Individual countries' environment agencies commission higher spatial resolution models of air pollution to assess compliance with air quality regulations, such as DEFRA's air pollution models for the UK [46].

Changes to Tropospheric O_3 Concentration Over Time

Rapid industrialisation, fossil fuel combustion, and land use change caused a global increase in O_3 concentrations in the 19th century, but the magnitude of change is uncertain due to the limitations of contemporary O_3 measurements [15]. After his discovery of O_3, Professor Schönbein developed the first method of measuring O_3 concentration using paper strips coated in starch and potassium iodide, named the Schönbein ozonoscope [47], however this only provided relative, semi-quantitative measurements. The only reliable quantitative O_3 measurements from the 19th Century were made at the Paris Municipal Observatory in Park Montsouris, from 1876 to 1907 under Chief Chemist Albert Lévy by bubbling air through aqueous iodide and arsenite solution [48]. Volz and Kley reconstructed this original method in 1988 and found it produced results similar to the modern ultraviolet absorption method [49]. Yeung et al analysed the clumped-isotope composition of molecular oxygen trapped in polar firn and ice from 1590 to 2016 AD alongside atmospheric chemistry model simulations to reconstruct changes in tropospheric O_3, and found concentrations increased by up to 40% between 1590-1958 [50]. This is a smaller increase than estimated by atmospheric transport model simulations [51]. European O_3 observations indicate a further significant increase in average O_3 concentrations between the 1950s and 2000 [15], although the precise magnitude is uncertain [50].

From the 1980s onwards, continuous and reliable O_3 measurements are available from ozonesondes and aircraft. In the 1970s and 80s background O_3 concentrations increased sharply [52], Christiansen et al reported a 4.3% increase per decade in near

surface O_3 concentrations from 1980 based on ozonesondes data [53]. Significant regulatory efforts in the 1990s reduced NO_x emissions in North America and Europe, leading to a decrease in O_3 maxima [53] and a plateau in tropospheric O_3 production according to modelling [51], however background O_3 shows an increasing trend across the globe [52, 53]. Observations indicate increasing O_3 concentrations in urban areas since the 1990s [54]. In southern hemisphere O_3 is increasing both in background concentrations and peak concentrations [53]. Precursor emissions have shifted towards the northern tropics in recent decades [51]. Since 2010, the southern hemisphere has experienced increasing O_3 concentrations (although monitoring stations are more sparse), while the northern hemisphere has shown mixed patterns [15]. Globally the trend in surface O_3 concentrations has been mixed whether data come from monitoring stations, ozonesondes or satellite retrievals [55], but where O_3 concentrations have plateaued they have levelled off at high concentrations. Parrish et al found the North American West Coast shows signs of a slight decrease in O_3 concentration since 2000 [56], whereas studies in China and Spain have observed significant increases [57, 58].

Future Tropospheric O_3 Dynamics

Future tropospheric O_3 pollution will depend on the extent of precursor emission reductions, importantly NO_x , VOCs, and methane emissions all need to decrease to reduce O_3 pollution [59]. Modelling approaches have found that O_3 may not decrease even with NO_x and VOCs precursor controls if methane is not also tackled [60, 61]. Climate change may result in meteorological conditions in the troposphere which favour O_3 production closer to emission sources [62], leading to significant increases in O_3 pollution in Asia [63]. Under the "middle of the road" SSP 370 Scenario, the 6th IPCC assessment report predicts the global tropospheric O_3 burden will continue to increase until 2100 [64].

Surface O_3 in the UK

In the UK, O_3 exposure is highest in upland and rural areas [65]. Overall, the hourly O_3 exceedance above 50 ppb have decreased since 1992-2019 [66], but background

concentrations have plateaued at a high level. The Automatic Urban and Rural air quality monitoring Network (AURN) provides O_3 concentration monitoring across the UK. Since 2000 there has been little change in O_3 concentration in rural sites, but upward trends in some urban and suburban sites due to local reductions in NO_x [65]. Methane emissions are set to become more important to the level of O_3 pollution in the UK as NO_x emissions decrease [65]. The impact of climate change on net O_3 pollution in the UK is uncertain, but the 2021 Air Quality Expert Group Report states "As other air pollutants in the UK continue to decline it seems likely that the importance of ozone will grow" [65].

1.2.2 The Effect of O_3 on Plants

Leaf Level Effects

O_3 enters the leaf via the stomata and rapidly decomposes into reactive oxygen species (ROS) in the extracellular space which cause oxidative damage and trigger a range of stress responses [67, 68]. Under acute O_3 exposure, the sudden increase in ROS in the leaf triggers several signalling cascades via protein phosphorylation, plant hormones, and calcium signals which induce rapid changes in protein activity, gene expression, and metabolism [68]. Acute O_3 stress results in programmed cell death and foliar lesions, via a process similar to the hypersensitive response [69]. Chronic low level O_3 exposure by contrast may not produce visible foliar damage but reduces photosynthetic activity, decreases growth, and induces premature senescence [70]. The first observations of visible O_3 damage in plants were reported in Los Angeles in 1952 in a mixed conifer forest [71].

Acute O_3 stress causes the breakdown of chlorophyll and carotene pigments [72]. O_3 induced reduction in chlorophyll and carotene been shown across many plant types including Acer species [73], maize [74], lettuce [75], spinach [76, 77], and sage [78], among others.

O_3 reduces photosynthetic productivity in plant via three key mechanisms: reduced Ribulose-1,5-bisphosphate carboxylase/oxygenase (Rubisco) content and activity, oxidation of cell membranes, and reduced stomatal conductance [79, 80].

The combination of these effects reduce the net productivity of plants under O_3 stress [81].

Rubisco is the key enzyme at the heart of photosynthesis, it catalyses the carboxylation of ribulose-1,5-bisphosphate (RuBP) in the Calvin-Benson-Bassham cycle [82, 83]. O_3 reduces Rubisco activity and concentration [84, 85]. Reduced Rubisco activity under O_3 stress has been linked to reduced transcription of rbcS1 protein [86].

O_3 causes oxidation of cell membranes via lipid peroxidation, an oxidative chain reaction in which free radicals convert unsaturated membrane fatty acids into lipid peroxides [87]. O_3 induced lipid peroxidation can be measured by an assay of malondialdehyde (MDA) [88]. Novotný et al showed MDA increases under O_3 in forest vegetation, although MDA content reflects oxidative stressors generally. MDA increase under O_3 exposure in lettuce [75], spinach [77], and has been shown to correlate with O_3 sensitivity in rice cultivars [89].

The Effects of O_3 Exposure on Stomata

Generally, acute O_3 exposure triggers stomatal closure [90], this process is induced by the increase in ROS in guard cells under O_3 stress via the protein SLAC1 and protein kinase OST1 [91]. Stomatal density and size have also been reported to decrease under O_3 stress [92]. On average, stomatal conductance of trees in experimental studies decreased by 13% under O_3 exposure [93], leading to reductions in photosynthetic activity.

O_3 stress also reduces the sensitivity of stomatal dynamics to other stressors, for example Paoletti et al identified slower stomatal closure in response to light and leaf wounding up to 10 days after O_3 treatment in *Arbutus unedo*[94]. This effect has been termed "stomatal sluggishness" and has been observed across physiognomic classes [95–97]. The extent of stomatal sluggishness in response to O_3 depends on O_3 flux and the capacity of the plant to detoxify ROS [98]. Stomatal sluggishness reduces the water use efficiency (WUE) of O_3 exposed plants by up to 20% [98], although O_3 induced reductions in photosynthetic activity also reduce

WUE [99]. The water use strategy of plants affects stomatal dynamics under O_3 stress [100]. Huntingford et al proposed a simple way to include the stomatal sluggishness response in Earth system models [101], but this is often still missing from modelling analyses of the effects of O_3.

For a given ambient O_3 concentration, the amount of O_3 stress experienced by a plant depends on stomatal conductance. Broad differences in O_3 sensitivity between different functional groups can be partially explained by differences in stomatal conductance and therefore the O_3 dosage received by the plant. Sensitivity to O_3 across woody species is strongly related to stomatal flux per unit leaf area as well as leaf mass per unit area (LMA) [102, 103]. Similar results have been found across a range of bioenergy C4 species such as maize, sorghum, and switchgrass [104].

As explained, O_3 stress affects stomatal dynamics and O_3 dosage is dependent on stomatal conductance. Stomatal O_3 uptake can be calculated from stomatal conductance [105], this has been formulated for risk assessments via the Deposition of O_3 for Stomatal Exchange (DO_3SE) model [106–108]. Stomatal flux based approaches to O_3 risk assessments have been proposed including phytotoxic O_3 doses (PODY, [109]). Stomatal O_3 flux approaches are now recommended for regulatory efforts [107, 108, 110–113].

Due to reduced stomatal conductance under low water conditions, drought has been shown to protect vegetation from O_3 damage via reduced dosage. Water stress was shown to mitigate O_3 stress in poplar trees via reduced stomatal flux and increased chlorophyll and carotenes [114]. Similar results have been reported in Norway spruce exposed to O_3 stress and mild drought [115], and in Acer species [73]. However, in the short term O_3 induced stomatal sluggishness may increase stomatal water loss due to delayed responses to changing conditions such as variable light [116]. O_3 also decreases investment in root growth across tree species [117], which may have negative effects on the ability of trees to cope with low water conditions.

Detoxification of O_3 in Plants

Plants can detoxify the ROS produced when O_3 enters the leaf via production of antioxidant secondary metabolites. Under O_3 stress, carbon is redirected from growth towards secondary metabolism in the phenylpropanoid, alkaloid, or isoprenoid pathways [118]. The phenylpropanoid pathway results in elevated phenolic compounds under O_3 stress [119, 120]. The effect of O_3 on the alkaloid pathway is not well understood, but polyamines (an important alkaloid precursor) are associated with O_3 tolerance in plants, via inhibition of ethylene production and direct ROS scavenging [118, 121]. Via the isoprenoid pathway, terpene production increases under elevated O_3. Terpenes are a type of biogenic VOC (BVOC) released by plants under abiotic stress, BVOCs can also act as a precursor for O_3 production leading to positive feedback loops in acutely O_3 exposed trees, particularly in urban areas [122–124].

The xanthophyll pool (a group of photoprotective carotenoid pigments which dissipate excess light energy) increases under O_3 stress [115, 125]. Ascorbic acid (also known as vitamin C) is the most abundant antioxidant in plants, and is associated with O_3 stress tolerance [76, 115]. Enhancing ascorbic acid levels in transgenic tobacco plants limits the negative effects of O_3 on photosynthesis [126]. The exact relationship between ascorbic acid and O_3 sensitivity is still under investigation [127], but generally greater antioxidant capacity increases the O_3 tolerance of plants [128].

The Combined Effects of Elevated CO_2 and O_3 on Plants

Elevated CO_2 (eCO_2) has been suggested to mitigate the negative effects of O_3 in plants, because it has a stimulating effect on photosynthesis – the CO_2 fertilisation effect [129]. ECO_2 increases photosynthesis and radiation use efficiency [130, 131], and so may offset the negative effects of O_3 on net photosynthesis [72, 93, 132, 133]. However, several experimental studies have shown that eCO_2 only partially offsets the negative effects of O_3 [133–135].

ECO_2 causes reduced stomatal conductance, which increases WUE and reduces exposure to O_3 [90, 136, 137]. Higher photosynthetic yield under elevated eCO_2

may compensate for increased secondary metabolite investment and detoxification demands under O_3 stress. Although eCO_2 induces stomatal closure [130], studies have found eCO_2 does not mitigate O_3 induced stomatal sluggishness [138]. Klingberg et al argue that the risk of future O_3 concentrations on vegetation will be counteracted by the stimulatory effects of rising CO_2, but this analysis only assessed stomatal conductance and did not include stomatal sluggishness [139]. Average atmospheric CO_2 concentrations will continue to increase while fossil fuels are burned, and are predicted to reach 550 ppm by 2050 if humanity continues along its current path [140]. Therefore, it is important to consider both elevated CO_2 and O_3 when predicting vegetation productivity and risk in the future.

The Effect of O_3 Exposure on Tree Growth

This thesis focuses on the effects of O_3 on trees, in particular temperate broadleaf trees. Although the effects of O_3 have been more extensively studied in crops, trees are crucial for the Earth's carbon balance [141] and reforestation efforts. Open top chambers, fumigated greenhouses, and free-air concentration enrichment (FACE) facilities have been used to study the effects of O_3 on trees. Generally, broadleaf trees are more sensitive to O_3 than coniferous species [102, 142, 143].

Experimental studies have shown O_3 exposure reduces growth in young trees [72], and offsets eCO_2 stimulated growth [144, 145]. Wittig et al's meta-analysis of the effect of O_3 on tree growth estimated current ambient O_3 concentrations of 40 ppb in the northern hemisphere already reduce the biomass of trees by 7% on average [117]. Wittig et al also reported that root to shoot biomass ratio decreases under O_3 stress across tree species [117]. In the Kranzberger forest FACE O_3 experiment, a mature section of forest was exposed to twice ambient O_3 concentrations for several years [146]. Elevated O_3 decreased bole volume in European beech by 44%, although the same effect was not seen in Norway spruce [147]. The relationships between O_3 flux and growth reduction in tree species have been derived from young trees in experiments, but when tested the flux-response relationship applied well to mature beech trees in Switzerland where O_3 stress caused an estimated 19.5% reduction in

the growth of deciduous forests [148]. O_3 was shown to reduce tree ring width in a range of European forest species in a high resolution dendrology analysis [149].

The Effect of O_3 Exposure on Tree Phenology

O_3 stress is known to accelerate the loss of leaves (senescence) in deciduous tree species [72]. O_3 induced acceleration of senescence has been observed in Japanese beech [150], and the sun leaves of European beech [151] based on measurements of chlorophyll fluorescence over time. Ribas et al also found accelerated senescence related processes in Mediterranean tree species under O_3 stress, but the extent of this response varied by species [152]. Similarly, Pell et al found O_3 accelerated senescence in black cherry and poplar trees, but not in sugar maple or red oak [153]. More recently, O_3 was shown to be the dominant factor in the timing of the end of the growth season across plant functional types in the Tibetan Plateau [154]. There is also some evidence that elevated O_3 delays leaf budding in urban tree species [155]. Therefore, O_3 exposure has important effects on the phenology of trees in particular relating to the timing of senescence and therefore the length of the growth season.

The Effect of O_3 Exposure on Forest Species

The differences in O_3 tolerance described above yield species specific differences in O_3 tolerance. At the community scale, O_3 pollution can therefore leaf to shifts in species dominance in favour of O_3 tolerance species [156, 157]. O_3 induced changes in species composition have been demonstrated in grasslands [158, 159], but the effect of O_3 on forest species composition is more challenging to test. Additionally, O_3 pollution can affect nutrient cycling in forests by altering litter decomposition [160, 161]. O_3 pollution negatively effects key pollinators via changes in VOC signalling and foliar quality [162–164]. O_3 pollution therefore is likely to have long term and multi-trophic level impacts on forest ecosystems although further research is needed to understand dose-specific responses in mature forests.

The effect of O_3 Exposure on Forest Carbon Assimilation

The negative effects of O_3 on photosynthesis and energetic cost of detoxifying O_3 stress lead to reduced growth in trees [72]. The effect of current and future O_3 pollution on forest biomass and carbon assimilation has been evaluated using a range of modelling and measurement-based approaches, yielding mixed results. As highlighted by Cailleret et al, integrated approaches are needed to combine the results of controlled experiments with long-term monitoring and account for processes like acclimation [165].

Karlsson et al found substantial reductions in the carbon sequestration of managed forests in Europe from 2008-2012 using phytotoxic stomatal O_3 dose modelling alongside an air pollution chemical transport model [166]. This analysis identified coastal, mid-latitude regions as being at particular risk of exceeding phytotoxic O_3 levels, such as the UK, and estimated the carbon stock of European living forest biomass would increase by 31% if O_3 concentrations returned to pre-industrial levels [166]. Using long-term flux measurements across Mediterranean ecosystems, Fares et al found O_3 reduced carbon assimilation by 12-19% [167]. In an analysis of the effect of O_3 on satellite derived gross primary productivity (GPP) in European forests across 37 sites, Proietti et al reported O_3 reduced GPP by 0.4-30% between 2000-2010 [168].

Conversely, Wang et al used gap model analysis to argue that while O_3 stress reduces plant productivity on an individual scale, at the ecosystem scale carbon assimilation may not be affected thanks to compensatory mechanisms and increasing dominance of O_3 tolerant species [157]. However, the O_3 tolerant species in their analysis also emit significantly more isoprenes, a type of BVOC which acts as a precursor for O_3 formation, which could lead to positive feedback loops yielding extreme local O_3 concentrations.

On balance, it is likely that O_3 pollution is having a significant effect on the growth and carbon assimilation of forests and will continue to do so in the future. Fuhrer et al found 40% of global ecoregions were O_3 polluted in 2000, and that even under the optimistic RCP4.5 scenario O_3 exposure would increase in half of all

ecoregions [169]. The negative effects of O_3 on vegetation can also enhance climatic change: Arnold et al simulated the global climate response to O_3 induced changes in plant transpiration and found an increase in annual surface temperature of up to +1.5 K due to the effects of O_3 on vegetation in polluted areas [170]. Therefore the effects of O_3 pollution on global vegetation, while uncertain in magnitude, are highly important in understanding the role of vegetation in coping with and compensating for anthropogenic climate change as well as restoring ecosystems (see [171]).

1.2.3 Monitoring O_3 Damage to Vegetation

Current Monitoring Methods

Monitoring the effects of air pollutants, including O_3, on natural and semi-natural vegetation is specified in Article 9 of the European National Emission Ceilings Directive [172]. This continues to apply under UK Law via the National Emission Ceilings Regulations [173]. The current methodology for monitoring the effect of O_3 on vegetation is to survey plants for visible foliar injury caused by O_3 [174].

Acute O_3 damage causes visual symptoms to leaves which include characteristic stippling, chlorosis, and necrosis [175–177]. Stipples are very small "pinprick" dark dots which occur between the veins of the leaf [174]. Chlorosis is a loss of chlorophyll pigmentation and in the case of O_3 damage can appear in discrete patches termed mottles [174]. Necrotic areas in the palisade mesophyll may also occur, sometimes referred to as flecks [176]. Visual symptoms of O_3 damage affect mature sun-exposed leaves the most [174]. Figure 1.1 demonstrates characteristic intervenous chlorotic mottles and necrotic flecks, as well as brown discolouration in a beech leaf experimentally exposed to elevated O_3. Acute O_3 stress can also lead to crown defoliation [174].

The International Co-operative Programme on Assessment and Monitoring of Air Pollution Effects on Forests (ICP Forests) launched in 1985 aims to monitor the effects of air pollution across Europe, it reports to the United Nations Economic Commission for Europe (UNECE). ICP Forests monitoring comprises of Level I: large scale forest crown condition surveys across 16km by 16km sample plots;



Figure 1.1: High resolution scan of a dried beech leaf exposed to elevated O_3 for 4 months.

and Level II: intensive forest observations alongside air quality monitoring [178]. In a recent publication, ICP Forests reported visible foliar O_3 injury on 38% of the observed broadleaved woody species across Europe, significantly correlated with O_3 exposure [179].

Although ICP Forests run routine inter-calibration courses, and have applied data quality limits, concerns remain about the objectivity of manual leaf inspection for visible foliar O_3 injury [180–182]. Monitoring via visual foliar injury relies on trained experts and is inherently limited in spatial coverage. Visible foliar O_3 injury is associated with decreased photosynthetic activity in sensitive species, but there is uncertainty in the suitability of visible symptoms to predict forest growth reduction [183].

Other methods of monitoring O_3 damage include the use of O_3 protectant chemicals and sensitive indicator species. Ethylenediurea (EDU) can prevent O_3 induced foliar injury and growth losses in plants, and can be used to verify O_3 induced symptoms in the field where O_3 monitoring is not available [184]. While the mode of action of EDU protection against O_3 damage remains unclear, EDU

is an effective O_3 protectant in larch and poplar saplings [185, 186]. Pyroligneous acid, also known as wood vinegar or wood distillate also protects O_3 sensitive species against oxidative damage, and has been proposed as a method for verifying O_3 induced foliar symptoms [187, 188]. Sensitive species can also be used as biomonitors of O_3 stress, for example the O_3 sensitive tobacco strain Bel-W3 has been widely used [189], as well as clover [190, 191]. Black Cherry trees have been used across North America for biomonitoring of O_3 exposure [192]. While protectant chemicals and biomonitoring species offer useful verification of O_3 damage in the field, a more quantitative approach is needed to assess the extent of O_3 damage to forests on large spatial scales.

Introduction to Vegetation Spectroscopy

The visible foliar injuries induced by O_3 damage, as well as changes to pigment concentrations, mean O_3 damage is a good candidate for spectral monitoring. Vegetation spectroscopy uses the interaction of light energy across the electromagnetic spectrum with plant surfaces to infer information about plants. Light can be absorbed, reflected, or transmitted when it hits the surface of vegetation, and vegetation spectroscopy uses the specific wavelengths and intensities of reflected light to gather information about the plant's chemical composition, structure, and water content. Specific components in plants, such as pigments, have distinct patterns of absorption and reflectance at specific wavelengths – a spectral signature. For example, it is visible to the naked eye that chlorophyll pigments absorb red and blue visible light but reflect green wavelengths. Vegetation spectroscopy extends visual analysis of plant health into the ultraviolet, and into the infrared regions of the electromagnetic spectrum, allowing high-throughput and quantitative remote monitoring of plant health.

Vegetation spectroscopy has been applied to many areas, including disease detection [193], crop productivity [194], and forest health [195]. Depending on the number and precision of wavelengths captured, spectrometers can be either multi or hyperspectral. Hyperspectral spectrometers capture a continuous spectrum

of reflectance data in narrow bands, whereas multispectral spectrometers collect data over a limited number of broad wavelength bands. Hyperspectral analysis allows more detailed assessment of changes in vegetation's spectral signature at the individual wavelength level, but is more limited in remote applications although hyperspectral sensors are now becoming available even in satellite mounted applications [196].

The method of illumination also affects the information that can be acquired from vegetation spectroscopy. Remote sensing applications of spectroscopy rely of passive illumination by the sun, whereas laboratory or field spectrometers use active illumination. Active illumination allows consistent comparisons between measurements taken in different places or at different times, without corrections for solar intensity and weather effects. Active illumination also results in a much higher signal to noise ratio, and so is used when high precision spectroscopy is desired.

The Application of Vegetation Spectroscopy to Study O_3 Damage in Vegetation

Visible foliar injuries caused by acute O_3 stress were first measured using reflectance spectroscopy of visible light by Runeckles and Rech in 1975 on leaf discs taken from bean plants exposed to elevated O_3 treatment [197]. Similar early experiments in tomatoes and soybean found changes in visible reflectance relating to chlorophyll content in plants visibly damaged by high O_3 exposure [198, 199]. Wheat experiences chlorosis under acute O_3 stress, accompanied by a shift in the position of the red edge reflectance towards longer wavelengths [200, 201], and reduced Normalized Difference Vegetation Index (NDVI) intensity [202]. Clover is sensitive to O_3 and has been used as a bioindicator of O_3 exposure for crops. Clover canopies suffering O_3 induced foliar injury have increased green reflectance, reduced near infrared (NIR) reflectance, and the position of the red-edge is shifted towards longer wavelengths [200, 203].

Under acute O_3 stress coniferous needles develop chlorotic mottling, which was first detected in the reflectance of stacks of needles via increased red wavelength reflectance [204]. In both natural O_3 gradients and open top chamber experiments, visible O_3 damage to Ponderosa pine needles was detected in the reflectance spectra

as a broadening of the chlorophyll absorption band and a shift in the position of the red edge towards longer wavelengths [205, 206]. Similar spectral results were found in Norway spruce needles with visual O_3 injury [207]. Loblolly pine needles also develop chlorosis and necrosis under O_3 stress, accompanied by increased visible light reflectance and decreased NIR reflectance intensity [208]. However, not all coniferous species are sensitive to O_3 stress, no visual injury or changes in needle reflectance were found in white pine or Scots pine saplings experimentally exposed to elevated O_3 [209].

These early applications of reflectance spectroscopy to detect O_3 stress relied upon visible foliar injury and intense exposure to high O_3 concentrations to detect changes in reflectance at the end of treatment, as summarised by Meroni et al's 2009 review paper [210]. These studies were also limited in the limited wavelength ranges available for analysis by field spectrometers, constrained to the visible and NIR spectrum and low spectral resolutions.

Building on this body of work, Meroni et al used more modern spectrometers with higher spectral resolution and wider wavelength ranges to pioneer spectral O_3 stress detection before visual symptoms develop, first in poplar clones and then clover [211, 212]. In both species the photochemical reflective index (PRI, [213]) alongside steady state chlorophyll fluorescence responded to O_3 treatment before visual foliar injury developed [211, 212]. O_3 stress has been shown to affect the chlorophyll a fluorescence dynamics of woody plants due to photosystem damage and photosynthetic downregulation, as summarised by Bussotti et al [214]. Early detection of O_3 stress via hyperspectral analysis has now also been demonstrated in sage [215] and pomegranate cultivars [216]. Recent hyperspectral analysis of O_3 stress in symptomatic soybeans confirmed earlier findings relating to changes in the green reflectance peak and red-edge shift towards longer wavelengths [217].

In 2002 Diem et al used satellite derived vegetation indices to demonstrate a reduction in green reflectance linked to O_3 induced foliar injury in sensitive Ponderosa pines [218]. More recently, visible O_3 injury in sensitive pine species in

Sierra Nevada and Catalonia has been remotely sensed using airborne hyperspectral images using PRI among other vegetation indices [219].

1.3 Thesis Aims

Broadleaf or deciduous temperate forests make up 15% of global forest cover and are one of Earth's major biomes [220, 221]. Broadleaf temperate forests are significant carbon stores, responsible for 24.5±9.4 PgC storage [222]. Broadleaf woody species have lower LMA [223], and higher stomatal conductance than conifers [224], consequently deciduous broadleaves are more vulnerable to O_3 damage [102]. Despite their global importance and sensitivity to O_3, there has been little research into the spectral response of temperate broadleaf species to O_3 compared to conifers and food crops. This thesis aims to contribute to this knowledge gap by establishing the spectral signature of O_3 damage in temperate broadleaf trees, with the aim of applying this technique to more effectively monitor the extent of O_3 on broadleaf temperate forests.

Objectives

1. To experimentally identify the hyperspectral signature of O_3 damage in temperate broadleaf species.

2. To test hyperspectral O_3 damage detection in mature temperate broadleaf trees outside experimental conditions.

3. To compare the effects of elevated CO_2 on leaf reflectance with the effects of O_3, with future monitoring under 2050 atmospheric conditions in mind.

4. To explore the suitability of spectral O_3 damage detection for a remote sensing application.

Chapter 2 addresses Objective 1 by asking "what is the spectral signature of O_3 damage in broadleaf saplings?" in the context of a chronic O_3 manipulation experiment. I found a distinct signal of O_3 damage which was modulated by dosage,

and varied between species but was unified by key changes in the width and intensity of the green reflectance peak, and the short-wavelength infrared region.

Chapter 3 expands upon this experiment by addressing Objective 2, and asking whether the O_3 damage signal identified in Chapter 2 is also found in mature temperate broadleaf trees exposed to naturally elevated O_3. I found that the changes in the width and intensity of the green reflectance peak and red-edge identified in saplings also occurred in mature trees exposed to elevated O_3, although I did not observe the short-wavelength infrared signal. In both Chapter 2 and 3 I found that whole-spectra methods of analysis (utilising machine learning) captured the multivariate signal of O_3 damage better than traditional vegetation index based approaches.

In Chapter 4 I used the BIFoR FACE CO_2 enrichment experiment to investigate Objective 3, asking how experimentally elevated CO_2 in a mature temperate broadleaf forest affected hyperspectral leaf reflectance and whether elevated CO_2 would interfere with spectral O_3 damage detection. I did not find a significant effect of elevated CO_2 on leaf reflectance, although there was an increase in one vegetation index linked to senescence. Although O_3 and CO_2 were not experimentally combined, this investigation shows that the signal of O_3 damage is stronger than and distinct from any impact elevated CO_2 may have on leaf reflectance. Hyperspectral O_3 damage detection therefore should not be affected by the elevated levels of CO_2 expected in the coming decades.

Chapter 5 tackles Objective 4 by trialling a correlative satellite analysis of the vegetation index which responded most strongly to O_3 damage in Chapters 2 and 3 with cumulative O_3 exposure. This analysis did not yield a significant correlation, and was constrained by the low spatial and temporal resolution of the available data. Chapter 5 also discusses in detail the datasets which would be needed to carry out a more sophisticated remote analysis of O_3 damage to forests, and explores different approaches of scaling up the leaf level signal I have identified to a remote methodology.

References

[1] C.F Schönbein. "On the Odour Accompanying Electricity and on the Probability of its Dependence on the Presence of a New Substance". In: *Philosophical Magazine* III.17 (1840), pp. 293–4.

[2] J. L. Soret. "Recherches sur la densite de l'ozone". In: *C. R. Hebd. Seances Acad. Sci.* Ser. C 64 (1867), pp. 904–8.

[3] Mordecai B Rubin. "THE HISTORY OF OZONE. THE SCHÖNBEIN PERIOD, 1839-1868". In: *Bull. Hist. Chem* 26.1 (2001).

[4] Michaela Hegglin et al. *Twenty Questions and Answers About the Ozone Layer: 2014 update*. Geneva, Switzerland: World Meteorological Organization, Jan. 2015, p. 84.

[5] D. S. Stevenson et al. "Tropospheric ozone changes, radiative forcing and attribution to emissions in the Atmospheric Chemistry and Climate Model Intercomparison Project (ACCMIP)". In: *Atmospheric Chemistry and Physics* 13.6 (Mar. 15, 2013). Publisher: Copernicus GmbH, pp. 3063–3085. DOI: 10.5194/acp-13-3063-2013.

[6] Marcello Iriti and Franco Faoro. "Oxidative Stress, the Paradigm of Ozone Toxicity in Plants and Animals". In: *Water, Air, and Soil Pollution* 187.1 (Jan. 1, 2008), pp. 285–301. DOI: 10.1007/s11270-007-9517-7.

[7] Marissa N. DeLang et al. "Mapping Yearly Fine Resolution Global Surface Ozone through the Bayesian Maximum Entropy Data Fusion of Observations and Model Output for 1990–2017". In: *Environmental Science & Technology* 55.8 (Apr. 20, 2021). Publisher: American Chemical Society, pp. 4389–4398. DOI: 10.1021/acs.est.0c07742.

[8] Paul S. Monks. "Gas-phase radical chemistry in the troposphere". In: *Chemical Society Reviews* 34.5 (2005), p. 376. DOI: 10.1039/b307982c.

[9] C. E. Junge. "Global ozone budget and exchange between stratosphere and troposphere". In: *Tellus* 14.4 (1962), pp. 363–377. DOI: 10.1111/j.2153-3490.1962.tb01349.x.

[10] A. Stohl et al. "Stratosphere-troposphere exchange: A review, and what we have learned from STACCATO". In: *Journal of Geophysical Research: Atmospheres* 108 (D12 2003). DOI: 10.1029/2002JD002490.

[11] C. A. McLinden et al. "Stratospheric ozone in 3-D models: A simple chemistry and the cross-tropopause flux". In: *Journal of Geophysical Research: Atmospheres* 105 (D11 2000), pp. 14653–14665. DOI: 10.1029/2000JD900124.

[12] J. R. Olson et al. "Seasonal differences in the photochemistry of the South Pacific: A comparison of observations and model results from PEM-Tropics A and B". In: *Journal of Geophysical Research: Atmospheres* 106 (D23 2001), pp. 32749–32766. DOI: 10.1029/2001JD900077.

[13] P. J. Young et al. "Pre-industrial to end 21st century projections of tropospheric ozone from the atmospheric chemistry and climate model intercomparison project (ACCMIP)". In: *Atmospheric Chemistry and Physics* 13 (2013), pp. 2063–2090. DOI: 10.5194/acp-13-2063-2013.

[14] Xiao Lu, Lin Zhang, and Lu Shen. "Meteorology and Climate Influences on Tropospheric Ozone: a Review of Natural Sources, Chemistry, and Transport Patterns". In: *Current Pollution Reports* 5.4 (Dec. 1, 2019). Company: Springer Distributor: Springer Institution: Springer Label: Springer Number: 4 Publisher: Springer International Publishing, pp. 238–260. DOI: 10.1007/s40726-019-00118-3.

[15] O. R. Cooper et al. "Global distribution and trends of tropospheric ozone: An observation-based review". In: *Elementa: Science of the Anthropocene* 2 (July 10, 2014). Ed. by Detlev Helmig and Paul Palmer, p. 000029. DOI: 10.12952/journal.elementa.000029.

[16] Samuel J. Oltmans and Hiram Levy. "Surface ozone measurements from a global network". In: *Atmospheric Environment* 28.1 (Jan. 1, 1994), pp. 9–24. DOI: 10.1016/1352-2310(94)90019-1.

[17] Juseon Bak et al. "Temporal variability of tropospheric ozone and ozone profiles in the Korean Peninsula during the East Asian summer monsoon: insights from multiple measurements and reanalysis datasets". In: *Atmospheric Chemistry and Physics* 22.21 (Nov. 4, 2022), pp. 14177–14187. DOI: 10.5194/acp-22-14177-2022.

[18] Martin G. Schultz et al. "Tropospheric Ozone Assessment Report: Database and Metrics Data of Global Surface Ozone Observations". In: *Elem Sci Anth* 5.0 (Oct. 18, 2017), p. 58. DOI: 10.1525/elementa.244.

[19] Wenxiu Zhang et al. "Parsimonious estimation of hourly surface ozone concentration across China during 2015–2020". In: *Scientific Data* 11 (May 14, 2024), p. 492. DOI: 10.1038/s41597-024-03302-3.

[20] Clara Betancourt et al. "Global, high-resolution mapping of tropospheric ozone – explainable machine learning and impact of uncertainties". In: *Geoscientific Model Development* 15.11 (June 3, 2022). Publisher: Copernicus GmbH, pp. 4331–4354. DOI: 10.5194/gmd-15-4331-2022.

[21] Anne M. Thompson et al. "Chapter 4 - Ozonesondes: Instrumentation and Data Applications". In: NTRS Author Affiliations: University of Maryland, Baltimore County, Forschungszentrum Jülich, Science Systems and Applications (United States), Goddard Space Flight Center NTRS Document ID: 20230002057 NTRS Research Center: Goddard Space Flight Center (GSFC). Sept. 15, 2022.

[22] Environment {and} Climate Change Canada. *World Ozone and Ultraviolet Radiation Data Centre (WOUDC).*

[23] Ryan M. Stauffer. *Southern Hemisphere ADditional OZonesondes, data archive.* DOI: https://doi.org/10.57721/SHADOZ-V06.

[24] Jian Xu et al. "Remote Sensing of Tropospheric Ozone from Space: Progress and Challenges". In: *Journal of Remote Sensing* 4 (Aug. 2, 2024). Publisher: American Association for the Advancement of Science, p. 0178. DOI: 10.34133/remotesensing.0178.

[25] Matthew S. Johnson et al. "TOLNet validation of satellite ozone profiles in the troposphere: impact of retrieval wavelengths". In: *Atmospheric Measurement Techniques* 17.8 (May 2, 2024). Publisher: Copernicus GmbH, pp. 2559–2582. DOI: 10.5194/amt-17-2559-2024.

[26] Glenn E. Shaw. "Atmospheric Ozone: Determination by Chappuis-Band Absorption". In: *Journal of Applied Meteorology (1962-1982)* 18.10 (1979). Publisher: American Meteorological Society, pp. 1335–1339.

[27] Herbert M. Pickett. "THz spectroscopy of the atmosphere". In: Optoelectronics '99 - Integrated Optoelectronic Devices. Ed. by Mark S. Sherwin. San Jose, CA, Apr. 29, 1999, pp. 2–6. DOI: 10.1117/12.347109.

[28] John P. Burrows et al. "The Global Ozone Monitoring Experiment (GOME): Mission Concept and First Scientific Results." In: *Journal of the Atmospheric Sciences* 56 (Jan. 1, 1999), pp. 151–175. DOI: 10.1175/1520-0469(1999)056<0151:TGOMEG>2.0.CO;2.

[29] Rosemary Munro et al. "The GOME-2 instrument on the Metop series of satellites: instrument design, calibration, and level 1 data processing – an overview". In: *Atmospheric Measurement Techniques* 9.3 (Mar. 24, 2016). Publisher: Copernicus GmbH, pp. 1279–1301. DOI: 10.5194/amt-9-1279-2016.

[30] Pieternel F. Levelt et al. "The Ozone Monitoring Instrument: overview of 14 years in space". In: *Atmospheric Chemistry and Physics* 18.8 (Apr. 24, 2018). Publisher: Copernicus GmbH, pp. 5699–5745. DOI: 10.5194/acp-18-5699-2018.

[31] Mengzhen Xie et al. "A Study on the Retrieval of Ozone Profiles Using FY-3D/HIRAS Infrared Hyperspectral Data". In: *Remote Sensing* 15.4 (Jan. 2023). Number: 4 Publisher: Multidisciplinary Digital Publishing Institute, p. 1009. DOI: 10.3390/rs15041009.

[32] K. V. Chance et al. "Satellite measurements of atmospheric ozone profiles, including tropospheric ozone, from ultraviolet/visible measurements in the nadir geometry: a potential method to retrieve tropospheric ozone". In: *Journal of Quantitative Spectroscopy and Radiative Transfer* 57.4 (Apr. 1, 1997), pp. 467–476. DOI: 10.1016/S0022-4073(96)00157-4.

[33] G. M. Miles et al. "Tropospheric ozone and ozone profiles retrieved from GOME-2 and their validation". In: *Atmospheric Measurement Techniques* 8.1 (Jan. 22, 2015), pp. 385–398. DOI: 10.5194/amt-8-385-2015.

[34] Nora Mettig et al. "Ozone profile retrieval from nadir TROPOMI measurements in the UV range". In: *Atmospheric Measurement Techniques* 14.9 (Sept. 16, 2021). Publisher: Copernicus GmbH, pp. 6057–6082. DOI: 10.5194/amt-14-6057-2021.

[35] M. D. Müller et al. "Ozone profile retrieval from Global Ozone Monitoring Experiment (GOME) data using a neural network approach (Neural Network Ozone Retrieval System (NNORSY))". In: *Journal of Geophysical Research: Atmospheres* 108 (D16 2003). DOI: 10.1029/2002JD002784.

[36] Jack Fishman and Jack C. Larsen. "Distribution of total ozone and stratospheric ozone in the tropics: Implications for the distribution of tropospheric ozone". In: *Journal of Geophysical Research: Atmospheres* 92 (D6 1987), pp. 6627–6634. DOI: 10.1029/JD092iD06p06627.

[37] J. R. Ziemke, S. Chandra, and P. K. Bhartia. "Two new methods for deriving tropospheric column ozone from TOMS measurements: Assimilated UARS MLS/HALOE and convective-cloud differential techniques". In: *Journal of Geophysical Research: Atmospheres* 103 (D17 1998), pp. 22115–22127. DOI: 10.1029/98JD01567.

[38] Klaus-Peter Heue et al. “Tropospheric ozone retrieval by a combination of TROPOMI/S5P measurements with BASCOE assimilated data”. In: *Atmospheric Measurement Techniques* 15.19 (Oct. 4, 2022), pp. 5563–5579. DOI: 10.5194/amt-15-5563-2022.

[39] J. R. Ziemke, S. Chandra, and P. K. Bhartia. ““Cloud slicing”: A new technique to derive upper tropospheric ozone from satellite measurements”. In: *Journal of Geophysical Research: Atmospheres* 106 (D9 2001), pp. 9853–9867. DOI: 10.1029/2000JD900768.

[40] J. R. Ziemke et al. “Tropospheric ozone determined from Aura OMI and MLS: Evaluation of measurements and comparison with the Global Modeling Initiative’s Chemical Transport Model”. In: *Journal of Geophysical Research: Atmospheres* 111 (D19 2006). DOI: 10.1029/2006JD007089.

[41] Matilda A. Pimlott et al. “Long-term satellite trends of European lower-tropospheric ozone from 1996–2017”. In: *EGUsphere* (Dec. 16, 2024). Publisher: Copernicus GmbH, pp. 1–26. DOI: 10.5194/egusphere-2024-3717.

[42] Richard J. Pope et al. “Investigation of spatial and temporal variability in lower tropospheric ozone from RAL Space UV–Vis satellite products”. In: *Atmospheric Chemistry and Physics* 23.23 (Dec. 5, 2023). Publisher: Copernicus GmbH, pp. 14933–14947. DOI: 10.5194/acp-23-14933-2023.

[43] *Sentinel-5 A Satellite Mission Summary | CEOS Database*. URL: https://database.eohandbook.com/database/missionsummary.aspx?missionID=641 (visited on 03/03/2025).

[44] D. Simpson et al. “The EMEP MSC-W chemical transport model – technical description”. In: *Atmospheric Chemistry and Physics* 12.16 (Aug. 31, 2012). Publisher: Copernicus GmbH, pp. 7825–7865. DOI: 10.5194/acp-12-7825-2012.

[45] D. Simpson et al. *Updates to the EMEP/MSC-W model, 2022–2023, in: Transboundary particulate matter, photo-oxidants, acidifying and eutrophying components*. 1\2023. The Norwegian Meteorological Insitutue, Oslo, Norway, 2023.

[46] Katherine L Pugsley et al. *Technical report on UK supplementary modelling assessment under the Air Quality Standards Regulations 2010 for 2022*. 2022.

[47] Rumen D. Bojkov. “Surface Ozone During the Second Half of the Nineteenth Century”. In: *Journal of Climate and Applied Meteorology* 25.3 (1986). Publisher: American Meteorological Society, pp. 343–352.

[48] Albert Lévy. *Annuaire de l’Observ. de Montsouris*. Paris: Gauthier-Villars, 1878. 495-505.

[49] Andreas Volz and Dieter Kley. “Evaluation of the Montsouris series of ozone measurements made in the nineteenth century”. In: *Nature* 332.6161 (Mar. 1988). Publisher: Nature Publishing Group, pp. 240–242. DOI: 10.1038/332240a0.

[50] Laurence Y. Yeung et al. “Isotopic constraint on the twentieth-century increase in tropospheric ozone”. In: *Nature* 570.7760 (June 2019). Publisher: Nature Publishing Group, pp. 224–227. DOI: 10.1038/s41586-019-1277-1.

[51] A. T. Archibald et al. “Tropospheric Ozone Assessment Report: A critical review of changes in the tropospheric ozone burden and budget from 1850 to 2100”. In: *Elementa: Science of the Anthropocene* 8.1 (Dec. 30, 2020), p. 034. DOI: 10.1525/elementa.2020.034.

[52] Roxanne Vingarzan. “A review of surface ozone background levels and trends”. In: *Atmospheric Environment* 38.21 (2004), pp. 3431–3442. DOI: https://doi.org/10.1016/j.atmosenv.2004.03.030.

[53] Amy Christiansen et al. “Multidecadal increases in global tropospheric ozone derived from ozonesonde and surface site observations: can models reproduce ozone trends?” In: *Atmospheric Chemistry and Physics* 22.22 (Nov. 21, 2022). Publisher: Copernicus GmbH, pp. 14751–14782. DOI: 10.5194/acp-22-14751-2022.

[54] Pierre Sicard. “Ground-level ozone over time: An observation-based global overview”. In: *Current Opinion in Environmental Science & Health* 19 (Feb. 1, 2021), p. 100226. DOI: 10.1016/j.coesh.2020.100226.

[55] A. Gaudel et al. “Tropospheric Ozone Assessment Report: Present-day distribution and trends of tropospheric ozone relevant to climate and global atmospheric chemistry model evaluation”. In: *Elementa: Science of the Anthropocene* 6 (Jan. 1, 2018). Ed. by Detlev Helmig and Alastair Lewis, p. 39. DOI: 10.1525/elementa.291.

[56] D. D. Parrish et al. “Lower tropospheric ozone at northern midlatitudes: Changing seasonal cycle”. In: *Geophysical Research Letters* 40.8 (2013), pp. 1631–1636. DOI: 10.1002/grl.50303.

[57] Ana Santurtún et al. “Surface ozone concentration trends and its relationship with weather types in Spain (2001–2010)”. In: *Atmospheric Environment* 101 (Jan. 1, 2015), pp. 10–22. DOI: 10.1016/j.atmosenv.2014.11.005.

[58] T. Wang et al. “Increasing surface ozone concentrations in the background atmosphere of Southern China, 1994–2007”. In: *Atmospheric Chemistry and Physics* 9.16 (Aug. 31, 2009). Publisher: Copernicus GmbH, pp. 6217–6227. DOI: 10.5194/acp-9-6217-2009.

[59] Zhenze Liu et al. “Tropospheric ozone changes and ozone sensitivity from present-day to future under shared socio-economic pathways”. In: (Aug. 19, 2021). DOI: 10.5194/acp-2021-689.

[60] Steven T. Turnock et al. “The impact of future emission policies on tropospheric ozone using a parameterised approach”. In: *Atmospheric Chemistry and Physics* 18.12 (June 28, 2018). Publisher: Copernicus GmbH, pp. 8953–8978. DOI: 10.5194/acp-18-8953-2018.

[61] O. Wild et al. “Modelling future changes in surface ozone: a parameterized approach”. In: *Atmospheric Chemistry and Physics* 12.4 (Feb. 21, 2012). Publisher: Copernicus GmbH, pp. 2037–2054. DOI: 10.5194/acp-12-2037-2012.

[62] Prodromos Zanis et al. “Climate change penalty and benefit on surface ozone: a global perspective based on CMIP6 earth system models”. In: *Environmental Research Letters* 17.2 (Feb. 1, 2022), p. 024014. DOI: 10.1088/1748-9326/ac4a34.

[63] Huimin Li et al. "Climate-driven deterioration of future ozone pollution in Asia predicted by machine learning with multi-source data". In: *Atmospheric Chemistry and Physics* 23.2 (Jan. 23, 2023), pp. 1131–1145. DOI: 10.5194/acp-23-1131-2023.

[64] Intergovernmental Panel on Climate Change (IPCC). "Short-Lived Climate Forcers". In: *Climate Change 2021: The Physical Science Basis. Contribution of Working Group I to the Sixth Assessment Report of the Intergovernmental Panel on Climate Change*. Cambridge: Cambridge University Press, 2021, pp. 817–922.

[65] Air Quality Expert Group. *Ozone in the UK – recent trends and future projections*. UK Department for Environment, Food and Rural Affairs, 2021.

[66] Florencia M. R. Diaz et al. "Ozone Trends in the United Kingdom over the Last 30 Years". In: *Atmosphere* 11.5 (May 21, 2020), p. 534. DOI: 10.3390/atmos11050534.

[67] Christine H Foyer and Graham Noctor. "Oxidant and antioxidant signalling in plants: a re-evaluation of the concept of oxidative stress in a physiological context". In: *Plant, Cell & Environment* 28.8 (2005). Publisher: Wiley Online Library, pp. 1056–1071.

[68] Julia P. Vainonen and Jaakko Kangasjärvi. "Plant signalling in acute ozone exposure". In: *Plant, Cell & Environment* 38.2 (2015), pp. 240–252. DOI: 10.1111/pce.12273.

[69] Mulpuri V. Rao, Jennifer R. Koch, and Keith R. Davis. "Ozone: a tool for probing programmed cell death in plants". In: *Plant Molecular Biology* 44.3 (Oct. 1, 2000), pp. 345–358. DOI: 10.1023/A:1026548726807.

[70] Sagar V. Krupa. "Joint Effects of Elevated Levels of Ultraviolet-B Radiation, Carbon Dioxide and Ozone on Plants". In: *Photochemistry and Photobiology* 78.6 (2003), pp. 535–542. DOI: 10.1562/0031-8655(2003)0780535JEOELO2.0.CO2.

[71] A. J. Haagen-Smit. "Chemistry and Physiology of Los Angeles Smog". In: *Industrial & Engineering Chemistry* 44.6 (June 1952), pp. 1342–1346. DOI: 10.1021/ie50510a045.

[72] N. E. Grulke and R. L. Heath. "Ozone effects on plants in natural ecosystems". In: *Plant Biology* 22 (S1 2020), pp. 12–37. DOI: 10.1111/plb.12971.

[73] Lifan Wang et al. "The Effects of Dual Ozone and Drought Stresses on the Photosynthetic Properties of Acer rubrum and A. pictum". In: *Forests* 14.5 (May 2023). Number: 5 Publisher: Multidisciplinary Digital Publishing Institute, p. 998. DOI: 10.3390/f14050998.

[74] L. Leitao, O. Bethenod, and J.-P. Biolley. "The Impact of Ozone on Juvenile Maize (Zea mays L.) Plant Photosynthesis: Effects on Vegetative Biomass, Pigmentation, and Carboxylases (PEPc and Rubisco)". In: *Plant Biology* 9.4 (2007), pp. 478–488. DOI: 10.1055/s-2007-964942.

[75] Angeles Calatayud and Eva Barreno. "Response to ozone in two lettuce varieties on chlorophyll *a* fluorescence, photosynthetic pigments and lipid peroxidation". In: *Plant Physiology and Biochemistry* 42.6 (June 1, 2004), pp. 549–555. DOI: 10.1016/j.plaphy.2004.05.002.

[76] Sumita Kumari, Madhoolika Agrawal, and Supriya Tiwari. "Impact of elevated CO2 and elevated O3 on *Beta vulgaris* L.: Pigments, metabolites, antioxidants, growth and yield". In: *Environmental Pollution* 174 (Mar. 1, 2013), pp. 279–288. DOI: 10.1016/j.envpol.2012.11.021.

[77] Takeshi Sakaki, Noriaki Kondo, and Kiyoshi Sugahara. "Breakdown of photosynthetic pigments and lipids in spinach leaves with ozone fumigation: Role of active oxygens". In: *Physiologia Plantarum* 59.1 (1983), pp. 28–34. DOI: 10.1111/j.1399-3054.1983.tb06566.x.

[78] Elisa Pellegrini et al. "Ecophysiological and antioxidant traits of Salvia officinalis under ozone stress". In: *Environmental Science and Pollution Research* 22.17 (Sept. 1, 2015). Company: Springer Distributor: Springer Institution: Springer Label: Springer Number: 17 Publisher: Springer Berlin Heidelberg, pp. 13083–13093. DOI: 10.1007/s11356-015-4569-5.

[79] Pierre Dizengremel. "Effects of ozone on the carbon metabolism of forest trees". In: *Plant Physiology and Biochemistry* 39.9 (Sept. 1, 2001), pp. 729–742. DOI: 10.1016/S0981-9428(01)01291-8.

[80] D. Lombardozzi, J. P. Sparks, and G. Bonan. "Integrating O_3 influences on terrestrial processes: photosynthetic and stomatal response data available for regional and global modeling". In: *Biogeosciences* 10.11 (Nov. 1, 2013). Publisher: Copernicus GmbH, pp. 6815–6831. DOI: 10.5194/bg-10-6815-2013.

[81] Elizabeth Ainsworth et al. "The Effects of Tropospheric Ozone on Net Primary Productivity and Implications for Climate Change *". In: *Annual review of plant biology* 63 (Feb. 9, 2012), pp. 637–61. DOI: 10.1146/annurev-arplant-042110-103829.

[82] J. A. Bassham et al. "The Path of Carbon in Photosynthesis. XXI. The Cyclic Regeneration of Carbon Dioxide Acceptor[1]". In: *Journal of the American Chemical Society* 76.7 (Apr. 1954), pp. 1760–1770. DOI: 10.1021/ja01636a012.

[83] Matteo Gionfriddo, Kun Zang, and Manajit Hayer-Hartl. "The challenge of engineering Rubisco for improving photosynthesis". In: *FEBS Letters* 597.13 (2023), pp. 1679–1680. DOI: 10.1002/1873-3468.14678.

[84] M S Dann and E J Pell. "Decline of rubisco activity and net photosynthesis in ozone-treated potato foliage. [Solanum tuberosum]". In: vol. 83:4. Plant Physiol., Suppl.; (United States). United States: Pennsylvania State Univ., University Park, Apr. 1987.

[85] Eva J. Pell, Nancy A. Eckardt, and Richard E. Glick. "Biochemical and molecular basis for impairment of photosynthetic potential". In: *Photosynthesis Research* 39.3 (Mar. 1, 1994). Company: Springer Distributor: Springer Institution: Springer Label: Springer Number: 3 Publisher: Kluwer Academic Publishers, pp. 453–462. DOI: 10.1007/BF00014598.

[86] Eleni Goumenaki et al. "Mechanisms underlying the impacts of ozone on photosynthetic performance". In: *Environmental and Experimental Botany* 69.3 (Dec. 1, 2010), pp. 259–266. DOI: 10.1016/j.envexpbot.2010.04.011.

[87] Zhengwei Cai. "Lipid Peroxidation". In: *Encyclopedia of Toxicology (Second Edition)*. Ed. by Philip Wexler. New York: Elsevier, Jan. 1, 2005, pp. 730–734. DOI: 10.1016/B0-12-369400-0/00564-0.

[88] Radek Novotný et al. “Assessment of ozone impact on forest vegetation using visible foliar injury, AOT40F exposure index and MDA concentration in two meteorologically contrasting years”. In: *Journal of Forest Science* 71.1 (Jan. 28, 2025). Publisher: Journal of Forest Science, pp. 40–56. DOI: 10.17221/57/2024-JFS.

[89] Zaisheng Shao et al. “Identification of key responsive leaf traits for ozone tolerance in six modern *indica* and *japonica* rice cultivars (*Oryza sativa* L.) over two years”. In: *Agriculture, Ecosystems & Environment* 349 (June 15, 2023), p. 108451. DOI: 10.1016/j.agee.2023.108451.

[90] Elena Paoletti and Nancy E. Grulke. “Does living in elevated CO2 ameliorate tree response to ozone? A review on stomatal responses”. In: *Environmental Pollution*. Forests Under Changing Climate, Enhanced UV and Air Pollution 137.3 (Oct. 1, 2005), pp. 483–493. DOI: 10.1016/j.envpol.2005.01.035.

[91] Triin Vahisalu et al. “Ozone-triggered rapid stomatal response involves the production of reactive oxygen species, and is controlled by SLAC1 and OST1”. In: *The Plant Journal* 62.3 (2010), pp. 442–453. DOI: 10.1111/j.1365-313X.2010.04159.x.

[92] P. Li et al. “Stomatal characteristics and ozone dose-response relationships for six greening tree species”. In: *Shengtai Xuebao/ Acta Ecologica Sinica* 38.8 (2018), pp. 2710–2721. DOI: 10.5846/stxb201705220945.

[93] Victoria E. Wittig, Elizabeth A. Ainsworth, and Stephen P. Long. “To what extent do current and projected increases in surface ozone affect photosynthesis and stomatal conductance of trees? A meta-analytic review of the last 3 decades of experiments”. In: *Plant, Cell & Environment* 30.9 (2007), pp. 1150–1162. DOI: 10.1111/j.1365-3040.2007.01717.x.

[94] Elena Paoletti. “Ozone slows stomatal response to light and leaf wounding in a Mediterranean evergreen broadleaf, Arbutus unedo”. In: *Environmental Pollution* 134.3 (Apr. 2005), pp. 439–445. DOI: 10.1016/j.envpol.2004.09.011.

[95] Gina Mills et al. “Chronic exposure to increasing background ozone impairs stomatal functioning in grassland species”. In: *Global Change Biology* 15.6 (June 2009). Publisher: John Wiley & Sons, Ltd, pp. 1522–1533. DOI: 10.1111/j.1365-2486.2008.01798.x.

[96] Elena Paoletti and Nancy E. Grulke. “Ozone exposure and stomatal sluggishness in different plant physiognomic classes”. In: *Environmental Pollution* 158.8 (Aug. 1, 2010), pp. 2664–2671. DOI: 10.1016/j.envpol.2010.04.024.

[97] Serena Wagg et al. “Stomata are less responsive to environmental stimuli in high background ozone in Dactylis glomerata and Ranunculus acris”. In: *Environmental Pollution (Barking, Essex: 1987)* 175 (Apr. 2013), pp. 82–91. DOI: 10.1016/j.envpol.2012.11.027.

[98] Yasutomo Hoshika et al. “Determinants of stomatal sluggishness in ozone-exposed deciduous tree species”. In: *Science of The Total Environment* 481 (May 2014), pp. 453–458. DOI: 10.1016/j.scitotenv.2014.02.080.

[99] Pin Li et al. "Combining carbon and oxygen isotopic signatures to identify ozone-induced declines in tree water-use efficiency". In: *Tree Physiology* 41.12 (Dec. 4, 2021). Ed. by Lucas Cernusak, pp. 2234–2244. DOI: 10.1093/treephys/tpab041.

[100] Yasutomo Hoshika et al. "Water use strategy affects avoidance of ozone stress by stomatal closure in Mediterranean trees—A modelling analysis". In: *Plant, Cell & Environment* 43.3 (2020), pp. 611–623. DOI: 10.1111/pce.13700.

[101] Chris Huntingford et al. "Technical note: A simple theoretical model framework to describe plant stomatal "sluggishness" in response to elevated ozone concentrations". In: *Biogeosciences* 15.17 (Sept. 12, 2018), pp. 5415–5422. DOI: 10.5194/bg-15-5415-2018.

[102] Zhaozhong Feng et al. "A unifying explanation for variation in ozone sensitivity among woody plants". In: *Global Change Biology* 24.1 (2018), pp. 78–84. DOI: 10.1111/gcb.13824.

[103] Pin Li et al. "Differences in ozone sensitivity among woody species are related to leaf morphology and antioxidant levels". In: *Tree Physiology* 36.9 (Sept. 1, 2016), pp. 1105–1116. DOI: 10.1093/treephys/tpw042.

[104] S. Li et al. "Testing unified theories for ozone response in C4 species". In: *Global Change Biology* (2022). DOI: 10.1111/gcb.16108.

[105] P. G. Jarvis, John Lennox Monteith, and Paul Egerton Weatherley. "The interpretation of the variations in leaf water potential and stomatal conductance found in canopies in the field". In: *Philosophical Transactions of the Royal Society of London. B, Biological Sciences* 273.927 (Jan. 1997). Publisher: Royal Society, pp. 593–610. DOI: 10.1098/rstb.1976.0035.

[106] L. D. Emberson et al. "Modelling and Mapping Ozone Deposition in Europe". In: *Water, Air, and Soil Pollution* 130.1 (Aug. 1, 2001). Company: Springer Distributor: Springer Institution: Springer Label: Springer Number: 1 Publisher: Kluwer Academic Publishers, pp. 577–582. DOI: 10.1023/A:1013851116524.

[107] L. D. Emberson et al. "Modelling stomatal ozone flux across Europe". In: *Environmental Pollution* 109.3 (Sept. 1, 2000), pp. 403–413. DOI: 10.1016/S0269-7491(00)00043-9.

[108] Gina Mills et al. *Chapter 3: Mapping critical levels for vegetation.* ICP Vegetation, 2017.

[109] Alessandra De Marco et al. "Assessing the role of soil water limitation in determining the Phytotoxic Ozone Dose (PODY) thresholds". In: *Atmospheric Environment* 147 (Dec. 1, 2016), pp. 88–97. DOI: 10.1016/j.atmosenv.2016.09.066.

[110] Y. Hoshika et al. "Ozone risk assessment with free-air controlled exposure (FACE) experiments: A critical revisit". In: *Environmental Research* 255 (2024). DOI: 10.1016/j.envres.2024.119215.

[111] Gina Mills et al. "Evidence of widespread effects of ozone on crops and (semi-)natural vegetation in Europe (1990–2006) in relation to AOT40- and flux-based risk maps". In: *Global Change Biology* 17.1 (2011), pp. 592–613. DOI: 10.1111/j.1365-2486.2010.02217.x.

[112] Elena Paoletti et al. "Towards long-term sustainability of stomatal ozone flux monitoring at forest sites". In: *Sustainable Horizons* 2 (Mar. 1, 2022), p. 100018. DOI: 10.1016/j.horiz.2022.100018.

[113] Pierre Sicard et al. "An epidemiological assessment of stomatal ozone flux-based critical levels for visible ozone injury in Southern European forests". In: *Science of The Total Environment* 541 (Jan. 15, 2016), pp. 729–741. DOI: 10.1016/j.scitotenv.2015.09.113.

[114] Feng Gao et al. "Water stress mitigates the negative effects of ozone on photosynthesis and biomass in poplar plants". In: *Environmental Pollution* 230 (Nov. 1, 2017), pp. 268–279. DOI: 10.1016/j.envpol.2017.06.044.

[115] G. Kronfuß et al. "Effects of ozone and mild drought stress on gas exchange, antioxidants and chloroplast pigments in current-year needles of young Norway spruce [Picea abies (L.) Karst.]" In: *Trees* 12.8 (Aug. 1, 1998). Company: Springer Distributor: Springer Institution: Springer Label: Springer Number: 8 Publisher: Springer-Verlag, pp. 482–489. DOI: 10.1007/PL00009730.

[116] Elena Paoletti, Nancy E. Grulke, and Rainer Matyssek. "Ozone Amplifies Water Loss from Mature Trees in the Short Term But Decreases It in the Long Term". In: *Forests* 11.1 (Jan. 2020). Number: 1 Publisher: Multidisciplinary Digital Publishing Institute, p. 46. DOI: 10.3390/f11010046.

[117] Victoria E. Wittig et al. "Quantifying the impact of current and future tropospheric ozone on tree biomass, growth, physiology and biochemistry: a quantitative meta-analysis". In: *Global Change Biology* 15.2 (2009), pp. 396–424. DOI: 10.1111/j.1365-2486.2008.01774.x.

[118] Aditya Abha Singh et al. "Secondary metabolites responses of plants exposed to ozone: an update". In: *Environmental Science and Pollution Research* 30.38 (Aug. 1, 2023). Company: Springer Distributor: Springer Institution: Springer Label: Springer Number: 38 Publisher: Springer Berlin Heidelberg, pp. 88281–88312. DOI: 10.1007/s11356-023-28634-2.

[119] Fitzgerald L. Booker, Kent O. Burkey, and Alan M. Jones. "Re-evaluating the role of ascorbic acid and phenolic glycosides in ozone scavenging in the leaf apoplast of Arabidopsis thaliana L". In: *Plant, Cell & Environment* 35.8 (Aug. 2012), pp. 1456–1466. DOI: 10.1111/j.1365-3040.2012.02502.x.

[120] Stephen C. Grace. "Phenolics as Antioxidants". In: *Antioxidants and Reactive Oxygen Species in Plants*. John Wiley & Sons, Ltd, 2005, pp. 141–168.

[121] Wolf Bors et al. "Polyamines as radical scavengers and protectants against ozone damage". In: *Phytochemistry* 28.6 (Jan. 1, 1989), pp. 1589–1595. DOI: 10.1016/S0031-9422(00)97805-1.

[122] Marina Liaskoni et al. "The long-term impact of biogenic volatile organic compound emissions on urban ozone patterns over central Europe: contributions from urban and rural vegetation". In: *Atmospheric Chemistry and Physics* 24.23 (Dec. 10, 2024). Publisher: Copernicus GmbH, pp. 13541–13569. DOI: 10.5194/acp-24-13541-2024.

[123] Delia M. Pinto et al. "Plant Volatile Organic Compounds (VOCs) in Ozone (O3) Polluted Atmospheres: The Ecological Effects". In: *Journal of Chemical Ecology* 36.1 (Jan. 1, 2010), pp. 22–34. DOI: 10.1007/s10886-009-9732-3.

[124] Yan Yang et al. “Emissions of Biogenic Volatile Organic Compounds from Plants: Impacts of Air Pollutants and Environmental Variables”. In: *Current Pollution Reports* 11.1 (Dec. 1, 2025). Company: Springer Distributor: Springer Institution: Springer Label: Springer Number: 1 Publisher: Springer International Publishing, pp. 1–18. DOI: 10.1007/s40726-024-00339-1.

[125] R. Alonso et al. “Interactive effects of ozone and drought stress on pigments and activities of antioxidative enzymes in Pinus halepensis”. In: *Plant, Cell & Environment* 24.9 (2001), pp. 905–916. DOI: https://doi.org/10.1046/j.0016-8025.2001.00738.x.

[126] Zhong Chen and Daniel R. Gallie. “Increasing Tolerance to Ozone by Elevating Foliar Ascorbic Acid Confers Greater Protection against Ozone Than Increasing Avoidance”. In: *Plant Physiology* 138.3 (July 2005), pp. 1673–1689. DOI: 10.1104/pp.105.062000.

[127] Erika Bellini and Mario C. De Tullio. “Ascorbic Acid and Ozone: Novel Perspectives to Explain an Elusive Relationship”. In: *Plants* 8.5 (May 2019). Number: 5 Publisher: Multidisciplinary Digital Publishing Institute, p. 122. DOI: 10.3390/plants8050122.

[128] Tatyana Chernikova et al. “Ozone tolerance and antioxidant enzyme activity in soybean cultivars”. In: *Photosynthesis Research* 64.1 (Apr. 1, 2000). Company: Springer Distributor: Springer Institution: Springer Label: Springer Number: 1 Publisher: Kluwer Academic Publishers, pp. 15–26. DOI: 10.1023/A:1026500911237.

[129] P Ciais et al. *Carbon and other biogeochemical cycles. Climate change 2013: the physical science basis. Contribution of working group I to the fifth assessment report of the intergovernmental panel on climate change*. Cambridge: Cambridge University Press, 2013.

[130] Bert G. Drake, Miquel A. Gonzàlez-Meler, and Steve P. Long. “MORE EFFICIENT PLANTS: A Consequence of Rising Atmospheric CO2?” In: *Annual Review of Plant Biology* 48 (Volume 48, 1997 June 1, 1997). Publisher: Annual Reviews, pp. 609–639. DOI: 10.1146/annurev.arplant.48.1.609.

[131] Jindong Sun et al. “FACE-ing the global change: Opportunities for improvement in photosynthetic radiation use efficiency and crop yield”. In: *Plant Science* 177.6 (Dec. 1, 2009), pp. 511–522. DOI: 10.1016/j.plantsci.2009.08.003.

[132] John C. Volin, Peter B. Reich, and Thomas J. Givnish. “Elevated carbon dioxide ameliorates the effects of ozone on photosynthesis and growth: species respond similarly regardless of photosynthetic pathway or plant functional group”. In: *The New Phytologist* 138.2 (Feb. 1998), pp. 315–325. DOI: 10.1046/j.1469-8137.1998.00100.x.

[133] B. A Wustman et al. “Effects of elevated CO2 and O3 on aspen clones varying in O3 sensitivity: can CO2 ameliorate the harmful effects of O3?” In: *Environmental Pollution* 115.3 (Dec. 1, 2001), pp. 473–481. DOI: 10.1016/S0269-7491(01)00236-6.

[134] H. Kobayakawa and K. Imai. "Effects of the interaction between ozone and carbon dioxide on gas exchange, photosystem II and antioxidants in rice leaves". In: *Photosynthetica* 49.2 (June 1, 2011). Company: Springer Distributor: Springer Institution: Springer Label: Springer Number: 2 Publisher: Springer Netherlands, pp. 227–238. DOI: 10.1007/s11099-011-0024-0.

[135] I. F. McKee, P. K. Farage, and S. P. Long. "The interactive effects of elevated CO2 and O3 concentration on photosynthesis in spring wheat". In: *Photosynthesis Research* 45.2 (Aug. 1, 1995). Company: Springer Distributor: Springer Institution: Springer Label: Springer Number: 2 Publisher: Kluwer Academic Publishers, pp. 111–119. DOI: 10.1007/BF00032582.

[136] E.L. Fiscus et al. "Elevated CO2 reduces O3 flux and O3-induced yield losses in soybeans: possible implications for elevated CO2 studies1". In: *Journal of Experimental Botany* 48.2 (Feb. 1, 1997), pp. 307–313. DOI: 10.1093/jxb/48.2.307.

[137] Harry Harmens et al. "Implications of climate change for the stomatal flux of ozone: A case study for winter wheat". In: *Environmental Pollution*. Critcial Levels for Ozone Effects on Vegetation: Further Applying and Developing the Flux Concept 146.3 (Apr. 1, 2007), pp. 763–770. DOI: 10.1016/j.envpol.2006.05.018.

[138] Yuqing Lyu et al. "Effects of ozone on stomatal ozone uptake in leaves of *Fagus crenata* seedlings grown under different CO_2 concentrations". In: *Journal of Forest Research* (Nov. 23, 2023), pp. 1–8. DOI: 10.1080/13416979.2023.2283981.

[139] J. Klingberg et al. "Ozone risk for vegetation in the future climate of Europe based on stomatal ozone uptake calculations". In: *Tellus A* 63.1 (2011), pp. 174–187. DOI: 10.1111/j.1600-0870.2010.00465.x.

[140] IPCC. *Climate Change 2021 – The Physical Science Basis: Working Group I Contribution to the Sixth Assessment Report of the Intergovernmental Panel on Climate Change*. Cambridge University Press, 2023. DOI: 10.1017/9781009157896.

[141] R. K. Dixon et al. "Carbon Pools and Flux of Global Forest Ecosystems". In: *Science* 263.5144 (Jan. 14, 1994). Publisher: American Association for the Advancement of Science, pp. 185–190. DOI: 10.1126/science.263.5144.185.

[142] Elke Bergmann, Jürgen Bender, and Hans-Joachim Weigel. "Impact of tropospheric ozone on terrestrial biodiversity: A literature analysis to identify ozone sensitive taxa". In: *Journal of Applied Botany and Food Quality* 90 (Feb. 1, 2017), pp. 83–105. DOI: 10.5073/JABFQ.2017.090.012.

[143] H. Saxe. "Physiological responses of trees to ozone - interactions and mechanisms." In: *Current Topics in Plant Biology, Volume 3*. Publisher: Research Trends. 2002, pp. 27–55.

[144] J. G Isebrands et al. "Growth responses of *Populus tremuloides* clones to interacting elevated carbon dioxide and tropospheric ozone". In: *Environmental Pollution* 115.3 (Dec. 1, 2001), pp. 359–371. DOI: 10.1016/S0269-7491(01)00227-5.

[145] Kevin E. Percy et al. "Altered performance of forest pests under atmospheres enriched by CO2 and O3". In: *Nature* 420.6914 (Nov. 28, 2002), pp. 403–407. DOI: 10.1038/nature01028.

[146] Rainer Matyssek et al. "Forest Trees Under Air Pollution as a Factor of Climate Change". In: *Trees in a Changing Environment*. ISSN: 1572-5561. Springer, Dordrecht, 2014, pp. 117–163. DOI: 10.1007/978-94-017-9100-7_7.

[147] Hans Pretzsch et al. "Tree and stand growth of mature Norway spruce and European beech under long-term ozone fumigation". In: *Environmental Pollution*. Facing the Future: Evidence from Joint AspenFACE, SoyFACE and SFB 607 Meeting 158.4 (Apr. 1, 2010), pp. 1061–1070. DOI: 10.1016/j.envpol.2009.07.035.

[148] Sabine Braun, Christian Schindler, and Beat Rihm. "Growth losses in Swiss forests caused by ozone: Epidemiological data analysis of stem increment of *Fagus sylvatica* L. and *Picea abies* Karst." In: *Environmental Pollution* 192 (Sept. 1, 2014), pp. 129–138. DOI: 10.1016/j.envpol.2014.05.016.

[149] A. Augustaitis. "Intra-annual variation of stem circumference of tree species prevailing in hemi-boreal forest on hourly scale in relation to meteorology, solar radiation and surface ozone fluxes". In: *Atmosphere* 12.8 (2021). DOI: 10.3390/atmos12081017.

[150] Mitsutoshi Kitao et al. "Increased phytotoxic O3 dose accelerates autumn senescence in an O3-sensitive beech forest even under the present-level O3". In: *Scientific Reports* 6.1 (Sept. 7, 2016). Publisher: Nature Publishing Group, p. 32549. DOI: 10.1038/srep32549.

[151] Birgit Gielen et al. "Chronic ozone exposure affects leaf senescence of adult beech trees: a chlorophyll fluorescence approach". In: *Journal of Experimental Botany* 58.4 (Mar. 1, 2007), pp. 785–795. DOI: 10.1093/jxb/erl222.

[152] Àngela Ribas et al. "Ozone exposure induces the activation of leaf senescence-related processes and morphological and growth changes in seedlings of Mediterranean tree species". In: *Environmental Pollution* 134.2 (Mar. 1, 2005), pp. 291–300. DOI: 10.1016/j.envpol.2004.07.026.

[153] E. J. Pell et al. "Differential response of four tree species to ozone-induced acceleration of foliar senescence". In: *Plant, Cell & Environment* 22.7 (1999), pp. 779–790. DOI: 10.1046/j.1365-3040.1999.00449.x.

[154] Y. Bao, H. Tian, and X. Wang. "Effects of climate change and ozone on vegetation phenology on the Tibetan Plateau". In: *Science of the Total Environment* 932 (2024). DOI: 10.1016/j.scitotenv.2024.172780.

[155] Yijing Wang et al. "Responses of spring leaf phenological and functional traits of two urban tree species to air warming and/or elevated ozone". In: *Plant Physiology and Biochemistry* 179 (May 15, 2022), pp. 158–167. DOI: 10.1016/j.plaphy.2022.03.015.

[156] E. Paoletti. "Ozone impacts on forests." In: *CABI Reviews* 2007 (Apr. 9, 2008). Publisher: CABI, 13 pp. DOI: 10.1079/PAVSNNR20072068.

[157] Bin Wang et al. "Forests and ozone: productivity, carbon storage and feedbacks". In: *Scientific Reports* 6.1 (Feb. 22, 2016). Publisher: Nature Publishing Group, p. 22133. DOI: 10.1038/srep22133.

[158] H. Calvete-Sogo et al. "Heterogeneous responses to ozone and nitrogen alter the species composition of Mediterranean annual pastures". In: *Oecologia* 181.4 (Aug. 1, 2016), pp. 1055–1067. DOI: 10.1007/s00442-016-3628-z.

[159] Kerstin V. Wedlich et al. "Effects of ozone on species composition in an upland grassland". In: *Oecologia* 168.4 (Apr. 1, 2012), pp. 1137–1146. DOI: 10.1007/s00442-011-2154-2.

[160] Daniela Baldantoni, Massimo Fagnano, and Anna Alfani. "Tropospheric ozone effects on chemical composition and decomposition rate of *Quercus ilex* L. leaves". In: *Science of The Total Environment* 409.5 (Feb. 1, 2011), pp. 979–984. DOI: 10.1016/j.scitotenv.2010.11.022.

[161] Marcello Vitale et al. "Plant Species-Specific Litter Decomposition Rates Are Directly Affected by Tropospheric Ozone: Analysis of Trends and Modelling". In: *Water, Air, & Soil Pollution* 230.12 (Dec. 14, 2019), p. 311. DOI: 10.1007/s11270-019-4339-y.

[162] Evgenios Agathokleous et al. "Ozone affects plant, insect, and soil microbial communities: A threat to terrestrial ecosystems and biodiversity". In: *Science Advances* 6.33 (Aug. 1, 2020). Publisher: American Association for the Advancement of Science Section: Research Article, eabc1176. DOI: 10.1126/sciadv.abc1176.

[163] Noboru Masui et al. "Ozone disrupts the communication between plants and insects in urban and suburban areas: an updated insight on plant volatiles". In: *Journal of Forestry Research* 32.4 (Aug. 1, 2021), pp. 1337–1349. DOI: 10.1007/s11676-020-01287-4.

[164] J.M.W. Ryalls et al. "Anthropogenic air pollutants reduce insect-mediated pollination services". In: *Environmental Pollution* 297 (2022). DOI: 10.1016/j.envpol.2022.118847.

[165] Maxime Cailleret et al. "Ozone effects on European forest growth—Towards an integrative approach". In: *Journal of Ecology* 106.4 (2018), pp. 1377–1389. DOI: 10.1111/1365-2745.12941.

[166] Per Erik Karlsson et al. *Ozone causes substantial reductions in the carbon sequestration of managed European forests*. Dec. 16, 2024. DOI: 10.5194/egusphere-2024-3742.

[167] Silvano Fares et al. "Tropospheric ozone reduces carbon assimilation in trees: estimates from analysis of continuous flux measurements". In: *Global Change Biology* 19.8 (2013), pp. 2427–2443. DOI: 10.1111/gcb.12222.

[168] C. Proietti et al. "A multi-sites analysis on the ozone effects on Gross Primary Production of European forests". In: *Science of The Total Environment* 556 (June 2016), pp. 1–11. DOI: 10.1016/j.scitotenv.2016.02.187.

[169] Jürg Fuhrer et al. "Current and future ozone risks to global terrestrial biodiversity and ecosystem processes". In: *Ecology and Evolution* 6.24 (2016), pp. 8785–8799. DOI: 10.1002/ece3.2568.

[170] S. R. Arnold et al. "Simulated Global Climate Response to Tropospheric Ozone-Induced Changes in Plant Transpiration". In: *Geophysical Research Letters* 45.23 (Dec. 16, 2018), pp. 13070–13079. DOI: 10.1029/2018GL079938.

[171] Michael P. Perring et al. "Out of sight, Out of mind — but not Out of scope: the need to consider ozone (O3) in restoration science, policy, and practice". In: *Restoration Ecology* 30.7 (2022), e13622. DOI: 10.1111/rec.13622.

[172] *DIRECTIVE (EU) 2016/ 2284 OF THE EUROPEAN PARLIAMENT AND OF THE COUNCIL on the reduction of national emissions of certain atmospheric pollutants, amending Directive 2003/ 35/ EC and repealing Directive 2001/ 81/ EC*. 2016.

[173] *The National Emission Ceilings Regulations*. 2018.

[174] M. Schaub et al. *Part VIII: Monitoring of Ozone Injury.* UNECE ICP Forests Programme Co-ordinating Centre, Thünen Institute of Forest Ecosystems, 2016, pp. 1221–1226.

[175] Sarah Brace, David L. Peterson, and Darci. Bowers. *A guide to ozone injury in vascular plants of the Pacific Northwest.* PNW-GTR-446. Portland, OR: U.S. Department of Agriculture, Forest Service, Pacific Northwest Research Station, 1999, PNW–GTR–446. DOI: 10.2737/PNW-GTR-446.

[176] P. Sicard et al. « Dommages forestiers et pollution à l'ozone dans les réserves naturelles : le cas de l'arolle dans le sud-est de la France - ». In : *Forêt Méditerranéenne* XXXI.3 (2010), p. 273.

[177] Michael Treshow. "Ozone damage to plants". In: *Environmental Pollution (1970)* 1.2 (Oct. 1, 1970), pp. 155–161. DOI: 10.1016/0013-9327(70)90016-9.

[178] A Michel et al. *Forest Condition in Europe: The 2024 Assessment. ICP Forests Technical Report under the UNECE Convention on Long-range Transboundary Air Pollution (Air Convention).* 2024.

[179] Marco Ferretti et al. "The fingerprint of tropospheric ozone on broadleaved forest vegetation in Europe". In: *Ecological Indicators* 158 (Jan. 1, 2024), p. 111486. DOI: 10.1016/j.ecolind.2023.111486.

[180] F. Bussotti et al. "Assessment of ozone visible symptoms in the field: perspectives of quality control". In: *Environmental Pollution*. Native Plants as Bioindicators of Air Pollutants: Contributed Papers to a Symposium held in conjunction with the 34th Air Pollution Workshop 125.1 (Sept. 1, 2003), pp. 81–89. DOI: 10.1016/S0269-7491(03)00095-2.

[181] Filippo Bussotti, Alberto Cozzi, and Marco Ferretti. "Field Surveys of Ozone Symptoms on Spontaneous Vegetation. Limitations and Potentialities of the European Programme". In: *Environmental Monitoring and Assessment* 115.1 (Apr. 1, 2006). Company: Springer Distributor: Springer Institution: Springer Label: Springer Number: 1 Publisher: Kluwer Academic Publishers, pp. 335–348. DOI: 10.1007/s10661-006-6558-0.

[182] M Schaub et al. *Part VIII: Monitoring of Ozone Injury. Version 2020-1.* Eberswalde, Germany: Thünen Institute of Forest Ecosystems, 2020.

[183] Riccardo Marzuoli et al. "Assessing the Impact of Ozone on Forest Trees in An Integrative Perspective: Are Foliar Visible Symptoms Suitable Predictors for Growth Reduction? A Critical Review". In: *Forests* 10.12 (Dec. 2019). Number: 12 Publisher: Multidisciplinary Digital Publishing Institute, p. 1144. DOI: 10.3390/f10121144.

[184] William J. Manning et al. "Ethylenediurea (EDU): A research tool for assessment and verification of the effects of ground level ozone on plants under natural conditions". In: *Environmental Pollution* 159.12 (Dec. 1, 2011), pp. 3283–3293. DOI: 10.1016/j.envpol.2011.07.005.

[185] Evgenios Agathokleous, Mitsutoshi Kitao, and Takayoshi Koike. "Ethylenediurea (EDU) effects on hybrid larch saplings exposed to ambient or elevated ozone over three growing seasons". In: *Journal of Forestry Research* 33.1 (Feb. 2022), pp. 117–135. DOI: 10.1007/s11676-021-01352-6.

[186] G. Carriero et al. "Effects of long-term ambient ozone exposure on biomass and wood traits in poplar treated with ethylenediurea (EDU)". In: *Environmental Pollution* 206 (Nov. 1, 2015), pp. 575–581. DOI: 10.1016/j.envpol.2015.08.014.

[187] Andrea Vannini and Alessandro Petraglia. "Correction: Vannini, A.; Petraglia, A. Wood Distillate Mitigates Ozone-Induced Visible and Photosynthetic Plant Damage: Evidence from Ozone-Sensitive Tobacco (Nicotiana tabacum L.) BelW3. Horticulturae 2024, 10, 480". In: *Horticulturae* 10.12 (Dec. 2024). Number: 12 Publisher: Multidisciplinary Digital Publishing Institute, p. 1281. DOI: 10.3390/horticulturae10121281.

[188] Andrea Vannini et al. "Foliar Application of Wood Distillate Alleviates Ozone-Induced Damage in Lettuce (Lactuca sativa L.)" In: *Toxics* 10.4 (Apr. 5, 2022), p. 178. DOI: 10.3390/toxics10040178.

[189] William J Manning. "The use of plants as bioindicators of ozone". In: *Proceedings of the International Symposium on Air Pollution and Climate Change Effects on Forest Ecosystems* (1998), p. 19.

[190] Allen S. Heagle et al. "Response of a white clover indicator system to tropospheric ozone at eight locations in the United States". In: *Water, Air, and Soil Pollution* 85.3 (Dec. 1, 1995). Company: Springer Distributor: Springer Institution: Springer Label: Springer Number: 3 Publisher: Kluwer Academic Publishers, pp. 1373–1378. DOI: 10.1007/BF00477173.

[191] Carla Zuliani Sandrin et al. "Ozone Biomonitoring with White Clover Clones: The First Experience in Brazil". In: *CLEAN – Soil, Air, Water* 46.12 (2018), p. 1800377. DOI: 10.1002/clen.201800377.

[192] John W. Coulston, Gretchen C. Smith, and William D. Smith. "Regional Assessment of Ozone Sensitive Tree Species Using Bioindicator Plants". In: *Environmental Monitoring and Assessment* 83.2 (Apr. 1, 2003). Company: Springer Distributor: Springer Institution: Springer Label: Springer Number: 2 Publisher: Kluwer Academic Publishers, pp. 113–127. DOI: 10.1023/A:1022578506736.

[193] Sreekala G. Bajwa, John C. Rupe, and Johnny Mason. "Soybean Disease Monitoring with Leaf Reflectance". In: *Remote Sensing* 9.2 (Feb. 2017). Number: 2 Publisher: Multidisciplinary Digital Publishing Institute, p. 127. DOI: 10.3390/rs9020127.

[194] Micol Rossini et al. “High resolution field spectroscopy measurements for estimating gross ecosystem production in a rice field”. In: *Agricultural and Forest Meteorology* 150.9 (Aug. 15, 2010), pp. 1283–1296. DOI: 10.1016/j.agrformet.2010.05.011.

[195] G. Masaitis, G. Mozgeris, and A. Augustaitis. “Spectral reflectance properties of healthy and stressed coniferous trees”. In: *iForest - Biogeosciences and Forestry* 6.1 (2013). Publisher: SISEF - Italian Society of Silviculture and Forest Ecology Section: Remote Sensing and Information System, p. 30. DOI: 10.3832/ifor0709-006.

[196] Debra Werner. *Planet shares information on Tanager hyperspectral constellation.* SpaceNews. Sept. 19, 2022. URL: https://spacenews.com/planet-hyperspectral-details/ (visited on 03/29/2025).

[197] V. C. Runeckles and H. M. Resh. “The assessment of chronic ozone injury to leaves by reflectance spectrophotometry”. In: *Atmospheric Environment (1967)* 9.4 (Apr. 1, 1975), pp. 447–452. DOI: 10.1016/0004-6981(75)90131-6.

[198] William W Cure. “Canopy Reflectance of Soybean as Affected by Chronic Doses of Ozone in Open-Top Field Chambers”. In: (1988).

[199] Schutt J, Rowland R, and Heggestad H. “Identification of injury resulting from atmospheric pollutants using reflectance measurements [Tomatoes, sulfur dioxide].” In: *Journal of Environmental Quality* 13 (1984).

[200] Martin Kraft et al. “Reflectance Measurements of Leaves for Detecting Visible and Non-visible Ozone Damage to Crops”. In: *Journal of Plant Physiology* 148.1 (Jan. 1, 1996), pp. 148–154. DOI: 10.1016/S0176-1617(96)80307-5.

[201] E. Leblanc, C.S.T. Daughtry, and C.L. Mulchi. “Remote sensing of crop responses to ozone and carbon dioxide treatments”. In: *IGARSS ’96. 1996 International Geoscience and Remote Sensing Symposium* 1 (1996). Conference Name: IGARSS ’96. 1996 International Geoscience and Remote Sensing Symposium ISBN: 9780780330689 Place: Lincoln, NE, USA Publisher: IEEE, pp. 224–226. DOI: 10.1109/IGARSS.1996.516298.

[202] Bernardo FT Rudorff et al. “Growth, radiation use efficiency, and canopy reflectance of wheat and corn grown under elevated ozone and carbon dioxide atmospheres”. In: *Remote sensing of Environment* 55.2 (1996). Publisher: Elsevier, pp. 163–173.

[203] J. H. Williams and T. W. Ashenden. “Differences in the spectral characteristics of white clover exposed to gaseous pollutants and acid mist”. In: *New Phytologist* 120.1 (1992), pp. 69–75. DOI: 10.1111/j.1469-8137.1992.tb01059.x.

[204] Walter E. Westman and Curtis V. Price. “Spectral changes in conifers subjected to air pollution and water stress: Experimental studies”. In: *IEEE Transactions on Geoscience and Remote Sensing* 26 (Jan. 1, 1988). NTRS Author Affiliations: NASA Ames Research Center, USGS, Water Resources Div., Trenton NTRS Report/Patent Number: ISSN: 0196-2892 NTRS Document ID: 19880037705 NTRS Research Center: Legacy CDMS (CDMS).

[205] B. Curtiss and S.L. Ustin. "Parameters Affecting Reflectance Of Coniferous Forests In The Region Of Chlorophyll Pigment Absorption". In: *12th Canadian Symposium on Remote Sensing Geoscience and Remote Sensing Symposium,* 12th Canadian Symposium on Remote Sensing Geoscience and Remote Sensing Symposium, vol. 4. July 1989, pp. 2633–2636. DOI: 10.1109/IGARSS.1989.577951.

[206] Susan L. Ustin and Brian Curtiss. "Spectral characteristics of ozone-treated conifers". In: *Environmental and Experimental Botany* 30.3 (July 1, 1990), pp. 293–308. DOI: 10.1016/0098-8472(90)90041-2.

[207] C. I. Essery and A. P. Morse. "The impact of ozone and acid mist on the spectral reflectance of young Norway spruce trees". In: *International Journal of Remote Sensing* 13.16 (Nov. 1, 1992), pp. 3045–3054. DOI: 10.1080/01431169208904101.

[208] Gregory A. Carter et al. "Response of Leaf Spectral Reflectance in Loblolly Pine to Increased Atmospheric Ozone and Precipitation Acidity". In: *Journal of Experimental Botany* 43 (Jan. 1, 1992). ADS Bibcode: 1992JEBot..43..577C, pp. 577–584. DOI: 10.1093/jxb/43.4.577.

[209] Outi Meinander et al. "Scots Pines after Exposure to Elevated Ozone and Carbon Dioxide Probed by Reflectance Spectra and Chlorophyll *a* Fluorescence Transients". In: *Journal of Plant Physiology* 148.1 (Jan. 1, 1996), pp. 229–236. DOI: 10.1016/S0176-1617(96)80319-1.

[210] Michele Meroni et al. "Using optical remote sensing techniques to track the development of ozone-induced stress". In: *Environmental Pollution.* Special Issue Section: Ozone and Mediterranean Ecology: Plants, People, Problems 157.5 (May 1, 2009), pp. 1413–1420. DOI: 10.1016/j.envpol.2008.09.018.

[211] M Meroni et al. "Assessing Steady-state Fluorescence and PRI from Hyperspectral Proximal Sensing as Early Indicators of Plant Stress: The Case of Ozone Exposure". In: *Sensors* 8.3 (Jan. 2008). Number: 3 Publisher: Molecular Diversity Preservation International, pp. 1740–1754. DOI: 10.3390/s8031740.

[212] M Meroni et al. "Leaf level early assessment of ozone injuries by passive fluorescence and photochemical reflectance index". In: *International Journal of Remote Sensing* 29.17 (Mar. 2008), pp. 5409–5422. DOI: 10.1080/01431160802036292.

[213] J. A. Gamon, L. Serrano, and J. S. Surfus. "The photochemical reflectance index: an optical indicator of photosynthetic radiation use efficiency across species, functional types, and nutrient levels". In: *Oecologia* 112.4 (Nov. 1, 1997), pp. 492–501. DOI: 10.1007/s004420050337.

[214] Filippo Bussotti et al. "Ozone stress in woody plants assessed with chlorophyll a fluorescence. A critical reassessment of existing data". In: *Environmental and Experimental Botany.* Chlorophyll Fluorescence: from Theory to (Good) Practice 73 (Nov. 1, 2011), pp. 19–30. DOI: 10.1016/j.envexpbot.2010.10.022.

[215] Marchica et al. "Early Detection of Sage (Salvia officinalis L.) Responses to Ozone Using Reflectance Spectroscopy". In: *Plants* 8.9 (Sept. 12, 2019), p. 346. DOI: 10.3390/plants8090346.

[216] Antonella Calzone et al. "Oxidative stress assessment by a spectroscopic approach in pomegranate plants under a gradient of ozone concentrations". In: *Environmental and Experimental Botany* 182 (Feb. 2021), p. 104309. DOI: 10.1016/j.envexpbot.2020.104309.

[217] Nichole Gosselin et al. "Using Visual Ozone Damage Scores and Spectroscopy to Quantify Soybean Responses to Background Ozone". In: *Remote Sensing* 12.1 (Jan. 2020). Number: 1 Publisher: Multidisciplinary Digital Publishing Institute, p. 93. DOI: 10.3390/rs12010093.

[218] Jeremy E. Diem. "Remote Assessment of Forest Health in Southern Arizona, USA: Evidence for Ozone-Induced Foliar Injury". In: *Environmental Management* 29.3 (Mar. 1, 2002), pp. 373–384. DOI: 10.1007/s00267-001-0011-5.

[219] Shawn C Kefauver. "Using topographic and remotely sensed variables to assess ozone injury to conifers in the Sierra Nevada (USA) and Catalonia (Spain)". In: *Remote Sensing of Environment* (2013), p. 11.

[220] Timothy Wade et al. "Distribution and Causes of Global Forest Fragmentation". In: *Conservation Ecology* 7.2 (Sept. 4, 2003). Publisher: The Resilience Alliance. DOI: 10.5751/ES-00530-070207.

[221] World Resources Institute. *Global Forest Review, 2024*. Washington DC: World Resources Institute, Apr. 4, 2024.

[222] Martin Thurner et al. "Carbon stock and density of northern boreal and temperate forests". In: *Global Ecology and Biogeography* 23.3 (2014), pp. 297–310. DOI: 10.1111/geb.12125.

[223] Hendrik Poorter et al. "Causes and consequences of variation in leaf mass per area (LMA): a meta-analysis". In: *New Phytologist* 182.3 (2009), pp. 565–588. DOI: 10.1111/j.1469-8137.2009.02830.x.

[224] W. J. Bond. "The tortoise and the hare: ecology of angiosperm dominance and gymnosperm persistence". In: *Biological Journal of the Linnean Society* 36.3 (1989), pp. 227–249. DOI: 10.1111/j.1095-8312.1989.tb00492.x.

.

2

Reflections of stress: Ozone damage in broadleaf saplings can be identified from hyperspectral leaf reflectance.

Contents

2.1 Commentary 42
2.2 Manuscript 43
2.2.1 Abstract 45
2.2.2 Introduction 46
2.2.3 Material and Methods 48
2.2.4 Results 53
2.2.5 Discussion 71
2.2.6 Conclusions 75
2.2.7 Acknowledgements 75
2.2.8 CRediT authorship contribution statement 75
References 76

2.1 Commentary

The following paper was published in Environmental Research (issue 360, November 2024). In this study I utilised a controlled experimental set up to investigate the effect of O_3 exposure on the leaf reflectance of broadleaf saplings, across a range of O_3 concentrations. I took a significant amount of other physiological and

biochemical measurements alongside leaf reflectance, but these were not included in the published manuscript for brevity. The majority of these additional investigations yielded null results, and are presented in full in Appendix B.

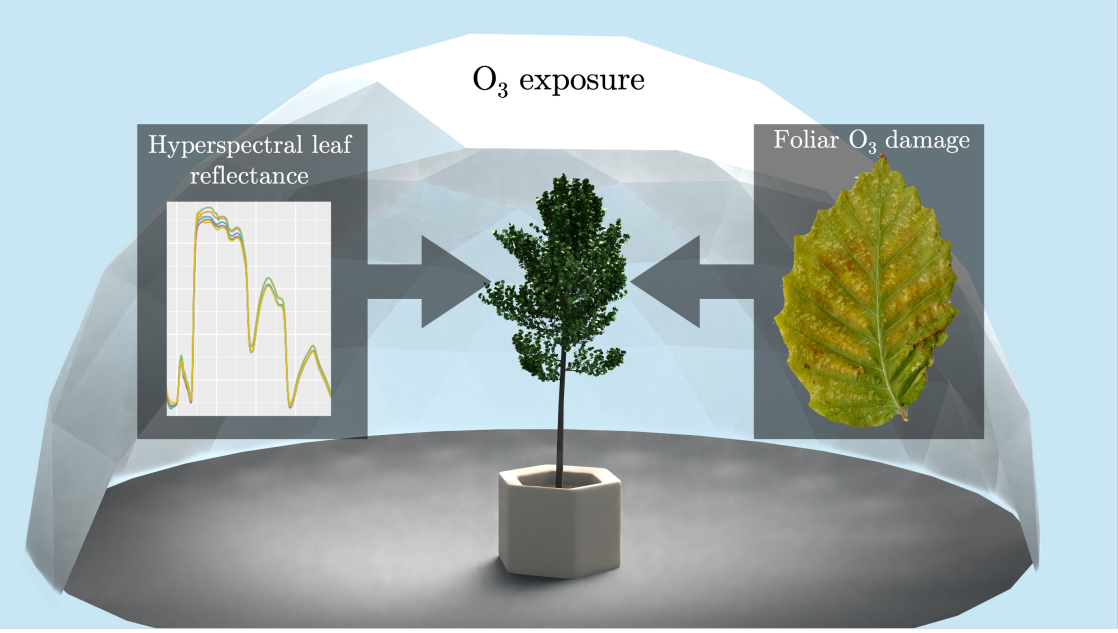


Figure 2.1: Graphical abstract depicting the O_3 exposure experiment.

2.2 Manuscript

Reflections of stress: Ozone damage in broadleaf saplings can be identified from hyperspectral leaf reflectance

Anna Lee Jones[a], Adam Ormondroyd[b], Felicity Hayes[c,d], Elizabeth S. Jeffers[a,d]

[a]*Department of Biology, University of Oxford, South Parks Road, Oxford, UK*
[b]*Kavli Institute for Cosmology, University of Cambridge, Madingley Road, Cambridge, UK*

2. Reflections of stress: Ozone damage in broadleaf saplings can be identified from hyperspectral leaf reflectance. *44*

[c] *UK Centre for Ecology & Hydrology, Environment Centre Wales, Deiniol Road, Bangor, UK*
[d] *Joint senior authors*

Environmental Pollution Volume 360, 1 November 2024, 124642

2.2.1 Abstract

Tropospheric ozone (O_3) causes widespread damage to vegetation; however, monitoring of O_3 induced damage is often reliant on manual leaf inspection. Reflectance spectroscopy of vegetation can identify and detect unique spectral signatures of different abiotic and biotic stressors. In this study, we tested the use of hyperspectral leaf reflectance to detect O_3 stress in alder, beech, birch, crab apple, and oak saplings exposed to five long-term O_3 regimes (ranging from daily target maxima of 30 ppb O_3 to 110 ppb). Hyperspectral reflectance varied significantly between O_3 treatments, both in whole spectra analysis and when simplified to representative components. O_3 damage had a multivariate impact on leaf reflectance, underpinned by changes in pigment balance, water content and structural composition. Vegetation indices derived from reflectance which characterised the visible green peak were able to differentiate between O_3 treatments. Iterative normalised difference spectral indices across the hyperspectral wavelength range were correlated to visual damage scores to identify significant wavelengths for O_3 damage detection. We propose a new Ozone Damage Index (OzDI), which characterises the reflectance peak in the short-wave infrared region and outperformed existing vegetation indices in terms of correlation to O_3 treatment. These results demonstrate the potential application of hyperspectral reflectance as a high throughput method of O_3 damage detection in a range of common broadleaf species.

Keywords: Tropospheric ozone, Reflectance spectroscopy, Forest monitoring, Temperate forest, Air pollution, Vegetation index.

2.2.2 Introduction

At ground level, O_3 is a highly oxidising pollutant which is toxic to both plant [1] and animal life [2], and is a potent greenhouse gas [3]. Tropospheric O_3 is formed by photocatalysis of a free radical mechanism between nitrous oxides (NO_x), hydrocarbons, and volatile organic compounds (VOCs) [4].

Tropospheric O_3 pollution has increased globally since 1950s [5], and although O_3 precursor emissions have plateaued in Europe and North America since the 1990s resulting in a decrease in extreme O_3 events, long-range transport of anthropogenic O_3 precursors continues to raise European baselines [6]. Background tropospheric O_3 concentrations are predicted to continue to rise in the northern hemisphere until at least the end of the century. O_3 induced injury is widespread in European vegetation, including crops [7] and trees [8].

O_3 uptake causes oxidative damage to plants by the oxidation of lipids, peptides, and nucleic acids through the induction of reactive oxygen species (ROS) [9]. ROS alter rubisco activity and content [10], leading to photoinhibition. Stomatal conductance is reduced in response to O_3 which limits transpiration and CO_2 uptake [11]. O_3 can be detoxified within the plant by antioxidising compounds such as superoxide dismutase and peroxidases [12].

Foliar O_3 damage includes stippling, chlorosis and necrosis [13], and can be visually differentiated from other biotic and abiotic stressors in broadleaf trees by the size, shape, and location of the damage [14, 15]. Stippling occurs on the upper leaf surface between veins as dots of brown to black pigmentation. Chlorosis is a loss of chlorophyll and appears in discrete patches known as mottles. Small discrete areas of dead tissue in the palisade mesophyll, known as fleck, also occur.

O_3 stressed vegetation shows decreased primary productivity [16], which limits the ability of vegetation to produce biomass and sequester carbon. Models based on experimental data estimate the reduction in the gross primary productivity (GPP) of European forests due to O_3 stress from 2000 to 2010 range between 0.4% and 30% [17]. Verification of the extent and location of O_3 damage to forest landscapes would be required to confirm the reduction of GPP attributable to

O_3 exposure. Furthermore, the impact of long-term or variable O_3 exposure on ecosystem productivity is complex to predict due to the interacting effects of O_3 stress with temperature, carbon dioxide (CO_2), water, and nitrogen availability.

Visible foliar O_3 injury is variable between species and requires experienced human identification to differentiate it from other stressors, and crown defoliation is not specific to O_3 stress [14]. Full assessment of foliar O_3 damage also requires access to the upper crown exposed to the sun [18]. A versatile and efficient method of measuring O_3 damage to trees would allow more widespread monitoring of the impacts of O_3 and justify responses in terms of precursor emissions control and species selection for O_3 exposed sites.

Vegetation spectroscopy uses the light reflectance or fluorescence of living vegetation to assess plant health at a variety of spatial scales. The high-throughput nature of spectroscopy allows rapid and non-destructive monitoring of plant health, including remote monitoring of large or inaccessible areas when spectroscopic instruments are mounted on unmanned aerial vehicles, aircraft, or satellites. Field spectroscopy, taken at the single plant or leaf level provides a higher signal-to-noise ratio measurement than remote spectroscopy but is still comparable to satellite-derived spectral signatures, and can be correlated to physiological and biochemical measurements taken in situ. Field spectroscopy, therefore, bridges the spatial gap between leaf-level measurements of productivity and ecosystem measurements of plant health derived from satellite data.

Symptoms of acute O_3 exposure such as visible foliar injury have been successfully detected using vegetation indices in some O_3 sensitive species [19, 20]. Reflectance spectroscopy has detected O_3 stress in leaves before injury is visible for several sensitive species such as white clover [21], soybean [22, 23], pomegranate [24], and sage [25]. Similar techniques have been applied to a few tree species, such as the study by Gäb et al. on *Fagus sylvatica* (common beech), which used near-infrared (NIR) spectroscopy to successfully predict the concentration of O_3 treatment during one growth season [26].

Spectroscopic detection of O_3 damage has not been trialled in temperate broadleaf tree species beyond common beech. Most trials have also focused on acute O_3 exposure in the range of 200 ppb for relatively short periods (24 hours to one month) [24, 25, 27]. Chronic O_3 exposure (such as 60 ppb during daylight hours for several weeks) is more commonly experienced by broadleaf forests and is predicted to increase over the next century [28]. Considering this, detecting damage to vegetation exposed realistic long-term O_3 concentrations is most relevant to the management of terrestrial carbon stocks.

This study aimed to characterise the reflectance profile of O_3 damage in a range of temperate broadleaf species under controlled conditions. We set out to test whether hyperspectral reflectance measurements could differentiate between saplings exposed to different O_3 regimes. Based on the successful detection of acute O_3 damage by reflectance spectroscopy in sensitive crops, we predicted clear differences in the spectral signatures of saplings exposed to ambient versus elevated O_3. The high resolution of hyperspectral leaf reflectance also has the potential to differentiate more finely between intermediate O_3 concentrations. Different tree species show varying degrees of O_3 sensitivity [29] and so we also expected species specific responses to be visible in the reflectance signature of O_3 stress. We chose a mixture of temperate species common to broadleaf forests, reforestation, and hedge planting initiatives, which are reported to have varying tolerance to O_3 [30]. A nitrogen fixing species, alder, was included based on evidence that nitrogen-fixing symbioses offer some resistance to O_3 stress [29]. In the context of reforestation initiatives, O_3 damage detection in cell grown saplings is particularly pertinent.

2.2.3 Material and Methods

Plant Materials

On April 4, 2022, twenty cell-grown, two-year-old alder *Alnus cordata*, birch *Betula pendula*, crab apple *Malus sylvestris*, oak *Quercus robur*, beech *Fagus sylvatica* saplings (Cheviot Trees Ltd, UK) were potted into 6.5 l tubs containing a 3 : 1 ratio by volume of peat-free Nursery Stock compost (Sinclair, UK) and John Innes

No.2 (J. Arthur Bowers, UK). Saplings were kept outside for four weeks at the Air Pollution Facility to establish before O_3 treatment began. Saplings were irrigated by hand three times weekly with additional watering on days of hot weather. On June 2, 2022, the saplings were stratified into three height categories by species. From these groups, the saplings were randomly distributed between five O_3 treatments at ambient temperature. The saplings were exposed to experimental conditions in the solardomes from June 2, 2022 until October 14, 2022.

Treatments

This experiment took place at the UK Center for Ecology & Hydrology's air pollution facility at Abergwyngregyn, North Wales (53.2°N, 4.0°W). O_3 was delivered in solardomes, dome-shaped glasshouses of 3 m diameter and 2.1 m height as described previously [29].

The solardomes were ventilated at two air changes per minute with charcoal filtered air to which O_3 was added to give the desired concentration. O_3 was generated using concentrated oxygen (PT20 O_3 generator, Ozone Industries, and AirSep NewLife Intensity 10L Oxygen Concentrator, CAIRE Inc. USA). O_3 delivery was controlled by LabVIEW software (version 2015, National Instruments, USA). O_3 concentrations within the solardomes were measured every 30 min (for 5 min) using two O_3 analysers (49i Thermo Fisher Scientific, USA) of matched calibration. Air temperature, relative humidity, and light were also monitored inside the solardomes (Skye Instruments, UK).

The solardomes' weekly O_3 profiles were based on data from a UK upland O_3 episode as previously described [29], and target concentrations were increases above and below this profile. The weekly O_3 profile featured five consecutive "high" O_3 days where the O_3 concentration was raised from 20 ppb overnight to the target maximum from 10:00–18:00, followed by two "low" O_3 days where concentration for all domes peaked at 30 ppb. This profile better replicates the dynamics of real O_3 episodes than a constant elevated exposure regime and has been used for many successful O_3 exposure experiments [31–33]. The target peaks of the five solardomes

were 30 ppb, 50 ppb, 65 ppb, 80 ppb, and 110 ppb. The seasonal averages of the O_3 concentration per treatment dome are summarised in Table 2.1.

O_3 Treatment	Seasonal O_3 24h average (ppb)	Daytime O_3 average (ppb)	Daytime Average AOT40 (ppb)	Sapling species	Number of replicates per species
OZ1, lowest O_3	23.29	25.76	0	Oak, beech, crab apple, alder, birch	3, 3, 5, 5, 5 (respectively)
OZ2, low O_3	32.97	39.16	5.37	Oak, beech, crab apple, alder, birch	3, 3, 5, 5, 5 (respectively)
OZ3, medium O_3	36.65	47.97	12.11	Oak, beech, crab apple, alder, birch	3, 3, 5, 5, 5 (respectively)
OZ4, high O_3	38.16	56.31	21.68	Oak, beech, crab apple, alder, birch	3, 3, 5, 5, 5 (respectively)
OZ5, highest O_3	45.87	66.63	31.53	Oak, beech, crab apple, alder, birch	3, 3, 5, 5, 5 (respectively)

Table 2.1: Average O_3 concentrations, test species and number of replicates per solardome. Daytime is defined as 10:00–18:00.

Plant Measurements

Growth After one month of O_3 treatment and again after four months, the height and diameter of the basal stem were measured for all saplings. The relative difference in height and basal stem diameter between months one and four was calculated as a percentage growth over the treatment period. Alder, birch, and crab apple saplings were measured again in August 2023 after wintering outside under ambient conditions.

O_3 Damage Score The extent of visible foliar O_3 damage to saplings each month was determined according to the following simple damage score devised to be time efficient and applicable to all test species. Damage score 1, healthy green leaves with no visible O_3 damage. Damage score 2, interveinal stippling or mottles on less than half of the leaves, by area or percentage of affected leaves. Damage score 3,

stippling or mottles on half or more of the leaves, by area or percentage of affected leaves. Damage score 4, stippling or mottles present and flecks covering less than half the leaves, by area or percentage of leaves affected. Damage score 5, stippling or mottles present and flecks of over half the leaves, by area or percentage of leaves affected. Images exemplifying each damage score are included in Appendix B, Table B.1. Mean damage score for each species and treatment per month was calculated. Any other notable observations about sapling health were also recorded monthly.

Leaf spectroscopy

Reflectance spectra of the adaxial leaf surface from 350 nm to 2500 nm were collected using an HR-1024i with leaf clip, Spectra Vista Corp, USA including an active light source. The HR-1024i spectrometer consisted of three dispersion grating spectrometers with overlapping wavelength ranges:
VNIR, 1.5 nm sampling interval, 350 nm to 1000 nm range; SWIR1, 3.8 nm sampling interval, 1000 nm to 1890 nm range; SWIR2, 2.5 nm sampling interval, 1890 nm to 2500 nm range.

The spectrometer was referenced using the incorporated leaf clip reflective standard every 5 minutes during measurements. Dark signal baseline correction was applied by the HR-1024i automatically, a dark spectrum was taken before each reflectance measurement. Once per month during O_3 treatment, reflectance spectra were taken from three leaves from three replicates of each species per O_3 treatment. The three leaves were chosen as one from each third of the vertical span of the sapling's leaf cover.

Spectral analysis Reflectance spectra were imported and processed as a spectral library in Python 3 using the SpecDAL package [34, 35]. The overlapping regions of the three component spectrometers in the HR-1024i were stitched. Reflectance measurements were interpolated to correspond to 1 nm interval wavelengths. The absolute reflectance was derived by multiplying the relative reflectance by the known reflectance of the reference panel.

Further processing of the spectral library was carried out in R using the hyperSpec package [36]. An average reflectance spectrum was calculated for each species, month and O_3 treatment.

Permutational multivariate analysis of variance (PERMANOVA) was performed using the vegan R package [37] as a non-parametric geometric partitioning of variance to test the contributions of species, O_3 treatment and length of exposure as explanatory factors of spectral variation. The Bray method was used to calculate pairwise distances from the spectral matrix and 999 permutations were used.

Principal component analysis (PCA) was used to visualise the key regions of variability within the hyperspectral library by dimensionality reduction. PCA was applied to the entire range of wavelengths measured 350 nm to 2500 nm. Principal components of the spectral library were calculated for each O_3 treatment and species.

Partial least squares discriminant analysis (PLS-DA) was used as an extension of PCA to build classification models based on principal components. We built a PLS-DA model which predicted the O_3 treatment leaves had been exposed to based on their hyperspectral reflectance spectra (350 nm to 2500 nm). PLS-DA was used due to the ordinal nature of the O_3 treatments in this experiment. PLS-DA was used built using the mdatools R package [38]. For each species, the optimum number of principal components was assessed to maximise the model's accuracy. A randomly selected 70% of the spectral library was used to calibrate the model and the remaining 30% used to cross validate it.

Vegetation Indices A range of vegetation indices which correlate to plant health and stress were calculated from leaf reflectance data and assessed for their ability to distinguish between O_3 treatments. Full equations for all vegetation indices calculated can be found in Appendix B, Table B.2.

Normalised Difference Spectral Indices To identify the spectral wavelengths that could best indicate O_3 damage, normalised difference spectral indices (NDSI)

analysis was used. NDSI is defined as:

$$NDSI\,(i,j) = \frac{R_i - R_j}{R_i + R_j} \tag{2.1}$$

where Ri is the absolute reflectance of wavelength i and subscripts are wavelengths in nm. All possible combinations of wavelengths (i and j) were used to calculate all NDSI for each plant species, month and treatment. The linear relationships between the average O_3 damage score and NDSIs per species, month and treatment were examined. A heat map of the absolute value of the Pearson correlation coefficient r between O_3 damage score and NDSI was generated using data collected throughout the growing season. The heat maps were produced using Python 3 packages: correlation arrays were created using NumPy, and plotted with matplotlib [39, 40].

Statistical Analyses Statistical analysis of the results of sapling growth and vegetation indices derived from reflectance data, were carried out in R using the inbuilt Stats package and mdatools. Non-parametric tests were used where data failed to pass normality and homogeneity of variance testing, as detailed in results.

2.2.4 Results

Plant Measurements

Growth O_3 treatment did not significantly affect the percentage growth of saplings between June and October 2022, as tested with the Kruskal-Wallis chi-square test ($\chi^2 = 9.5791$, d.o.f. = 6, $P = 0.144$), Appendix B Figure B.1. The interaction between species and O_3 treatment was also not significant ($F = 3.2419$, d.o.f. = 22, $P = 0.344$).

Alder, birch, and crab apple saplings were overwintered in ambient conditions (October 2022 - May 2023) and then returned to their previous ozone treatment domes for a further growth season. O_3 treatment had a significant effect on change in height between October 2022 and August 2023 (ANOVA, $F(2, 42) = 5.21$, $P < 0.01$) (Appendix B, Figure B.2). Post hoc analysis using the Tukey HSD test indicates that saplings exposed to high O_3 treatment (OZ5) grew significantly less between

October 2022 and August 2023 (mean = 1.47, std. dev. = 5.41) than saplings in either the intermediate (mean = 8.56, std. dev. = 7.59) or low (mean = 8.31, std. dev. = 7.28) O_3 treatments.

O_3 Damage Score The O_3 induced damage scores of saplings increased with elevated O_3 treatment (Figure 2.2). Ordinal logistic regression between average O_3 damage score and O_3 treatment showed that for each unit increase in average damage score, the odds ratio of the sapling being exposed to high O_3 treatment increased on average by 12.94 ($P = 8.34\times10^{-5}$). Furthermore, McFadden's pseudo-R^2 value for this model was estimated to be 0.403, thereby indicating a robust positive correlation between O_3 damage score and the concentration of O_3 treatment.

When separated by species, all species except crab apple show increasing O_3 damage scores under higher O_3 treatments. Crab apple saplings showed a more mixed pattern, although damage free saplings (score 1) were only found in the lower O_3 treatments.

When separated by species, all species except crab apple show increasing O_3 damage scores under higher O_3 treatments. Crab apple saplings showed a more mixed pattern, although damage free saplings (score 1) were only found in the lower O_3 treatments.

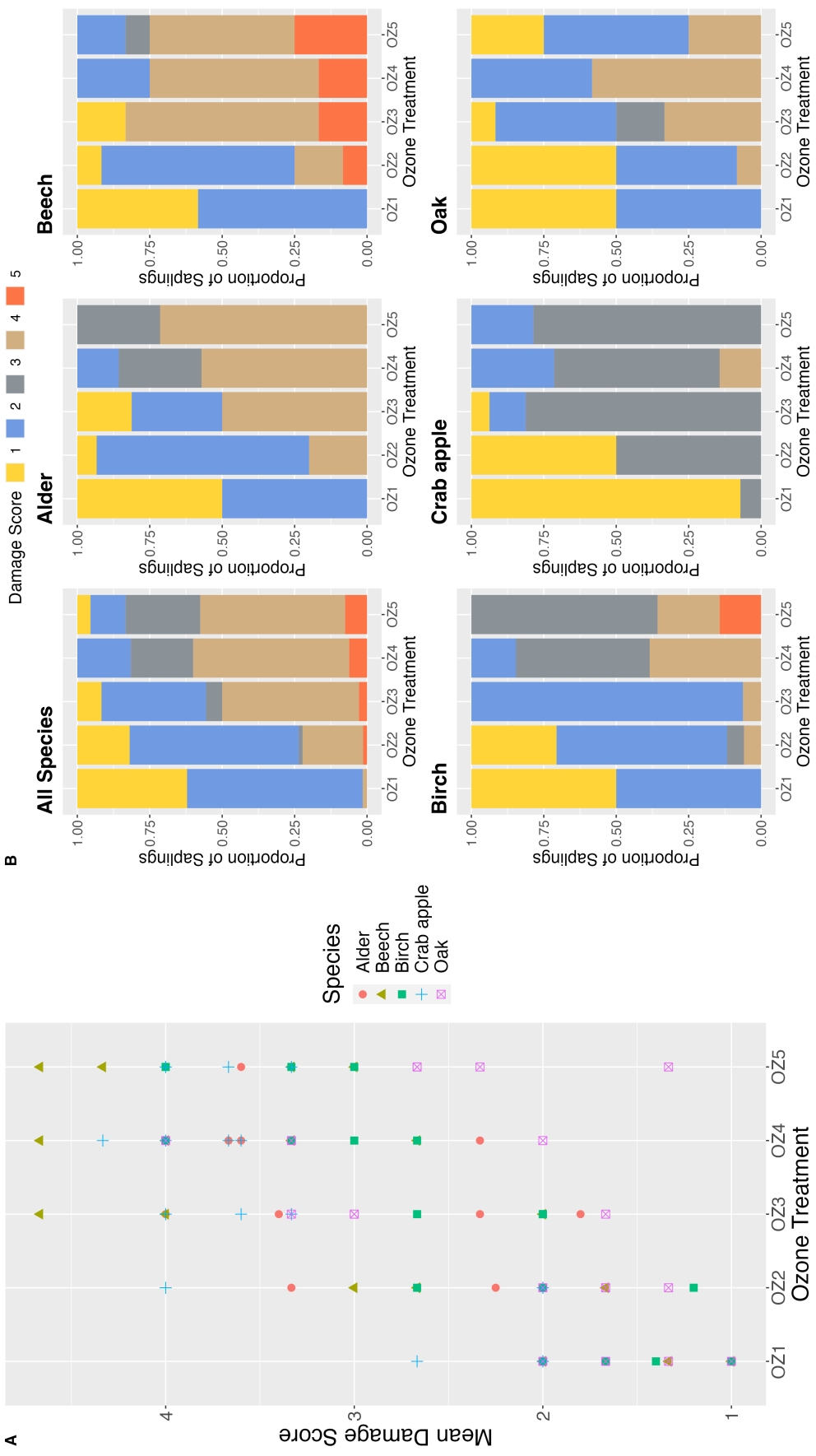


Figure 2.2: O_3 damage to saplings following exposure to O_3 with A) Mean O_3 damage score and B) proportion of saplings in each damage category.

Leaf Spectroscopy

For each species, leaf clip reflectance spectroscopy showed clear differences between the spectra of saplings grown in different O_3 treatments (Figure 2.3). Key regions of differentiation between O_3 treatments included the green peak in the visible range (~540 nm); the NIR region (800 nm to 1500 nm); the water absorption bands at 1440 nm and 1900 nm; and the infrared peak at 2220 nm. In July in the highest O_3 treatment, reflectance spectra feature an absorption peak at 750 nm caused by chlorophyll fluorescence.

In the visible light region of the spectra, the trough in reflectance between 400 nm to 500 nm caused by absorbance of blue/violet light by chlorophyll-A is shallower in saplings exposed to high O_3 concentrations. When all species are averaged, the reflectance trough is deepest in saplings exposed to ambient O_3 (OZ1) and shallowest in saplings exposed to the highest O_3 treatment (OZ5), indicating lower chlorophyll.

The green reflectance peak at 550 nm attributed to chlorophyll, and is reduced in saplings exposed to the highest O_3 concentration (OZ5) compared to ambient conditions (OZ1) when all species are averaged. At the species level, beech, birch, and crab apple saplings all show a reduced green peak when exposed to high O_3 concentration. However, alder and oak saplings had increased green peak reflectance under high O_3 conditions.

The reflective region in the NIR characterised by three broad peaks between 750 nm to 1400 nm is attributed to cell structure. High O_3 exposure reduced the NIR reflectance of saplings. This was particularly marked in alder, beech, and birch saplings. In all species except birch, saplings exposed to intermediate O_3 (OZ3) had the highest NIR reflectance.

The water absorption bands at 1440 nm and 1900 nm were slightly reduced in saplings exposed to higher O_3 concentrations. This was most marked in crab apple and beech. In all species, saplings exposed to intermediate O_3 concentration (OZ3) had increased reflectance between 1440 nm and 1900 nm.

The SWIR reflectance peak at 2220 nm is associated with cellulose, sugar, and starch content of the leaf [41]. In beech, crab apple, and birch saplings this

reflectance peak was reduced under high O_3 exposure (OZ5) compared to ambient exposure (OZ1). Conversely, in alder and oak the 2220 nm reflectance peak was slightly higher in saplings exposed to the highest O_3 concentration (OZ5) than those exposed to ambient concentration (OZ1). In all species except birch, saplings exposed to intermediate O_3 concentration (OZ3) had a higher 2220 nm reflectance peak than saplings exposed to ambient (OZ1) or high O_3 (OZ5).

Two-way permutation analysis of variance showed that the effect of species, O_3 treatment (and the interaction between the two) were significant on the reflectance spectra of sapling leaves (Appendix B, Table B.3). When each month's spectra were analysed separately, O_3 treatment had a significant effect on leaf reflectance in every month of measurement (July, August, September $P < 0.001$, October $P = 0.014$).

Inclusion of the month of measurement showed a highly significant effect on the reflectance spectra of sapling leaves ($P < 0.001$). O_3 treatment and month of measurement had a significant interactive effect ($P < 0.001$). The interaction between species, O_3 treatment, and month was also significant ($P = 0.040$).

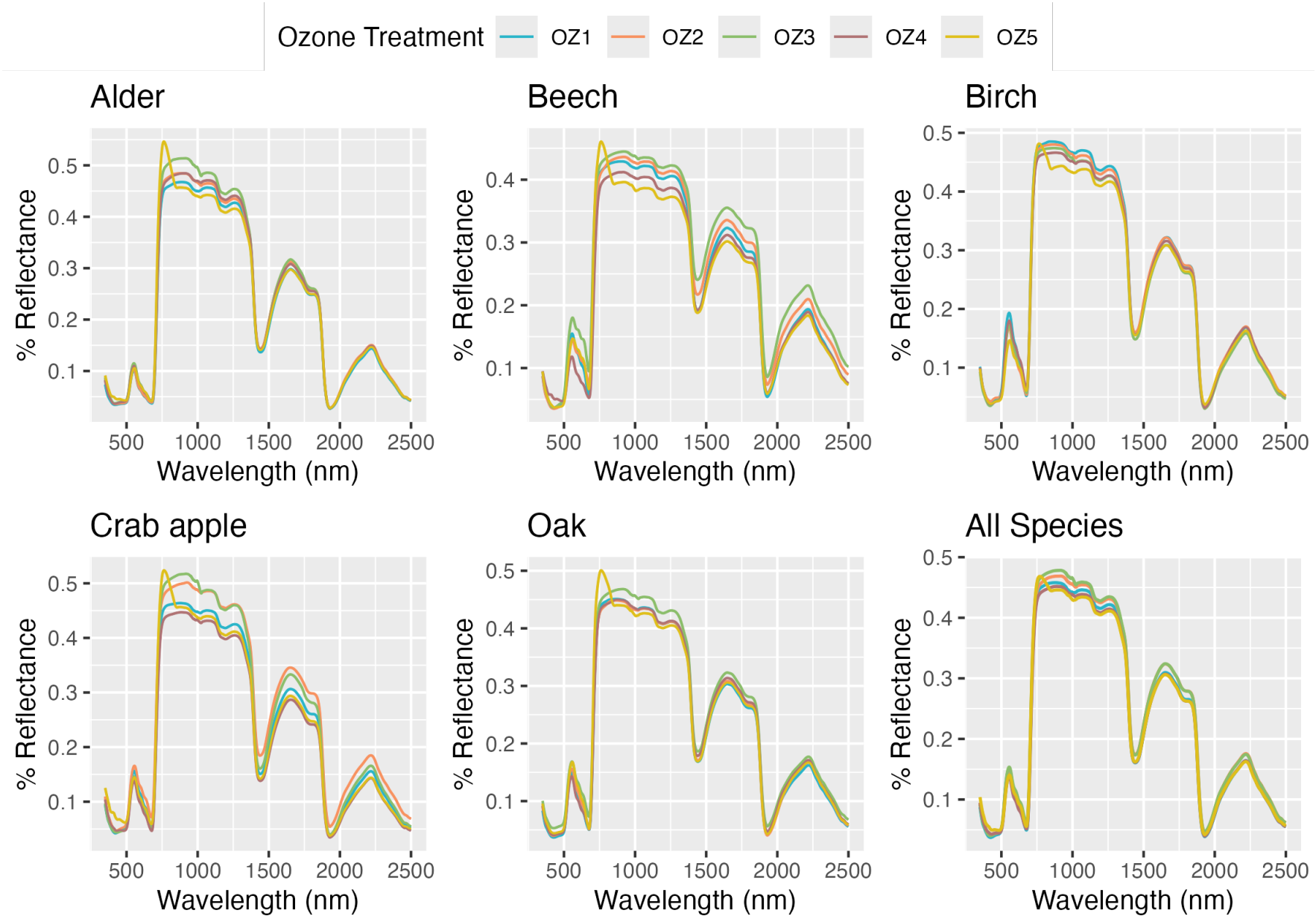


Figure 2.3: Monthly average leaf clip reflectance spectra from alder, beech, birch, crab apple, oak saplings exposed to different O_3 treatments, July to October 2022.

Principal Component Analysis Principal component analysis (PCA) on the hyperspectral library of leaf reflectance spectra showed that the first four principal components explained 95.4% of the total variation in the dataset. The first principal component (PC1) accounted for 59.3% of the total variation, while the second (PC2), third (PC3), and fourth (PC4) components explained 23%, 9.1%, 4% of the variation, respectively. PC1 is loaded evenly across the entire wavelength range, suggesting it captures the overall shape of the leaf reflectance curve (Figure 2.4). Component 2 relates highly to the red edge associated with chlorophyll content around 680 nm. The third component relates strongly to the green reflectance peak at 540 nm and the red edge.

A large amount of the variation explained by the first two principal components relates to differences between species, as indicated by the strong spatial clustering of species in Appendix B Figure B.14. When species were plotted separately against the second and third principal components (Figure 2.4), clustering emerged for the highest and lowest ozone treatments. Separation of the highest and lowest ozone treatments by principal components 2 and 3 was clearest in oak saplings.

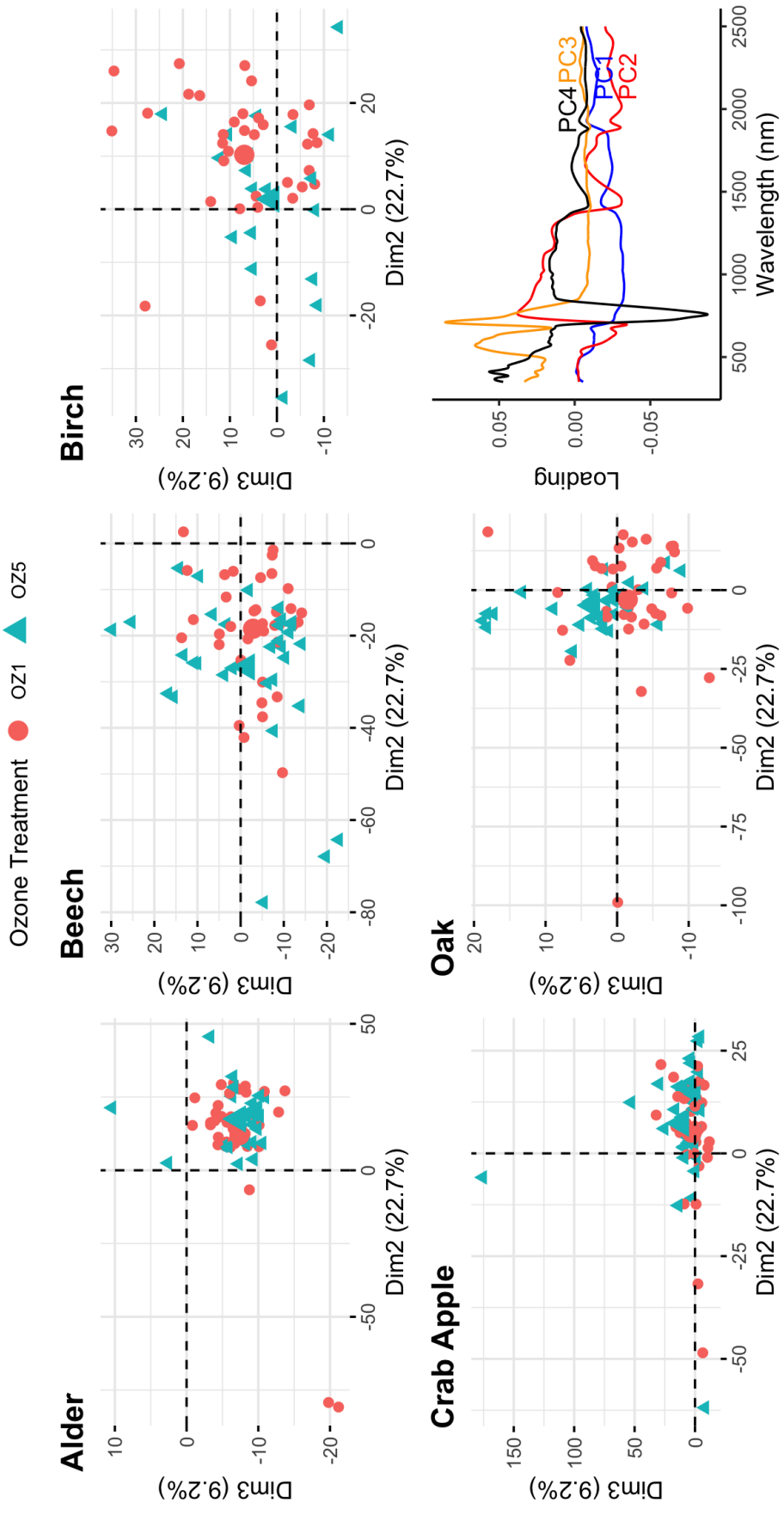


Figure 2.4: Principal Component visualisation of the highest and lowest O_3 treatments, split by species alongside the loading plot showing the wavelengths at which each of the first four principal components captures the most variation in the hyperspectral library of leaf reflectance.

Partial Least Squares Discriminant Analysis The PLS-DA models built for each species were able to discriminate accurately between saplings exposed to different O_3 treatments based on the hyperspectral reflectance spectra of leaves.

For beech leaves, 34 components were optimal for O_3 treatment classification, which was a significant dimensionality reduction from the original hyperspectral data (Appendix B, Figure B.17. The overall accuracy of O_3 treatment classification of this model was 0.872. Classification of beech leaves exposed to the highest treatment was most accurate (0.923). The prediction plot of the cross validation dataset showed that most misclassifications were assigned to neighbouring O_3 treatments (e.g. leaves exposed to OZ4 misclassified as being exposed to OZ5 or OZ3). When only the highest and lowest O_3 treatments were used (OZ1 and 5), a PLS-DA model with only 16 components was 87.9% accurate at classifying leaf spectra to the correct O_3 treatment.

For oak saplings, a PLS-DA model comprised of 40 components produced an overall model accuracy of 0.859 (Appendix B, Figure B.20). The model's accuracy varied across the five O_3 treatments, with the highest accuracy seen for classifying leaves exposed to the highest O_3 treatment OZ5 (0.902), and the lowest accuracy for OZ1 (0.797).

For alder saplings, a PLS-DA with 34 components, produced an overall accuracy of 0.913 (Appendix B, Figure B.16). For birch saplings, the optimal number of components for PLS-DA was 34, which produced an overall model accuracy of 0.898 (Appendix B, Figure B.18). For crab apple the optimal number of components for PLS-DA was 37, which produced an overall model accuracy of 0.907 (Appendix B, Figure B.19).

These PLS-DA results show that O_3 exposure of leaves can be predicted from their hyperspectral reflectance. The calibration and validation datasets contained a random mix of spectra from different months, therefore classification of leaves to the correct O_3 treatment is not dependent on seasonality.

Vegetation Indices From the range of well-known vegetation indices calculated from leaf reflectance data, O_3 treatment only had a significant main effect on modified chlorophyll absorption in reflectance index (MCARI) (Figure 2.5). Species and O_3 treatment had a significant interactive effect on all vegetation indices, as did the interaction of month and O_3 treatment. The MCARI results are explored in detail below. Photochemical reflectance index (PRI) and Plant senescence reflectance index (PSRI) results are also described as they were not suitable for PERMANOVA analysis. Full results for normalised difference vegetation index (NDVI) and red edge normalised difference vegetation index (RENDVI) can be found in the Appendix B Figures B.24 and B.25.

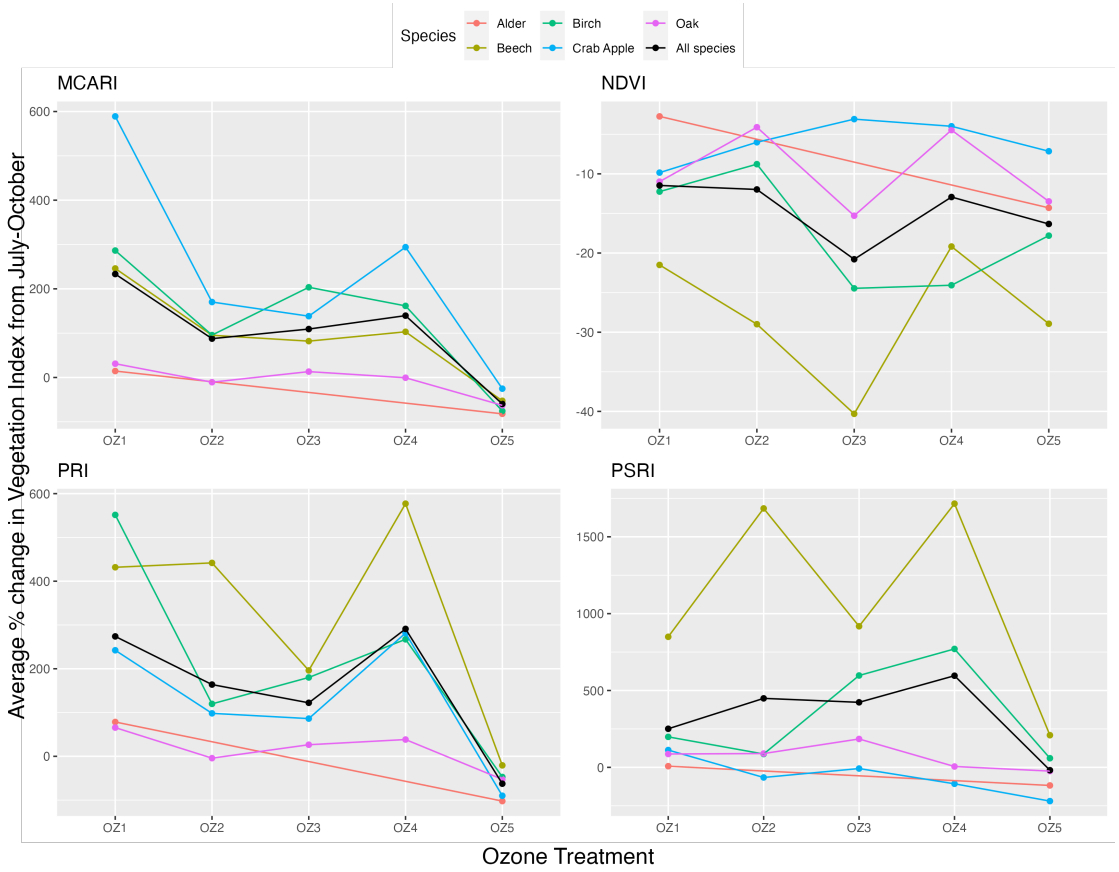


Figure 2.5: Percentage change in vegetation indices from July-October across different O_3 treatments, coloured by species.

Higher MCARI values correspond to a lower relative abundance of chlorophyll in the leaf. Broadly the MCARI of saplings increased during the growth season, as seen in Figure 2.5, reflecting a seasonal decrease in chlorophyll. Although

analysis of MCARI variance showed a significant main effect of ozone treatment, correlative analysis did not find a significant relationship between MCARI and ozone treatment ($\rho = -0.0239$, $P = 0.467$). This suggests although MCARI differed significantly between treatments, the relationship between ozone treatment and MCARI was not linear.

In terms of species-specific responses, we found that alder saplings showed limited changes in MCARI between O_3 treatments and over the growth season. The other four species showed the temporal dynamics described above and a clear difference in the MCARI of saplings in the highest O_3 treatment, as shown in Figure 2.5.

Generally, the PRI of the saplings increased during the experimental period, except the saplings exposed to the highest O_3 treatment (Figure 2.5, and Appendix B Figure B.22). The average PRI of saplings was not significantly affected by O_3 treatment alone in analysis of variance (Kruskal-Wallis, $P > 0.05$), although a weak but significant positive correlation of PRI with ozone treatment was found ($\rho = 0.116$, $P < 0.001$).

Patterns in PSRI over time and with O_3 exposure vary by species, as visualised in Appendix B Figure B.23. PSRI of saplings in the highest O_3 treatment, OZ5, was significantly greater than those in all other treatments (Wilcoxon test, $P < 0.001$). However, the average PSRI of all species and months was not significantly affected by O_3 treatment overall (Kruskal-Wallis, $P > 0.05$). Correlative analysis revealed a weak but significant positive correlation of PSRI with ozone treatment as an ordinal variable ($\rho = 0.125$, $P < 0.001$).

Overall, the only vegetation index that showed significant differentiation between O_3 treatments and correlation with O_3 concentration across all species was MCARI. Other indices were able to distinguish between the highest and lowest O_3 treatments or differentiate O_3 treatments in some species. All vegetation indices were significantly affected by seasonal and interspecific variation.

Normalised Difference Spectral Indices To determine the best wavelengths to use for a normalised difference spectral index (NDSI) specific to O_3 stress, the strength of correlation between pairs of wavelengths and visual ozone damage were analysed as per Equation 2.1 and plotted as a heat map in Figure 2.6.

When all species were combined, wavelengths in the 2200 nm to 2300 nm SWIR region were identified as having the strongest Pearson Correlation to O_3 damage scores (Figure 2.6). The combination of wavelengths with the highest correlation to O_3 damage was 2204 nm and 2248 nm, with a Pearson Correlation of 0.438.

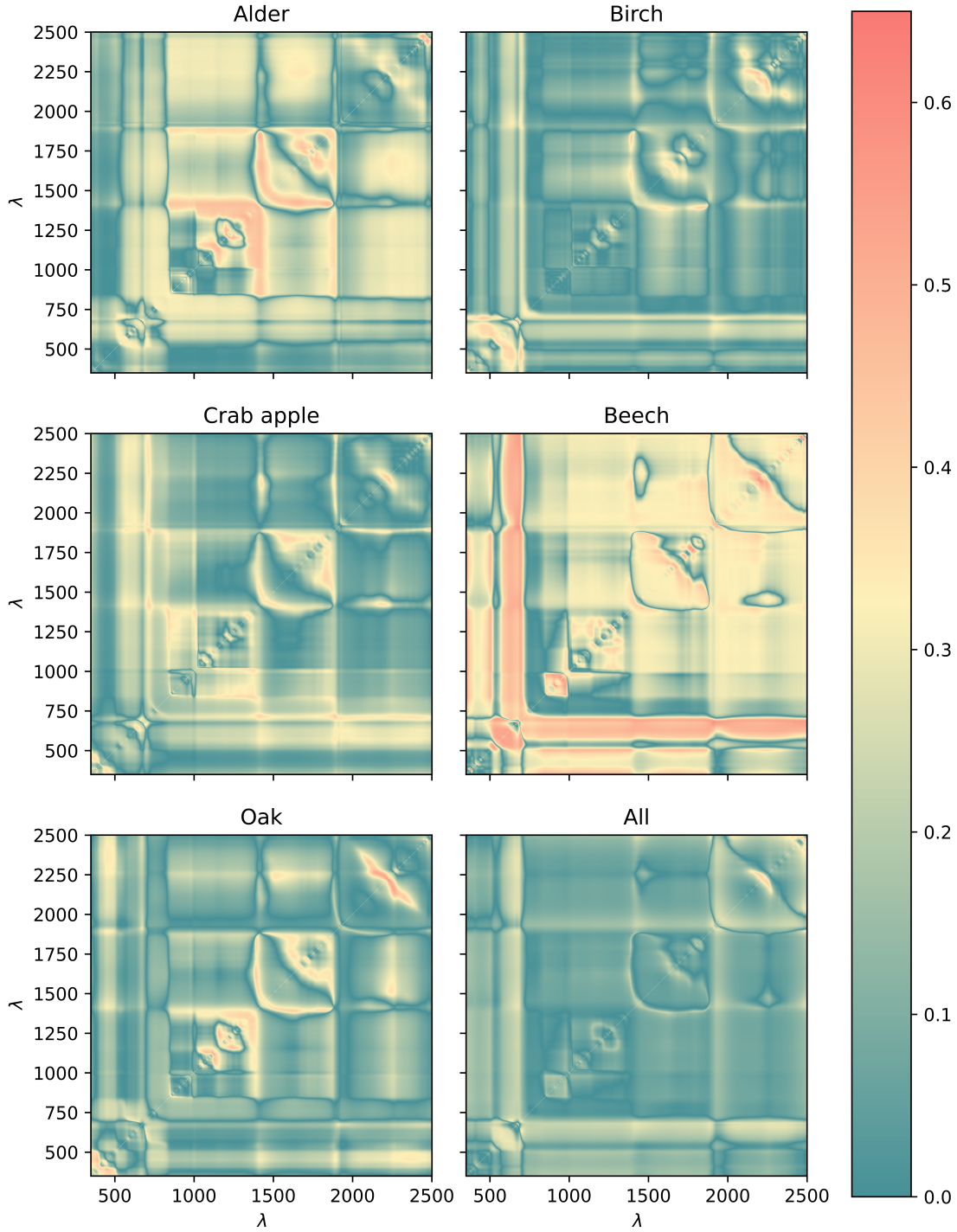


Figure 2.6: Heat map of the Pearson's correlation coefficient between the normalised difference spectral index (NDSI) and visual O_3 damage score for all saplings, O_3 treatments and months of measurement.

These wavelengths were used to form a new reflective index specific to foliar O_3 damage:

$$\text{Ozone Damage Index (OzDI)} = \frac{A_{2204} - A_{2248}}{A_{2204} + A_{2248}}, \tag{2.2}$$

where A_λ is the absorbance of wavelength λ.

OzDI ranged between 0.01 and 0.04, and increased over the growth season (Figure 2.7, All Species). On average saplings exposed to ambient O_3 (OZ1) the OzDI of saplings was lowest in July, increased significantly by August and then remained stable until October. Saplings exposed to high O_3 (OZ5) showed a step-wise increase in OzDI each month. The highest OzDI values were seen in October in the highest O_3 treatment.

The highest OzDI values were seen in crab apple and beech saplings exposed to high O_3 (OZ4 and OZ5) in September and October. The lowest OzDI values were in Alder and Oak saplings in low O_3 treatments in July. The average OzDI value was highest in the highest O_3 treatment in all species except oak, where OzDI was highest in the OZ4 treatment (Figure 2.7, oak).

In this experiment, a cut off of OzDI ≥ 0.03 could be used to identify O_3 stressed saplings. Only saplings exposed to the highest two O_3 treatments had OzDI values ≥ 0.03, although a seasonal and species-specific approach may be more precise.

OzDI performed well compared to existing vegetation indexes in differentiating O_3treatments and when correlatively analysed. Spearman's rank correlation coefficient was calculated to determine the relationship between ozone treatment (as an ordinal variable) and OzDI value of leaves. The results indicate a significant positive relationship ($\rho = 0.180$, $P < 0.001$) with a stronger correlative coefficient than any of the other pre-existing vegetation indices tested (as detailed in Section 2.2.4).

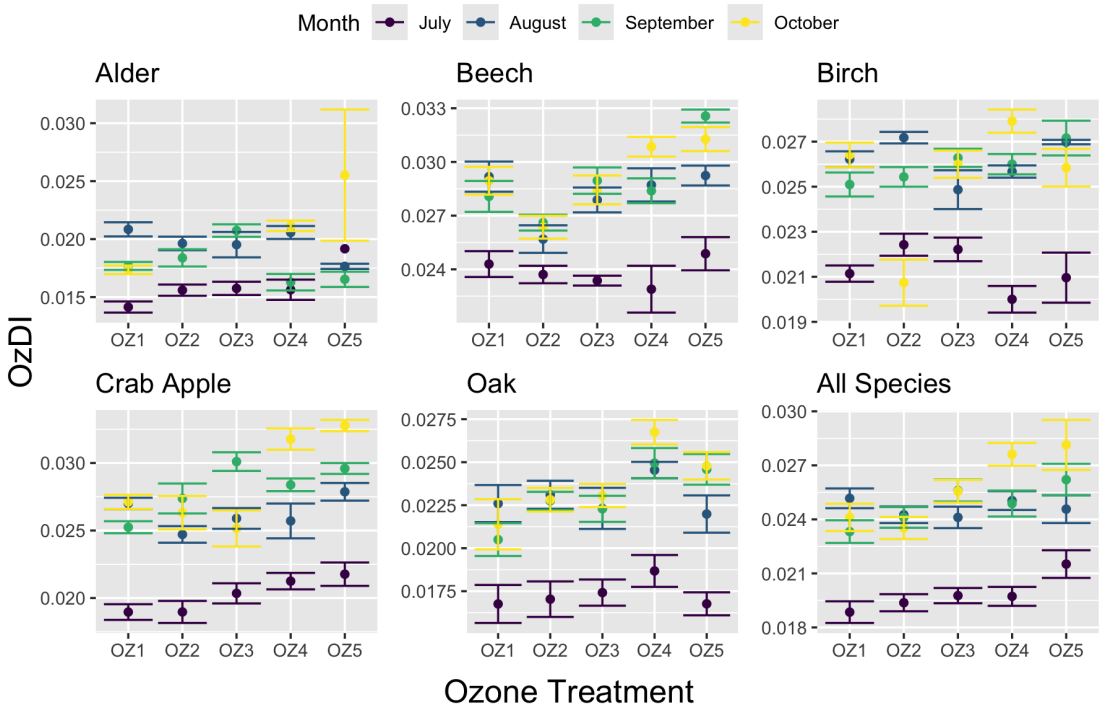


Figure 2.7: OzDI vegetation index split by species in different ozone treatments, coloured by month of measurement.

In permutational analysis, variation in OzDI was more highly correlated to O_3 treatment, species and month than NDVI, RENDVI or MCARI in terms of F-Statistic (Table 2.2). There was also a highly significant interaction between the effects of species and O_3 treatment, species and month, O_3 treatment and month, and species, O_3 treatment and month ($F = 4.452$, $F = 5.16$, $F = 5.55$, $F = 1.71$ respectively, all $P < 0.001$).

The strength of correlation between pairs of wavelengths and visual ozone damage were also analysed for each species, and the performance of the species specific NDSI compared to OzDI.

In alder, the normalised difference of 1209 nm and 1218 nm was most strongly correlated to visual O_3 damage with a Pearson Correlation of 0.512. Spearman's rank correlation coefficient was calculated to determine the relationship between ozone treatment (as an ordinal variable) and the normalised difference of 1209 nm and 1218 nm for Alder saplings only. The results indicate a non-significant relationship ($\rho = 0.0058$, $P > 0.05$). When only alder saplings were analysed, OzDI had a positive relationship to ozone treatment ($\rho = 0.15$, $P = 0.0498$).

For birch saplings, the normalised difference between 674 nm and 680 nm correlated most strongly O_3 damage score, with a Pearson Correlation of 0.51. SWIR reflectance between 2200 nm and 2300 nm was also strongly correlated to visual O_3 damage in birch. Spearman's rank correlation analysis between this NDSI and ozone treatment of birch saplings did not show a relationship ($\rho = -0.00528$, $P > 0.05$). In birch saplings, OzDI showed a non-signficant positive relationship to ozone treatment ($\rho = 0.137$, $P > 0.05$).

O_3 damage score in crab apple saplings was most highly correlated to the normalised difference of 2210 nm and 2228 nm, with a Pearson Correlation of 0.421. Spearman's rank correlation between ozone treatment and the normalised difference of 1209 nm and 1218 nm for crab apple saplings indicates a non-significant relationship ($\rho = 0.0742$, $P > 0.05$). When only crab apple saplings were analysed, OzDI had a strong positive relationship to ozone treatment ($\rho = 0.332$, $P < 0.001$).

For beech saplings the normalised difference of 956 nm and 958 nm was most strongly correlated to visual O_3 damage in beech, with a Pearson Correlation of 0.597. Spearman's rank correlation analysis between this NDSI and ozone treatment of beech saplings showed a significant negative relationship ($\rho = -0.175$, $P = 0.017$). In beech saplings, OzDI showed a highly significant positive relationship to ozone treatment ($\rho = 0.291$, $P < 0.001$).

In oak, the normalised difference of 2221 nm and 2222 nm was most strongly correlated to visual O_3 damage, with a Pearson Correlation of 0.577. These wavelengths characterise a similar part of the infrared spectrum as OzDI. Spearman's rank correlation analysis between this NDSI and ozone treatment of oak saplings showed a significant positive relationship ($\rho = 0.285$, $P < 0.001$). In oak saplings, OzDI also showed a highly significant positive relationship to ozone treatment ($\rho = 0.301$, $P < 0.001$).

OzDI also outperformed the species specific normalised different indices calculated when tested across the entire spectral library. The alder specific NDSI (1209 nm and 1218 nm) did not correlate significantly with ozone treatment when analysed for all species. Neither did the birch NDSI of 674 nm and 680 nm. The crab apple NDSI (2210 nm and 2228 nm) was significantly positively correlated with ozone treatment across all species, but less strongly than OzDI ($\rho = 0.115$, $P < 0.001$). Similarly, the beech NDSI (956 nm and 958 nm) was significantly negatively correlated with ozone treatment across all species, but less strongly than OzDI ($\rho = -0.110$, $P < 0.001$). The oak NDSI (2221 nm and 2222 nm) was also significantly correlated with ozone treatment across all species, but again less strongly than OzDI ($\rho = -0.113$, $P < 0.001$).

Vegetation Index	NDVI			RENDVI			MCARI			OzDI		
	d.o.f.	F	P	d.o.f.	F	P	d.o.f.	F	P	d.o.f.	F	P
Species	4	24.06	0.001***	4	91.02	0.001***	4	70.92	0.001***	4	182.44	0.001***
O_3	4	1.94	0.075	4	1.97	0.069	4	3.79	0.002**	4	31.38	0.001***
Treatment												
Month	3	31.83	0.001***	3	47.84	0.001***	3	13.89	0.001***	3	182.12	0.001***
Species $\times O_3$	16	2.41	0.002**	16	4.99	0.001***	16	3.96	0.001***	16	4.45	0.001***
Treatment												
Species $\times$Month	12	5.03	0.001***	12	9.77	0.001***	12	10.66	0.001***			
O_3 Treatment $\times$Month	12	1.40	0.13	12	2.89	0.001***	12	4.32	0.001***	12	5.55	0.001***
Species $\times O_3$ Treatment $\times$Month	46	0.9070	0.668	46	1.03	0.373.	46	1.49	0.003**	46	1.71	0.001***

Table 2.2: 3-way permutational analysis of variance results for the impact of species, O_3 treatment and month of measurement on selected vegetation indices and the new OzDI index. 'd.o.f.' represents degrees of freedom. F represents the F statistic. Significance codes for P-values: ***: $P \leq 0.001$, **: $P \leq 0.01$, not stated: $P > 0.05$. 999 permutations were used, and the Bray method was used to calculate pairwise distances from the spectral matrix.

2.2.5 Discussion

All species exhibited characteristic foliar O_3 damage when exposed to high O_3 treatments, consistent with previous studies that have reported a positive relationship between O_3 exposure and visual leaf injury [22, 42]. Although the growth of saplings during initial treatment was not affected by O_3, high O_3 reduced growth in the saplings measured one year after initial exposure. Carry-over effects on sapling growth following O_3 stress were also found in several other studies [43, 44].

The combination of visible foliar damage and reduced growth in the following season indicates that the saplings experienced O_3 damage proportional to O_3 exposure.

The hyperspectral leaf reflectance of saplings exposed to different O_3 concentrations showed clear differentiation despite the large seasonal and interspecific variation. A sharp reflectance peak at 750 nm was visible in all leaves in the highest O_3 treatment in July. Chlorophyll fluoresces at 750 nm [45], it is likely this peak is caused by fluorescence influencing the reflectance spectrum. Models based on the principal components of the hyperspectral dataset were able to accurately predict the O_3 treatment which new leaf spectra had been exposed to. The changes in reflectance of the visible region in saplings exposed to high O_3 corroborate the visible injury observed. Leaf reflectance spectra indicate changes in the carbohydrate content within the leaf associated with the cellulose reflectance peak, which may be related to the carry over effects of O_3 on the growth of the saplings observed. Therefore, changes in hyperspectral reflectance support the physical measurements that detected O_3 damage.

Hyperspectral data is rapid to collect and the leaf clip attachment with active light source produces a high signal to noise ratio. The number of repeats of physiological and physical measurements taken was limited by their time-consuming nature, whereas over 1450 spectra were taken capturing variation between leaves, saplings, and treatments. The high number of spectra measured allowed the effect of O_3 to be identified amongst other strong sources of variation such as species and seasonality. Outside of a controlled experimental environment, the repeatability and high throughput advantages of spectral data would be even more pronounced.

Changes in hyperspectral reflectance of saplings exposed to high O_3 also revealed additional responses not identified by other measurements. For example, high O_3 reduced NIR reflectance which is associated with the cellular structure and spongy mesophyll of the leaf. Previous studies have found cellular structure to be modified under high O_3 exposure in broadleaf species [46].

NDSI analysis showed species specific differences in the wavelengths most strongly correlated to visible ozone damage, however none of these outperformed OzDI in terms of correlation to ozone treatment across all species. The species specific NDSI for crab apple and oak characterised a very similar part of the SWIR region as OzDI. For leaf reflectance measurements taken with a lower resolution spectrometer, OzDI could be rounded to 2200 nm and 2250 nm to characterise this key peak.

Our NDSI analysis revealed a stronger correlation between visible O_3 injury and the SWIR region of leaf reflectance than regions associated with pigments. Reflectance in the SWIR region is associated with leaf cellulose, starch, and sugar content, as well as water content [41, 47]. Studies have found O_3 stress reduces the hemicellulose content of leaves [46].

The variation in OzDI between O_3 treatments may therefore be accompanied by changes in the cellulose, starch, and sugar content in O_3 stressed leaves, as well as the reduced water content due to stomatal closure.

Hyperspectral reflectance also revealed the complexity of O_3 responses which are not always linear. In several regions of the spectra, such as the green reflectance peak and NIR, the saplings in intermediate O_3 treatments had the highest reflectance. Hormesis describes the stimulatory effect of low doses of pollutants or toxins on plants and animals. A hormetic response to O_3 has been identified in many studies, as summarised by Agathaokleous et al [48]. Chlorophyll concentration is known to show hormetic dynamics in response to low doses of toxins including O_3 [49]. Understanding the complexities of dosage-dependent O_3 responses is vital to assess O_3 damage in natural settings, and hyperspectral reflectance provided higher resolution insight into the dose response of foliar O_3 damage.

Vegetation indices calculated from the hyperspectral reflectance were able to show changes in the response to O_3 stress over time. The high PRI and MCARI of saplings in the highest O_3 treatment during the first month of O_3 treatment suggests an initial acute O_3 response which was not maintained over chronic exposure, potentially showing acclimation to high O_3 stress. NDVI characterises the red-edge like MCARI but does not include the green peak, and did not show this trend. This indicated the initial increase in MCARI and PRI in response to high O_3 was underpinned by changes in the green peak reflectance. A fall in green peak reflectance can either be caused by a drop in chlorophyll or carotenoids or an increase in anthocyanin concentration. Anthocyanins are an anti-oxidant known to be upregulated in response to the oxidative stress caused by high O_3 exposure [50].

Although our study used saplings, there is evidence to suggest similar O_3 damage is found between young and mature trees. Visible O_3 injury to beech saplings in phytotrons was found at similar AOT40 levels to mature trees at a free air manipulation experiment [51]. Other research has shown inconsistent scaling of leaf-level responses to O_3 between juvenile and mature trees, dependent on compensation mechanisms and stomatal responses [52, 53]. In light of this, although our results indicate hyperspectral detection of O_3 damage is a viable method in broadleaf species, application of this method to mature trees and outside controlled conditions would require further testing. For reforestation however, hyperspectral detection of O_3 damage to young saplings is highly relevant and could be deployed to help understand variable success rates in planting initiatives.

The controlled conditions of the solardomes allow characterisation of O_3 damage using a lower number of replicates than would be needed in the field, due to reduced microclimate variability. However, in forests O_3 deposition varies along vertical profiles and temporally due to canopy fluxes [54]. Any field trial of hyperspectral detection of O_3 damage would need to capture this microclimatic variability particularly for saplings in the understory.

Hyperspectral data generally is much more scalable than traditional methods of O_3 damage detection. Hyperspectral instruments can be mounted on UAVs or

aircraft. Vegetation indices can be translated across spectroscopy instruments of varying resolution to including multispectral sensors. Leaf scale detection of O_3 damage may be upscaled to canopy level detection, although this would require further study to ascertain the strength of the O_3 damage signal when remotely sensing reflectance.

Leaf reflectance was significantly affected by O_3 treatment at all measurement points throughout the growth season, although in by the end of the season this effect was weaker. O_3 is known to have a cumulative damaging effect on vegetation [55], however, seasonality has a large influence on the reflectance of deciduous trees due to changes in pigments and water content as senescence approaches. In all analyses the effect of species and month of measurement was greater than the effect of O_3 treatment, emphasising the importance of taking into account these variables when assessing O_3 damage. For example a higher than average OzDI would need to be interpreted in context of the species and when in the growth season the measurement was taken, as is the case for most vegetation indices used to measure plant stress.

Changes in the reflectance signal of O_3 damaged leaves were broadly shared by all the broadleaf species tested, despite some species-specific differences. This suggests that canopy level analysis of O_3 damage could be feasible using a mixed species model, although this approach would need to be further tested in adult trees. Canopy level assessment of O_3 damage via hyperspectral reflectance would allow rapid evaluation of the impacts of tropospheric O_3 on forests, only currently possible by labour-intensive or destructive methods. To reliably attribute foliar damage to O_3, other abiotic and biotic stressors would need to be excluded. The changes to reflectance in the visible region and some vegetation indices (such as MCARI) observed are common to many stress responses. However, the multivariate changes observed throughout the fully hyperspectral range are more likely to be unique to ozone stress. Trialling hyperspectral detection of foliar O_3 damage in adult trees alongside high resolution O_3 measurements would be a prudent next step in the development of remote sensing O_3 damage to forests.

2.2.6 Conclusions

Our results demonstrate that hyperspectral reflectance can be used to identify O_3 damage in broadleaf saplings and differentiate between plants exposed to different concentrations of O_3 exposure. Hyperspectral leaf reflectance was able to distinguish saplings exposed to different O_3 treatments despite high inter and intra-specific variation. The entire hyperspectral reflectance profile of O_3 damaged leaves indicates a multivariate signal of O_3 damage, comprised of changes in pigments, leaf structure and water content. Wavelengths in the SWIR used to develop the new OzDI index could be used in conjunction with MCARI to predict the O_3 exposure of broadleaf trees in a seasonal and species based context. This work represents a critical first step in developing a remote sensing assessment for O_3 damage to forests, which now needs to be tested in adult trees and non-experimental settings.

2.2.7 Acknowledgements

This work was supported by the Natural Environment Research Council [grant number NE/S007474/1]. The SVC HR-1024i, leaf clip- reflectance probe attachment, and reflectance panels, were loaned from the National Environment Research Council Field Spectroscopy Facility (NERC FSF) under FSF internal loan number 884.1121. The authors gratefully acknowledge NERC FSF for this loan, and for the training and technical advice provided.

2.2.8 CRediT authorship contribution statement

Anna Lee Jones: Writing – review & editing, Writing – original draft, Visualization, Validation, Software, Resources, Project administration, Methodology, Investigation, Formal analysis, Data curation, Conceptualization. **Adam Ormondroyd:** Writing – review & editing, Software, Formal analysis. **Felicity Hayes:** Writing – review & editing, Supervision, Methodology. **Elizabeth S. Jeffers:** Writing – review & editing, Supervision, Conceptualization.

References

[1] Elizabeth Ainsworth et al. "The Effects of Tropospheric Ozone on Net Primary Productivity and Implications for Climate Change *". In: *Annual review of plant biology* 63 (Feb. 9, 2012), pp. 637–61. DOI: 10.1146/annurev-arplant-042110-103829.

[2] Daniela Nuvolone, Davide Petri, and Fabio Voller. "The effects of ozone on human health". In: *Environmental Science and Pollution Research* 25.9 (Mar. 1, 2018), pp. 8074–8088. DOI: 10.1007/s11356-017-9239-3.

[3] L. J. Mickley et al. "Radiative forcing from tropospheric ozone calculated with a unified chemistry-climate model". In: *Journal of Geophysical Research: Atmospheres* 104 (D23 1999), pp. 30153–30172. DOI: https://doi.org/10.1029/1999JD900439.

[4] H. Levy. "Normal Atmosphere: Large Radical and Formaldehyde Concentrations Predicted". In: *Science* 173.3992 (July 9, 1971). Publisher: American Association for the Advancement of Science Section: Reports, pp. 141–143. DOI: 10.1126/science.173.3992.141.

[5] Roxanne Vingarzan. "A review of surface ozone background levels and trends". In: *Atmospheric Environment* 38.21 (2004), pp. 3431–3442. DOI: https://doi.org/10.1016/j.atmosenv.2004.03.030.

[6] A. Gaudel et al. "Tropospheric Ozone Assessment Report: Present-day distribution and trends of tropospheric ozone relevant to climate and global atmospheric chemistry model evaluation". In: *Elementa: Science of the Anthropocene* 6 (Jan. 1, 2018). Ed. by Detlev Helmig and Alastair Lewis, p. 39. DOI: 10.1525/elementa.291.

[7] Gina Mills et al. "Evidence of widespread effects of ozone on crops and (semi-)natural vegetation in Europe (1990–2006) in relation to AOT40- and flux-based risk maps". In: *Global Change Biology* 17.1 (2011), pp. 592–613. DOI: 10.1111/j.1365-2486.2010.02217.x.

[8] Elena Gottardini et al. *Spatial and temporal distribution of ozone symptoms across Europe from 2002 to 2014*. ICP, 2016, p. 14.

[9] A. Francini et al. "Metabolic changes in white clover clones exposed to ozone". In: *Environmental and Experimental Botany* 60.1 (May 2007), pp. 11–19. DOI: 10.1016/j.envexpbot.2006.06.004.

[10] H. Saxe. "Physiological responses of trees to ozone - interactions and mechanisms." In: *Current Topics in Plant Biology, Volume 3*. Publisher: Research Trends. 2002, pp. 27–55.

[11] Victoria E. Wittig, Elizabeth A. Ainsworth, and Stephen P. Long. "To what extent do current and projected increases in surface ozone affect photosynthesis and stomatal conductance of trees? A meta-analytic review of the last 3 decades of experiments". In: *Plant, Cell & Environment* 30.9 (2007), pp. 1150–1162. DOI: 10.1111/j.1365-3040.2007.01717.x.

[12] J. Kangasjärvi et al. "Plant defence systems induced by ozone". In: *Plant, Cell & Environment* 17.7 (1994), pp. 783–794. DOI: 10.1111/j.1365-3040.1994.tb00173.x.

[13] P. Sicard et al. « Dommages forestiers et pollution à l'ozone dans les réserves naturelles : le cas de l'arolle dans le sud-est de la France - ». In : *Forêt Méditerranéenne* XXXI.3 (2010), p. 273.

[14] Sarah Brace, David L. Peterson, and Darci. Bowers. *A guide to ozone injury in vascular plants of the Pacific Northwest.* PNW-GTR-446. Portland, OR: U.S. Department of Agriculture, Forest Service, Pacific Northwest Research Station, 1999, PNW–GTR–446. DOI: 10.2737/PNW-GTR-446.

[15] Michael Treshow. "Ozone damage to plants". In: *Environmental Pollution (1970)* 1.2 (Oct. 1, 1970), pp. 155–161. DOI: 10.1016/0013-9327(70)90016-9.

[16] M. R. Ashmore. "Assessing the future global impacts of ozone on vegetation". In: *Plant, Cell & Environment* 28.8 (2005), pp. 949–964. DOI: 10.1111/j.1365-3040.2005.01341.x.

[17] C. Proietti et al. "A multi-sites analysis on the ozone effects on Gross Primary Production of European forests". In: *Science of The Total Environment* 556 (June 2016), pp. 1–11. DOI: 10.1016/j.scitotenv.2016.02.187.

[18] M. Schaub et al. *Part VIII: Monitoring of Ozone Injury.* UNECE ICP Forests Programme Co-ordinating Centre, Thünen Institute of Forest Ecosystems, 2016, pp. 1221–1226.

[19] Jeremy E. Diem. "Remote Assessment of Forest Health in Southern Arizona, USA: Evidence for Ozone-Induced Foliar Injury". In: *Environmental Management* 29.3 (Mar. 1, 2002), pp. 373–384. DOI: 10.1007/s00267-001-0011-5.

[20] Shawn C Kefauver. "Using topographic and remotely sensed variables to assess ozone injury to conifers in the Sierra Nevada (USA) and Catalonia (Spain)". In: *Remote Sensing of Environment* (2013), p. 11.

[21] M Meroni et al. "Assessing Steady-state Fluorescence and PRI from Hyperspectral Proximal Sensing as Early Indicators of Plant Stress: The Case of Ozone Exposure". In: *Sensors* 8.3 (Jan. 2008). Number: 3 Publisher: Molecular Diversity Preservation International, pp. 1740–1754. DOI: 10.3390/s8031740.

[22] Nichole Gosselin et al. "Using Visual Ozone Damage Scores and Spectroscopy to Quantify Soybean Responses to Background Ozone". In: *Remote Sensing* 12.1 (Jan. 2020). Number: 1 Publisher: Multidisciplinary Digital Publishing Institute, p. 93. DOI: 10.3390/rs12010093.

[23] Moon S. Kim et al. "Assessment of Combined Effects of Elevated Tropospheric O3 and CO2 on Soybean under Well-Watered and Restricted Soil Moisture Conditions by Multispectral Fluorescence Imaging Techniques". In: *Digital Imaging and Spectral Techniques: Applications to Precision Agriculture and Crop Physiology.* John Wiley & Sons, Ltd, 2004, pp. 223–253.

[24] Antonella Calzone et al. "Oxidative stress assessment by a spectroscopic approach in pomegranate plants under a gradient of ozone concentrations". In: *Environmental and Experimental Botany* 182 (Feb. 2021), p. 104309. DOI: 10.1016/j.envexpbot.2020.104309.

[25] Marchica et al. "Early Detection of Sage (Salvia officinalis L.) Responses to Ozone Using Reflectance Spectroscopy". In: *Plants* 8.9 (Sept. 12, 2019), p. 346. DOI: 10.3390/plants8090346.

[26] Martina Gäb et al. "NIR-spectroscopic investigation of foliage of ozone-stressed Fagus sylvatica trees". In: *Journal of Forest Research* 11.2 (Apr. 1, 2006), pp. 69–75. DOI: 10.1007/s10310-005-0186-3.

[27] M Meroni et al. "Leaf level early assessment of ozone injuries by passive fluorescence and photochemical reflectance index". In: *International Journal of Remote Sensing* 29.17 (Mar. 2008), pp. 5409–5422. DOI: 10.1080/01431160802036292.

[28] IPCC. *Climate Change 2021 – The Physical Science Basis: Working Group I Contribution to the Sixth Assessment Report of the Intergovernmental Panel on Climate Change*. Cambridge University Press, 2023. DOI: 10.1017/9781009157896.

[29] Felicity Hayes, Jennifer Williamson, and Gina Mills. "Species-Specific Responses to Ozone and Drought in Six Deciduous Trees". In: *Water, Air, & Soil Pollution* 226.5 (Apr. 24, 2015), p. 156. DOI: 10.1007/s11270-015-2428-0.

[30] Zhaozhong Feng et al. "A unifying explanation for variation in ozone sensitivity among woody plants". In: *Global Change Biology* 24.1 (2018), pp. 78–84. DOI: 10.1111/gcb.13824.

[31] Clare Brewster, Nathalie Fenner, and Felicity Hayes. "Chronic ozone exposure affects nitrogen remobilization in wheat at key growth stages". In: *Science of The Total Environment* 908 (Jan. 15, 2024), p. 168288. DOI: 10.1016/j.scitotenv.2023.168288.

[32] Hattie R. Roberts et al. "Chronic tropospheric ozone exposure reduces seed yield and quality in spring and winter oilseed rape". In: *Agricultural and Forest Meteorology* 316 (Apr. 1, 2022), p. 108859. DOI: 10.1016/j.agrformet.2022.108859.

[33] Amanda J. Holder and Felicity Hayes. "Substantial yield reduction in sweet potato due to tropospheric ozone, the dose-response function". In: *Environmental Pollution* 304 (July 2022), p. 119209. DOI: 10.1016/j.envpol.2022.119209.

[34] Young Lee. *SpecDAL 2.0.0*. 2017.

[35] Guido Van Rossum and Fred L. Drake. *Python 3 Reference Manual*. Scotts Valley, CA: CreateSpace, 2009.

[36] Claudia Beleites and Valter Sergo. *hyperSpec: a package to handle hyperspectral data sets in R*. Version R Package Version 0.100.2. 2017.

[37] Jari Oksanen et al. *vegan: Community Ecology Package*. 2008.

[38] Sergey Kucheryavskiy. "mdatools – R package for chemometrics". In: *Chemometrics and Intelligent Laboratory Systems* 198 (Mar. 15, 2020), p. 103937. DOI: 10.1016/j.chemolab.2020.103937.

[39] Charles R. Harris et al. "Array programming with NumPy". In: *Nature* 585 (2020), pp. 357–362. DOI: 10.1038/s41586-020-2649-2.

[40] John D Hunter. "Matplotlib: A 2D graphics environment". In: *Computing in science & engineering* 9.3 (2007). Publisher: IEEE, pp. 90–95.

[41] Paul J Curran. "Remote sensing of foliar chemistry". In: *Remote Sensing of Environment* 30.3 (Dec. 1, 1989), pp. 271–278. DOI: 10.1016/0034-4257(89)90069-2.

[42] A. J. Clark et al. "Beech (Fagus sylvatica) response to ozone exposure assessed with a chlorophyll a fluorescence performance index". In: *Environmental Pollution* 109.3 (Sept. 1, 2000), pp. 501–507. DOI: 10.1016/S0269-7491(00)00053-1.

[43] E. Oksanen and A. Saleem. "Ozone exposure results in various carry-over effects and prolonged reduction in biomass in birch (Betula pendula Roth)". In: *Plant, Cell & Environment* 22.11 (1999), pp. 1401–1411. DOI: 10.1046/j.1365-3040.1999.00501.x.

[44] Johanna Riikonen et al. "Carbon gain and bud physiology in Populus tremuloides and Betula papyrifera grown under long-term exposure to elevated concentrations of CO2 and O3". In: *Tree Physiology* 28.2 (Feb. 1, 2008), pp. 243–254. DOI: 10.1093/treephys/28.2.243.

[45] Pablo J. Zarco-Tejada et al. "Chlorophyll Fluorescence Effects on Vegetation Apparent Reflectance: I. Leaf-Level Measurements and Model Simulation". In: *Remote Sensing of Environment* 74.3 (Dec. 1, 2000), pp. 582–595. DOI: 10.1016/S0034-4257(00)00148-6.

[46] Elina Oksanen et al. "Structural characteristics and chemical composition of birch (Betula pendula) leaves are modified by increasing CO2 and ozone". In: *Global Change Biology* 11.5 (2005), pp. 732–748. DOI: 10.1111/j.1365-2486.2005.00938.x.

[47] T. Cheng, B. Rivard, and A. Sánchez-Azofeifa. "Spectroscopic determination of leaf water content using continuous wavelet analysis". In: *Remote Sensing of Environment* 115.2 (Feb. 15, 2011), pp. 659–670. DOI: 10.1016/j.rse.2010.11.001.

[48] Evgenios Agathokleous et al. "A quantitative assessment of hormetic responses of plants to ozone". In: *Environmental Research* 176 (Sept. 1, 2019), p. 108527. DOI: 10.1016/j.envres.2019.108527.

[49] Evgenios Agathokleous, ZhaoZhong Feng, and Josep Peñuelas. "Chlorophyll hormesis: Are chlorophylls major components of stress biology in higher plants?" In: *Science of The Total Environment* 726 (July 15, 2020), p. 138637. DOI: 10.1016/j.scitotenv.2020.138637.

[50] Linda Chalker-Scott. "Environmental Significance of Anthocyanins in Plant Stress Responses". In: *Photochemistry and Photobiology* 70.1 (1999), pp. 1–9. DOI: 10.1111/j.1751-1097.1999.tb01944.x.

[51] M. Baumgarten et al. "Seasonal ozone response of mature beech trees (*Fagus sylvatica*) at high altitude in the Bavarian forest (Germany) in comparison with young beech grown in the field and in phytotrons". In: *Environmental Pollution* 109.3 (Sept. 1, 2000), pp. 431–442. DOI: 10.1016/S0269-7491(00)00046-4.

[52] T.E. Kolb and R. Matyssek. "Limitations and perspectives about scaling ozone impacts in trees". In: *Developments in Environmental Science*. Vol. 3. Elsevier, 2003, pp. 141–173. DOI: 10.1016/S1474-8177(03)03006-7.

[53] T. E Kolb et al. "Issues in scaling tree size and age responses to ozone: a review". In: *Environmental Pollution* 98.2 (Nov. 12, 1997), pp. 195–208. DOI: 10.1016/S0269-7491(97)00132-2.

[54] Angelo Finco et al. "Characterization of ozone deposition to a mixed oak–hornbeam forest – flux measurements at five levels above and inside the canopy and their interactions with nitric oxide". In: *Atmospheric Chemistry and Physics* 18.24 (Dec. 18, 2018). Publisher: Copernicus GmbH, pp. 17945–17961. DOI: 10.5194/acp-18-17945-2018.

[55] Per Erik Karlsson et al. "Evidence for Impacts of Near-ambient Ozone Concentrations on Vegetation in Southern Sweden". In: *AMBIO: A Journal of the Human Environment* 38.8 (Dec. 2009), pp. 425–432. DOI: 10.1579/0044-7447-38.8.425.

2. Reflections of stress: Ozone damage in broadleaf saplings can be identified from hyperspectral leaf reflectance. *81*

.

3

On mature reflection: Ozone damage can be detected in oak trees by hyperspectral reflectance.

Contents

3.1 Commentary 82
3.2 Manuscript 83
3.2.1 Highlights 85
3.2.2 Abstract 85
3.2.3 Introduction 85
3.2.4 Methods 89
3.2.5 Results 93
3.2.6 Discussion 105
3.2.7 Conclusions 109
3.2.8 Acknowledgements 110
3.2.9 CRediT authorship contribution statement 111
References 112

3.1 Commentary

The following paper was published in Ecological Indicators (Volume 172, March 2025). In this paper I build upon the controlled experiment in Chapter 2 by expanding to mature trees under a natural range of O_3 concentrations. I found

similar signals of O_3 damage in the hyperspectral leaf reflectance of mature trees, compared to the saplings in Chapter 2. The supplementary material published with this paper is presented in Appendix C.

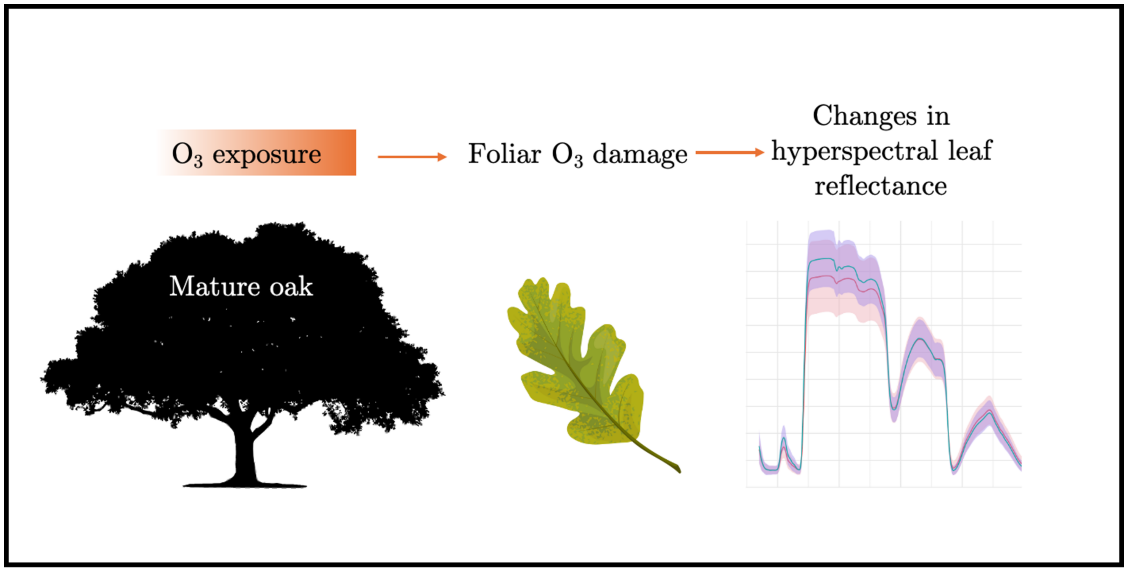


Figure 3.1: Chapter 3 graphical abstract.

3.2 Manuscript

On mature reflection: Ozone damage can be detected in oak trees by hyperspectral reflectance.

Anna Lee Jones[a], Christian Pfrang[b,c], Felicity Hayes[d], Elizabeth S. Jeffers[a]

[a] *Department of Biology, University of Oxford, South Parks Road, Oxford, UK*
[b] *School of Geography, Earth and Environmental Sciences, University of Birmingham, Birmingham, UK*
[c] *Birmingham Institute of Forest Research, University of Birmingham, Birmingham, UK*

3. On mature reflection: Ozone damage can be detected in oak trees by hyperspectral reflectance. *84*

[d]*UK Centre for Ecology & Hydrology, Environment Centre Wales, Deiniol Road, Bangor, UK*

Ecological Indicators, Volume 172, March 2025, 113263

3.2.1 Highlights

- Wytham woods has significantly higher ozone (O_3) than BIFoR FACE forest.
- O_3 induced changes in leaf reflectance can be identified in mature *Quercus robur*.
- O_3 affected green reflectance peak and red-edge reflectance of leaves.
- Hyperspectral monitoring is a new method of detecting O_3 damage to forests.

3.2.2 Abstract

At the near-surface, ozone (O_3) is a toxic pollutant which has reached dangerously high concentrations across the world and is predicted to continue to rise. O_3 reduces the growth, productivity and resilience of trees but the extent of O_3 damage to forests is uncertain. To develop a high throughput method of monitoring O_3 damage to forests, we pioneer hyperspectral monitoring of O_3 damage in adult oak trees across a range of naturally occurring O_3 concentrations. Using a machine learning approach, we demonstrate accurate prediction of O_3 exposure of trees from hyperspectral leaf reflectance alone. This method could be used for forest level assessments of O_3 damage. Vegetation indices characterising green reflectance and red-edge track O_3 induced changes in leaf reflectance. Vegetation indices have the potential to scale up O_3 damage monitoring across spatial scales. As O_3 concentrations continue to rise globally, understanding the extent of O_3 damage to forests is crucial to effectively harness the carbon sequestration potential of forests. We demonstrate the exciting potential of spectral monitoring of O_3 damage in mature trees under natural conditions.

Keywords: Air pollution, forests, spectroscopy, vegetation indices, forest health.

3.2.3 Introduction

O_3 is highly oxidising, and direct contact with O_3 at the ground level is toxic to both plant and animal life [1, 2]. Ground-level or tropospheric O_3 is a secondary pollutant formed by sunlight induced reactions of nitrogen oxides and volatile organic

compounds [3]. Tropospheric O_3 concentrations have been increasing since the 1950s when reliable global monitoring began [4]. Despite controls on vehicular emissions of nitrogen oxides, background tropospheric O_3 concentrations are increasing and are predicted to continue to rise for the rest of the century [5–8].

When O_3 enters leaves via the stomata, it causes oxidative stress and triggers a range of defence mechanisms [9] including the hypersensitive response [10] and antioxidant synthesis [11]. In the short term, O_3 exposure induces stomatal closure and a reduction in photosynthetic activity [12]. Long-term O_3 exposure results in altered allocation of carbon [13], reduced vegetation productivity [14, 15] and altered ecosystem dynamics [16, 17].

The carbon sequestration of European forest ecosystems may be significantly hindered by O_3 exposure, although modelling studies predict the extent of primary production loss to O_3 varies spatially [18]. In a meta-analysis of the impact of O_3 on tree growth, Wittig et al showed that the root-to-shoot ratio was significantly reduced by elevated O_3 across a range of species [19]. O_3 sensitivity varies widely across tree species [20], associated with differences in uptake and leaf-area-index [21] and by detoxification capacity [22]. O_3 exposure may lead to changes in community composition and diversity in forests [16]. Plant-soil-microbe interactions in forests are affected by O_3 exposure and resulting changes to leaf litter, which impacts nutrient cycling [16]. O_3 exposure also alters the abundance and community composition of insects in forests [23], particularly beneficial invertebrates [24]. O_3 therefore has a range of important effects on forest health and productivity.

Article 9 of the European National Emission Ceilings Directive specifies the negative impacts of air pollutants including O_3 on natural and semi-natural vegetation should be monitored "... through a cost-effective and risk-based approach, based on a network of monitoring sites..." [25]. Monitoring of the impacts of air pollution based upon this directive continues to apply under UK law [26]. O_3 induced leaf damage can be identified in vegetation by visible foliar injury such as stippling, chlorosis and necrosis [27–29]. Currently, the Convention on Long-range Transboundary Air Pollution (CLRTAP) and its International Co-operative

Programme on Assessment and Monitoring of Air Pollution Effects on Forests (ICP Forests) recommends the assessment by visible foliar O_3 injury and crown defoliation [30]. Manual leaf inspection is currently the only wide-scale indicator of O_3 impact on vegetation [30, 31]. Visible foliar O_3 injury is associated with decreased photosynthetic activity in sensitive species , but there is uncertainty in the suitability of visible symptoms to predict forest growth reduction [32]. Manual leaf inspection is inherently limited in coverage, accuracy and speed [33]. To extend the spatial and temporal coverage of assessment of the impact of O_3 on forests, a more versatile and high throughput method is required that does not rely solely on manual leaf inspection. Assessing the extent of O_3 damage to forests is particularly important in light of ambitious reforestation targets [34], many of which are planned for O_3 exposed sites. Projections of carbon sequestration by afforestation, such as the European Commission's 3 Billion Tree Planting Pledge project, do not account for inhibition of productivity and growth by O_3 exposure [35]. A comprehensive assessment of O_3 damage to forests over large spatial scales is a crucial component of both effective afforestation and monitoring the health of existing forests.

Vegetation spectroscopy uses the reflectance of light or fluorescence from vegetation to assess plant health at a range of spatial scales. Hyperspectral reflectance captures a continuous spectrum of reflectance across a range of wavelengths, versus multispectral reflectance which is confined to discrete bands of wavelengths but is more readily available. O_3 induced changes to plant health and visible foliar injury have been successfully detected using leaf reflectance in a range of species including indicator species [36], crops [37–40], and some trees [41–44]. In our previous study we characterised O_3 induced changes in the hyperspectral reflectance of a range of broadleaf saplings during one growth season of controlled O_3 exposure [45]. Hyperspectral leaf reflectance was able to differentiate between O_3 treatments and revealed a multivariate signal of O_3 damage comprised of changes in the green reflectance peak, red-edge, water absorption bands, and short wavelength infrared region. To our knowledge, no investigations have examined O_3 induced changes in the leaf reflectance of mature deciduous trees.

Pedunculate oak (*Quercus robur*) is the second most abundant broadleaf species in the UK (accounting for 16% of broadleaved woodland), is the most common principal species, and is the largest broadleaf contributor to the UK's standing stock of timber [46]. Pedunculate oak also occur widely across the temperate biome and their range extends from Europe to Iran. Pedunculate oak attracts up to 2,300 associated species, of which 300 are obligate oak species [47]. In an examination of 69 European tree species under projected climate conditions, Pedunculate oak (alongside *Fagus sylvatica* and *Quercus petraea*) was one of the only species to have high future potential to contribute to timber production, carbon uptake and habitat value [48]. Additionally Pedunculate oak is highly valued by forest managers as an iconic cultural species as well as for its timber [49]. Pedunculate oak is therefore an important species in temperate regions and predicted to be a crucial species in the future of temperate broadleaf forests.

The effect of O_3 exposure on Pedunculate oak has been investigated under experimental conditions using seedlings and sapling trees [50]. O_3 exposure increased photoinhibition of photosynthesis in Pedunculate oak saplings [51], and reduced assimilation [52]. O_3 exposure decreased chlorophyll content in Pedunculate oak [53], but increased total carotenoid content and flavonoids [54]. O_3 exposure of Pedunculate oak saplings reduced overall biomass [55, 56], and reduced root biomass compared to shoots [57]. Pedunculate oak is more sensitive to O_3 than other species of oak [54, 56]. To date, no studies have studied the effects of elevated O_3 on mature Pedunculate oak [50].

Tropospheric O_3 has a significant effect on the health and productivity of forests but wide-scale assessment of the impact of O_3 is limited by current monitoring methods. The objectives of this study were to investigate the difference in hyperspectral leaf reflectance between a low O_3 and high O_3 site, and to compare O_3 induced changes in leaf reflectance of mature trees under natural conditions to the spectral signature of O_3 damage we had experimentally elucidated in our previous study [45]. This study represents a crucial step in developing a high-throughput and scalable

method for O_3 damage detection in broadleaf trees, by trialling hyperspectral detection in mature pedunculate oak trees in natural settings.

3.2.4 Methods

Study sites

Our study sites were two UK broadleaf woodlands with similar land use history and climate but differing predicted O_3 profiles.

Wytham Woods (UK, 51° 46' N, 1° 20' W) is a 400 ha research woodland owned by the University of Oxford. We accessed the canopy using the 13 m canopy walkway located in secondary woodland [58] within the Smithosonian Institution ForestGEO plot established in 2008 [59]. The dominant soil of the plot is a well-drained Lithomorphic clay soil of Sherbourne series, above the Coral Rag limestone [59, 60]. This area of Wytham is known to have been woodland since at least the 18th Century, and probably much longer [61]. This region of the woods is dominated by sycamore maple (*Acer psuedoplatanus*) and pedunculate oak (*Quercus robur*), as well as small numbers of common beech (*Fagus sylvatica*) [59]. Ring counts of fallen trees and anecdotal evidence suggest pedunculate oak at this site are between 150-200 years old [62]. From the canopy walkway, 17 oak branches were accessible for measurements originating from four mature trees. Oak leaves emerged in early May in 2023. The long-term average rainfall of Wytham Woods is 717 mm, and average temperature 10 degreeCelsius (1993-2007) [60]. Air temperature was recorded hourly from the Flux tower located close to our monitoring plot. Daily rainfall was taken from the Radcliffe Meteorological Observatory in Central Oxford due to technical issues in the Wytham Woods rainfall monitoring equipment.

Birmingham Institute for Forest Research Free-Air CO_2 Enrichment facility ('BIFoR FACE', UK, 52° 47' N, 2° 18' W) is a 21 ha broadleaf woodland. It is semi-natural with over 200 years continuous cover, dominated by 180 year old pedunculate oak [63]. The woodland also features sycamore maple, hazel (*Corylus avellana*), common hawthorn (*Cretaegus monogyna*) and ash (*Fraxinus excelsior*). The dominant soil is Dystric Cambisol with sandy clay texture, and the underlying

geology is Helsby Sandstone [64]. BIFoR FACE has 30 m diameter experimental arrays, three of which are dosed with elevated CO_2, and three of which are controls dosed with ambient air [63]. Our measurements were taken in two of the control arrays. In each control array we sampled two mature oak trees which were accessible at the canopy level, totalling four trees. Oak leaves emerged in early May in 2023. The long-term annual rainfall average is 690 mm and average annual temperature is 9 degreeCelsius [65]. The mean hourly rainfall recorded by four rain gauges at the bottom of the BIFoR FACE meteorological towers (TR-525M, Texas Electronics, Dallas, Texas) was totalled per day of measurement. Daily mean air temperature was averaged across four sensors mounted on the BIFoR FACE meteorological towers (HMP155RH, Vaisala, Helsinki, Finland).

The average accumulated O_3 exposure over the threshold of 40 ppb (AOT40) from May to July for the closest four 1 km cells in Defra's 2022 Pollution Climate Mapping Model were calculated for each site [66]. The average modelled background O_3 AOT40 for the BIFoR site was 4341.75 µg m^{-3} h (for O_3 1 ppb = 1.96 µg m^{-3}). This is below the UK AOT40 objective for the protection of vegetation from O_3 damage (<6000 µg m^{-3} h) [67]. The average modelled background O_3 AOT40 for the Wytham site is 6045.5 µg m^{-3} h, this exceeds the protective threshold. Wytham Woods was designated as an O_3 polluted site based on this data, and BIFoR FACE ambient arrays designated as a lower O_3 site.

O_3 Monitoring

The O_3 concentrations of both sites were monitored using Palmes-type O_3 diffusion tubes (Gradko International) between June and October 2023. Diffusion tubes were deployed at canopy level in two locations on the canopy walkway at Wytham woods and at canopy level in the two ambient arrays at BIFoR FACE. Diffusion tubes consist of a fluorinated ethylene polymer tube fitted with an absorbent cap and porosity filter to prevent ingress of particulate nitrate. Diffusion tubes were exposed on site for 2-4 weeks and then analysed by Gradko International via ion chromatography, yielding an average O_3 concentration for the exposure period.

The measurement uncertainty of this analysis was quoted as ±10% and exposure periods are given in Appendix C, Table C.1.

Leaf Reflectance Sampling

We measured reflectance spectra of adaxial leaf surfaces in the canopy of each site approximately every two weeks (see sampling dates in Appendix C, Table C.1). Reflectance spectra were taken in the range 350 nm to 2500 nm with a HR-1024i spectrometer with a leaf clip and an active light source (Spectra Vista Corp, USA). The HR-1024i spectrometer is comprised of three dispersion grating spectrometers with overlapping wavelength ranges: Very Near Infrared (VNIR), 1.5 nm sampling interval, 350 nm to 1000 nm range; Short Wavelength Infrared 1 (SWIR1), 3.8 nm sampling interval, 1000 nm to 1890 nm range; SWIR2, 2.5 nm sampling interval, 1890 nm to 2500 nm range.

The spectrometer was referenced using the incorporated leaf clip reflective standard every five minutes during measurements. Dark signal baseline correction is applied by the HR-1024i automatically, a dark spectrum is taken before each reflectance measurement. In Wytham Woods, five leaves per accessible branch were sampled per session, totalling 85 leaves from four trees. At BIFoR FACE twenty leaves were sampled from each accessible tree per measurement session, totalling 80 leaves from four trees. All leaves sampled were full developed mature leaves, without visible herbivory or mildew from the sun exposed canopy.

Hyperspectral Processing

Leaf reflectance spectra were imported and processed as a spectral dataset in Python 3 using the SpecDAL package [68]. The overlapping regions of the three component spectrometers in the HR-1024i were stitched. Reflectance measurements were interpolated to correspond to 1.0 nm interval wavelengths. Absolute reflectance was derived from the relative reflectance by multiplying by the known reflectance of the reference panel.

Hyperspectral Analysis

Further processing of the spectral dataset was carried out in R using the 'Hyperspec' package [69]. We explored the hyperspectral dataset by principal component analysis (PCA). Hyperspectral data contains many correlated variables (the wavelengths at which reflectance was sampled). We examined the clustering of spectra by site and measured O_3 concentration when plotted against combinations of principal components.

We used Partial Least-Squares Regression (PLSR) analysis as a machine learning approach to examine the relationship between hyperspectral reflectance as the predictor and O_3 concentration as the response variable. PLSR uses the least squares method to fit a linear model using partial least squares components as predictors and prevents over-fitting when predictor variables are highly correlated, as is the case in hyperspectral data. PLSR was performed in R using the PLS package [70]. Per measurement session (one session per unique site/date combination) the hyperspectral data was split into test and train (30:70) and then within the test and train datasets an average spectrum was measurement session. PLSR with K-fold cross validation was applied to the train dataset and the optimal number of components was selected by minimising the root mean square error of prediction (RMSEP). This model was then applied to the test dataset and its performance in predicting O_3 concentration from hyperspectral leaf reflectance was evaluated.

To identify the spectral wavelengths most correlated to O_3 concentration, normalised difference spectral indices (NDSI) analysis was used. NDSI is defined as:

$$NDSI\,(i,j) = \frac{R_i - R_j}{R_i + R_j} \tag{3.1}$$

where R_i is the absolute reflectance of wavelength i, and subscripts are wavelengths in nm. The average leaf reflectance spectra per measurement session (unique site/date combination) was calculated and used for NDSI analysis. All possible combinations of wavelengths (i and j) were used to calculate all NDSI. The linear relationships between the O_3 concentration and NDSIs were examined. A heat map of the absolute value of the Pearson correlation coefficient r between O_3 concentration

and NDSI was generated. The heat maps were produced using Python 3 packages: correlation arrays were created using NumPy[71], and plotted with matplotlib [72].

The NDSI with the highest correlation to O_3 concentration was compared to common vegetation indices via correlation analysis. OzDI, an infrared vegetation index corresponding to O_3 induced leaf injury in saplings derived from our previous O_3 manipulation experiment was included [45]. The formula of the pre-existing vegetation indices used are given in Table 3.1.

Vegetation Index	Equation	Reference
Normalised Difference Vegetation Index	$NDVI = \frac{\rho_{800}-\rho_{670}}{\rho_{800}+\rho_{670}}$	[73]
Modified Chlorophyll Absorption Ratio Index	$MCARI = \left[(\rho_{700}-\rho_{670}) - 0.2 \times (\rho_{700}-\rho_{550})\right] \times \frac{\rho_{700}}{\rho_{670}}$	[74]
Red Edge Normalised Difference Vegetation Index	$RENDVI = \frac{\rho_{750}-\rho_{705}}{\rho_{750}+\rho_{705}}$	[75, 76]
Photochemical Reflectance Index	$PRI = \frac{\rho_{570}-\rho_{530}}{\rho_{570}+\rho_{530}}$	[77, 78]
Plant Senescence Reflectance Index	$PSRI = \frac{\rho_{680}-\rho_{500}}{\rho_{750}}$	[75]
Sapling Ozone Damage Index	$OzDI = \frac{\rho 2204-\rho 2248}{\rho 2204+\rho 2248}$	[45]

Table 3.1: Formulae of common vegetation indices used to measure plant health and tested for sensitivity to O_3 damage.

3.2.5 Results

O_3 and Meteorological Monitoring

Mean 24 hour O_3 concentration over June to October 2023 was 35.54 ppb at Wytham Woods and 26.89 ppb at BIFoR FACE. The O_3 profiles of the two sites were significantly different (Mann-Whitney, $Z = 0, P = 0.0022$). At every measurement point throughout the season Wytham Woods had higher O_3 exposure than BIFoR FACE (Figure 3.2), O_3 concentrations at Wytham were also more

variable. Cumulative O_3 concentration is also displayed in Figure 3.2. This monitoring data, combined with Defra's AOT40 modelling for 2022 confirms that Wytham Woods is an O_3 polluted site. The maximum O_3 concentration recorded was 53.54 ppb, the average at Wytham Woods between the 7th and 27th of July 2023. The lowest O_3 concentration recorded was 24.24 ppb at BIFoR FACE between 25th July and 10th August 2023. O_3 concentration did not correlate significantly with date of measurement ($r_\tau = 31, P = 0.84$, Appendix C figure C.2).

Throughout the measurement period (22/06/2023-06/10/2023), the average daily air temperature recorded at BIFoR FACE was 15.88 °C, and average daily rainfall was 2.14 mm. The total rainfall in the measurement period was 242.3 mm.

At Wytham Woods in the measurement period (27/06/2023-12/10/2023), the average daily air temperature was 16.29 °C. The average daily rainfall at the Radcliffe Observatory was 2.57 mm, and total rainfall in the measurement period was 277.7 mm [79].

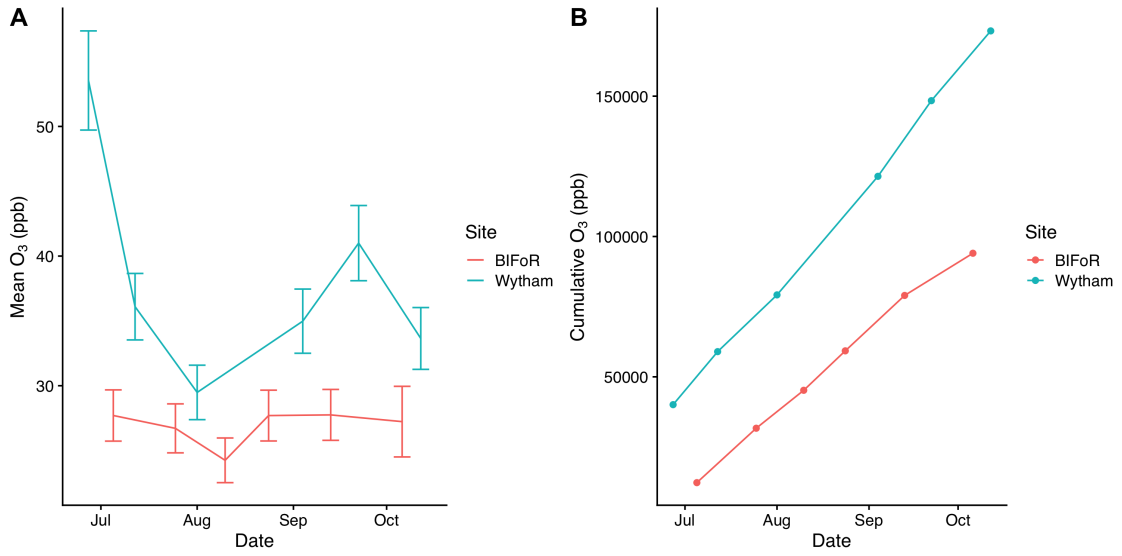


Figure 3.2: Time series of O_3 concentrations at Wytham Woods (blue) and BIFoR FACE facility (red) from July to October 2023. A: Mean hourly O_3 concentrations in ppb calculated from the preceding measurement period, error bars represent the mean measurement uncertainty at each time point. B: Cumulative O_3 dosage in ppb hour from 26th June 2023 at BIFoR FACE facility, and from the 27th June 2023 at Wytham woods.

Visual Observations

In Wytham Woods, pinprick white dots (stippling) were observed on the adaxial leaf surface of oaks (Appendix C, Figure C.1), no stippling was observed at BIFoR FACE. Stippling indicates a programmed cell death response, which occurs in response to O_3 stress but may also indicate other stressors. The stippling of oak leaves at Wytham Woods avoided the veins and was more prevalent on leaves at the ends of branches, which is typical of O_3 induced injury. Herbivory and mildew on some leaf surfaces were also observed at both sites, leaf reflectance measurements were not taken from affected leaves.

Hyperspectral Leaf Reflectance

The average hyperspectral reflectance of oak leaves from Wytham Woods and BIFoR FACE exhibited a pattern of typical foliar reflectance but differed in intensity at key regions of the spectrum (Figure 3.3). The intensity of the green reflectance peak (∼540 nm) was greater in leaves from Wytham Woods, as was the triple reflectance peak in the Near Infrared (750 nm to 1300 nm. At the water absorption bands (1400 nm and 1900 nm), leaves from BIFoR FACE had shallower reflectance troughs than leaves from Wytham Woods. Leaves from BIFoR FACE also had increased reflectance intensity in the short wavelength infrared peak at 2200 nm compared to leaves from Wytham Woods.

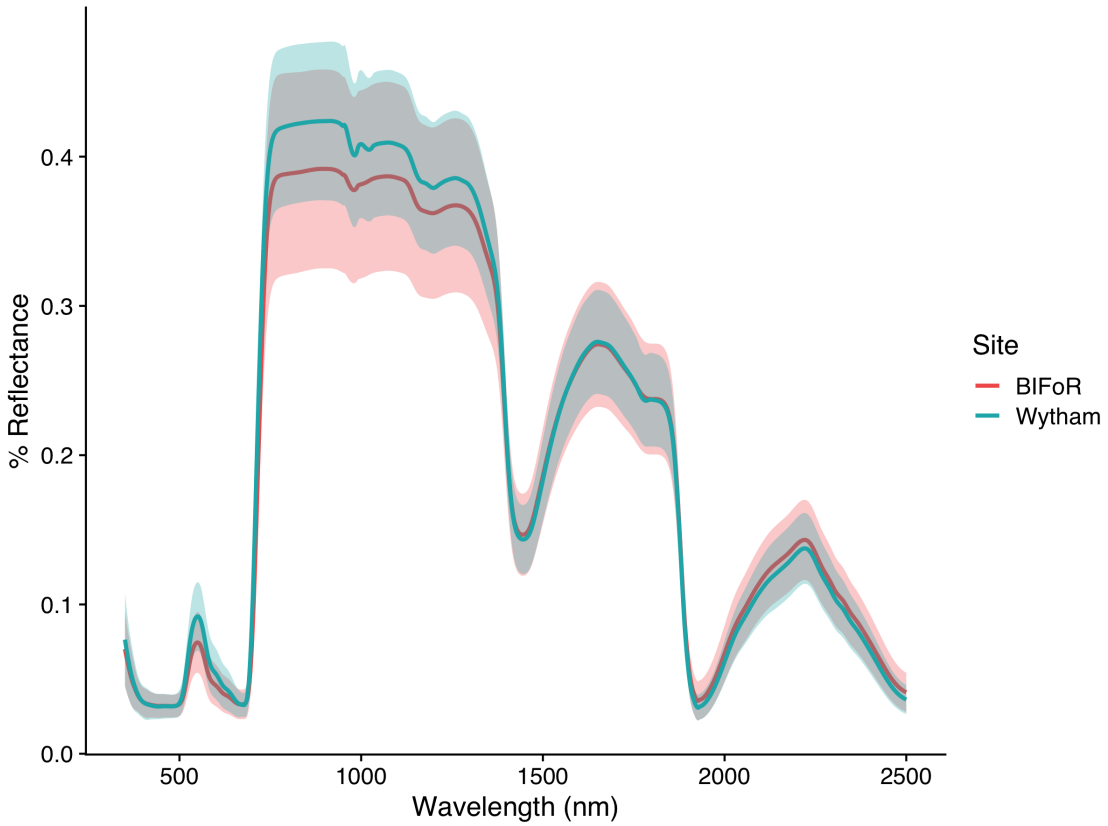


Figure 3.3: Average hyperspectral leaf reflectance per site displayed as a solid line (BIFoR FACE facility in red, Wytham Woods in blue), with ± standard deviation surrounding the mean in shading (BIFoR FACE facility in light red, Wytham Woods in light blue).

Principal Component Analysis

The first four principal components of the hyperspectral dataset of leaf reflectance were cumulatively able to explain 98.8% of the variance in the dataset (PC1 84.78%, PC2 11.44%, PC3 1.99%, PC4 0.6%). The Scree Plot of principal components can be found in the Appendix C, Figure C.3. The first principal component (PC1) was loaded most heavily by wavelengths in the near-infrared (NIR) and infrared (Figure 3.4A). PC1 captures the generic profile of leaf reflectance spectra, and so summarises differences in overall reflectance intensity. The second principal component (PC2) was negatively correlated with wavelengths in the Red-Edge and NIR, and positively correlated with wavelengths in the infrared (Figure 3.4A). The third principal component (PC3) was strongly loaded by wavelengths in the green peak and red edge, commonly used to assess chlorophyll content (Figure 3.4A). Principal component four (PC4) was loaded heavily by the lower boundary of wavelengths measured by the spectrometer (∼350 nm), and negatively correlated to the Near infrared (Figure 3.4A).

Figure 3.4B-D shows the clustering of leaf reflectance spectra coloured by measurement site against combinations of the first three principal components. There is separation of leaf reflectance spectra from BIFoR FACE versus Wytham Woods in all three combinations of PCs, but components two and three achieve the clearest distinction between sites (Figure 3.4C). The reflectance spectra of leaves at BIFoR FACE versus Wytham Woods can be discriminated by principal components, and therefore differ. The difference in reflectance spectra between the two sites correlates with cumulative O_3 concentration (Figure 3.4E), and average O_3 concentration (Appendix C Figure C.4) but not with date of measurement (Appendix C Figure C.2). Leaf reflectance clustered most clearly by average and cumulative O_3 concentration when plotted against the first two principal components (Figure 3.4E).

The reflectance spectra of leaves from BIFoR FACE versus Wytham Woods are therefore distinct and the differences between the sites correlate with both average and cumulative O_3 concentration. The variation in reflectance spectra is best characterised by the overall intensity of leaf reflectance (PC1) combined with

the intensity of the green peak (PC3), Red-Edge (PC1, 2 and 3) and infrared reflectance peaks.

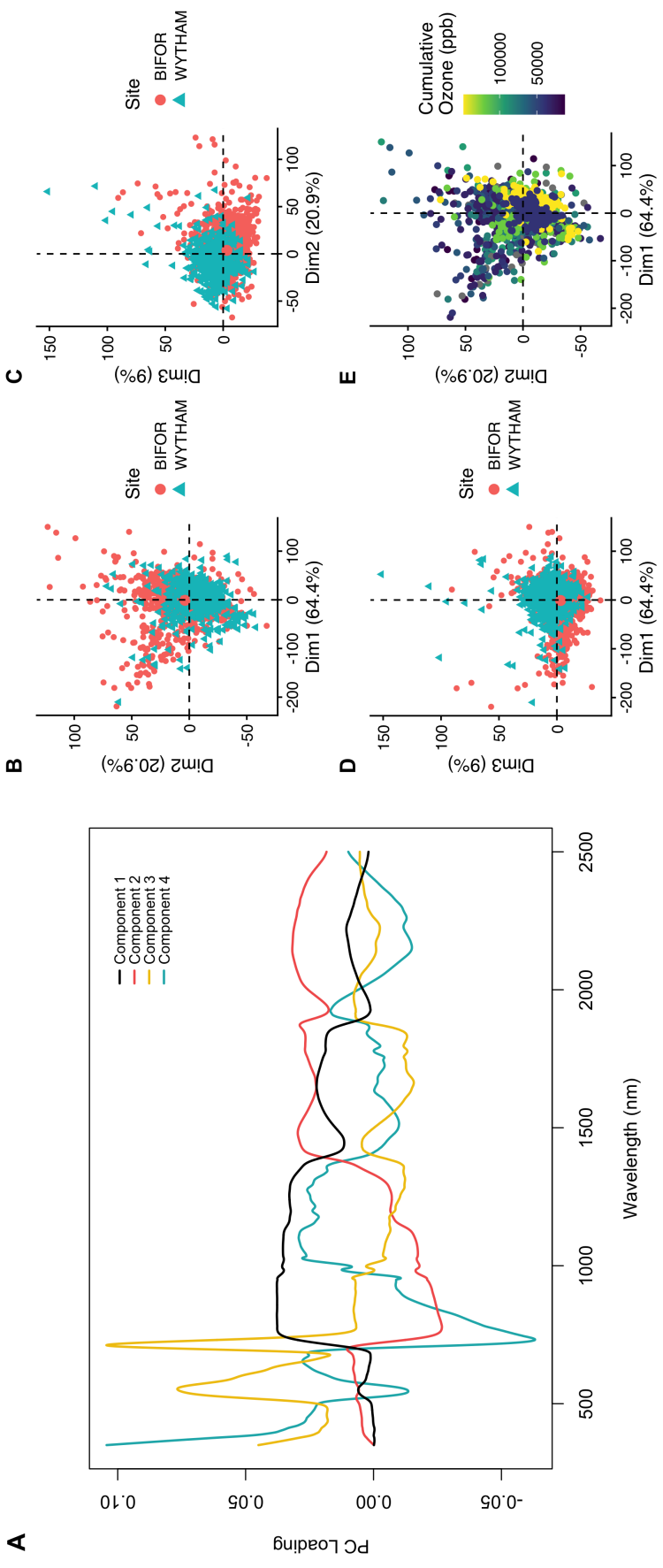


Figure 3.4: Principal component analysis of hyperspectral leaf reflectance from the two study sites (BIFoR in red, Wytham in blue). A: Loadings of the first four principal component (PC) across the spectrum of wavelengths measured. B: Leaf reflectance coloured by site against PC1 and PC2. C: leaf reflectance coloured by site against PC2 and PC3. D: Leaf reflectance coloured by site against PC1 and PC3. E: Leaf reflectance coloured by cumulative O_3 concentration in ppb against PC1 and PC2.

Partial Least Squares Regression Analysis

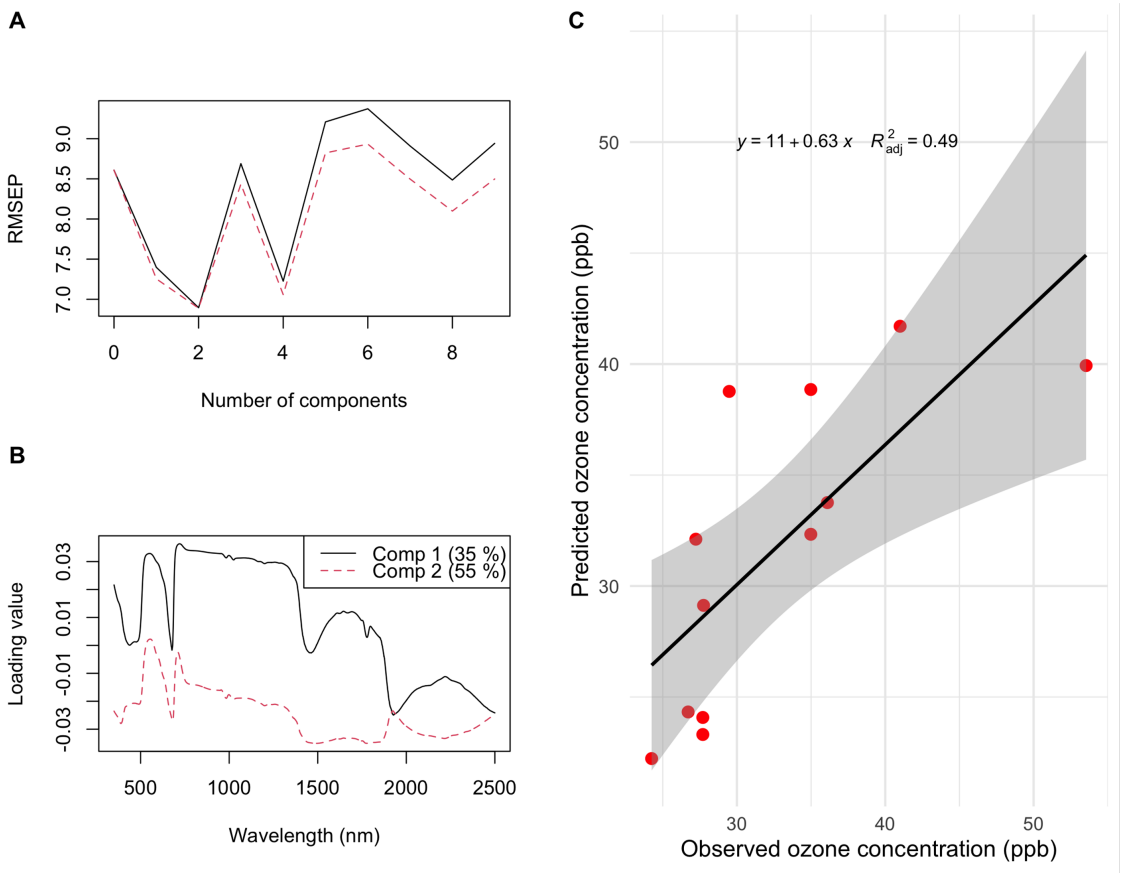


Figure 3.5: Partial least squares regression (PLSR) model validation and predictions of O_3 concentration from hyperspectral leaf reflectance. A: PLSR root mean square error prediction (RMSEP) versus number of model components. B: Loadings of the first two PLS components across the range of reflectance wavelengths measured. C: O_3 concentrations predicted by the model versus observed O_3 concentrations, based on hyperspectral leaf reflectance of the test dataset.

We selected a two component PLSR model for our analysis, based on minimisation of RMSEP in the train dataset (Figure 3.5A). These two latent variables explained 89% of variance in the reflectance data (component 1: 37%, component 2: 52%) and 56% of variance in O_3 concentration. Component 1 was strongly positively loaded by reflectance in the green peak, NIR, and to a weaker extent negatively loaded in the SWIR (Figure 3.5B). Component 2 also featured the Red Edge and was strongly negatively loaded in SWIR of the spectrum (Figure 3.5B). When the PLSR model with 2 components was used to predict O_3 values from the test spectral dataset, it achieved RMSE of 5.33, $R^2 = 0.588$ and $MAE = 4.34$. Figure 3.5C

shows the capacity of the model to predict O_3 concentrations (as an indicator of the stress due to O_3) experienced by the leaves based on their reflectance spectra alone, which are a close match to observed O_3 concentrations. The accuracy of prediction of O_3 concentration decreases at higher concentrations, as shown by the confidence boundaries in Figure 3.5C. The coefficient of the line of best fit is 0.63, indicating the model somewhat underestimates O_3 concentration on average.

Normalised Difference Spectral Indices Analysis

The correlation of all possible normalised difference indices to O_3 concentration is displayed as a heat map in Figure 3.6. NDSIs which combined one wavelength Red Edge (740 nm to 760 nm) and a wavelength above 760 nm were highly correlated to O_3 concentration (Figure 3.6). Combinations of wavelengths between 500 nm to 750 nm were also highly correlated to O_3 concentration, these wavelengths characterise the shape of the green reflectance peak and Red Edge. Many other wavelength combinations were strongly correlated to O_3 concentration, including wavelengths from 1900 nm to 2000 nm and combinations of $\sim$ 1500 to 2000+ nm. The combination of wavelengths most highly correlated with O_3 concentration were 515 nm and 647 nm, which characterise the width and intensity of the green reflectance peak. This index will be referred to as "Max NDSI".

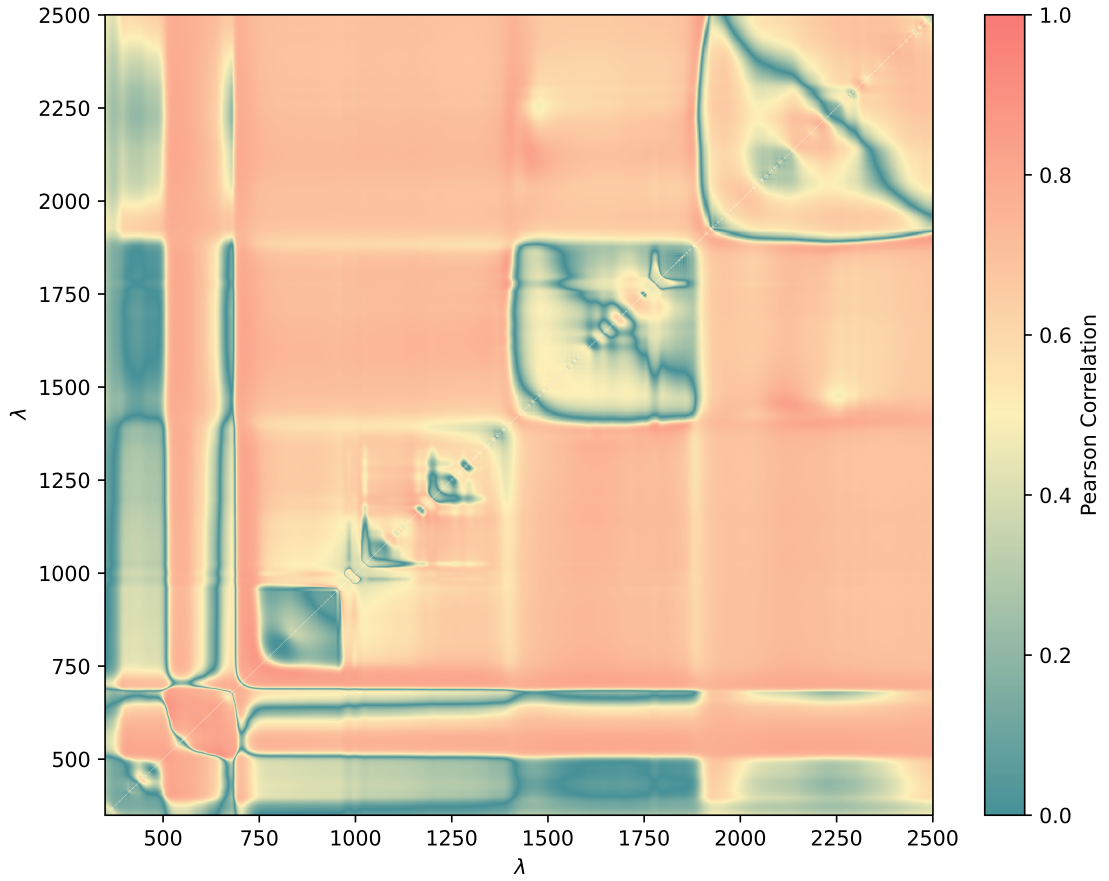


Figure 3.6: Heat map of the Pearson correlation of the normalised difference of wavelength combinations to O_3 concentration. Lambda, λ, represents wavelength in nm.

Vegetation Indices

Some pre-existing vegetation indices showed strong relationships with average O_3 concentration (Figure 3.7) and weaker relationships with cumulative O_3 concentration (Appendix C Figure C.6 and Table 3.2). Modified Chlorophyll Absorption Ratio Index (MCARI) was significantly correlated with average O_3 (Table 3.2). MCARI combines reflectance intensities at 700, 670 and 550 nm (Table 3.1), and is inversely related to chlorophyll content. MCARI showed a strong positive correlation with O_3 concentration ($r(10) = 0.826,\ P < 0.001$). MCARI was not correlated with date of measurement ($r(12) = 0.161,\ P = 0.96$), but was significantly higher at Wytham Woods than BIFoR FACE ($t(13) = -6.42,\ P < 0.001$).

Normalised Difference Vegetation Index (NDVI) was weakly positively correlated to average O_3 concentration (Figure 3.7A), but this relationship was not significant (Table 3.2). NDVI was significantly positively correlated with cumulative O_3 concentration (Appendix C Figure C.6A, $r(10) = 0.690,\ P = 0.0131$). PSRI was negatively correlated with average O_3 concentration (Figure 3.7D), but again this relationship was not significant (Table 3.2). There was no clear relationship between OzDI and average O_3 concentration (Figure 3.7f). OzDI was significantly positively correlated with cumulative O_3 concentration (Appendix C Figure C.6F, $r(10) = 0.661,\ P = 0.0193$), however there was a clear site specific difference in the correlation of this relationship

The Max NDSI calculated from this hyperspectral dataset as described above, was positively correlated with average O_3 concentration (Figure 3.7E). The strong positive correlation between Max NDSI and average O_3 concentration was statistically significant ($r(10) = 0.839,\ P < 0.001$).

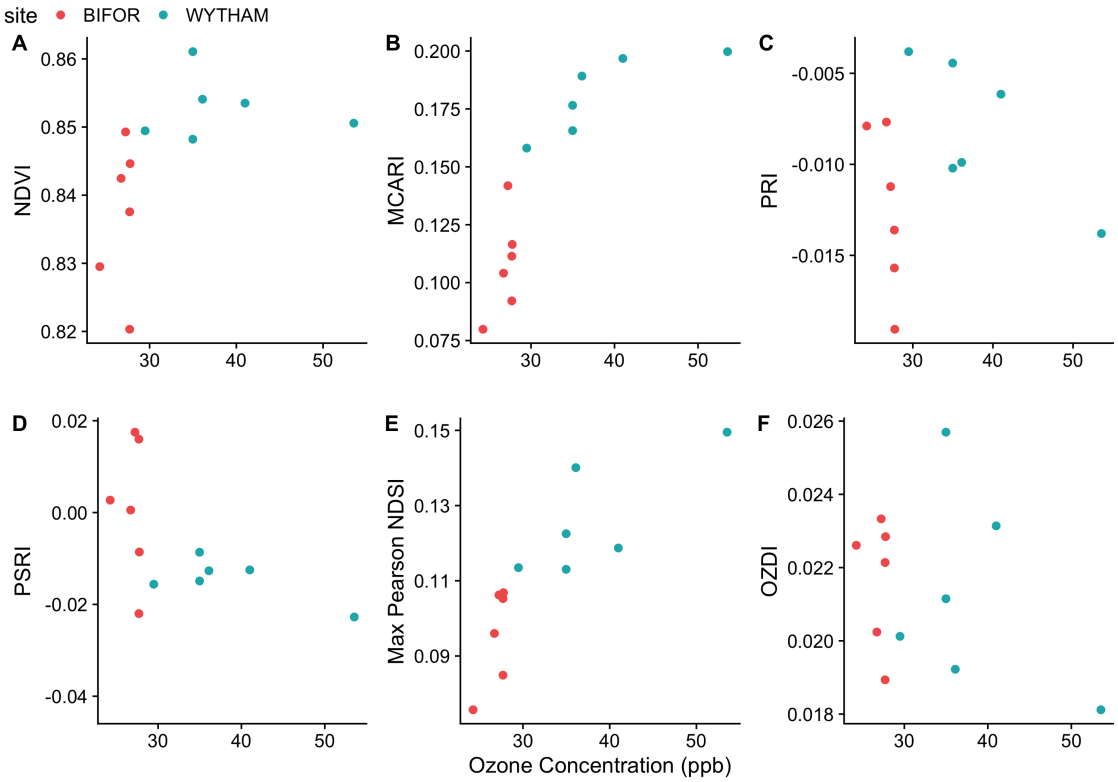


Figure 3.7: Vegetation indices plotted against O_3 concentration, coloured by site of measurement (BIFoR in red, Wytham Woods in blue).

Vegetation Index	Correlation	Degrees of Freedom	T Value	P Value
NDVI	0.52	10	1.92	0.0832
MCARI	0.826	10	4.63	0.000933 ***
PRI	0.0273	10	0.0864	0.933
PSRI	-0.563	10	-2.15	0.0569
Max NDSI	0.839	10	4.88	0.000639 ***
OzDI	-0.301	10	-0.997	0.342

Table 3.2: Results of Pearson Correlation analysis of different vegetation indices against average O_3 concentration. *** indicates P value < 0.001

3.2.6 Discussion

Our O_3 monitoring in Wytham Woods demonstrates the site is exposed to damaging levels of O_3, as predicted by the Defra's Pollution Climate Mapping Model. The meteorological conditions of the two sites were similar in terms of rainfall and temperature, however other factors such as light availability, humidity, and soil nutrients may also affect leaf reflectance [80]. The scope of this study did not include the measurement of additional meteorological factors which may differ between the two woodlands, meaning hyperspectral features which correlated with O_3 over time and without site specific differences are more robust such as the PLSR analysis. The canopy in Wytham Woods was significantly more O_3 exposed than BIFoR FACE, and the differences in leaf reflectance between the two sites indicate foliar changes induced by O_3 damage.

The cumulative exposure of vegetation to O_3 determines the magnitude of damage [81]. AOT40 has been adopted widely as a metric of "accumulate O_3 over threshold 40 ppb" intended to capture vegetation damaging levels of O_3 exposure for compliance monitoring. However, there is developing scientific consensus that a stomatal flux-based approach gives a more accurate assessment of the risk of O_3 damage to vegetation [82–84]. Stomatal O_3 flux is affected by atmospheric and stomatal conductivity [85]. There are a range of species specific or vegetation type PODy flux models which calculate the cumulative exceedance of critical levels of stomatal O_3 flux, based on O_3 concentration, temperature, humidity, light and soil moisture [86]. Hourly monitoring of these parameters was beyond the scope of this study, and so we use simple O_3 concentration and cumulative O_3 concentration as a proxy for O_3 dosage which has obvious limitations in terms of understanding the dose of O_3 received.

The O_3 induced change in leaf reflectance we identified is multivariate, key regions of the spectrum include the green reflectance peak, red edge, and NIR. The hyperspectral reflectance profile of oak leaves at Wytham Woods, the high O_3 site, was increased in the height and width of the green reflectance peak (500 nm to 570 nm) and the Near Infrared triple peak (750 nm to 1300 nm). In the water

absorption peaks (1400 nm and 1900 nm), and infrared peak at 2200 nm the leaf reflectance of the high and low O_3 was more similar, although slightly reduced under high O_3. Unsupervised variable reduction (PCA) and supervised variable reduction (PLSR) both highlighted the green reflectance peak and near infrared triple peak as key regions for summarising the variability in hyperspectral reflectance profiles. The high spectral resolution and wavelength range of our measurements allow a more detailed understanding of the spectral shifts underpinning changes in vegetation indices and the multivariate differences in leaf reflectance between a low and high O_3 site.

The indices most strongly related to average O_3 exposure independent of site (max NDSI and MCARI) characterise the intensity and width of the green reflectance peak (500 nm to 650 nm). Several early experimental studies found changes in this region associated with O_3 damage in other species [87, 88]. PRI characterises the top of the green reflectance peak at 550 nm but did not respond significantly to O_3 exposure in neither our field or experimental study, whereas max NDSI and MCARI characterise the broader green reflectance peak by inclusion of a wavelength at 640 nm to 670 nm. The green reflectance peak is influenced by chlorophyll, carotene and anthocyanin pigment concentrations in combination [76]. Chlorophyll content decreases during ozone stress [89], whereas anthocyanins are an anti-oxidant upregulated to in response to the oxidative stress caused by high ozone [90]. MCARI was developed to estimate chlorophyll A concentration [74], but is also influenced by xanthophyll and carotene concentration [91]. NDVI characterises the red edge and is dominated by chlorophyll A concentration but did not respond to O_3 exposure. In O_3 exposed oak saplings, a significant increase in total carotenoids (including carotene and xanthophylls) has been observed experimentally [54]. Together these results indicate the broader green reflectance peak is a key component of the signal of O_3 damage in leaf reflectance, likely underpinned by changes in the relative concentration of chlorophyll, carotene, and xanthophyll pigments.

The effects of O_3 on oak species was reviewed by Cotrozzi in a meta-analysis which concluded that although oak species are broadly resistant to large changes in biomass

under elevated O_3 damage, they undergo significant physiological impairment [50]. O_3 exposure reduced the maximum rate of carboxylation, electron transport rate, conductance parameters and stomatal responsivity in 2 year-old *Quercus robur* [92]. Phenols play a key role in the antioxidant response of oak species [50]. These physiological effects may relate to the changes we have observed in the green peak leaf reflectance peak, but further studies are needed to identify the precise leaf level changes underpinning changes in leaf reflectance in response to O_3. A further limitation of current knowledge of the effects of O_3 on forests is a lack of studies on mature trees, which we sought to address although this limited our study to a 'natural experiment' with many uncontrolled variables in comparison to the many O_3 manipulation studies on young trees.

Leaf reflectance is affected by many factors, besides O_3 damage, such as drought [93], disease [94], and leaf traits [95]. However, the changes in leaf reflectance we found corresponded strongly to O_3 concentration changes within as well as between the two sites. Our machine learning model of hyperspectral reflectance was able to accurately predict O_3 exposure from reflectance data, independent of study site. Furthermore, we also demonstrated that MCARI and the Max NDSI responded linearly to O_3 concentrations across both sites. Date of measurement did not have a significant relationship with O_3 concentration, and did not significantly affect MCARI. In our previous experimental study, the MCARI of oak saplings also changed significantly under different O_3 exposure regimes [45]. The principal components of the hyperspectral dataset show similarities between the present field study and our previous controlled experiment, suggesting broadly similar regions of variation in the leaf reflectance spectra. The width of the green reflectance peak (characterised by MCARI and Max NDSI) was important in differentiating between O_3 treatments in our previous controlled experiment, as well as in the present field study.

Conversely, the short wavelength infrared region (SWIR) which varied strongly with foliar O_3 damage in our previous controlled experiment did not show a relationship with O_3 concentration in the present field study. There are several

possible reasons for this: maximum O_3 concentrations measured in the field were lower than the highest O_3 treatment in our previous experiment and so changes in the SWIR may only be triggered at higher O_3 concentrations. Some studies have also found that juvenile trees are more sensitive to O_3 stress than mature tress due to higher stomatal uptake and therefore dosage of O_3 [96]. Alternatively, the SWIR region may be affected by O_3 in saplings but not in mature trees. Stress responses are known to differ between saplings and mature trees for example in response to drought in *Quercus rubra* [97], other studies of *Quercus* and deciduous species have found age-related differences in leaf traits and gas exchange patterns [98, 99]. The SWIR region of leaf reflectance is associated with foliar cellulose, starch, and sugar content, as well as water content [100, 101] and so may be affected differently by O_3 stress in saplings versus mature trees. Conversely, some studies have shown similar responses to O_3 stress in saplings and mature trees [102]. These two explanations for the difference in SWIR response between our two studies (lower O_3 exposure/uptake and differences in ontogeny) are not mutually exclusive.

We have demonstrated using a machine learning approach that O_3 exposure in mature trees can be detected from hyperspectral leaf reflectance (PLSR analysis), which could be used to indicate locally damaging O_3 concentrations. Tropospheric O_3 monitoring is sparse in coverage, and focusses on urban versus suburban sites in the UK [7]. The O_3 exposure of most forests is unknown, and monitoring requires expensive automated gas analysers or regular lab analysis of diffusion tubes. Leaf reflectance therefore represents an exciting new method of identifying damage inducing O_3 concentrations in forests, confirmed by air pollution models. We took leaf level reflectance measurements directly from the canopy, but scaling this method up to remote measurements taken via unmanned aerial vehicles (UAV, or drones) would allow widespread assessment of O_3 induced damage in forests.

Although this study focussed on oak, our previous O_3 exposure experiment showed oak reflectance in saplings responded similarly to other broadleaf species (beech, birch, alder and crab apple). MCARI differed significantly with O_3 treatment across beech, birch, crab apple as well as oak in our experimental study. Meroni

et al reported similar changes in the green peak and red edge in *Populus nigra* [87]. We hypothesize hyperspectral detection of O_3 damage using analysis of the green peak and red edge in mature trees could be expanded beyond oak to other deciduous species. The canopies of natural or semi natural deciduous forests are often a mixture of different species, and so expanding detection of O_3 damage to a deciduous species mix will be important for developing a remote sensing method of O_3 damage detection.

The spectral method of O_3 damage detection we have tested is more scalable and consistent than manual inspection of foliar damage. Hyperspectral measurements are not subjectively influence by the assessor, unlike manual inspection methods. Standardisation training for human O_3 damage assessors can improve the subjectivity of their measurements, but differences remain and training takes significant resources [33]. Hyperspectral measurements on the other hand are objective, standardised by referencing, and can be taken by non-experts. Hyperspectral measurements can also be taken remotely via UAV, aircraft and satellite although scaling spectral intensity across spatial scales can be challenging [103]. Vegetation indices are directly scalable however because by taking the ratio of intensity at different wavelengths, they are not dependant on absolute intensity of reflectance. MCARI has a strong relationship with O_3 exposure and can be calculated from multispectral satellites with global coverage over several decades such as Sentinel 2 and Landsat 8. Standard multispectral satellite bands could not be used to calculate Max NDSI but hyperspectral satellite products such as EnMAP could be used on a landscape scale to assess O_3 damage to vegetation. This study demonstrates the potential for specific changes in leaf reflectance to be used to monitor O_3 damage on larger spatial scales in a new application of remote sensing.

3.2.7 Conclusions

Our study has shown a clear signal of O_3 damage can be detected from hyperspectral leaf reflectance in adult oak trees under a range of naturally occurring O_3 concentrations. Hyperspectral leaf reflectance can be used to accurately predict O_3 exposure,

which could be scaled up for forest level assessments of damage inducing O_3 exposure. O_3 induced changes in leaf reflectance can be tracked using vegetation indices such as MCARI, which could be used establish remote sensing of O_3 damage to forests. As O_3 concentrations continue to rise globally, understanding the extent of O_3 damage to forests is crucial to effectively harness the carbon sequestration potential of forests. We have demonstrated the exciting potential of spectral monitoring of O_3 damage in mature trees, which now needs to be generalised beyond oak and scaled up to a remote sensing methodology.

3.2.8 Acknowledgements

This work was supported by the Natural Environment Research Council [grant number NE/S007474/1]. The SVC HR-1024i, leaf clip- reflectance probe attachment, and reflectance panels, were loaned from the National Environment Research Council Field Spectroscopy Facility (NERC FSF) under FSF internal loan number 915.1122. The authors gratefully acknowledge NERC FSF for this loan, and for the training and technical advice provided.

Fieldwork carried out at the Birmingham Institute of Forest Research FACE Facility was coordinated by Dr Kris Hart and academically supervised by Prof Christian Pfrang. The authors would like to thank Peter Miles for his enthusiasm and facilitation of canopy access at BIFoR FACE. BIFoR FACE meteorological data was collected and managed by the following contributors: Curioni G., Denny G., Downes T.M., Harper N.J., Hart K.M., Mackenzie A.R., Miles P., Ullah S., Tekinay F. The BIFoR FACE facility is a research infrastructure project supported by the JABBS Foundation and the University of Birmingham. The facility has received support for scientific studies from the Biotechnology and Biological Sciences Research Council (BBSRC), Ecological Continuity Trust (ECT), JABBS Foundation, the John Horseman Trust, the Natural Environment Research Council (NERC), National Science Foundation (NSF), the Woodland Trust and the Newton Fund.

We would also like to thank Alex Black, Yadvinder Mahli and Curt Lambeth for facilitating canopy access in Wytham Woods and meteorological data.

3.2.9 CRediT authorship contribution statement

Anna Lee Jones: Writing – review & editing, Writing – original draft, Visualization, Validation, Software, Project administration, Methodology, Investigation, Formal analysis, Data curation, Conceptualization. **Christian Pfrang:** Writing – review & editing, Supervision. **Felicity Hayes:** Writing – review & editing, Supervision. **Elizabeth S. Jeffers:** Writing – review & editing, Supervision, Conceptualization.

References

[1] Gabriele Donzelli and Maria Morales Suarez-Varela. "Tropospheric Ozone: A Critical Review of the Literature on Emissions, Exposure, and Health Effects". In: *Atmosphere* 15.7 (July 2024). Number: 7 Publisher: Multidisciplinary Digital Publishing Institute, p. 779. DOI: 10.3390/atmos15070779.

[2] Allen S. Lefohn et al. "Tropospheric ozone assessment report: Global ozone metrics for climate change, human health, and crop/ecosystem research". In: *Elementa: Science of the Anthropocene* 6.27 (Apr. 6, 2018). Ed. by Detlev Helmig and Alastair Lewis. DOI: 10.1525/elementa.279.

[3] P. S. Monks et al. "Tropospheric ozone and its precursors from the urban to the global scale from air quality to short-lived climate forcer". In: *Atmospheric Chemistry and Physics* 15.15 (Aug. 13, 2015). Publisher: Copernicus GmbH, pp. 8889–8973. DOI: 10.5194/acp-15-8889-2015.

[4] IPCC. *Climate Change 2021 – The Physical Science Basis: Working Group I Contribution to the Sixth Assessment Report of the Intergovernmental Panel on Climate Change*. Cambridge University Press, 2023. DOI: 10.1017/9781009157896.

[5] Amy Christiansen et al. "Multidecadal increases in global tropospheric ozone derived from ozonesonde and surface site observations: can models reproduce ozone trends?" In: *Atmospheric Chemistry and Physics* 22.22 (Nov. 21, 2022). Publisher: Copernicus GmbH, pp. 14751–14782. DOI: 10.5194/acp-22-14751-2022.

[6] O. R. Cooper et al. "Global distribution and trends of tropospheric ozone: An observation-based review". In: *Elementa: Science of the Anthropocene* 2 (July 10, 2014). Ed. by Detlev Helmig and Paul Palmer, p. 000029. DOI: 10.12952/journal.elementa.000029.

[7] Douglas P. Finch and Paul I. Palmer. "Increasing ambient surface ozone levels over the UK accompanied by fewer extreme events". In: *Atmospheric Environment* 237 (Sept. 15, 2020), p. 117627. DOI: 10.1016/j.atmosenv.2020.117627.

[8] Paul T. Griffiths et al. "Tropospheric ozone in CMIP6 simulations". In: *Atmospheric Chemistry and Physics* 21.5 (Mar. 18, 2021). Publisher: Copernicus GmbH, pp. 4187–4218. DOI: 10.5194/acp-21-4187-2021.

[9] Heinrich Sandermann Jr. "Ozone and Plant Health". In: *Annual Review of Phytopathology* 34.1 (1996), pp. 347–366. DOI: 10.1146/annurev.phyto.34.1.347.

[10] Jaakko Kangasjärvi, Pinja Jaspers, and Hannes Kollist. "Signalling and cell death in ozone-exposed plants". In: *Plant, Cell & Environment* 28.8 (2005), pp. 1021–1036. DOI: 10.1111/j.1365-3040.2005.01325.x.

[11] Yogesh K Sharma and Keith R Davis. "The Effects of Ozone on Antioxidant Responses in Plants". In: *Free Radical Biology and Medicine* 23.3 (Jan. 1, 1997), pp. 480–488. DOI: 10.1016/S0891-5849(97)00108-1.

[12] A. Clyde Hill and Niel Littlefield. "Ozone. Effect on apparent photosynthesis, rate of transpiration, and stomatal closure in plants". In: *Environmental Science and Technology* 3 (Jan. 1, 1969). ADS Bibcode: 1969EnST....3...52H, pp. 52–56. DOI: 10.1021/es60024a002.

[13] Christian P. Andersen. "Source–sink balance and carbon allocation below ground in plants exposed to ozone". In: *New Phytologist* 157.2 (2003), pp. 213–228. DOI: 10.1046/j.1469-8137.2003.00674.x.

[14] M. R. Ashmore. "Assessing the future global impacts of ozone on vegetation". In: *Plant, Cell & Environment* 28.8 (2005), pp. 949–964. DOI: 10.1111/j.1365-3040.2005.01341.x.

[15] B. Felzer et al. "Effects of ozone on net primary production and carbon sequestration in the conterminous United States using a biogeochemistry model". In: *Tellus B: Chemical and Physical Meteorology* 56.3 (Jan. 1, 2004), pp. 230–248. DOI: 10.3402/tellusb.v56i3.16415.

[16] Evgenios Agathokleous et al. "Ozone affects plant, insect, and soil microbial communities: A threat to terrestrial ecosystems and biodiversity". In: *Science Advances* 6.33 (Aug. 1, 2020). Publisher: American Association for the Advancement of Science Section: Research Article, eabc1176. DOI: 10.1126/sciadv.abc1176.

[17] J.M.W. Ryalls et al. "Anthropogenic air pollutants reduce insect-mediated pollination services". In: *Environmental Pollution* 297 (2022). DOI: 10.1016/j.envpol.2022.118847.

[18] C. Proietti et al. "A multi-sites analysis on the ozone effects on Gross Primary Production of European forests". In: *Science of The Total Environment* 556 (June 2016), pp. 1–11. DOI: 10.1016/j.scitotenv.2016.02.187.

[19] Victoria E. Wittig, Elizabeth A. Ainsworth, and Stephen P. Long. "To what extent do current and projected increases in surface ozone affect photosynthesis and stomatal conductance of trees? A meta-analytic review of the last 3 decades of experiments". In: *Plant, Cell & Environment* 30.9 (2007), pp. 1150–1162. DOI: 10.1111/j.1365-3040.2007.01717.x.

[20] Elke Bergmann, Jürgen Bender, and Hans-Joachim Weigel. "Impact of tropospheric ozone on terrestrial biodiversity: A literature analysis to identify ozone sensitive taxa". In: *Journal of Applied Botany and Food Quality* 90 (Feb. 1, 2017), pp. 83–105. DOI: 10.5073/JABFQ.2017.090.012.

[21] Zhaozhong Feng et al. "A unifying explanation for variation in ozone sensitivity among woody plants". In: *Global Change Biology* 24.1 (2018), pp. 78–84. DOI: 10.1111/gcb.13824.

[22] Pin Li et al. "Differences in ozone sensitivity among woody species are related to leaf morphology and antioxidant levels". In: *Tree Physiology* 36.9 (Sept. 1, 2016), pp. 1105–1116. DOI: 10.1093/treephys/tpw042.

[23] Michael L. Hillstrom and Richard L. Lindroth. "Elevated atmospheric carbon dioxide and ozone alter forest insect abundance and community composition". In: *Insect Conservation and Diversity* 1.4 (2008), pp. 233–241. DOI: 10.1111/j.1752-4598.2008.00031.x.

[24] James M. W. Ryalls et al. "Air pollution disproportionately impairs beneficial invertebrates: a meta-analysis". In: *Nature Communications* 15.1 (July 11, 2024). Publisher: Nature Publishing Group, p. 5447. DOI: 10.1038/s41467-024-49729-5.

[25] *DIRECTIVE (EU) 2016/ 2284 OF THE EUROPEAN PARLIAMENT AND OF THE COUNCIL on the reduction of national emissions of certain atmospheric pollutants, amending Directive 2003/ 35/ EC and repealing Directive 2001/ 81/ EC*. 2016.

[26] *The National Emission Ceilings Regulations*. 2018.

[27] Sarah Brace, David L. Peterson, and Darci. Bowers. *A guide to ozone injury in vascular plants of the Pacific Northwest.* PNW-GTR-446. Portland, OR: U.S. Department of Agriculture, Forest Service, Pacific Northwest Research Station, 1999, PNW–GTR–446. DOI: 10.2737/PNW-GTR-446.

[28] P. Sicard et al. « Dommages forestiers et pollution à l'ozone dans les réserves naturelles : le cas de l'arolle dans le sud-est de la France - ». In : *Forêt Méditerranéenne* XXXI.3 (2010), p. 273.

[29] Michael Treshow. "Ozone damage to plants". In: *Environmental Pollution (1970)* 1.2 (Oct. 1, 1970), pp. 155–161. DOI: 10.1016/0013-9327(70)90016-9.

[30] M. Schaub et al. *Part VIII: Monitoring of Ozone Injury.* UNECE ICP Forests Programme Co-ordinating Centre, Thünen Institute of Forest Ecosystems, 2016, pp. 1221–1226.

[31] Marco Ferretti et al. "The fingerprint of tropospheric ozone on broadleaved forest vegetation in Europe". In: *Ecological Indicators* 158 (Jan. 1, 2024), p. 111486. DOI: 10.1016/j.ecolind.2023.111486.

[32] Riccardo Marzuoli et al. "Assessing the Impact of Ozone on Forest Trees in An Integrative Perspective: Are Foliar Visible Symptoms Suitable Predictors for Growth Reduction? A Critical Review". In: *Forests* 10.12 (Dec. 2019). Number: 12 Publisher: Multidisciplinary Digital Publishing Institute, p. 1144. DOI: 10.3390/f10121144.

[33] F. Bussotti et al. "Assessment of ozone visible symptoms in the field: perspectives of quality control". In: *Environmental Pollution*. Native Plants as Bioindicators of Air Pollutants: Contributed Papers to a Symposium held in conjunction with the 34th Air Pollution Workshop 125.1 (Sept. 1, 2003), pp. 81–89. DOI: 10.1016/S0269-7491(03)00095-2.

[34] Thomas Abeli and Andrea Di Giulio. "Risks of massive tree planting in Europe should be considered by the EU Forestry Strategy 2030". In: *Restoration Ecology* 31.5 (2023), e13834. DOI: 10.1111/rec.13834.

[35] *COMMUNICATION FROM THE COMMISSION TO THE EUROPEAN PARLIAMENT, THE COUNCIL, THE EUROPEAN ECONOMIC AND SOCIAL COMMITTEE AND THE COMMITTEE OF THE REGIONS New EU Forest Strategy for 2030: The 3 Billion Tree Planting Pledge For 2030*. 2021.

[36] M Meroni et al. "Assessing Steady-state Fluorescence and PRI from Hyperspectral Proximal Sensing as Early Indicators of Plant Stress: The Case of Ozone Exposure". In: *Sensors* 8.3 (Jan. 2008). Number: 3 Publisher: Molecular Diversity Preservation International, pp. 1740–1754. DOI: 10.3390/s8031740.

[37] Antonella Calzone et al. "Oxidative stress assessment by a spectroscopic approach in pomegranate plants under a gradient of ozone concentrations". In: *Environmental and Experimental Botany* 182 (Feb. 2021), p. 104309. DOI: 10.1016/j.envexpbot.2020.104309.

[38] Nichole Gosselin et al. "Using Visual Ozone Damage Scores and Spectroscopy to Quantify Soybean Responses to Background Ozone". In: *Remote Sensing* 12.1 (Jan. 2020). Number: 1 Publisher: Multidisciplinary Digital Publishing Institute, p. 93. DOI: 10.3390/rs12010093.

[39] Moon S. Kim et al. "Assessment of Combined Effects of Elevated Tropospheric O3 and CO2 on Soybean under Well-Watered and Restricted Soil Moisture Conditions by Multispectral Fluorescence Imaging Techniques". In: *Digital Imaging and Spectral Techniques: Applications to Precision Agriculture and Crop Physiology*. John Wiley & Sons, Ltd, 2004, pp. 223–253.

[40] Marchica et al. "Early Detection of Sage (Salvia officinalis L.) Responses to Ozone Using Reflectance Spectroscopy". In: *Plants* 8.9 (Sept. 12, 2019), p. 346. DOI: 10.3390/plants8090346.

[41] Jeremy E. Diem. "Remote Assessment of Forest Health in Southern Arizona, USA: Evidence for Ozone-Induced Foliar Injury". In: *Environmental Management* 29.3 (Mar. 1, 2002), pp. 373–384. DOI: 10.1007/s00267-001-0011-5.

[42] Martina Gäb et al. "NIR-spectroscopic investigation of foliage of ozone-stressed Fagus sylvatica trees". In: *Journal of Forest Research* 11.2 (Apr. 1, 2006), pp. 69–75. DOI: 10.1007/s10310-005-0186-3.

[43] Shawn C Kefauver. "Using topographic and remotely sensed variables to assess ozone injury to conifers in the Sierra Nevada (USA) and Catalonia (Spain)". In: *Remote Sensing of Environment* (2013), p. 11.

[44] M Meroni et al. "Leaf level early assessment of ozone injuries by passive fluorescence and photochemical reflectance index". In: *International Journal of Remote Sensing* 29.17 (Mar. 2008), pp. 5409–5422. DOI: 10.1080/01431160802036292.

[45] Anna Lee Jones et al. "Reflections of stress: Ozone damage in broadleaf saplings can be identified from hyperspectral leaf reflectance". In: *Environmental Pollution* 360 (Nov. 1, 2024), p. 124642. DOI: 10.1016/j.envpol.2024.124642.

[46] *Forestry Statistics 2023: Chapter 1 - Woodland Area & Planting*. Alice Holt: Forest Research, 2023.

[47] R. J. Mitchell et al. "Collapsing foundations: The ecology of the British oak, implications of its decline and mitigation options". In: *Biological Conservation* 233 (May 1, 2019), pp. 316–327. DOI: 10.1016/j.biocon.2019.03.040.

[48] Johannes Wessely et al. "A climate-induced tree species bottleneck for forest management in Europe". In: *Nature Ecology & Evolution* 8.6 (Apr. 29, 2024), pp. 1109–1117. DOI: 10.1038/s41559-024-02406-8.

[49] Liz O'Brien et al. "Managing Trees Species of High Social and Cultural Value: Forest Manager Attitudes towards Pest and Disease Risks to Oak in Britain". In: *Forests* 15.10 (Oct. 2024). Number: 10 Publisher: Multidisciplinary Digital Publishing Institute, p. 1695. DOI: 10.3390/f15101695.

[50] Lorenzo Cotrozzi. "The effects of tropospheric ozone on oaks: A global meta-analysis". In: *Science of The Total Environment* 756 (Feb. 20, 2021), p. 143795. DOI: 10.1016/j.scitotenv.2020.143795.

[51] P. K. Farage. "The effect of ozone fumigation over one season on photosynthetic processes of Quercus robur seedlings". In: *New Phytologist* 134.2 (1996), pp. 279–285. DOI: 10.1111/j.1469-8137.1996.tb04632.x.

[52] Vicent Calatayud et al. "Responses of evergreen and deciduous *Quercus* species to enhanced ozone levels". In: *Environmental Pollution* 159.1 (Jan. 1, 2011), pp. 55–63. DOI: 10.1016/j.envpol.2010.09.024.

[53] Filippo Bussotti et al. "Photosynthesis responses to ozone in young trees of three species with different sensitivities, in a 2-year open-top chamber experiment (Curno, Italy)". In: *Physiologia Plantarum* 130.1 (2007), pp. 122–135. DOI: 10.1111/j.1399-3054.2007.00894.x.

[54] Elisa Pellegrini et al. "Antioxidative responses of three oak species under ozone and water stress conditions". In: *Science of The Total Environment* 647 (Jan. 10, 2019), pp. 390–399. DOI: 10.1016/j.scitotenv.2018.07.413.

[55] Felicity Hayes, Jennifer Williamson, and Gina Mills. "Species-Specific Responses to Ozone and Drought in Six Deciduous Trees". In: *Water, Air, & Soil Pollution* 226.5 (Apr. 24, 2015), p. 156. DOI: 10.1007/s11270-015-2428-0.

[56] B.B. Moura et al. "Visible Foliar Injury and Ecophysiological Responses to Ozone and Drought in Oak Seedlings". In: *Plants* 11.14 (2022). DOI: 10.3390/plants11141836.

[57] Riccardo Marzuoli et al. "Biomass and physiological responses of Quercus robur (L.) young trees during 2 years of treatments with different levels of ozone and nitrogen wet deposition". In: *Trees* 30.6 (Dec. 1, 2016), pp. 1995–2010. DOI: 10.1007/s00468-016-1427-0.

[58] M. D. Morecroft et al. "Effects of climate and management history on the distribution and growth of sycamore (Acer pseudoplatanus L.) in a southern British woodland in comparison to native competitors". In: *Forestry* 81.1 (Feb. 29, 2008), pp. 59–74. DOI: 10.1093/forestry/cpm045.

[59] Nathalie Butt et al. *Initial Results from Establishment of a Long-term Broadleaf Monitoring Plot at Wytham Woods, Oxford, UK*. University of Oxford, Jan. 2009.

[60] M.E. Taylor, M.D. Morecroft, and H.R. Oliver. "The Physical Environment". In: *Wytham Woods: Oxford's Ecological Laboratory*. Ed. by Peter Savill et al. Oxford University Press, June 2, 2011. DOI: 10.1093/acprof:osobl/9780199605187.003.0002.

[61] Arnold John Grayson and Eustace Jones. *Notes on the history of Wytham Estate with special reference to the woodlands.* Oxford: Imperial Forestry Institute, 1956.

[62] M. D. Morecroft and J. M. Roberts. "Photosynthesis and stomatal conductance of mature canopy Oak (Quercus robur) and Sycamore (Acer pseudoplatanus) trees throughout the growing season". In: *Functional Ecology* 13.3 (1999), pp. 332–342. DOI: 10.1046/j.1365-2435.1999.00327.x.

[63] Kris M. Hart et al. "Characteristics of free air carbon dioxide enrichment of a northern temperate mature forest". In: *Global Change Biology* 26.2 (2020), pp. 1023–1037. DOI: 10.1111/gcb.14786.

[64] Richard J. Norby et al. "Enhanced woody biomass production in a mature temperate forest under elevated CO2". In: *Nature Climate Change* 14.9 (Sept. 2024). Publisher: Nature Publishing Group, pp. 983–988. DOI: 10.1038/s41558-024-02090-3.

[65] Richard J. Norby et al. "Model–data synthesis for the next generation of forest free-air CO2 enrichment (FACE) experiments". In: *New Phytologist* 209.1 (2016), pp. 17–28. DOI: 10.1111/nph.13593.

[66] UK AIR DEFRA. *Ozone AOT40 Modelled Background 2019-2023*. 2024.

[67] *The Air Quality Limit Values Regulations 2003*.

[68] Young Lee. *SpecDAL 2.0.0*. 2017.

[69] Claudia Beleites and Valter Sergo. *hyperSpec: a package to handle hyperspectral data sets in R*. Version R Package Version 0.100.2. 2017.

[70] Björn-Helge Mevik and Ron Wehrens. "The pls Package: Principal Component and Partial Least Squares Regression in R". In: *Journal of Statistical Software* 18 (Jan. 10, 2007), pp. 1–23. DOI: 10.18637/jss.v018.i02.

[71] Charles R. Harris et al. "Array programming with NumPy". In: *Nature* 585 (2020), pp. 357–362. DOI: 10.1038/s41586-020-2649-2.

[72] John D Hunter. "Matplotlib: A 2D graphics environment". In: *Computing in science & engineering* 9.3 (2007). Publisher: IEEE, pp. 90–95.

[73] J. W. Rouse et al. "Monitoring vegetation systems in the Great Plains with ERTS". In: NASA. Goddard Space Flight Center 3d ERTS-1 Symp., Vol. 1, Sect. A. NTRS Author Affiliations: Texas A&M Univ. NTRS Report/Patent Number: PAPER-A20 NTRS Document ID: 19740022614 NTRS Research Center: Legacy CDMS (CDMS). Jan. 1, 1974.

[74] C. S. T Daughtry et al. "Estimating Corn Leaf Chlorophyll Concentration from Leaf and Canopy Reflectance". In: *Remote Sensing of Environment* 74.2 (Nov. 1, 2000), pp. 229–239. DOI: 10.1016/S0034-4257(00)00113-9.

[75] Mark N. Merzlyak et al. "Non-destructive optical detection of pigment changes during leaf senescence and fruit ripening". In: *Physiologia Plantarum* 106.1 (1999), pp. 135–141. DOI: 10.1034/j.1399-3054.1999.106119.x.

[76] Daniel A Sims and John A Gamon. "Relationships between leaf pigment content and spectral reflectance across a wide range of species, leaf structures and developmental stages". In: *Remote Sensing of Environment* 81.2 (Aug. 2002), pp. 337–354. DOI: 10.1016/S0034-4257(02)00010-X.

[77] J. A. Gamon, L. Serrano, and J. S. Surfus. "The photochemical reflectance index: an optical indicator of photosynthetic radiation use efficiency across species, functional types, and nutrient levels". In: *Oecologia* 112.4 (Nov. 1, 1997), pp. 492–501. DOI: 10.1007/s004420050337.

[78] Josep Peñuelas, Iolanda Filella, and John A. Gamon. "Assessment of photosynthetic radiation-use efficiency with spectral reflectance". In: *New Phytologist* 131.3 (1995), pp. 291–296. DOI: 10.1111/j.1469-8137.1995.tb03064.x.

[79] Stephen Burt and Tim Burt. *Oxford Weather and Climate Since 1767 (Updated to 2023 from SOGE website.)* Oxford University Press, 2019. 513 pp.

[80] J. L. Baltzer and S. C. Thomas. "Leaf optical responses to light and soil nutrient availability in temperate deciduous trees". In: *American Journal of Botany* 92.2 (2005), pp. 214–223. DOI: 10.3732/ajb.92.2.214.

[81] Annemarie Bastrup-Birk et al. "Studying cumulative ozone exposures in Europe during a 7-year period". In: *Journal of Geophysical Research: Atmospheres* 102 (D20 1997), pp. 23917–23935. DOI: 10.1029/97JD01966.

[82] Gina Mills et al. "Evidence of widespread effects of ozone on crops and (semi-)natural vegetation in Europe (1990–2006) in relation to AOT40- and flux-based risk maps". In: *Global Change Biology* 17.1 (2011), pp. 592–613. DOI: 10.1111/j.1365-2486.2010.02217.x.

[83] Chiara Proietti et al. "Trends in tropospheric ozone concentrations and forest impact metrics in Europe over the time period 2000–2014". In: *Journal of Forestry Research* 32.2 (Apr. 2021), pp. 543–551. DOI: 10.1007/s11676-020-01226-3.

[84] Pierre Sicard et al. "An epidemiological assessment of stomatal ozone flux-based critical levels for visible ozone injury in Southern European forests". In: *Science of The Total Environment* 541 (Jan. 15, 2016), pp. 729–741. DOI: 10.1016/j.scitotenv.2015.09.113.

[85] Robert Guderian. *Air pollution by photochemical oxidants: formation, transport, control, and effects on plants*. Springer, 1985.

[86] Gina Mills et al. *Chapter 3: Mapping critical levels for vegetation*. ICP Vegetation, 2017.

[87] Michele Meroni et al. "Using optical remote sensing techniques to track the development of ozone-induced stress". In: *Environmental Pollution*. Special Issue Section: Ozone and Mediterranean Ecology: Plants, People, Problems 157.5 (May 1, 2009), pp. 1413–1420. DOI: 10.1016/j.envpol.2008.09.018.

[88] Susan L. Ustin and Brian Curtiss. "Spectral characteristics of ozone-treated conifers". In: *Environmental and Experimental Botany* 30.3 (July 1, 1990), pp. 293–308. DOI: 10.1016/0098-8472(90)90041-2.

[89] Linda L. Knudson, Theodore W. Tibbitts, and Gerald E. Edwards. "Measurement of Ozone Injury by Determination of Leaf Chlorophyll Concentration 1". In: *Plant Physiology* 60.4 (Oct. 1, 1977), pp. 606–608. DOI: 10.1104/pp.60.4.606.

[90] Linda Chalker-Scott. "Environmental Significance of Anthocyanins in Plant Stress Responses". In: *Photochemistry and Photobiology* 70.1 (1999), pp. 1–9. DOI: 10.1111/j.1751-1097.1999.tb01944.x.

[91] Richard Taylor-Zavala et al. "Quantifying Biochemical Traits over the Patagonian Sub-Antarctic Forests and Their Relation to Multispectral Vegetation Indices". In: *Remote Sensing* 13.21 (Jan. 2021). Number: 21 Publisher: Multidisciplinary Digital Publishing Institute, p. 4232. DOI: 10.3390/rs13214232.

[92] Yasutomo Hoshika et al. "Species-specific variation of photosynthesis and mesophyll conductance to ozone and drought in three Mediterranean oaks". In: *Physiologia Plantarum* 174.1 (2022), e13639. DOI: 10.1111/ppl.13639.

[93] Gerard Sapes et al. "Mechanistic links between physiology and spectral reflectance enable previsual detection of oak wilt and drought stress". In: *Proceedings of the National Academy of Sciences* 121.7 (Feb. 13, 2024). Publisher: Proceedings of the National Academy of Sciences, e2316164121. DOI: 10.1073/pnas.2316164121.

[94] Beth Fallon et al. "Spectral differentiation of oak wilt from foliar fungal disease and drought is correlated with physiological changes". In: *Tree Physiology* 40.3 (Mar. 11, 2020), pp. 377–390. DOI: 10.1093/treephys/tpaa005.

[95] Xi Yang et al. "Seasonal variability of multiple leaf traits captured by leaf spectroscopy at two temperate deciduous forests". In: *Remote Sensing of Environment* 179 (June 15, 2016), pp. 1–12. DOI: 10.1016/j.rse.2016.03.026.

[96] Angela J. Nunn et al. "Comparison of ozone uptake and sensitivity between a phytotron study with young beech and a field experiment with adult beech (*Fagus sylvatica*)". In: *Environmental Pollution*. Forests Under Changing Climate, Enhanced UV and Air Pollution 137.3 (Oct. 1, 2005), pp. 494–506. DOI: 10.1016/j.envpol.2005.01.036.

[97] J. Cavender-Bares and F. A. Bazzaz. "Changes in drought response strategies with ontogeny in Quercus rubra: implications for scaling from seedlings to mature trees". In: *Oecologia* 124.1 (July 1, 2000), pp. 8–18. DOI: 10.1007/PL00008865.

[98] Sonia Mediavilla and Alfonso Escudero. "Mature trees versus seedlings: Differences in leaf traits and gas exchange patterns in three co-occurring Mediterranean oaks". In: *Annals of Forest Science* 60.5 (July 1, 2003). Publisher: EDP Sciences, pp. 455–460. DOI: 10.1051/forest:2003038.

[99] Sean C. Thomas and William E. Winner. "Photosynthetic differences between saplings and adult trees: an integration of field results by meta-analysis". In: *Tree Physiology* 22.2 (Feb. 1, 2002), pp. 117–127. DOI: 10.1093/treephys/22.2-3.117.

[100] T. Cheng, B. Rivard, and A. Sánchez-Azofeifa. "Spectroscopic determination of leaf water content using continuous wavelet analysis". In: *Remote Sensing of Environment* 115.2 (Feb. 15, 2011), pp. 659–670. DOI: 10.1016/j.rse.2010.11.001.

[101] Paul J Curran. "Remote sensing of foliar chemistry". In: *Remote Sensing of Environment* 30.3 (Dec. 1, 1989), pp. 271–278. DOI: 10.1016/0034-4257(89)90069-2.

[102] Sabine Braun, Christian Schindler, and Beat Rihm. "Growth losses in Swiss forests caused by ozone: Epidemiological data analysis of stem increment of *Fagus sylvatica* L. and *Picea abies* Karst." In: *Environmental Pollution* 192 (Sept. 1, 2014), pp. 129–138. DOI: 10.1016/j.envpol.2014.05.016.

[103] Dominic Fawcett et al. "Multi-Scale Evaluation of Drone-Based Multispectral Surface Reflectance and Vegetation Indices in Operational Conditions". In: *Remote Sensing* 12.3 (Jan. 2020). Number: 3 Publisher: Multidisciplinary Digital Publishing Institute, p. 514. DOI: 10.3390/rs12030514.

3. On mature reflection: Ozone damage can be detected in oak trees by hyperspectral reflectance. *120*

.

4

The effect of elevated CO_2 on hyperspectral leaf reflectance in mature trees

Contents

4.1 Commentary 121
4.2 Manuscript 123
4.2.1 Abstract 124
4.2.2 Introduction 125
4.2.3 Methods 130
4.2.4 Results 135
4.2.5 Discussion 147
4.2.6 Conclusion 150
4.2.7 Acknowledgements 151
4.2.8 Funding 151
4.2.9 Data Availability 151
4.2.10 Declarations 152
References 152

4.1 Commentary

The following paper is under second review at the time of submission in Trees: Structure and Function. In this paper I investigate the effect of elevated CO_2 on *Quercus robur L.* leaf reflectance via the BIFoR FACE CO_2 enrichment experiment in

a mature forest. The aim of this research was to find out whether leaf reflectance will be altered by the CO_2 concentrations we are predicted to reach by 2050. Although this is an interesting question in and of itself, within the context of this thesis it is important to know if elevated CO_2 might affect the O_3 damage reflectance signal identified and tested in Chapter 2 and 3. I found that leaf reflectance was broadly unaffected by elevated CO_2 exposure, although one vegetation index related to senescence (PSRI) significantly increased. Therefore, elevated CO_2 does not have a strong effect on leaf reflectance and should not interfere with reflectance based O_3 monitoring even under the concentrations predicted for 2050 and beyond.

4.2 Manuscript

The effect of elevated CO_2 on hyperspectral leaf reflectance in mature trees

Anna Lee Jones[a], Anna Gardner[b,c], Felicity Hayes[d], Christian Pfrang[c,e], Elizabeth S. Jeffers[a]

[a]*Department of Biology, University of Oxford, South Parks Road, Oxford, UK*
[b]*School of Biological Sciences, University of Birmingham, Birmingham, UK*
[c]*Birmingham Institute of Forest Research, University of Birmingham, Birmingham, UK*
[d]*UK Centre for Ecology & Hydrology, Environment Centre Wales, Deiniol Road, Bangor, UK*
[c]*School of Geography, Earth and Environmental Sciences, University of Birmingham, Birmingham, UK*

Trees: Structure and Function, Under Review

4.2.1 Abstract

Key Message: Experimentally elevated CO_2 does not significantly alter the overall leaf reflectance of mature *Quercus robur L.*, but increases Plant Senescence Reflectance Index (PSRI) indicating a change in the ratio of chlorophyll to carotene content.

Abstract: Rising atmospheric CO_2 concentrations, driven by anthropogenic emissions, are projected to reach 550 ppm by 2050. Elevated CO_2 (eCO_2) is expected to have a fertilisation effect on forests, influencing productivity, water relations, and phenology. However, the impact of eCO_2 on leaf reflectance in mature forests remains poorly understood, despite its critical role in radiative transfer processes. Utilising the Birmingham Institute of Forest Research (BIFoR) Free-Air CO_2 Enrichment (FACE) experiment, we investigated the hyperspectral leaf reflectance of 180-year-old *Quercus robur L.* trees exposed to eCO_2 for seven years. Our results demonstrate that overall leaf reflectance under eCO_2 is similar to that of leaves exposed to ambient CO_2, but the Plant Senescence Reflectance Index (PSRI) is significantly increased under eCO_2. This index relates to the ratio of foliar chlorophyll and carotene pigments. These findings suggest that *Q. robur* canopy reflectance will not significantly shift under future CO_2 conditions, but the relative content of pigments will change, altering the reflectance of specific wavelengths and providing insights into the leaf level physiological and phenological responses of mature trees to eCO_2.

Keywords: Climate change, forests, leaf reflectance, spectroscopy, vegetation indices, forest health.

4.2.2 Introduction

Since 1850, net anthropogenic CO_2 emissions have reached 2400 (±240) Gt, with concentrations in 2019 surpassing levels observed over the past two million years [1]. Under the 'business as usual' RCP 8.5 scenario, atmospheric CO_2 concentrations are predicted to reach 550 ppm by 2050 [1]. Forests are a major component of the terrestrial carbon sink, absorbing 2.4 (±0.4) petagrams of carbon per year (Pg C year–1) globally [2]. CO_2 is the carbon input for photosynthesis in plants and elevated CO_2 (eCO_2) has a stimulating effect on photosynthesis, often referred to as the 'CO_2 fertilisation' effect [3]. CO_2 fertilisation of forests, leading to enhanced productivity, has been observed in recent decades [4, 5]. However, the long-term effect of eCO_2 on mature forests and their role as a carbon sink remains uncertain.

The fertilisation response of tree seedlings and saplings to eCO_2 has been extensively experimentally studied using Free Air CO_2 Enrichment (FACE) experiments (as reviewed by [6–8]). The first generation of FACE experiments provided valuable long-term observations of the effect of eCO_2 on young trees, such as sustained elevated photosynthetic rate [6] and increased fine-root production and throughput of root biomass into the soil [9]. However, these experiments were conducted in young tree plantations, limiting their application to understanding how mature forests will respond to eCO_2 [10, 11]. Notably, results from the Aspen FACE project revealed that responses observed in seedlings and young trees were not always sustained as the stand matured, emphasising the effect of tree age on eCO_2 responses [12]. Wood analysis of Quercus ilex exposed to a lifetime of eCO_2 (at a natural spring) revealed that most growth enhancement occurs when the tree is young [13], leading to ongoing questions about the growth responses of mature forests to eCO_2.

The second generation of FACE experiments seeks to explore the capacity of mature trees to response to eCO_2 across different biomes [14]. This study is based at BIFoR FACE, situated in a 180-year-old Quercus robur (Q. robur) dominated woodland in central England, which has shown increased photosynthetic activity and woody biomass production in the first seven years of eCO_2 exposure [15, 16]. These results contrast with the Eucalyptus FACE experiment (EucFACE) based

in Australia, where increased carbon uptake did not translate into greater carbon sequestration, likely due to phosphorous limitation [17]. As well as the eCO_2 crane experiment in Basel, where after 8 years of eCO_2 treatment, radial stem diameter was not affected in *Quercus petraea* or the other deciduous hardwoods tested [18].

In addition to changes in photosynthetic rate and tree growth, eCO_2 has also been shown to affect water relations in trees. In a synthesis of 13 long term experiments ($>$ 1 year), Medlyn et al found European forest trees exposed eCO_2 had 21% lower stomatal conductance [19], although a recent meta-analysis has shown that the eCO_2 induced increase in WUE was primarily due to increased photosynthesis rather than decreased stomatal conductance [20]. eCO_2 has been shown to increase water use efficiency in mature deciduous forests [21] and Quercus petraea saplings [22]. After 8 years of eCO_2 treatment, water use was significantly reduced in the Basel deciduous forest experiment [18], but at BIFoR FACE although tree's water use was lower on average under eCO_2 this change was not significant [23].

At the leaf level of trees, eCO_2 has been shown to decrease chlorophyll content. Onisch et al reported decreased chlorophyll in young *Picea* and *Fagus* saplings exposed to eCO_2 [24]; and Tausz et al found the needles of young *Picea abies* trees had lower chlorophyll when exposed to eCO_2 [25]. In mature forest grown trees, at the EucFACE experiment mature *Eucalyptus tereticornis* leaves had reduced pigment concentrations (chlorophyll and carotenes) per area [26]. In mature *Liquidambar styraciflua* (sweetgum) leaves from the Oak Ridge FACE experiment, after 12 years of eCO_2 exposure leaves had lower chlorophyll [27]. In the BIFoR FACE experiment, eCO_2 did not affect mass-based chlorophyll concentrations in mature *Q. robur* leaves, but area-based chlorophyll content significantly increased, which was attributed to increased leaf mass per unit area [28]. Similarly, mature *Quercus ilex* and *Quercus pubescens* trees exposed to eCO_2 by a natural spring did not show a significant change in the chlorophyll content of leaves [29].

ECO_2 has been reported to also decrease the nitrogen content of leaves per unit area [6, 7]. In mature *Liquidambar styraciflua* trees, foliar nitrogen decreased 17% under long term eCO_2 [27]. Reduced foliar nitrogen was also found in *Populus*

tremuloides, Betula papyrifera and *Acer saccharum* saplings [30]. It has been indicated that reduced foliar allocation of nitrogen to chlorophyll under eCO_2 follows total nitrogen content [26, 27]. eCO_2 has resulted in reduced foliar phenol content in *Quercus* species [31, 32], although some studies have found this effect is only temporary [33]. In the BIFoR FACE experiment, no significant effect of eCO_2 on the foliar nitrogen content of *Q. robur* foliar has been found [28].

Studies have also examined the effect of eCO_2 on leaf nutrient content, from the perspective of food sources for insects. In a range of deciduous species, saplings grown under eCO_2 have reduced foliar nutritional quality [33]. Carbohydrate concentrations, particularly starch, increase in young trees exposed to eCO_2 [30, 34, 35]. Combined with reduced nitrogen content, this results in increased foliar carbon to nitrogen (C:N) ratios. For example, at the BIFoR FACE experiment the foliar carbon content of fresh leaves was found to be significantly higher under eCO_2 [36].

ECO_2 also decreases the antioxidant content of tree leaves. For instance, in mature Mediterranean *Quercus* trees, eCO_2 reduced antioxidant enzyme activity and increased the ascorbate pool [29, 37]. In *Q. robur* seedlings, superoxide dismutase content decreased under eCO_2 [38] but this has not been investigated in mature *Q. robur* trees. In summary, eCO_2 has been shown to lead to a variety of effects on the phytochemistry of deciduous trees, and on oak trees in particular although there is more limited evidence for the effects on mature trees in forest settings.

Remote sensing of forest health, productivity and biodiversity relies on the reflectance spectra of leaves [39, 40]. Across visible to infrared wavelengths, leaf reflectance is influenced by factors such as pigments, leaf structural composition, and water content [41–43]. Despite its importance, few studies have examined the effect of eCO_2 on the leaf reflectance of mature trees, which could provide important insight into leaf-level changes underpinning forest fertilisation or acclimation. Hyperspectral reflectance data from forests is widely used to remotely sense leaf traits [44], classify species [45], and monitor forest health [46, 47] under natural conditions. Understanding how leaf reflectance will change under future CO_2 concentrations

is therefore crucial for accurately monitoring forest health and productivity in a changing climate.

Our study explores how the leaf reflectance of mature *Quercus robur L.* (*Q. robur*) is affected by eCO_2, using high-resolution leaf level spectroscopy in the range of 350–2500 nm. High-resolution spectroscopy represents a computational and analytical challenge due to large datasets and autocorrelation between wavelength variables; consequently, machine learning techniques are increasingly employed to identify key features in spectral datasets [48]. We used supervised and unsupervised machine learning analyses across the whole spectrum to identify principal components of variation and regions of the spectrum that change under eCO_2, alongside conventional vegetation index analysis. By combining this data-intensive approach with previous physiological and phenological studies from the BIFoR FACE experiment, our study asks how mature *Q. robur* leaf reflectance is affected by future CO_2 conditions.

Leaf-level hyperspectral reflectance studies on trees exposed to eCO_2 are limited and have found variable results. Thomas (2005) found an increase in the reflectance of photosynthetically active radiation (PAR; 400–700 nm) and a decrease in chlorophyll in a glasshouse eCO_2 study on tropical *Leguminosae* saplings [49]. In contrast, Carter et al. (2000) found no significant effect of eCO_2 on the reflectance of young *Acer saccharum* within a 400-850 nm range in open-top chambers [50]. In mature *Quercus pubescens* trees exposed to lifetime eCO_2 via natural springs, normalised difference vegetation index (NDVI) was not affected and nor was Photosynthetic Reflectance Index (PRI) despite photosynthetic enhancement [51]. Similarly, the Oak Ridge FACE experiment reported no significant changes in reflectance at the leaf or canopy level for a *Liquidambar styraciflua* monoculture under eCO_2 [52]. In the EucFACE experiment, harvested leaf reflectance in the PAR spectrum (400-700 nm) was not significantly affected by eCO_2 treatment [26]. However, Pintó-Marijuan et al. successfully used near-infrared (NIR; 1100–2500 nm) reflectance spectroscopy to examine pigment and antioxidant responses of *Quercus ilex* re-sprouts under eCO_2 [53]. Our study aims to expand on these findings by

examining a broad continuous range of hyperspectral reflectance (350–2500 nm) of leaves measured in situ in a mature *Q. robur* forest under eCO_2.

As highlighted, eCO_2 has been shown to affect water use in trees, which may affect the water content of leaves, and therefore water absorption reflectance bands, although this has not been well investigated. However, we do not expect to find a large effect of eCO_2 on water indices in the leaf reflectance of trees at the BIFoR experiment because eCO_2 has not significantly reduced overall tree water use [23]. Similarly, although eCO_2 has been broadly reported to reduce chlorophyll content, at the BIFoR FACE experiment no significant change has been found under eCO_2 in foliar chlorophyll content by mass [28], so we do not expect to find an effect of eCO_2 on chlorophyll-based indices such as NDVI or PRI. Since eCO_2 reduces foliar nitrogen content, one may expect nitrogen indices to decrease under eCO_2, but no CO_2 induced change in foliar nitrogen content has been found so far in the BIFoR experiment [28]. Increased foliar carbohydrate has been found at BIFoR FACE in trees exposed to eCO_2 which could lead to changes in the NIR reflectance of leaves [36]. Broadly, eCO_2 has been shown to decrease carotenoid content in plants [54] which could affect reflectance in the visible region, and the Plant Senescence Reflectance Index (PSRI) due to the reflectance profile of carotene pigment [43, 55].

The aim of our study is to investigate whether long-term eCO_2 changes the leaf reflectance of mature *Q. robur* trees in terms of total reflectance, spectral profile, and vegetation indices. The majority of the relevant literature indicates eCO_2 does not significantly affect the leaf reflectance of trees exposed over long time periods, particularly in mature trees. We therefore hypothesise that eCO_2 will not significantly affect the leaf reflectance profile or total reflectance but may affect specific regions linked to physiological or structural changes. By examining the entire wavelength range reflectance profile as well as traditional vegetation indices, we expect to find more nuanced changes in leaf reflectance.

4.2.3 Methods

Study Site

The Birmingham Institute of Forest Research (BIFoR) has operated a Free-Air Carbon Enrichment (FACE) experiment since 2015 at Mill Haft, Staffordshire, UK (52°48′3.6″ N, 2°18′0″ W). Mill Haft is 19.1 ha of deciduous woodland dominated by *Q. robur* (pedunculate oak) in the canopy and *Corylus avellana* (common hazel) in the understory, situated in a temperate maritime climate [56, 57]. The underlying geology is Helsby Sandstone, and the dominant soil type is Dystric Cambisol, with a sandy clay texture [16]. The long-term average annual temperature of the site is 9 °C, and the average annual rainfall is 690 mm [14]. Since the CO_2 fertilisation experiment began in 2017, mean hourly rainfall has been recorded by four rain gauges on the BIFoR FACE meteorological towers (TR-525M, Texas Electronics, Dallas, Texas), alongside daily mean air temperature (HMP155RH, Vaisala, Helsinki, Finland). During the measurement period of this study, the mean daily rainfall was 1.93 mm, and the mean daily temperature was 15.72 °C.

The BIFoR FACE facility is comprised of three experimental treatments across nine experimental arrays, each 30 m in diameter. The treatments are three "elevated CO_2" arrays (eCO_2) maintained at 150 ± 38 ppm above ambient CO_2, three control arrays exposed to ambient CO_2 (aCO_2), and three undisturbed woodland areas without fumigation infrastructure. In the present study, only four of the infrastructure arrays were studied due to logistical constraints related to tree canopy access. The fumigation infrastructure arrays have operated from budburst to leaf fall (early April to November) during daylight hours since April 2017, for full details of the experimental design, see Hart et al.[56].

Leaf Reflectance Sampling

We recorded the reflectance spectra of adaxial leaf surface of *Q. robur* in the sun exposed canopy of two aCO_2 and two eCO_2 arrays from July to October 2023. Leaf reflectance measurements were taken on 25th July 2023, 10th August 2023, 24th August 2023, and 6th October 2023. On each measurement day, approximately

30 leaf spectra were taken per tree from two trees per array (60 spectra per array). In total, 932 leaf spectra were recorded, with 469 from aCO_2 arrays and 463 from eCO_2 arrays.

Fully expanded leaves were selected that were in the light exposed crown, avoiding leaves with significant herbivory. From the leaves accessible which met these criteria, every third leaf was sampled until 30 spectra had been taken per tree.

Reflectance spectra were recorded using a high-performance single-beam field spectroradiometer over the range 350 nm to 2500 nm using a LC-RP Pro leaf clip with active light source (HR-1024i spectrometer, Spectra Vista Corp, USA). The HR-1024i spectrometer combines three dispersion grating spectrometers which overlap in their wavelength ranges to produce continuous spectra from 350 nm to 2500 nm. The Very Near Infrared (VNIR) spectrometer measures in the range of 350 nm to 1000 nm with a 1.5 nm sampling interval. The first SWIR spectrometer measures in the range of 1000 nm to 1890 nm with a 3.8 nm sampling interval. The second SWIR spectrometer measures in the range of 1890 nm to 2500 nm with a 2.5 nm sampling interval. The spectrometer was calibrated before use by the NERC Field Spectroscopy Facility. The leaf clip attachment is coupled to the spectroradiometer via a 25° armoured fibre optic. The leaf clip forms a seal around the leaf to exclude external light and is illuminated by an internal lamp. The leaf reflectance is integrated within the field of view, approximately 2 cm diameter. An integrating sphere was not used, this allowed time efficient sampling in the canopy and for flat broadleaf samples like oak leaves bi-directional (hotspot) view-illumination geometry is suitable due to the homogenous leaf surface [58]. An integration time of 2 s was used for all measurements.

During leaf reflectance measurements, the spectrometer was referenced using the leaf clip's incorporated reflective standard in the leaf clip every five minutes. The HR-1024i applies automatic dark signal baseline correction to every measurement by taking a dark spectrum before each reflectance measurement.

The leaf clip was attached to the adaxial surface in the centre of each leaf, to the left of the midvein, making sure to avoid smaller veins.

Hyperspectral Processing

All leaf reflectance spectra were imported and processed using the SpecDAL package [59] in Python 3 [60]. The overlapping regions of the spectra produced by the three spectrometers comprising the HR-1024i were stitched to give a continuous spectrum from 350 nm to 2500 nm. The original reflectance spectra were interpolated to obtain data at 1.0 nm wavelength intervals. Absolute reflectance was calculated by multiplying relative reflectance spectra by the laboratory calibrated reflectance of the leaf clip's reference standard panel (as calibrated by the NERC Field Spectroscopy Facility, panel manufactured by Spectra Vista Corp, USA).

Analysis of the hyperspectral dataset was carried out in R version 4.3.2 [61] using the following packages: hyperspec [62], hyperSpec.utils [63], readr [64], dplyr [65], tidyr [66], factoextra [67], caret [68], FactoMineR [69], tibble [70], scutr [71], kableExtra [72], stringr [73], and effectsize [74]. The following packages were used for data visualisation: ggplot2 [75], viridis [76], and ggpubr [77].

Hyperspectral Analysis

We calculated the mean total leaf reflectance for eCO_2 and aCO_2 exposed leaves by integrating reflectance across the wavelength range and assessed the effect of CO_2 treatment via linear mixed-effect modelling.

We calculated the first ten principal components of the hyperspectral dataset and evaluated the percentage of variance explained by each component. Principal component analysis is an unsupervised method of dimension reduction. We then analysed the difference in values of the first four components between CO_2 treatments by visualisation, followed by multivariate mixed-effect modelling.

To assess the degree of difference between leaf spectra exposed to elevated versus ambient CO_2, we tested the ability of a machine learning model to predict CO_2 treatment from leaf reflectance spectra. The spectral data were preprocessed with centring and scaling. Partial least squares discriminant analysis (PLSDA) models were trained on 70% of leaf reflectance measurements (evenly split between leaves measured in ambient and elevated arrays), using ten-fold cross-validation. PLSDA

models were calculated with up to 60 components, and the accuracy of models with different numbers of components was evaluated to select an optimum number of components. The PLSDA model with the optimum number of components was then applied to unseen test spectra, and we evaluated the accuracy of the model's predictions of which CO_2 treatment leaves had been exposed to. We used cumulative wavelength importance to understand which wavelength regions were most important for class separation in the PLSDA model.

Vegetation Indices

We calculated a range of vegetation indices from leaf reflectance spectra and compared the average vegetation index values of leaves exposed to elevated versus ambient CO_2 using mixed-effects modelling. The names, formulas, and original references of the vegetation indices are listed in Table 4.1.

Vegetation Index	Equation	Reference
Normalised Difference Vegetation Index	$NDVI = \frac{\rho_{800} - \rho_{670}}{\rho_{800} + \rho_{670}}$	[78]
Modified Chlorophyll Absorption Ratio Index	$MCARI = \left[(\rho_{700} - \rho_{670}) - 0.2 \times (\rho_{700} - \rho_{550})\right] \times \frac{\rho_{700}}{\rho_{670}}$	[79]
Photochemical Reflectance Index	$PRI = \frac{\rho_{570} - \rho_{530}}{\rho_{570} + \rho_{530}}$	[80, 81]
Plant Senescence Reflectance Index	$PSRI = \frac{\rho_{680} - \rho_{500}}{\rho_{750}}$	[55]
Normalised Difference Nitrogen Index	$NDNI = \frac{\log\left(\frac{1}{p_{1510}}\right) - \log\left(\frac{1}{p_{1680}}\right)}{\log\left(\frac{1}{p_{1510}}\right) + \log\left(\frac{1}{p_{1680}}\right)}$	[82, 83]
Normalised Difference Lignin Index	$NDLI = \frac{\log\left(\frac{1}{p_{1754}}\right) - \log\left(\frac{1}{p_{1680}}\right)}{\log\left(\frac{1}{p_{1754}}\right) + \log\left(\frac{1}{p_{1680}}\right)}$	[82–84]
Normalised Difference Water Index	$NDWI = \frac{p_{860} - p_{1240}}{p_{860} + p_{1240}}$	[85]
Normalised Phaeophytinisation Quotient Index	$NPQI = \frac{p_{415} - p_{435}}{p_{415} + p_{435}}$	[86–88]

Table 4.1: Formula of vegetation indices calculated from leaf reflectance.

Statistical Analysis: Mixed-Effects Modelling

Our dataset contains a hierarchical structure, individual leaves belong to separate trees, arranged in arrays, which then receive different CO_2 treatments. We also took measurements over time, introducing a time series element to our dataset. To explicitly include these sources of variation in our analysis of the effect of eCO_2 on different elements of leaf reflectance, we used linear mixed effects modelling. Mixed-effects modelling models the effect of fixed effects (such as CO_2 treatment) on response variables, as well as modelling the variation in response variable explained by random effects (such as hierarchical structure or time-series). Throughout our analysis we used variations of the model:

$$Response\ variable \sim\ CO_2 + (1|Tree) + (1|Tree : Date) \tag{4.1}$$

The tree ID was used as a random effect throughout because it explained significant amounts of variation, whereas the array number did not explain any further variance when included alongside tree ID. Date of measurement for a given tree also explained variance and so was included as a nested random effect. Model estimation was carried out using Restricted Maximum Likelihood (REML), with Satterthwaite's approximation for degrees of freedom. Multivariate mixed effects modelling was used to model the response of the first four principal components to CO_2 treatment.

When comparing CO_2 treatments, density plots are used instead of traditional box plots to display the data distribution.

4.2.4 Results

Integrated Leaf Reflectance

The average reflectance spectra of leaves exposed to aCO_2 versus eCO_2 are visualised in Fig. 4.1. Visually, the reflectance of leaves exposed to eCO_2 was higher than those exposed to aCO_2, except for the green reflectance peak. At the green reflectance peak (540 nm), leaves exposed to eCO_2 had slightly lower reflectance than leaves exposed to aCO_2. The position of the Red-Edge does not visually differ between

CO_2 treatments. The infrared reflectance peak between 2200 and 2400 nm was elevated and slightly shifted towards lower wavelengths under eCO_2.

The mean integrated reflectance for leaves exposed to eCO_2 was 436.67 (95% CI: 432.40 – 440.93), whereas under aCO_2 treatment it was 423.18 (95% CI: 416.34 – 430.02). Using a linear mixed-effects model, the average integrated leaf reflectance under aCO_2 was an intensity of 423.00 (Standard Error (SE) = 6.93). Under eCO_2 integrated leaf reflectance was on average 13 units higher or 3.07% (SE = 9.81, Satterthwaite's degrees of freedom (DF) = 5.97, Satterthwaite's P = 0.23), though this was not statistically significant. Random effects analysis of the date of measurement and tree ID showed that tree-to-tree variability in integrated leaf reflectance accounted for 72.77 variance (Standard Deviation (SD) = 8.53), while date of measurement accounted for 356.67 variance (SD = 18.89). The residual variance in integrated leaf reflectance was 3523.52, indicating large variability which was not explained by CO_2 treatment, the random effects of tree-to-tree, or date of measurement variability. Inclusion of the array number as a random effect in the model did not explain any further variance.

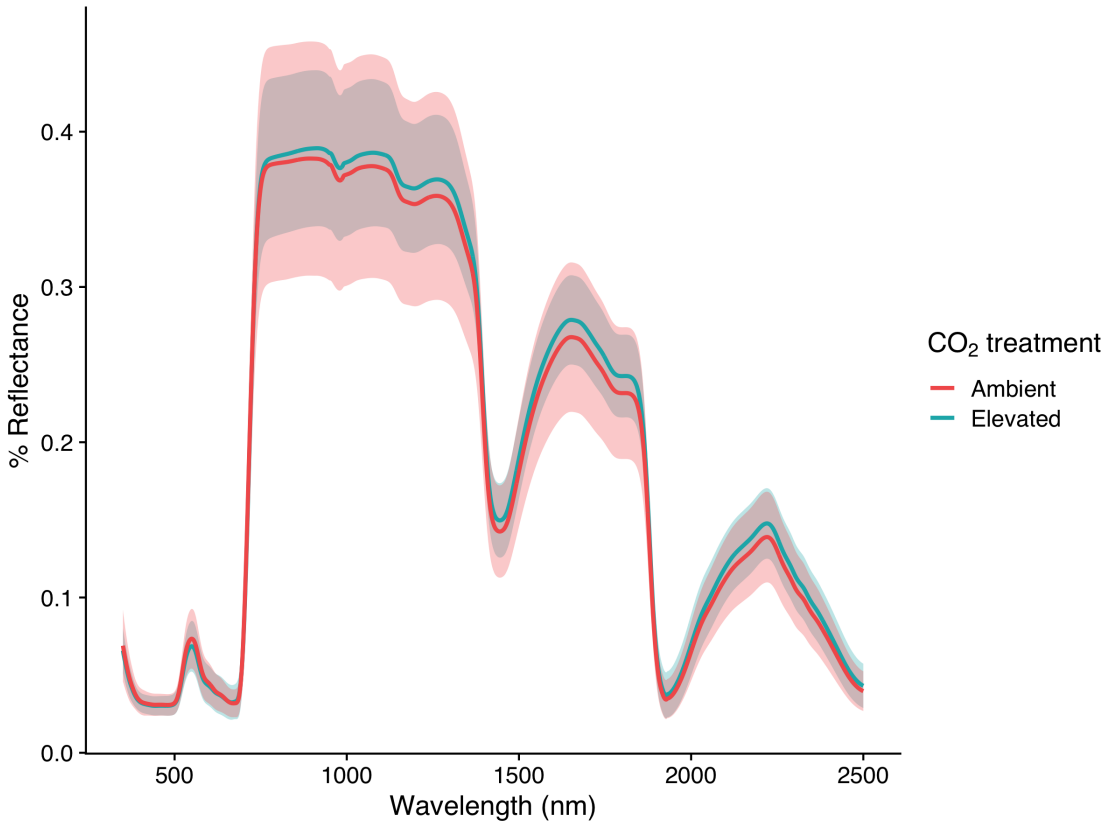


Figure 4.1: Average percentage leaf reflectance spectra across the range of 350–2500 nm of oak leaves exposed to ambient (red) versus elevated (blue) CO_2 treatments at the BIFoR FACE experiment. Shaded areas represent +/− one standard deviation, with red shading for ambient CO_2 and blue shading for elevated CO_2.

Leaf Reflectance Principal Component Analysis

The first four principal components (PCs) cumulatively explained 97.2% of the total variance in hyperspectral leaf reflectance (Fig. 4.2B, PC1: 64.66%, PC2: 23.33%, PC3: 7.04%, PC4: 2.31%). The first component (PC1) is loaded negatively loaded by wavelengths around the red-edge (Fig. 4.2A), while the second component (PC2) is positively loaded by the red-edge and wavelengths between 750 and 1500 nm. The third principal component (PC3) is strongly positively loaded by wavelengths characterising the green peak (550 nm) and red-edge (680–750 nm), and the fourth component (PC4) is strongly negatively loaded by wavelengths characterising the red edge (680–750 nm) and positively loaded by longer wavelengths. When individual leaf reflectance spectra are plotted against combinations of the first four principal components (Fig. 4.2C-F), the spectra show limited clustering by CO_2 dosage. Clustering by CO_2 dosage is clearer against components two and three (Fig. 4.2D), and three and four (Fig. 4.2F). As an unsupervised dimensionality reduction method, principal component analysis reveals that CO_2 treatment has a limited diverging effect on values of the first four principal components of leaf reflectance. Fig. 4.3 shows the difference in density distribution of principal component scores between CO_2 treatments, the clearest difference is in component three which has a narrower spread of lower scores under elevated CO_2 (Fig. 4.3C).

To assess whether CO_2 treatment significantly influenced leaf reflectance spectra as summarised by the first four principal components, we fitted a multivariate linear mixed-effects model with CO_2 treatment as a fixed effect and random intercepts for tree ID and nested date of measurement.

The model had an intercept of 0.066 (SE = 0.063) for ambient CO_2 and the fixed effect of eCO_2 treatment was estimated at –0.1324 (SE = 0.089). However, this difference was not statistically significant (DF = 5.9, P = 0.19). Random effects analyses indicated low between-group variation. The tree-to-tree variance was 0.01 (SD = 0.10) and among the tree-by-date combinations 0.016 (SD = 0.13), while the residual variance (i.e., variation among individual leaves) was substantially larger

(0.79; SD = 0.89). Adding the array as an additional level of random effect did not explain any further variation in the principal components of leaf reflectance spectra.

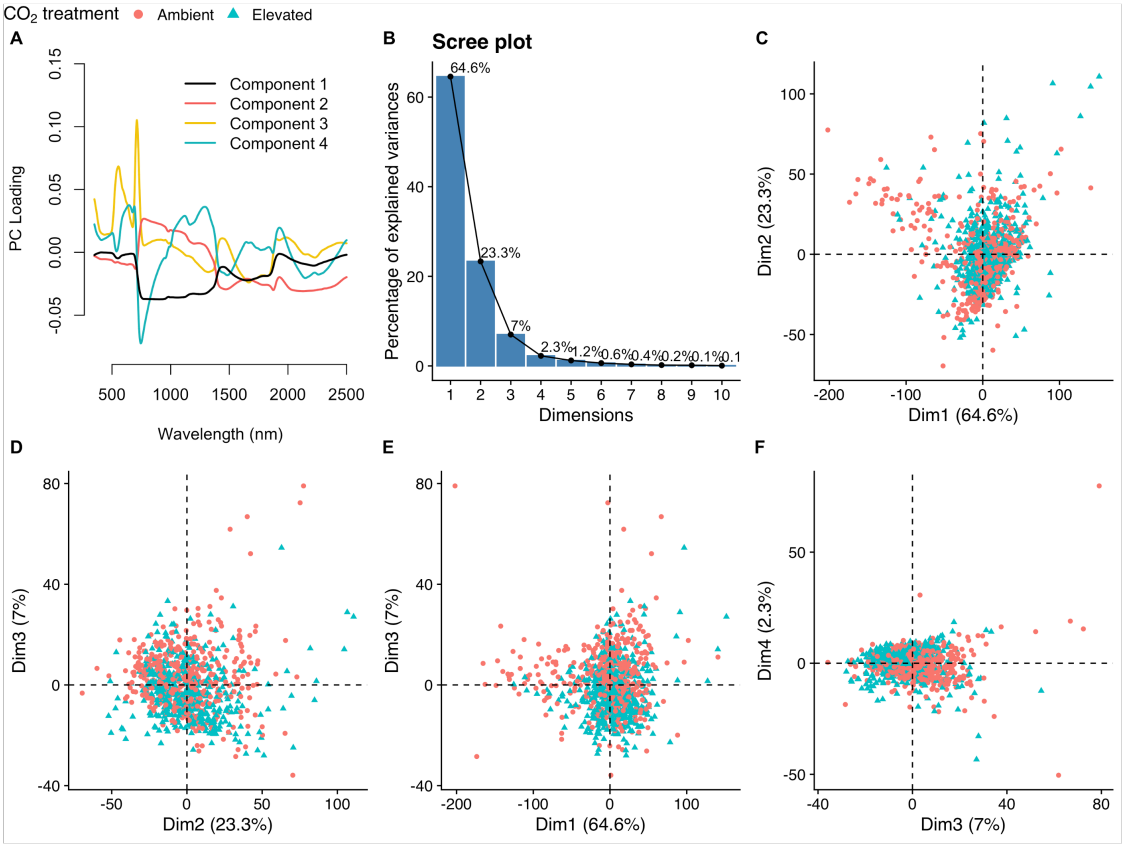


Figure 4.2: Principal component analysis (PCA) of the leaf reflectance spectra in the range 350–2500 nm of oak trees exposed to ambient (red) versus elevated (blue) CO_2 treatments at the BIFoR FACE experiment. A Wavelength (nm) loading of the first four principal components. B Scree plot of variance explained by increasing the number of principal component dimensions. C-F leaf reflectance of trees exposed to ambient (red) versus elevated (blue) CO_2 treatments, plotted against combinations of the first four principal components.

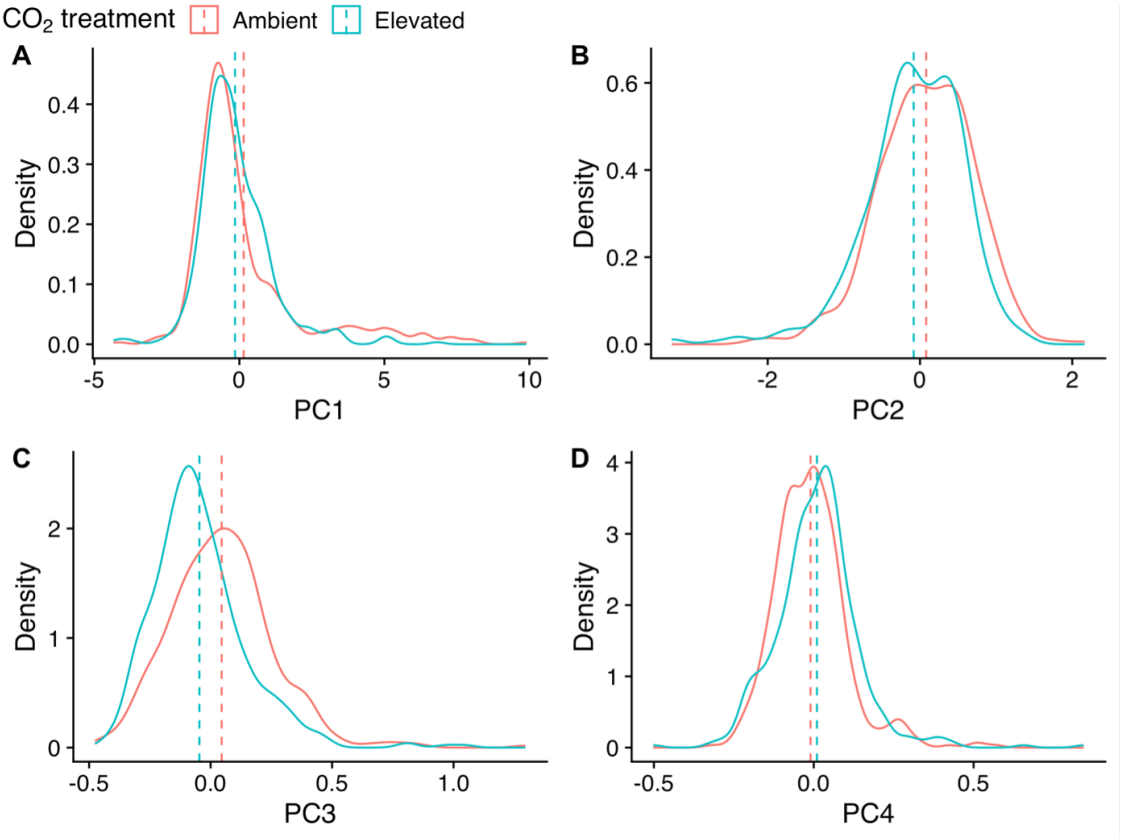


Figure 4.3: Density plots showing the distribution of values of the first four principal components (PC1-4) in leaf reflectance spectra of oak trees exposed to ambient (red lines) versus elevated (blue lines) CO_2 treatment. Vertical dashed lines indicate mean principal component value per treatment (ambient in red, elevated in blue). Panel A represents principal component 1, panel B represents principal component 2, panel C represents principal component 3, and panel D represents principal component 4. Data taken from mature *Quercus robur* trees at the BIFoR FACE experiment, Staffordshire.

Leaf Reflectance Partial Least Squares Discriminant Analysis (PLSDA)

Ten-fold cross-validation of the PLSDA model on the training dataset had the highest accuracy with 44 components (Fig. 4.4, accuracy = 0.89). The 44-component PLSDA model had an accuracy of 0.88 (95% confidence intervals: 0.84, 0.92) for assigning unknown leaf spectra to the correct CO_2 treatment, sensitivity was 0.89, and specificity was 0.87. Compared to the 'no information rate' (assigning all spectra to aCO_2 class), the PLSDA model was significantly more accurate ('no information rate' accuracy = 0.50, $P < 2e - 16$). Between the two classes (aCO_2 and eCO_2), error rates were not significantly different (McNemar's Test, $P = 0.73$). Fig. 4.5 visualises the cumulative importance of different wavelengths in separating the reflectance spectra of aCO_2 leaves from eCO_2 leaves. Key regions of importance include the upper edge of the green reflectance peak (565–580 nm), the water absorption region at 1400 nm, and the short-wave infrared peak at 1600–1720 nm. The 44-component PLSDA model was able to accurately separate leaf spectra exposed to aCO_2 from those exposed to eCO_2.

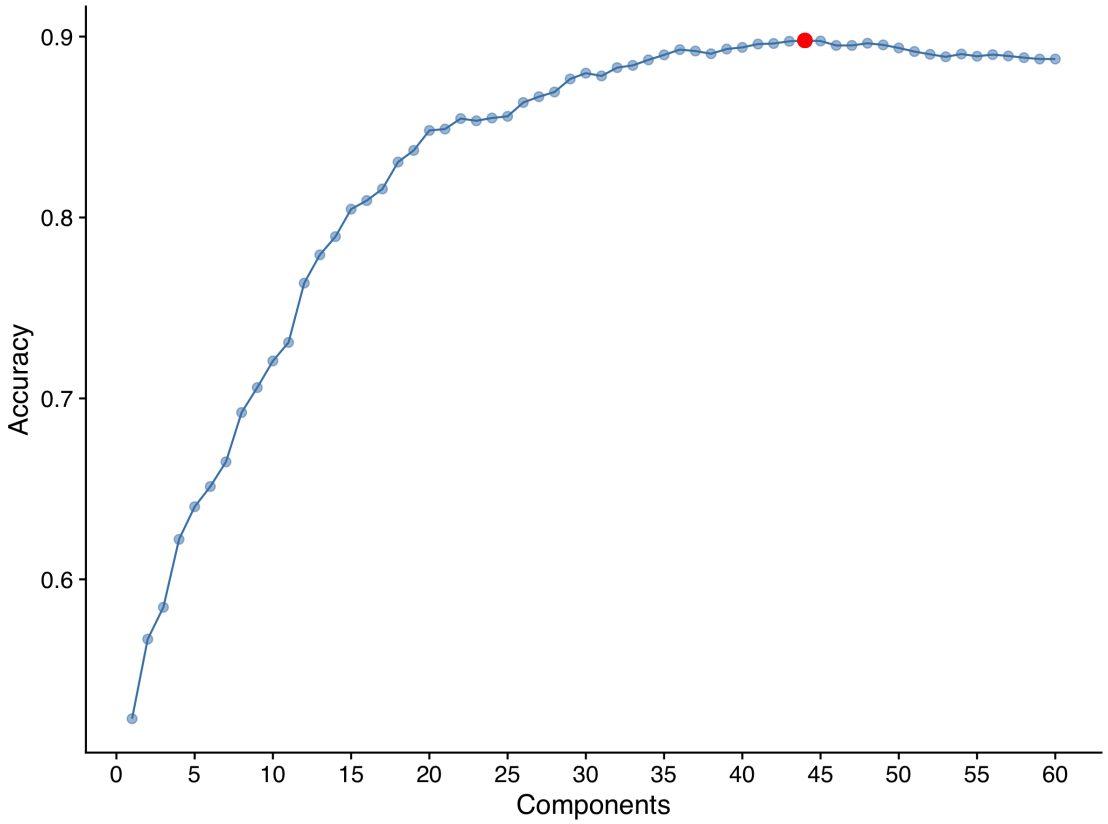


Figure 4.4: Cross-validation tuning of a partial least squares discriminant analysis (PLSDA) model to separate leaves exposed to elevated versus ambient CO_2 by their reflectance spectra. Model accuracy is plotted against number of model components, with the optimum number of model components for maximum accuracy highlighted as a red circle (44 components, 0.89 accuracy).

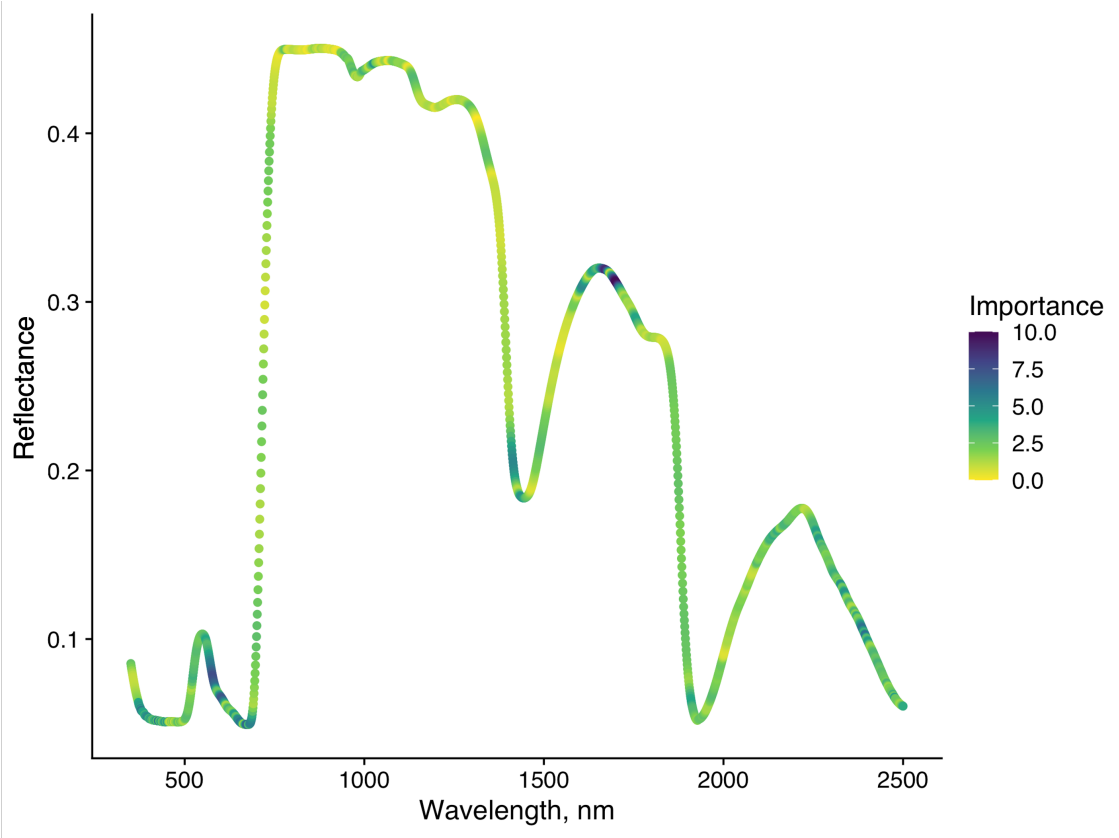


Figure 4.5: Cumulative wavelength (nm) importance for class separation of CO_2 treatments (ambient CO_2 versus elevated CO_2) by leaf reflectance spectra in partial least squares discriminant analysis (PLSDA) model. Colours indicate the importance of each wavelength to the discrimination model.

Vegetation indices

Linear mixed-effects models were fitted to examine the impact of CO_2 treatment on each vegetation index, with random intercepts for tree and for tree-by-date to account for the hierarchical structure. The results of these models are presented in Table 4.2. CO_2 treatment did not have a significant effect on the value of most of the vegetation indices tested except PSRI. Random-effect analysis revealed moderate tree-to-tree variation in all vegetation indices, and moderate variation between dates of measurement, although the majority of variation resided at the residual level indicating the predominant source of variation in most vegetation indices in this experiment was at the leaf level and was not affected by CO_2 treatment. Fig. 4.6 visualises the distributions of vegetation index values of leaves exposed to ambient or elevated CO_2. Although MCARI did not differ significantly between CO_2 treatments, the distribution of values under eCO_2 is much narrower than under aCO_2 indicating reduced variance in MCARI values under eCO_2, Fig. 4.6B. Similarly, there is a narrower distribution of values around the median NDNI (Fig. 4.6E) and NPQI (Fig. 4.6H) values in leaves exposed to eCO_2.

PSRI was significantly higher in leaves exposed to eCO_2 compared to aCO_2 (see Table 4.2, $+2.6 \times 10^2$ PSRI relative to aCO_2, $t(5.97) = 2.5$, $P = 0.049$, Fig. 4.3D). Random-effects analysis revealed moderate variability among trees (variance = 0.14, SD = 0.012) and dates (variance = 0.24, SD = 1.5×10^{-4}), although most of the variation resided at the residual level (variance = 1.8×10^{-3}, SD = 0.043). Leaves exposed to eCO_2 exhibited higher PSRI values throughout the measurement period, whereas the PSRI of leaves exposed to aCO_2 increased steadily from July to October. Fig. 4.6I shows how the average PSRI per CO_2 treatment changed over time.

Index	aCO_2		eCO_2 effect		T value	P value	Tree Variance		Date Variance		Residual Variance		Fig.
	Mean value	SE	Mean effect	SE			Value	SD	Value	SD	Value	SD	
NDVI	8.4×10^{-1}	7.9×10^{-3}	4.1×10^{-3}	1.1×10^{-2}	3.5×10^{-1}	7.4×10^{-1}	1.9×10^{-4}	1.4×10^{-2}	1.9×10^{-4}	1.4×10^{-2}	2.8×10^{-3}	5.3×10^{-2}	6A
MCARI	1.1×10^{-1}	1.6×10^{-2}	-1.0×10^{-2}	2.2×10^{-2}	-4.8×10^{-1}	6.5×10^{-1}	6.6×10^{-4}	2.6×10^{-2}	1.1×10^{-3}	3.3×10^{-2}	2.3×10^{-3}	4.8×10^{-2}	6B
PRI	-1.1×10^{-2}	4.5×10^{-3}	5.1×10^{-4}	6.4×10^{-3}	8.1×10^{-2}	9.4×10^{-1}	6.8×10^{-5}	8.3×10^{-3}	4.2×10^{-5}	6.4×10^{-3}	2.5×10^{-4}	1.6×10^{-2}	6C
PSRI	-3.1×10^{-3}	7.3×10^{-3}	2.6×10^{-2}	1.0×10^{-2}	2.5	4.9×10^{-2}*	1.4×10^{-4}	1.2×10^{-2}	2.4×10^{-4}	1.5×10^{-2}	1.8×10^{-3}	4.3×10^{-2}	6D
NDNI	1.1×10^{-1}	4.7×10^{-3}	2.8×10^{-3}	6.7×10^{-3}	4.2×10^{-1}	6.9×10^{-1}	7.7×10^{-5}	8.8×10^{-3}	3.8×10^{-5}	6.1×10^{-3}	2.3×10^{-4}	1.5×10^{-2}	6E
NDLI	3.5×10^{-2}	1.5×10^{-3}	-3.1×10^{-4}	2.2×10^{-3}	-1.4×10^{-1}	8.9×10^{-1}	8.3×10^{-6}	2.9×10^{-3}	3.0×10^{-6}	1.7×10^{-3}	2.5×10^{-5}	5.0×10^{-3}	6F
NDWI	3.1×10^{-2}	4.7×10^{-3}	-7.0×10^{-3}	6.6×10^{-3}	-1.1	3.3×10^{-1}	6.8×10^{-5}	8.2×10^{-3}	6.0×10^{-5}	7.7×10^{-3}	5.0×10^{-4}	2.2×10^{-2}	6G
NPQI	1.3×10^{-2}	1.7×10^{-3}	2.0×10^{-3}	2.4×10^{-3}	7.6	8.3×10^{-1}	4.1×10^{-6}	2.0×10^{-3}	2.5×10^{-5}	5.0×10^{-3}	1.3×10^{-4}	1.2×10^{-2}	6H

Table 4.2: Summary of linear mixed effect model results for vegetation indices of leaves exposed to ambient (aCO_2) or elevated CO_2 (eCO_2). In all model the degrees of freedom were 5.97, using Satterthwaite's method. P values marked with * indicate a statistically significant effect ($\alpha = 0.05$). All values are given to two significant figures in standard form.

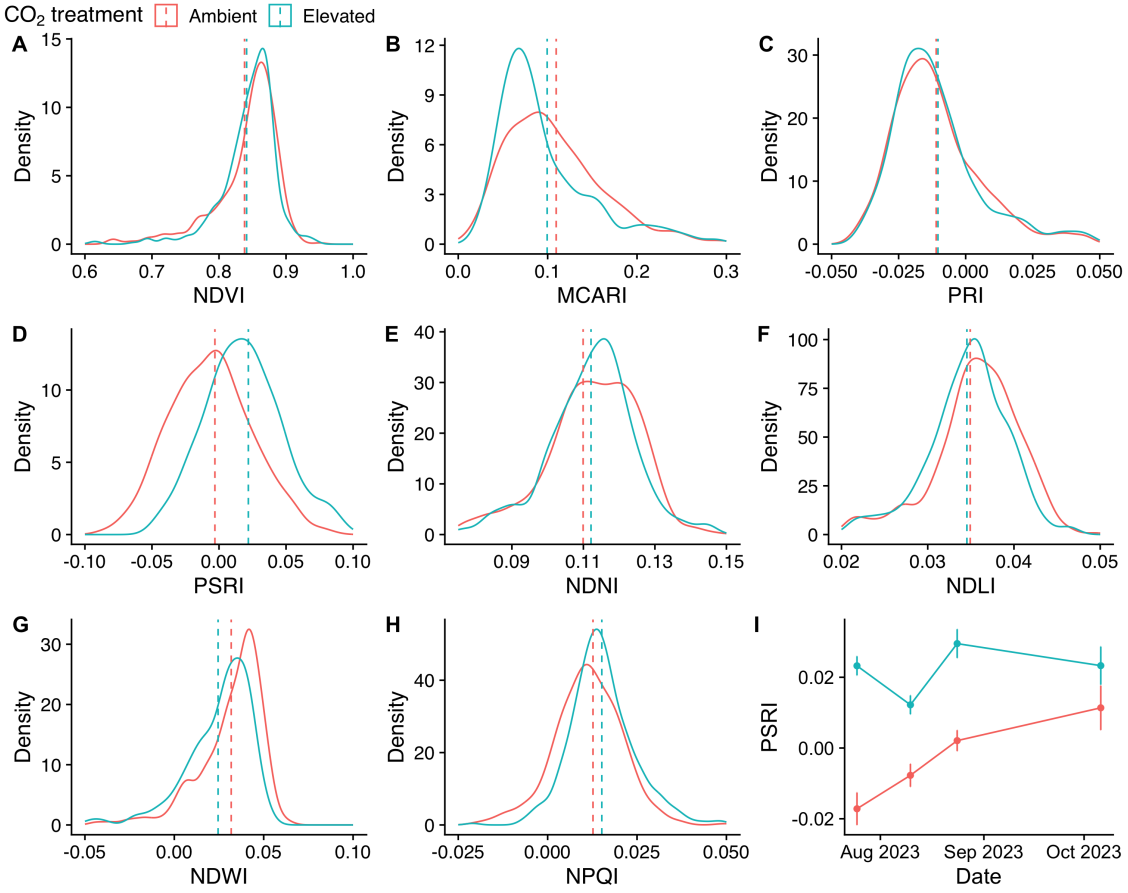


Figure 4.6: A-H: Density plots showing the distribution of values of range of vegetation indices of oak leaves exposed to ambient (in red) or elevated (in blue) CO_2 treatment. Dashed lines indicate the mean value of each vegetation index for each CO_2 treatment. I: Time series of mean Plant Senescence Reflectance Index (PSRI) for each CO_2 treatment.

4.2.5 Discussion

Our analysis shows that most regions of the leaf reflectance spectra of mature *Q. robur* were not significantly affected by eCO_2 treatment after seven years of eCO_2 exposure, except in the case of PSRI which was higher in eCO_2 exposed leaves.

In our study leaves exposed to eCO_2 showed a non-significant trend of increased the integrated leaf reflectance, 3.2% higher than leaves exposed to aCO_2. This result is in contrast to Thomas et al. who found a significant leaf reflectance under eCO_2 in saplings of tropical tree species, however, in their study the extent of reflectance increase varied from 9 to 23% by species and the number of replicates is unclear [49]. It has been suggested that such changes could affect forest albedo [49]. Forest albedo, which refers to the amount of solar radiation reflected back to the atmosphere by forests, plays a critical role in regulating the Earth's climate and is a source of uncertainty in the radiation budget of climate models [89]. Forest albedo is influenced not only by forest structure but also by leaf-level optical properties [90–92]. For example, in China, forest greening between 2002-2019 was accompanied by an increase in short-wave albedo [93]. Luyssaert et al highlighted the lack of consideration of changes to forest albedo in the management of forests aimed at offsetting CO_2 emissions [94]. Despite this, the effect of eCO_2 on forest albedo remains understudied. Our results suggest that in the long-term eCO_2 will not have a significant effect on the total leaf reflectance of mature *Q. robur*, and therefore would not be predicted to affect forest albedo. Further analysis is needed to understand how the total reflectance of different mature tree species will respond to future CO_2 concentrations, as well as the effect on temperate forest albedo.

As hypothesised, the spectral reflectance profile of leaves exposed to eCO_2 was similar to that of leaves exposed to aCO_2. The spectral signature as summarised by the first four principal components was not significantly affected by CO_2 treatment after accounting for hierarchical structure. The large residual in the mixed effects model of principal components suggests that most of the variation in leaf reflectance spectra arose at the leaf level rather than at the tree or temporal level. Most of the vegetation indices examined also did not respond to CO_2 treatment, although

the reduced spread of MCARI, NDNI, and NPQI values under eCO_2 could indicate some form of directional response. The majority of previous studies which have examined the effect of eCO_2 on the leaf reflectance of trees have also not found a significant eCO_2 effect in mature *Quercus pubescens* [51], in young Acer saccharum [50], in mature *Liquidambar styraciflua* [52], nor in mature *Eucalyptus tereticornis* [26]. Significantly increased reflectance in the green peak and red edge was reported in *Pinus strobus L.* exposed to eCO_2 [95]. eCO_2 induced spectral changes have also been reported in crops [96, 97]. On balance, the lack of eCO_2 response in the spectral profile of *Q. robur* in this study is in keeping with previous research in deciduous tree species. This suggests the spectral profile of future deciduous forests will not be broadly altered by future CO_2 concentrations.

Our PLSDA model is useful in highlighting the regions of the spectra which differed most between CO_2 treatments and so answering the question "how does eCO_2 affect leaf reflectance?" in a nuanced way. The key regions of differentiation were the upper edge of the green reflectance peak, the water absorption region at 1400 nm, and the shortwave infrared peak around 1650 nm. Firstly, the green reflectance peak is affected by the overlapping reflectance peaks of different chlorophyll, carotene and anthocyanin pigments [43], so changes in the upper edge green peak reflectance could reflect a change in one or multiple pigment concentrations.

The 1400 nm water absorption peak was also important in differentiating between leaves exposed to different CO_2 treatments. In a different species of oak (*Quercus agrifolia*), the 1650 nm peak has also been shown to correspond to leaf water status [98] but it has not been explicitly characterised in *Q. robur*. Generally, eCO_2 has been found to increase vegetation's water use efficiency (WUE) as a result of stomatal closure and/or increased photosynthetic activity [20, 99]. Additionally, in the BIFoR FACE experiment, there were no significant changes to water used under eCO_2.

Wavelengths in the 1650 nm reflectance peak were the most important in the PLSDA model's differentiation between CO_2 treatments. Tormena et al. (2019) also identified a response to eCO_2 in coffee leaf reflectance bands around 1657 nm and 1698 nm via PLSDA [97]. The 1650 nm peak is an indirect reflectance band,

due to chemicals such as cellulose [100] and affected by leaf water content [101, 102]. The cell wall hemicellulose content increased in *Betula pendula* leaves exposed to eCO_2 [103], but the effect of eCO_2 on leaf cellulose content in oak species has not been well examined. More broadly, eCO_2 has been shown to increase leaf carbohydrate content [30, 34, 35], and at the BIFoR FACE experiment foliar carbon content in fresh leaves was significantly higher under eCO_2 [36], which could include changes to cellulose content. While firm conclusions cannot be drawn from the PLSDA analysis, the importance of wavelengths in the upper green reflectance, water absorption band, and 1650 nm peak are useful to highlight as directions for future investigation of the foliar effects of eCO_2 in mature deciduous trees.

The one vegetation index which CO_2 treatment had a significant effect on was PSRI. PSRI is sensitive to the ratio of carotene to chlorophyll pigments in the leaf and is used as a quantitative measure of senescence-induced degradation of chlorophyll [55]. PSRI was significantly higher under eCO_2 and was elevated early in the growing season compared to trees exposed to aCO_2. This indicates changes in the relative content of carotenes and chlorophyll under eCO_2. Since no changes in chlorophyll content have been found with eCO_2 treatment at BIFoR FACE [28], the increase in PSRI is more likely to be due to increased carotene content than decreased chlorophyll. Reductions in carotene content with eCO_2 treatment have been found previously [54]. In the only study on Q. robur the decrease in carotenoid content under eCO_2 was not significant [104], but this study was on seedlings in pots so may not be transferable to adult trees in a mature forest. Norby et al. (2024) reported leaf loss started earlier in some years under eCO_2 at the BIFoR FACE experiment, which could also lead to earlier chlorophyll breakdown and elevated PSRI [16]. We would encourage future work to examine the pigment concentrations of leaves from the BIFoR FACE experiment via HPLC, to quantify the changes in carotenes indicated by our spectral data and how pigments change seasonally.

In large scale ecosystem manipulation experiments, like the BIFoR FACE experiment, engineering and financial constraints limit the number of replicate arrays and thus limit the "n" of the study. With small numbers of replicate arrays,

very large changes are needed between treatments to produce statistically significant results using traditional statistical methods [16]. Mixed effect modelling goes some way to address this issue. However, the value of observations from large ecosystem manipulation experiments should not be dismissed on account of the difficulty in producing statistically significant results while avoiding pseudo-replication [105].

4.2.6 Conclusion

Long-term exposure to eCO_2 did not significantly change the intensity of leaf reflectance or the overall spectra of mature *Q. robur* trees. However, the Plant Senescence Reflectance Index (PSRI) increased under eCO_2 conditions, indicating a change in the ratio of chlorophyll to carotene pigments. Our analysis also highlighted reflectance changes in the infrared spectrum, which may correspond to alterations in leaf water content and carbohydrate content. Hyperspectral leaf reflectance is a useful tool for understanding the consequences of future atmospheric CO_2 concentrations on foliar features such as pigments.

4.2.7 Acknowledgements

The SVC HR-1024i, leaf clip-reflectance probe attachment, and reflectance panels were loaned from the National Environment Research Council Field Spectroscopy Facility (NERC FSF) under FSF internal loan number 915.1122. The authors gratefully acknowledge NERC FSF for this loan, and for the training and technical advice provided. Fieldwork carried out at the Birmingham Institute of Forest Research FACE Facility was coordinated by Dr Kris Hart and academically supervised by Prof. Christian Pfrang. We would like to thank Prof. Rob Mackenzie for his help initiating this collaboration, and Peter Miles for his enthusiasm and facilitation of canopy access at BIFoR FACE. BIFoR FACE meteorological data was collected and managed by the following contributors: Curioni G., Denny G., Downes T.M., Harper N.J., Hart K.M., Mackenzie A.R., Miles P., Ullah S., Tekinay F. The BIFoR FACE facility is a research infrastructure project supported by the JABBS Foundation and the University of Birmingham.

4.2.8 Funding

This work was supported by the Natural Environment Research Council [grant number: NE/S007474/1]. The BIFoR FACE facility has received support for scientific studies from the Biotechnology and Biological Sciences Research Council (BBSRC), Ecological Continuity Trust (ECT), JABBS Foundation, the John Horseman Trust, the Natural Environment Research Council (NERC), National Science Foundation (NSF), the Woodland Trust and the Newton Fund.

4.2.9 Data Availability

The spectral dataset and analysis code used in this research will be freely available to download at https://doi.org/10.5281/zenodo.14610230 upon publication.

4.2.10 Declarations

Author's Contributions

ALJ, EJ and CP conceived the field experiment. ALJ collected, processed and analysed the data. AG contributed to the interpretation of the results by ALJ. ALJ wrote the first draft. All authors contributed to writing of the final draft.

Conflict of interest

The authors have no relevant financial or non-financial interests to disclose.

References

[1] IPCC. *Climate Change 2021 – The Physical Science Basis: Working Group I Contribution to the Sixth Assessment Report of the Intergovernmental Panel on Climate Change*. Cambridge University Press, 2023. DOI: 10.1017/9781009157896.

[2] Yude Pan et al. "The enduring world forest carbon sink". In: *Nature* 631.8021 (July 2024). Publisher: Nature Publishing Group, pp. 563–569. DOI: 10.1038/s41586-024-07602-x.

[3] P Ciais et al. *Carbon and other biogeochemical cycles. Climate change 2013: the physical science basis. Contribution of working group I to the fifth assessment report of the intergovernmental panel on climate change*. Cambridge: Cambridge University Press, 2013.

[4] Sophie Ruehr et al. "Evidence and attribution of the enhanced land carbon sink". In: *Nature Reviews Earth & Environment* 4.8 (Aug. 2023). Publisher: Nature Publishing Group, pp. 518–534. DOI: 10.1038/s43017-023-00456-3.

[5] Zaichun Zhu et al. "Greening of the Earth and its drivers". In: *Nature Climate Change* 6.8 (Aug. 2016). Publisher: Nature Publishing Group, pp. 791–795. DOI: 10.1038/nclimate3004.

[6] Elizabeth A. Ainsworth and Stephen P. Long. "What have we learned from 15 years of free-air CO2 enrichment (FACE)? A meta-analytic review of the responses of photosynthesis, canopy properties and plant production to rising CO2". In: *New Phytologist* 165.2 (2005), pp. 351–372. DOI: 10.1111/j.1469-8137.2004.01224.x.

[7] David S. Ellsworth et al. "Photosynthesis, carboxylation and leaf nitrogen responses of 16 species to elevated pCO2 across four free-air CO2 enrichment experiments in forest, grassland and desert". In: *Global Change Biology* 10.12 (2004), pp. 2121–2138. DOI: 10.1111/j.1365-2486.2004.00867.x.

[8] Julia Maschler et al. "Links across ecological scales: Plant biomass responses to elevated CO". In: *Global Change Biology* 28.21 (2022), pp. 6115–6134. DOI: 10.1111/gcb.16351.

[9] Richard J. Norby and Donald R. Zak. "Ecological Lessons from Free-Air CO2 Enrichment (FACE) Experiments". In: *Annual Review of Ecology, Evolution, and Systematics* 42 (Volume 42, 2011 Dec. 1, 2011). Publisher: Annual Reviews, pp. 181–203. DOI: 10.1146/annurev-ecolsys-102209-144647.

[10] Richard J. Norby et al. "Forest response to elevated CO2 is conserved across a broad range of productivity". In: *Proceedings of the National Academy of Sciences* 102.50 (Dec. 13, 2005). Publisher: Proceedings of the National Academy of Sciences, pp. 18052–18056. DOI: 10.1073/pnas.0509478102.

[11] U.S. DOE. *Free-Air CO2 Enrichment Experiments: Results, Lessons, and Legacy.* DOE/SC–0202. U.S. Department of Energy Office of Science, 2020.

[12] Andrew J. Burton et al. *IMPACTS OF INTERACTING ELEVATED ATMOSPHERIC CO2 AND O3 ON THE STRUCTURE AND FUNCTIONING OF A NORTHERN FOREST ECOSYSTEM: OPERATING AND DECOMMISSIONING THE ASPEN FACE PROJECT*. DOE-MTU-ER62125, 1135783. June 30, 2014, DOE–MTU–ER62125, 1135783. DOI: 10.2172/1135783.

[13] S. Hättenschwiler et al. "Thirty years of in situ tree growth under elevated CO2: a model for future forest responses?" In: *Global Change Biology* 3 (1997). DOI: 10.1046/j.1365-2486.1997.00105.x.

[14] Richard J. Norby et al. "Model–data synthesis for the next generation of forest free-air CO2 enrichment (FACE) experiments". In: *New Phytologist* 209.1 (2016), pp. 17–28. DOI: 10.1111/nph.13593.

[15] A Gardner et al. "Is photosynthetic enhancement sustained through three years of elevated CO2 exposure in 175-year-old Quercus robur?" In: *Tree Physiology* 42.1 (Jan. 1, 2022), pp. 130–144. DOI: 10.1093/treephys/tpab090.

[16] Richard J. Norby et al. "Enhanced woody biomass production in a mature temperate forest under elevated CO2". In: *Nature Climate Change* 14.9 (Sept. 2024). Publisher: Nature Publishing Group, pp. 983–988. DOI: 10.1038/s41558-024-02090-3.

[17] Mingkai Jiang et al. "The fate of carbon in a mature forest under carbon dioxide enrichment". In: *Nature* 580.7802 (Apr. 2020), pp. 227–231. DOI: 10.1038/s41586-020-2128-9.

[18] Martin K.-F. Bader et al. "Central European hardwood trees in a high-CO2 future: synthesis of an 8-year forest canopy CO2 enrichment project". In: *Journal of Ecology* 101.6 (2013), pp. 1509–1519. DOI: 10.1111/1365-2745.12149.

[19] B. E. Medlyn et al. "Stomatal conductance of forest species after long-term exposure to elevated CO2 concentration: a synthesis". In: *New Phytologist* 149.2 (2001), pp. 247–264. DOI: 10.1046/j.1469-8137.2001.00028.x.

[20] Anna Gardner et al. "Optimal stomatal theory predicts CO responses of stomatal conductance in both gymnosperm and angiosperm trees". In: *New Phytologist* 237.4 (2023), pp. 1229–1241. DOI: 10.1111/nph.18618.

[21] S. Leuzinger and C. Körner. "Water savings in mature deciduous forest trees under elevated CO2". In: *Global Change Biology* 13 (2007). DOI: 10.1111/j.1365-2486.2007.01467.x.

[22] Kojo Kwakye Ofori-Amanfo et al. "Interactive Effect of Elevated CO2 and Reduced Summer Precipitation on Photosynthesis is Species-Specific: The Case Study with Soil-Planted Norway Spruce and Sessile Oak in a Mountainous Forest Plot". In: *Forests* (2020). DOI: 10.3390/f12010042.

[23] Susan E. Quick et al. "Water usage of old-growth oak at elevated CO_2 in the FACE (Free-Air CO_2 Enrichment) of climate change". In: *Biogeosciences* 22.6 (Mar. 25, 2025). Publisher: Copernicus GmbH, pp. 1557–1581. DOI: 10.5194/bg-22-1557-2025.

[24] A. S. W. Onisch et al. "Effects of elevated CO 2 on chloroplast pigments of spruce (Picea abies) and beech (Fagus sylvatica) in model ecosystems as modified by provenance , soil type , and nitrogen supply". In: (2016).

[25] M. Tausz, De Kok, and I. Stulen. "Physiological responses of Norway spruce trees to elevated CO2 and SO2". In: *Journal of Plant Physiology* 148 (1996), pp. 362–367. DOI: 10.1016/S0176-1617(96)80266-5.

[26] Agnieszka Wujeska-Klause et al. "Leaf age and eCO2 both influence photosynthesis by increasing light harvesting in mature *Eucalyptus tereticornis* at EucFACE". In: *Environmental and Experimental Botany* 167 (Nov. 1, 2019), p. 103857. DOI: 10.1016/j.envexpbot.2019.103857.

[27] Jeffrey M. Warren et al. "Carbon dioxide stimulation of photosynthesis in Liquidambar styraciflua is not sustained during a 12-year field experiment". In: *AoB PLANTS* 7 (Jan. 1, 2015), plu074. DOI: 10.1093/aobpla/plu074.

[28] A. Gardner et al. "Are chlorophyll concentrations and nitrogen across the vertical canopy profile affected by elevated CO2 in mature Quercus trees?" In: *Trees* 36.6 (Dec. 1, 2022), pp. 1797–1809. DOI: 10.1007/s00468-022-02328-7.

[29] P. Schwanz and A. Polle. "Antioxidative systems, pigment and protein contents in leaves of adult mediterranean oak species (Quercus pubescens and Q. ilex) with lifetime exposure to elevated CO2." In: *The New phytologist* 140 3 (1998), pp. 411–423. DOI: 10.1111/J.1469-8137.1998.00290.X.

[30] Jep Agrell, Evan P. McDonald, and Richard L. Lindroth. "Effects of CO2 and light on tree phytochemistry and insect performance". In: *Oikos* 88.2 (2000), pp. 259–272. DOI: 10.1034/j.1600-0706.2000.880204.x.

[31] R. Tognetti and Jon D. Johnson. "The effect of elevated atmospheric CO2 concentration and nutrient supply on gas exchange, carbohydrates and foliar phenolic concentration in live oak (Quercus virginiana Mill.) seedlings". In: *Annals of Forest Science* 56 (1999), pp. 379–389. DOI: 10.1051/FOREST:19990503.

[32] Yoko Watanabe et al. "Effects of Elevated CO2 and Nitrogen Loading on the Defensive Traits of Three Successional Deciduous Broad-Leaved Tree Seedlings". In: *Forests* (2021). DOI: 10.3390/F12070939.

[33] S. Dury et al. "The effects of increasing CO2 and temperature on oak leaf palatability and the implications for herbivorous insects". In: *Global Change Biology* 4 (1998). DOI: 10.1046/j.1365-2486.1998.00102.x.

[34] P. D. Coley et al. "Effects of elevated CO2 on foliar chemistry of saplings of nine species of tropical tree". In: *Oecologia* 133 (2002), pp. 62–69. DOI: 10.1007/s00442-002-1005-6.

[35] Karl K. Kinney et al. "Effects of Co2 and No3– Availability on Deciduous Trees: Phytochemistry and Insect Performance". In: *Ecology* 78.1 (1997), pp. 215–230. DOI: 10.1890/0012-9658(1997)078[0215:EOCANA]2.0.CO;2.

[36] Aradhana J. Roberts et al. "Effects of Elevated Atmospheric CO2 Concentration on Insect Herbivory and Nutrient Fluxes in a Mature Temperate Forest". In: *Forests* 13.7 (July 2022). Number: 7 Publisher: Multidisciplinary Digital Publishing Institute, p. 998. DOI: 10.3390/f13070998.

[37] R. Marabottini et al. "Foliar antioxidant status of adult Mediterranean oak species (Quercus ilex L. and Q. pubescens Willd.) exposed to permanent CO2-enrichment and to seasonal water stress." In: *Environmental pollution* 115 3 (2001), pp. 413–23. DOI: 10.1016/S0269-7491(01)00231-7.

[38] P. Schwanz et al. "Responses of Antioxidative Systems to Drought Stress in Pendunculate Oak and Maritime Pine as Modulated by Elevated CO2". In: *Plant Physiology* 110.2 (Feb. 1, 1996), pp. 393–402. DOI: 10.1104/pp.110.2.393.

[39] Patrick Kacic and Claudia Kuenzer. "Forest Biodiversity Monitoring Based on Remotely Sensed Spectral Diversity—A Review". In: *Remote Sensing* 14.21 (Oct. 26, 2022), p. 5363. DOI: 10.3390/rs14215363.

[40] Angela Lausch et al. "Understanding Forest Health with Remote Sensing -Part I—A Review of Spectral Traits, Processes and Remote-Sensing Characteristics". In: *Remote Sensing* 8.12 (Dec. 2016). Number: 12 Publisher: Multidisciplinary Digital Publishing Institute, p. 1029. DOI: 10.3390/rs8121029.

[41] E. Baldini et al. "Leaf characteristics and optical properties of different woody species". In: *Trees* 12.2 (Dec. 1, 1997), pp. 73–81. DOI: 10.1007/s004680050124.

[42] Lois Grant. "Diffuse and specular characteristics of leaf reflectance". In: *Remote Sensing of Environment* 22.2 (July 1, 1987), pp. 309–322. DOI: 10.1016/0034-4257(87)90064-2.

[43] Daniel A Sims and John A Gamon. "Relationships between leaf pigment content and spectral reflectance across a wide range of species, leaf structures and developmental stages". In: *Remote Sensing of Environment* 81.2 (Aug. 2002), pp. 337–354. DOI: 10.1016/S0034-4257(02)00010-X.

[44] Litong Chen et al. "Predicting leaf traits of temperate broadleaf deciduous trees from hyperspectral reflectance: can a general model be applied across a growing season?" In: *Remote Sensing of Environment* 269 (Feb. 1, 2022), p. 112767. DOI: 10.1016/j.rse.2021.112767.

[45] Eetu Puttonen et al. "Tree species classification from fused active hyperspectral reflectance and LIDAR measurements". In: *Forest Ecology and Management* 260.10 (Oct. 15, 2010), pp. 1843–1852. DOI: 10.1016/j.foreco.2010.08.031.

[46] Rei Sonobe and Quan Wang. "Towards a Universal Hyperspectral Index to Assess Chlorophyll Content in Deciduous Forests". In: *Remote Sensing* 9.3 (Mar. 2017). Number: 3 Publisher: Multidisciplinary Digital Publishing Institute, p. 191. DOI: 10.3390/rs9030191.

[47] Pablo Torres et al. "The Role of Remote Sensing for the Assessment and Monitoring of Forest Health: A Systematic Evidence Synthesis". In: *Forests* 12.8 (Aug. 2021). Number: 8 Publisher: Multidisciplinary Digital Publishing Institute, p. 1134. DOI: 10.3390/f12081134.

[48] Carlos A. Meza Ramirez et al. "Applications of machine learning in spectroscopy". In: *Applied Spectroscopy Reviews* 56.8 (Nov. 26, 2021), pp. 733–763. DOI: 10.1080/05704928.2020.1859525.

[49] Sean C. Thomas. "Increased leaf reflectance in tropical trees under elevated CO2". In: *Global Change Biology* 11.2 (2005), pp. 197–202. DOI: 10.1111/j.1529-8817.2005.00907.x.

[50] Gregory A. Carter, Raj Bahadur, and Richard J. Norby. "Effects of elevated atmospheric CO2 and temperature on leaf optical properties in *Acer saccharum*". In: *Environmental and Experimental Botany* 43.3 (June 1, 2000), pp. 267–273. DOI: 10.1016/S0098-8472(00)00048-4.

[51] C. D. Stylinski et al. "Effects of lifelong [CO2] enrichment on carboxylation and light utilization of Quercus pubescens Willd. examined with gas exchange, biochemistry and optical techniques". In: *Plant, Cell & Environment* 23.12 (2000), pp. 1353–1362. DOI: 10.1046/j.1365-3040.2000.00638.x.

[52] Haley F. Wicklein et al. "Variation in foliar nitrogen and albedo in response to nitrogen fertilization and elevated CO2". In: *Oecologia* 169.4 (Aug. 1, 2012), pp. 915–925. DOI: 10.1007/s00442-012-2263-6.

[53] M. Pintó-Marijuan et al. "Antioxidant and photoprotective responses to elevated CO2 and heat stress during holm oak regeneration by resprouting, evaluated with NIRS (near-infrared reflectance spectroscopy)". In: *Plant Biology* 15 (s1 2013), pp. 5–17. DOI: 10.1111/j.1438-8677.2011.00538.x.

[54] Irakli Loladze et al. "Rising Atmospheric CO2 Lowers Concentrations of Plant Carotenoids Essential to Human Health: Meta-analysis." In: *Molecular nutrition & food research* (2019). DOI: 10.1002/mnfr.201801047.

[55] Mark N. Merzlyak et al. "Non-destructive optical detection of pigment changes during leaf senescence and fruit ripening". In: *Physiologia Plantarum* 106.1 (1999), pp. 135–141. DOI: 10.1034/j.1399-3054.1999.106119.x.

[56] Kris M. Hart et al. "Characteristics of free air carbon dioxide enrichment of a northern temperate mature forest". In: *Global Change Biology* 26.2 (2020), pp. 1023–1037. DOI: 10.1111/gcb.14786.

[57] A. Rob MacKenzie et al. "BIFoR FACE: Water–soil–vegetation–atmosphere data from a temperate deciduous forest catchment, including under elevated CO". In: *Hydrological Processes* 35.3 (2021), e14096. DOI: 10.1002/hyp.14096.

[58] Aarne Hovi et al. "Evaluation of Accuracy and Practical Applicability of Methods for Measuring Leaf Reflectance and Transmittance Spectra". In: *Remote Sensing* 10.1 (Jan. 2018). Number: 1 Publisher: Multidisciplinary Digital Publishing Institute, p. 25. DOI: 10.3390/rs10010025.

[59] Young Lee. *SpecDAL 2.0.0*. 2017.

[60] Guido Van Rossum and Fred L. Drake. *Python 3 Reference Manual*. Scotts Valley, CA: CreateSpace, 2009.

[61] R Core Team. *R: a language and environment for statistical computing*. manual. Vienna, Austria: R Foundation for Statistical Computing, 2023.

[62] Claudia Beleites and Valter Sergo. *hyperSpec: a package to handle hyperspectral data sets in R*. Version R Package Version 0.100.2. 2017.

[63] Konrad Mayer. *hyperSpec.utils: Utility functions to work with objects of the hyperSpec class*. manual. 2024.

[64] Hadley Wickham, Jim Hester, and Jennifer Bryan. *readr: Read rectangular text data*. 2024.

[65] Hadley Wickham et al. *dplyr: a grammar of data manipulation*. manual. 2023.

[66] Hadley Wickham, Davis Vaughan, and Maximilian Girlich. *tidyr: Tidy messy data*. manual. 2024.

[67] Alboukadel Kassambara and Fabian Mundt. *factoextra: Extract and visualize the results of multivariate data analyses*. manual. 2020.

[68] Kuhn and Max. "Building predictive models in R using the caret package". In: *Journal of Statistical Software* 28.5 (2008), pp. 1–26. DOI: 10.18637/jss.v028.i05.

[69] Sébastien Lê, Julie Josse, and François Husson. "FactoMineR: a package for multivariate analysis". In: *Journal of Statistical Software* 25.1 (2008), pp. 1–18. DOI: 10.18637/jss.v025.i01.

[70] Kirill Müller and Hadley Wickham. *tibble: Simple data frames*. manual. 2023.

[71] Keenan Ganz. *scutr: Balancing multiclass datasets for classification tasks*. manual. 2023.

[72] Hao Zhu. *kableExtra: Construct complex table with 'kable' and pipe syntax*. manual. 2024.

[73] Hadley Wickham. *stringr: Simple, consistent wrappers for common string operations*. manual. 2023.

[74] Mattan S. Ben-Shachar, Daniel Lüdecke, and Dominique Makowski. "effectsize: Estimation of effect size indices and standardized parameters". In: *Journal of Open Source Software* 5.56 (2020). Publisher: The Open Journal, p. 2815. DOI: 10.21105/joss.02815.

[75] Hadley Wickham. *ggplot2: Elegant graphics for data analysis*. 2016.

[76] Garnier et al. *Viridis - colorblind-friendly color maps for R*. 2024. DOI: 10.5281/zenodo.4679423.

[77] Alboukadel Kassambara. *ggpubr: 'ggplot2' based publication ready plots*. 2023.

[78] J. W. Rouse et al. "Monitoring vegetation systems in the Great Plains with ERTS". In: NASA. Goddard Space Flight Center 3d ERTS-1 Symp., Vol. 1, Sect. A. NTRS Author Affiliations: Texas A&M Univ. NTRS Report/Patent Number: PAPER-A20 NTRS Document ID: 19740022614 NTRS Research Center: Legacy CDMS (CDMS). Jan. 1, 1974.

[79] C. S. T Daughtry et al. "Estimating Corn Leaf Chlorophyll Concentration from Leaf and Canopy Reflectance". In: *Remote Sensing of Environment* 74.2 (Nov. 1, 2000), pp. 229–239. DOI: 10.1016/S0034-4257(00)00113-9.

[80] J. A. Gamon, L. Serrano, and J. S. Surfus. "The photochemical reflectance index: an optical indicator of photosynthetic radiation use efficiency across species, functional types, and nutrient levels". In: *Oecologia* 112.4 (Nov. 1, 1997), pp. 492–501. DOI: 10.1007/s004420050337.

[81] Josep Peñuelas, Iolanda Filella, and John A. Gamon. "Assessment of photosynthetic radiation-use efficiency with spectral reflectance". In: *New Phytologist* 131.3 (1995), pp. 291–296. DOI: 10.1111/j.1469-8137.1995.tb03064.x.

[82] Lydia Serrano, Josep Peñuelas, and Susan L Ustin. "Remote sensing of nitrogen and lignin in Mediterranean vegetation from AVIRIS data: Decomposing biochemical from structural signals". In: *Remote Sensing of Environment* 81.2 (Aug. 1, 2002), pp. 355–364. DOI: 10.1016/S0034-4257(02)00011-1.

[83] Th. Fourty et al. "Leaf optical properties with explicit description of its biochemical composition: Direct and inverse problems". In: *Remote Sensing of Environment* 56.2 (May 1, 1996), pp. 104–117. DOI: 10.1016/0034-4257(95)00234-0.

[84] Jerry M. Melillo, John D. Aber, and John F. Muratore. "Nitrogen and Lignin Control of Hardwood Leaf Litter Decomposition Dynamics". In: *Ecology* 63.3 (1982), pp. 621–626. DOI: 10.2307/1936780.

[85] Bo-cai Gao. "NDWI—A normalized difference water index for remote sensing of vegetation liquid water from space". In: *Remote Sensing of Environment* 58.3 (Dec. 1, 1996), pp. 257–266. DOI: 10.1016/S0034-4257(96)00067-3.

[86] J Peñuelas et al. "Reflectance assessment of mite effects on apple trees". In: *International Journal of Remote Sensing* 16.14 (Sept. 20, 1995), pp. 2727–2733. DOI: 10.1080/01431169508954588.

[87] J. D. Barnes et al. "A reappraisal of the use of DMSO for the extraction and determination of chlorophylls *a* and *b* in lichens and higher plants". In: *Environmental and Experimental Botany* 32.2 (Apr. 1, 1992), pp. 85–100. DOI: 10.1016/0098-8472(92)90034-Y.

[88] R. Ronen and Margalith Galun. "Pigment extraction from lichens with dimethyl sulfoxide (DMSO) and estimation of chlorophyll degradation". In: *Environmental and Experimental Botany* 24.3 (Aug. 1, 1984), pp. 239–245. DOI: 10.1016/0098-8472(84)90004-2.

[89] Sara Alibakhshi et al. "Quantitative analysis of the links between forest structure and land surface albedo on a global scale". In: *Remote Sensing of Environment* 246 (Sept. 1, 2020), p. 111854. DOI: 10.1016/j.rse.2020.111854.

[90] Hans Henniger et al. "A New Approach Combining a Multilayer Radiative Transfer Model with an Individual-Based Forest Model: Application to Boreal Forests in Finland". In: *Remote Sensing* 15.12 (June 12, 2023), p. 3078. DOI: 10.3390/rs15123078.

[91] D. Y. Hollinger et al. "Albedo estimates for land surface models and support for a new paradigm based on foliage nitrogen concentration". In: *Global Change Biology* 16.2 (2010), pp. 696–710. DOI: 10.1111/j.1365-2486.2009.02028.x.

[92] Félicien Meunier et al. "Liana optical traits increase tropical forest albedo and reduce ecosystem productivity". In: *Global Change Biology* 28.1 (2022), pp. 227–244. DOI: 10.1111/gcb.15928.

[93] Hao Yan et al. "Forest Greening Increases Land Surface Albedo During the Main Growing Period Between 2002 and 2019 in China". In: *JOURNAL OF GEOPHYSICAL RESEARCH-ATMOSPHERES* 126.6 (Mar. 27, 2021). Num Pages: 17 Place: Washington Publisher: Amer Geophysical Union Web of Science ID: WOS:000634788300006, e2020JD033582. DOI: 10.1029/2020JD033582.

[94] Sebastiaan Luyssaert et al. "Trade-offs in using European forests to meet climate objectives". In: *Nature* 562.7726 (Oct. 2018). Publisher: Nature Publishing Group, pp. 259–262. DOI: 10.1038/s41586-018-0577-1.

[95] Gregory A. Carter, Joanne Rebbeck, and Kevin E. Percy. "Leaf optical properties in Liriodendrontulipifera and Pinusstrobus as influenced by increased atmospheric ozone and carbon dioxide". In: *Canadian Journal of Forest Research* 25.3 (Mar. 1995). Publisher: NRC Research Press, pp. 407–412. DOI: 10.1139/x95-045.

[96] Sharon B. Gray, Orla Dermody, and Evan H. DeLucia. "Spectral reflectance from a soybean canopy exposed to elevated CO2 and O3". In: *Journal of Experimental Botany* 61.15 (Oct. 1, 2010), pp. 4413–4422. DOI: 10.1093/jxb/erq244.

[97] Cláudia Domiciano Tormena et al. "Potential biomonitoring of atmospheric carbon dioxide in Coffea arabica leaves using near-infrared spectroscopy and partial least squares discriminant analysis". In: *Environmental Science and Pollution Research* 26.29 (Oct. 1, 2019), pp. 30356–30364. DOI: 10.1007/s11356-019-06163-1.

[98] R. Pu et al. "Spectral absorption features as indicators of water status in coast live oak (Quercus agrifolia) leaves". In: *International Journal of Remote Sensing* 24.9 (2003), p. 1799.

[99] M. E. Gilbert et al. "Field confirmation of genetic variation in soybean transpiration response to vapor pressure deficit and photosynthetic compensation". In: *Field Crops Research* 124.1 (Oct. 9, 2011), pp. 85–92. DOI: 10.1016/j.fcr.2011.06.011.

[100] Paul J Curran. "Remote sensing of foliar chemistry". In: *Remote Sensing of Environment* 30.3 (Dec. 1, 1989), pp. 271–278. DOI: 10.1016/0034-4257(89)90069-2.

[101] F. M. DANSON et al. "High-spectral resolution data for determining leaf water content". In: *International Journal of Remote Sensing* 13.3 (Feb. 1, 1992), pp. 461–470. DOI: 10.1080/01431169208904049.

[102] Q. Tian et al. "Spectroscopic determination of wheat water status using 1650-1850 nm spectral absorption features". In: *International Journal of Remote Sensing* 22.12 (Jan. 1, 2001), pp. 2329–2338. DOI: 10.1080/01431160118199.

[103] Elina Oksanen et al. "Structural characteristics and chemical composition of birch (Betula pendula) leaves are modified by increasing CO2 and ozone". In: *Global Change Biology* 11.5 (2005), pp. 732–748. DOI: 10.1111/j.1365-2486.2005.00938.x.

[104] P. Schwanz and A. Polle. "Differential stress responses of antioxidative systems to drought in pendunculate oak (Quercus robur) and maritime pine (Pinus pinaster) grown under high CO(2) concentrations". In: *Journal of Experimental Botany* 52.354 (Jan. 2001), pp. 133–143.

[105] G. Matt Davies and Alan Gray. "Don't let spurious accusations of pseudoreplication limit our ability to learn from natural experiments (and other messy kinds of ecological monitoring)". In: *Ecology and Evolution* 5.22 (2015), pp. 5295–5304. DOI: 10.1002/ece3.1782.

4. The effect of elevated CO_2 on hyperspectral leaf reflectance in mature trees 161

.

5

An exploration of remote sensing ozone damage to forests

Contents

5.1 Abstract 162
5.2 Introduction 163
5.3 Methods 165
5.3.1 O_3 Input Data 165
5.3.2 Vegetation Indices 166
5.3.3 Forest Cover 167
5.3.4 Data Processing 167
5.3.5 Data Visualisation and Analysis 167
5.4 Results 168
5.5 Discussion 172
References 176

5.1 Abstract

This chapter investigates the relationship between ozone (O_3) exposure and satellite derived Modified Chlorophyll Absorption Reflectance Index (MCARI). I conducted this preliminary satellite analysis on forested regions in the UK, using modelled O_3 exposure data. While my previous leaf-level studies demonstrated that MCARI is sensitive to O_3 exposure, this analysis revealed no significant relationship between

satellite derived annual MCARI and cumulative O_3 exposure (summarised by AOT40) in UK forests. High variability in AOT40 and MCARI, along with limitations in spatial and temporal resolution, likely obscured potential patterns. This chapter also examines the challenges associated with scaling from leaf reflectance to remote sensing applications, addressing issues such as reduced signal-to-noise ratios and canopy structure. I highlight the necessity of higher-resolution O_3 exposure data, improved scaling methodologies, and further spectral analyses across vegetation types and at intermediate spatial scales.

5.2 Introduction

Although the effects of O_3 damage on the physiology and growth of some tree species have been well studied [1], the extent of global O_3 damage to forests is not well understood. Risk assessments based on O_3 concentration and flux have helped to estimate the risk to forests by O_3 [2], but wide-scale monitoring of the extent of O_3 damage is reliant on manual inspection of visible foliar injury [3]. Although visible foliar injury monitoring coordinated by the Convention on Long-range Transboundary Air Pollution (CLRTAP) and its International Co-operative Programme on Assessment and Monitoring of Air Pollution Effects on Forests (ICP Forests), has shown frequent foliar symptoms across Europe [3, 4], manual leaf inspection is inherently limited in coverage, accuracy, and speed [5]. My previous work has demonstrated spectral detection of O_3 damage in broadleaf temperate species [6, 7], which has the potential to be scaled up to a remote sensing application. A remote sensing approach to detecting O_3 damage to forests would allow comprehensive coverage over large spatial scales, as well as regularly repeated measurements to understand changing patterns over time.

There have been a small number of local studies assessing the relationship between remotely sensed indices and O_3 induced foliar injury. Kefauver et al found a significant relationship between the photochemical reflective index (PRI) and position of the red edge peak in canopy hyperspectral reflectance collected via aircraft with field assessments of visual injury in conifers in California and Catalonia

[8]. In Arizona, Diem found an association between NDVI and O_3 exposure between 1970s and 1990s in conifer canopies in Arizona [9]. More recent studies have focussed on the correlation between remotely sensed gross or net primary productivity (GPP, NPP) and O_3 measurements to attribute reductions in forest productivity to O_3 damage. Proietti et al found significant reductions in MODIS satellite derived GPP associated with O_3 exposure across 37 European forest sites between 2000-2010, although reductions in GPP ranged between 0.4 and 30% [10]. Shimizu et al assessed the linear correlation between NPP and O_3 concentrations above 40 ppb, and found reductions in NPP between 4 and 48% across different vegetation types in the Kanto region of Japan [11].

Within a range of broadleaf saplings and mature oak trees, I identified the Modified Chlorophyll Absorption Reflectance Index (MCARI) as the vegetation index most sensitive to O_3 exposure and most reflective of visible O_3-induced damage at the leaf level [6, 7]. Vegetation indices, in essence, quantify the ratio of reflected light intensity at two or more wavelengths. As relative, rather than absolute, measures of reflectance, they can be compared across varying measurement scales and methodologies. Based on my leaf-level analysis, I hypothesise that, at broader spatial scales, MCARI will increase with O_3 exposure in temperate broadleaf forests. However, I have not yet explored the extent to which my leaf level findings apply when analysed at the canopy scale. Additionally, when scaling up a signature found in leaf reflectance, the strength of the signal to noise ratio decreases as detection moves from the leaf level to more remote applications.

In this chapter, I present a preliminary satellite-based analysis examining the relationship between O_3 exposure and MCARI in the UK. Additionally, I outline a methodological framework for such analyses, acknowledging the limitations of the restricted spatio-temporal scope of this trial. This analysis is centred on the UK because my previous findings are specific to temperate deciduous broadleaf species, my experimental work was conducted in UK forests, additionally I was able to freely access high spatial resolution modelled O_3 exposure for the UK. The analysis is constrained to forested areas to ensure relevance to the studied ecosystems.

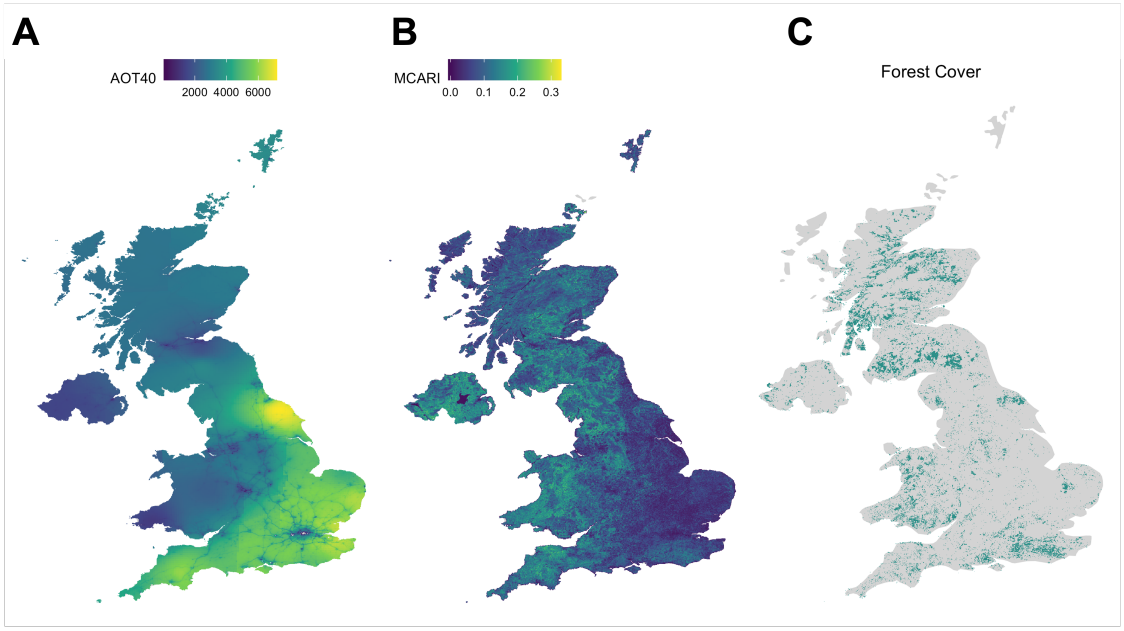


Figure 5.1: Visualisation of the input map layers used to analyse the correlation between annual O_3 concentrations above 40 ppb (AOT40, panel A) and the vegetation index MCARI (B). Layers B and C were cropped to the forested areas shown in blue C, taken from 2020 map of world forest cover. 2019 MCARI and AOT40 data are presented for illustrative purposes.

5.3 Methods

Surface level O_3 data is available from networks of monitoring sites, ozonesondes, satellite retrievals, as well as atmospheric models which combine these data sources. In the UK DEFRA commission 1 km resolution atmospheric model maps of O_3 each year for the purpose of monitoring compliance with air quality regulations [12, 13]. I used this data source because it was the highest spatial resolution O_3 exposure data freely available for the UK.

Initial mapping and data filtering was done in Google Earth Engine, a cloud based geospatial analysis software with an extensive satellite data library of publicly available data [14].

5.3.1 O_3 Input Data

I used the AOT40 annual background model provided by DEFRA's Pollution Climate Mapping Model as input O_3 data in this analysis [12]. AOT40 is the

accumulated excess of hourly O_3 concentration is above 40 ppb between 8:00 and 20:00 central European time from May to July per year. For each hour, the difference between the O_3 concentration and 40 ppb is added to a running total, expressed in ppb hours. AOT40 is the current European [15] and UK standard to assess whether vegetation is at risk from O_3 damage, with a target limit of $18\,000\,\mu g\,m^{-3}\,h$ in the UK [13]. DEFRA's AOT40 model data has a $1\,km^2$ spatial resolution and was analysed for the years 2019-2023. An example of the 2019 AOT40 data is shown in Figure 5.1, panel A.

5.3.2 Vegetation Indices

Of the pre-existing vegetation indices investigated in Chapters 2 and 3, MCARI was the most strongly and consistently correlated with O_3 exposure. MCARI was therefore chosen as the candidate satellite derived vegetation index for this analysis. MCARI was calculated from sentinel 2 data [16] over the UK from 2019-2023, according to Equation 5.1, where B stands for Band [17]

$$MCARI = ((B5 - B4) - 0.2(B5 - B3))\left(\frac{B5}{B4}\right) \tag{5.1}$$

Example MCARI data for 2019 is presented in Figure 5.1, panel B. I used Sentinel 2 data because it is publicly available and has high spatio-temporal resolution, however it is a multispectral satellite so has lower spectral resolution than hyperspectral satellite products. Sentinel 2 is available for cloud-based analysis in Google Earth Engine, which eliminates the data processing concerns associated with local analysis of high resolution satellite data.

The same methodology was also applied to NDVI and GRVI. GRVI is the closest multispectral vegetation index to the hyperspectral vegetation index calculated to be most strongly correlated to O_3 exposure in Chapter 3, and NDVI is widely used as an indicator of vegetation health. NDVI and GRVI were calculated as per Equation 5.2 [18] and Equation 5.3 [19], respectively. The results relating to these vegetation indices are presented in Appendix D.

$$NDVI = \frac{(B8 - B4)}{(B8 + B4)} \tag{5.2}$$

$$GRVI = \frac{(B3 - B4)}{(B3 - B4)} \tag{5.3}$$

5.3.3 Forest Cover

I limited the analysis to forested areas of the UK. Forest cover was taken from Potapov et al's map of 2020 global forest cover at 10 m spatial resolution based on Landsat data [20]. I chose this forest cover dataset because it is recent, freely available, has high spatial resolution and is based on global observations. I then down sampled the forest cover map of the UK to 1km resolution, 1 km^2 cells with over 75% forest cover were classed as forested. The resulting 1 km resolution UK forest cover map is shown in Figure 5.1, panel C.

5.3.4 Data Processing

The Sentinel 2 from June to October each year were filtered to only include cloudless images using the Sentinel 2 Quality Assurance cloud and cirrus bands. The median composite was then calculated for each year, MCARI was then calculated from the annual composite for year. The MCARI annual maps were then down sampled to 1 km resolution. An example of the 2019 MCARI data is shown in Figure 5.1, panel C.

The AOT40 O_3 layer and MCARI layer were masked by the forest cover layer, to yield an annual map of AOT40 and MCARI in forested areas of the UK for the years 2019-2023. These annual maps were then exported as geotiff files. A random sample of 20,000 forested cells was taken from the annual maps of each year and exported.

5.3.5 Data Visualisation and Analysis

Maps were plotted in R [21] using the packages terra [22], ggplot [23], viridis [24], cowplot [25], and ggpubr [26]. The package biscale [27] was used to calculate a bivariate variable for MCARI and AOT40 which was then visualised as a bivariate map. The AOT40 and MCARI of sampled cells were then normalised and correlatively analysed using a linear model.

5.4 Results

The AOT40 maps shown in Figure 5.2 demonstrate a strong spatial pattern of O_3 exposure across the UK. O_3 exposure is higher in the south of the UK, and in most years the highest AOT40 exposure in forested areas is found in the southernmost region, Cornwall. In 2019 AOT40 exposure was highest on the East coast in the North York Moors. In all years the AOT40 O_3 exposure of forested areas increased with latitude.

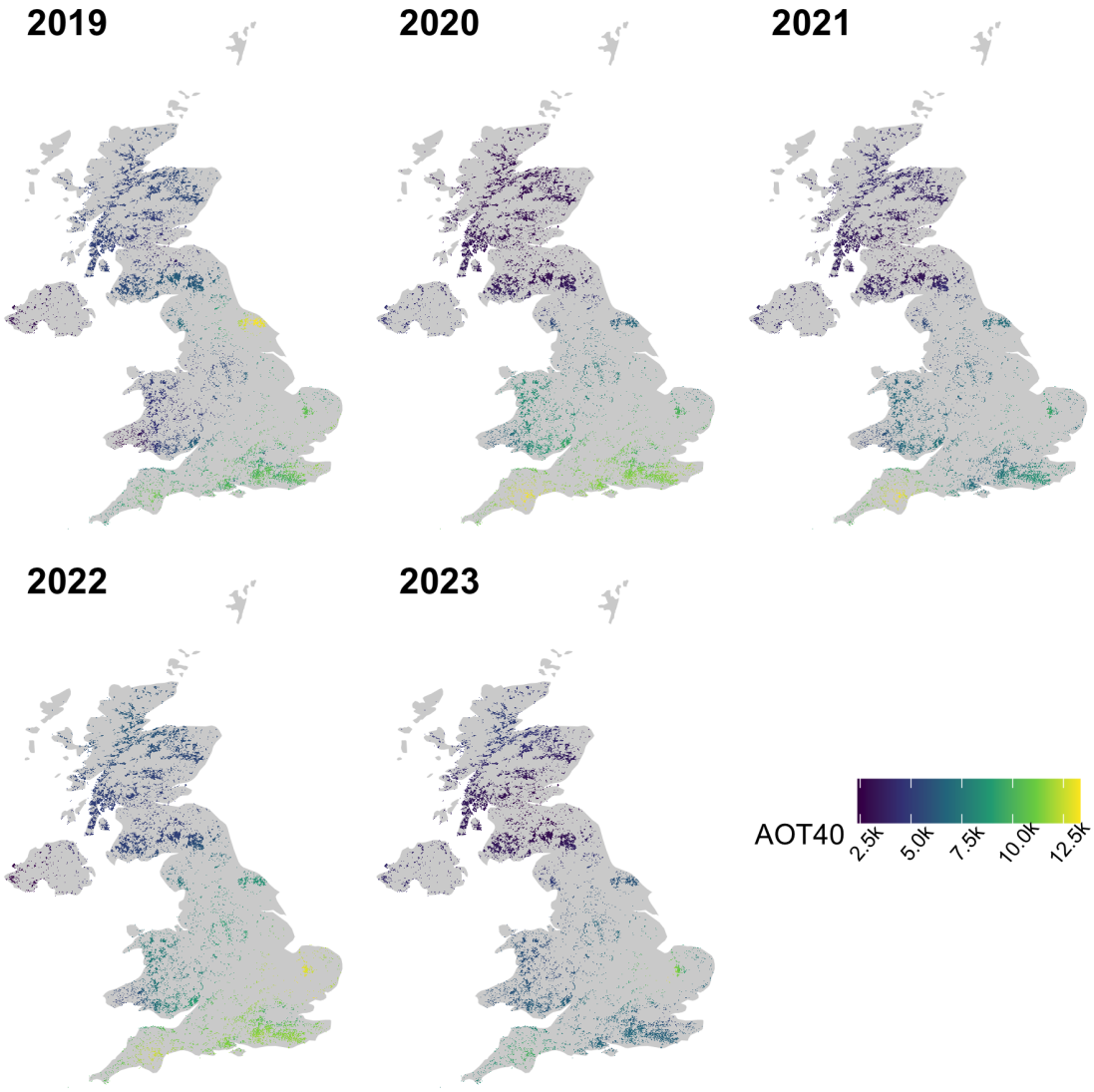


Figure 5.2: Maps of annual accumulated daytime O_3 exposure above 40 ppb between May and July, AOT40, in ppb hours, for forested areas of the UK 2019-2023.

Figure 5.3 shows annual median MCARI of forested areas. MCARI combines

reflectance intensities at 700, 670 and 550 nm (Equation 5.1), and is inversely related to chlorophyll content [17]. There was inter-annual variation in the median values of MCARI, but broadly forested areas in the west of the UK had higher MCARI corresponding to lower chlorophyll content.

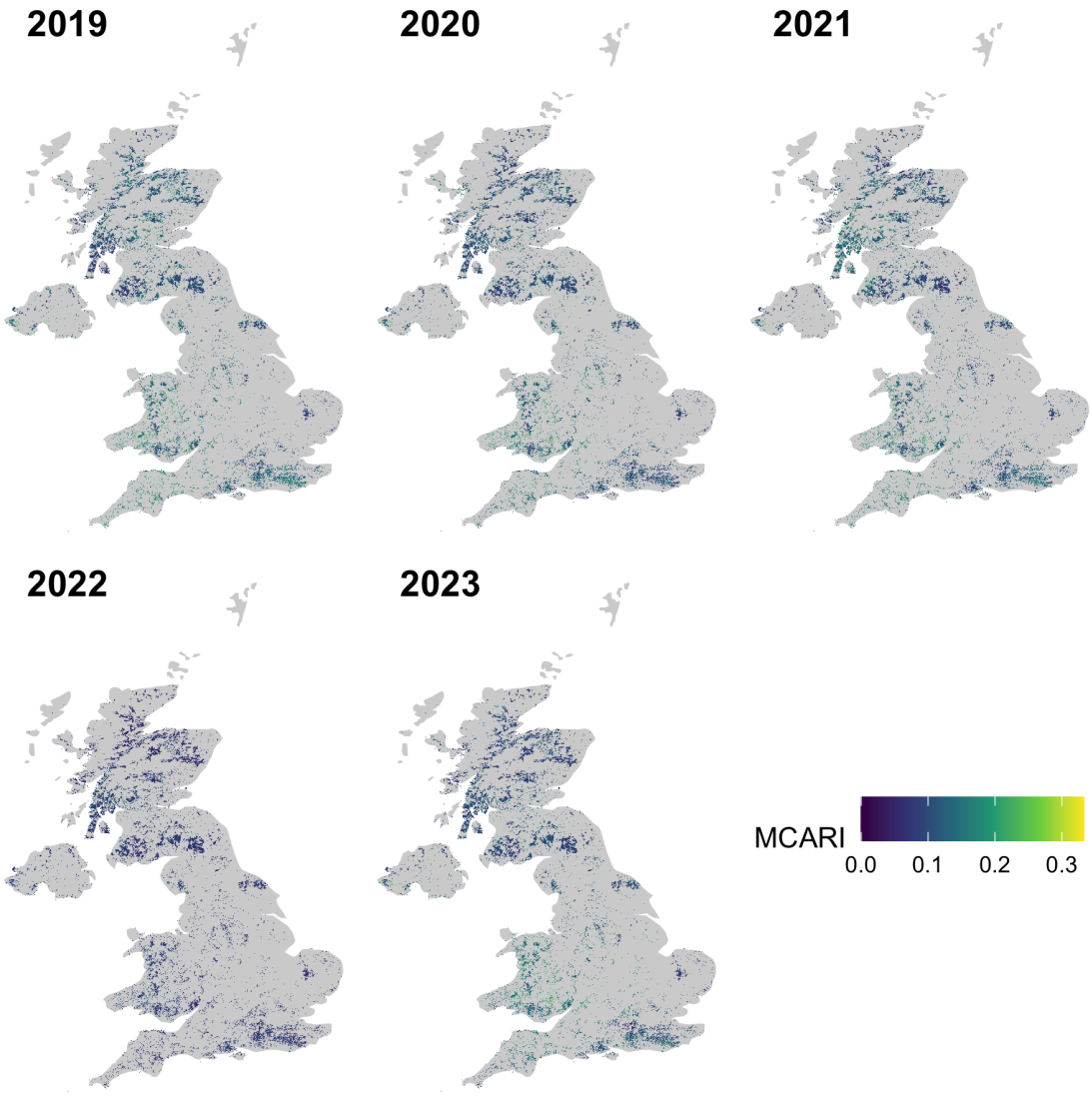


Figure 5.3: Maps of median annual MCARI of forested areas of the UK, calculated from Sentinel 2 data down sampled to 1 km spatial resolution.

The correlation between annual AOT40 and MCARI in forests areas of the UK is shown in Figure 5.4 and by the bivariate map in Figure 5.5. There was no significant relationship between AOT40 and MCARI for any of the years analysed. In 2023, a weak positive relationship is seen (Figure 5.4E, correlation coefficient

$= 0.27$, $R^2 = 0.07$) but this did not explain a significant proportion of the variance. As highlighted by the bivariate colour scheme in Figure 5.5, many forested areas had high MCARI without high AOT40 and vice versa.

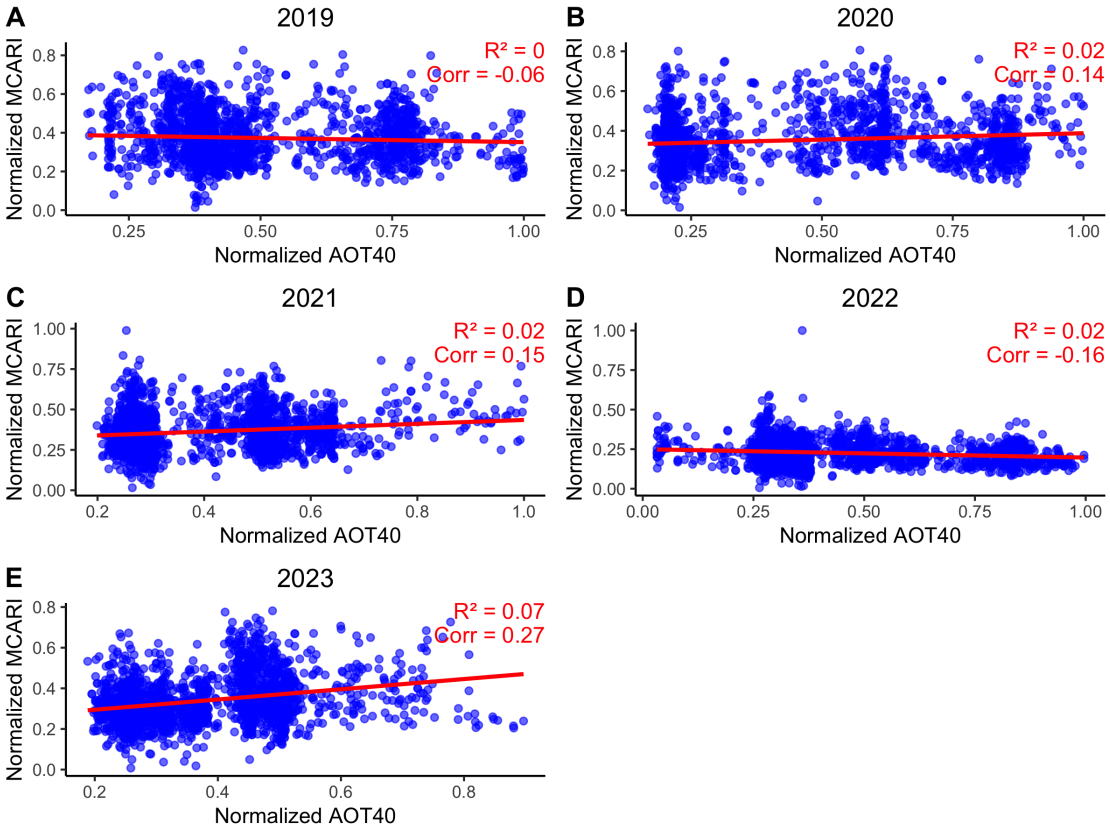


Figure 5.4: The correlative relationship between annual MCARI and AOT40 for 20,000 forested 1 km cells in the UK plotted in blue, fitted with linear models in red. The R^2 and correlation coefficient ($Corr$) are shown red text. Analysis for the years 2019-2023 are shown in panels A-E.

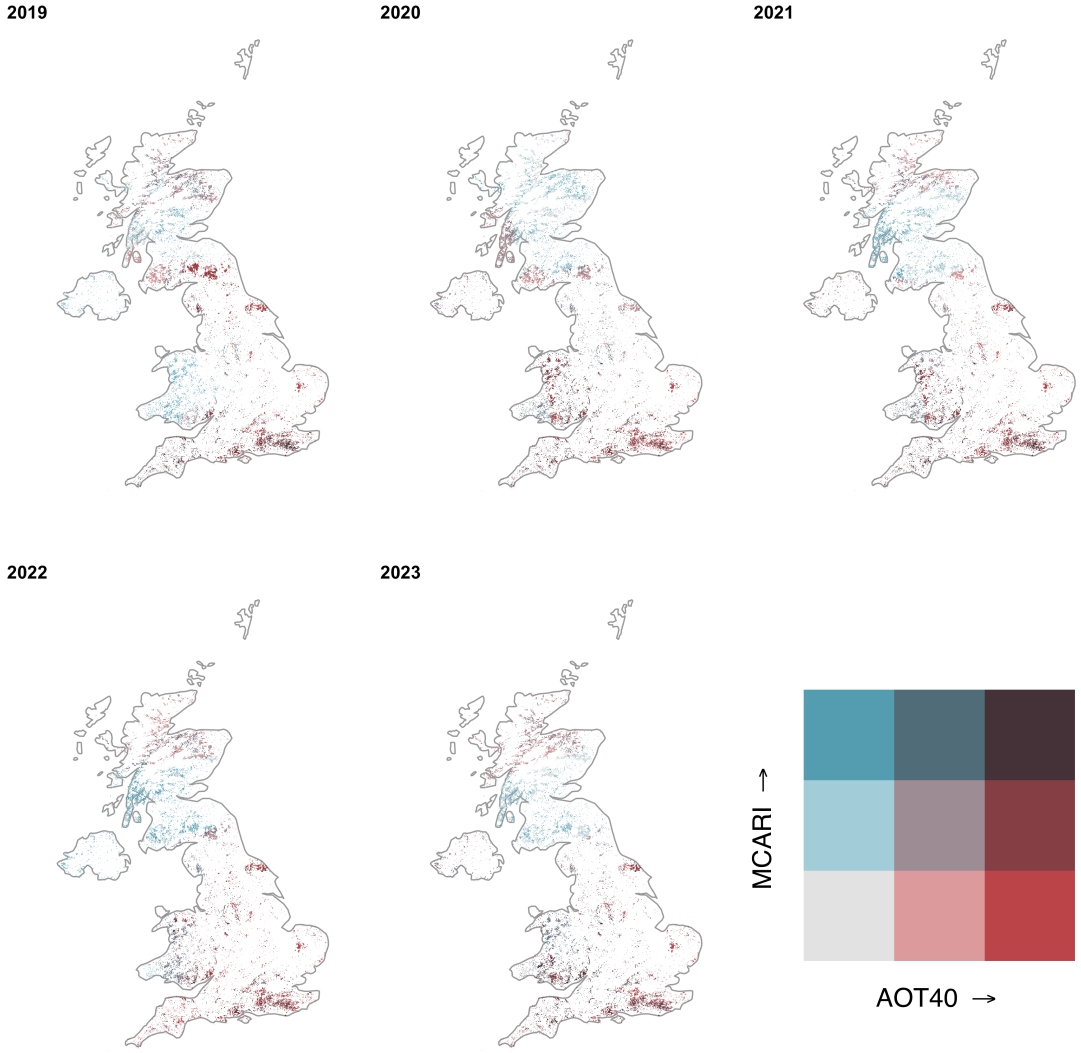


Figure 5.5: Bivariate maps of annual median MCARI against annual AOT40 for forested areas of the UK, at 1 km spatial resolution. Areas with high MCARI and low AOT40 are shown in bright blue, areas with high AOT40 and low MCARI are shown in bright red. Areas with both high AOT40 and MCARI are coloured dark purple, areas with both low AOT40 and MCARI are coloured in grey, as per the bivariate legend. The years 2019-2023 are presented.

5.5 Discussion

Based on my studies of leaf level reflectance under O_3 stress, I hypothesized that MCARI would increase with O_3 exposure (summarized by AOT40) in forested areas. I did not find this relationship in the annual analysis; however, I also did not find the inverse. Rather, no significant relationship was observed, and there were high levels of variability in AOT40 and MCARI. There are several possible reasons for this relating to the coarseness of this analysis. The spatial resolution of the analysis was limited by the 1 km resolution of the AOT40 data, meaning heterogeneity in MCARI across forested areas was lost, and only forests with 75% cover over 1 km were be included. Additionally, because the AOT40 data only gave annual averages, weekly MCARI values across the growth season had to be averaged, losing temporal resolution. Ideally, daily or weekly O_3 concentrations would be available at a higher spatial resolution such as 30 m. This would be particularly useful for countries like the UK where most forests are small. My previous studies have focussed on temperate deciduous broadleaves, and oak in particular, however in this analysis all forested areas were included. Without testing the effect of O_3 on temperate evergreen species' leaf reflectance, I cannot assume the same vegetation indices will be sensitive to O_3 damage as in broadleaf species.

In this analysis I have moved from directly measuring the leaf surface reflectance under an active light source (Chapters 2-4), to analysing satellite reflectance of forests. Although both methods rely on the reflectance of light from leaf surfaces, satellite measurements also include atmospheric effects and background reflectance of the soil. The light source in satellite monitoring is the sun, which is variable in intensity and so relative metrics of reflectance intensity such as vegetation indices must be used to compare between different times and places. The signal to noise ratio is much lower when remotely measuring canopy reflectance from space, compared with measuring leaf reflectance in a leaf clip. Therefore, it is possible the strength of the signal of O_3 damage which I found in Chapters 2 and 3 was not strong enough to be detected from satellites at the spatial and temporal resolution used.

Additionally, MCARI at the leaf level highly sensitive to changes in chlorophyll, but when measured from a satellite the background reflectance of the soil and other non-photosynthetic material influence the MCARI value [17]. NDVI is a more widely used measure of vegetation health from satellite measurements, but did not respond significantly to O_3 exposure in Chapters 2 and 3. Correlative analysis of NDVI and AOT40 is presented in Appendix D, but also did not show any relationship.

One strength of the AOT40 measurement is that it is cumulative, and it is well established than the cumulative exposure of vegetation to O_3 determines the magnitude of damage [28]. However, by only including concentrations above 40 ppb, chronic low level O_3 stress may be missed. Additionally, there is now consensus among experts that stomatal O_3 flux based metrics perform better than concentration-based metrics for assessing the risk of O_3 damage to vegetation [29–31]. Stomatal flux based metrics require additional meteorological information and are specific to different vegetation types or species [32]. Stomatal flux metrics are more complex to implement than concentration metrics, and the majority of regulations on air quality in the UK and Europe relating to ozone are also still based on concentration rather than flux-based metrics [13, 15].

More broadly, to effectively scale up leaf level detection of O_3 damage to a remote sensing technique, consideration needs to be given to canopy structure and radiative transfer. There are several approaches which can be used to scale leaf reflectance up to canopy reflectance for remote sensing involving multi-scale integration and different types of radiative transfer models. Multi-scale integration involves combining spectral data from different scales to improve the accuracy of remote forest monitoring. For example field measurements of leaf reflectance may be combined with measurements taken by spectrometers mounted on unmanned aerial vehicles (UAVs) as well as satellite imagery [33]. When moving between different spectral and spatial resolutions, downscaling can be used to help understand how different monitoring techniques relate to each other. For example, hyperspectral canopy reflectance measurements taken by UAV mounted hyperspectrometers can be spectrally downscaled to match the multispectral bands of specific satellites, which

can reveal the influence of other factors such as atmospheric interference. Higher spatial resolution data can be combined with satellite data to disentangle the contributions of soil and shade to the reflectance spectra, particularly in sparse forests.

In the context of remote sensing O_3 damage to forests, to effectively scale up from leaf level measurements, I would suggest simultaneously taking hyperspectral reflectance measurements at the leaf level using a field spectrometer and at the canopy level using a UAV mounted hyperspectrometer as a first step, in a temperate broadleaf forest with visible O_3 damage or O_3 FACE sapling experiment. This would allow the effects of canopy structure and solar illumination on leaf reflectance to be identified in the context of O_3 damage, as well as allowing whole spectral analysis alongside vegetation indices.

Radiative transfer models (RTMs) provide a consistent framework for understanding how light interacts with forest canopies, at the smallest spatial scale RTMs simulate the interaction of light with individual leaves via absorption, transmission and reflection such as the PROSPECT leaf optical properties model [34]. At the canopy level, RTMs include the effect of the 3D arrangement of leaves, branches and gaps in the canopy. At the canopy level, are many different types of RTM, such as 3D models (such as the DART model [35]), hybrid models (such as PROSAIL model [36]), coupled atmosphere-canopy models (such as the FLiES model [37]).

Bidirectional reflectance models are a type of RTM often applied to scaling canopy reflectance. These models consider directional characteristics of light reflection depending on the angle of incoming sunlight and viewing angle for various scales within the canopy to simulate the bidirectional reflectance distribution function [38]. Bidirectional reflectance models can also be used for discontinuous canopies by incorporating the shadow of tree crowns [39]. These models have been used to separate physiological versus directional effects on photosynthetic efficiency, monitored by the photochemical reflectance index (PRI, [40].

In conclusion, scaling from leaf reflectance to satellite remote sensing requires a comprehensive understanding of the relationships between leaf biophysical properties, canopy structure, and spectral reflectance. The integration of remote sensing

techniques at different spatial scales and radiative transfer models would be needed to accurately scale up my leaf level findings to a remote sensing application.

Another approach to understand the impact of O_3 on forests is to input O_3 stress response parameters in earth system models and assess the impact of O_3 on larger scale processes. High resolution changes in leaf reflectance under O_3 exposure could add detail to the O_3 response parameters included in earth system models such as JULES [41]. Model outputs could then inform the expected changes to canopy level parameters under O_3 stress.

As mentioned, the spatial and temporal resolution of the modelled O_3 data was a limiting factor in this analysis. A more comprehensive analysis could utilise European or global O_3 data, although there are trade-offs between spatial extent and the spatio-temporal resolution of the data. Future satellite retrievals of tropospheric O_3 may improve the availability of O_3 data and improve the accuracy of models which combine satellite derived and in situ O_3 measurements in areas with sparse in situ observations.

References

[1] Victoria E. Wittig et al. "Quantifying the impact of current and future tropospheric ozone on tree biomass, growth, physiology and biochemistry: a quantitative meta-analysis". In: *Global Change Biology* 15.2 (2009), pp. 396–424. DOI: 10.1111/j.1365-2486.2008.01774.x.

[2] Lisa D. Emberson, Patrick Büker, and Mike R. Ashmore. "Assessing the risk caused by ground level ozone to European forest trees: A case study in pine, beech and oak across different climate regions". In: *Environmental Pollution*. Air Pollution and Climate Change: A Global Overview of the Effects on Forest Vegetation 147.3 (June 1, 2007), pp. 454–466. DOI: 10.1016/j.envpol.2006.10.026.

[3] M. Schaub et al. *Part VIII: Monitoring of Ozone Injury*. UNECE ICP Forests Programme Co-ordinating Centre, Thünen Institute of Forest Ecosystems, 2016, pp. 1221–1226.

[4] Marco Ferretti et al. "The fingerprint of tropospheric ozone on broadleaved forest vegetation in Europe". In: *Ecological Indicators* 158 (Jan. 1, 2024), p. 111486. DOI: 10.1016/j.ecolind.2023.111486.

[5] F. Bussotti et al. "Assessment of ozone visible symptoms in the field: perspectives of quality control". In: *Environmental Pollution*. Native Plants as Bioindicators of Air Pollutants: Contributed Papers to a Symposium held in conjunction with the 34th Air Pollution Workshop 125.1 (Sept. 1, 2003), pp. 81–89. DOI: 10.1016/S0269-7491(03)00095-2.

[6] Anna Lee Jones. "On mature reflection: ozone damage can be detected in oak trees by hyperspectral reflectance." In: *In Preparation* (2024).

[7] Anna Lee Jones et al. "Reflections of stress: Ozone damage in broadleaf saplings can be identified from hyperspectral leaf reflectance". In: *Environmental Pollution* 360 (Nov. 1, 2024), p. 124642. DOI: 10.1016/j.envpol.2024.124642.

[8] Shawn C Kefauver. "Using topographic and remotely sensed variables to assess ozone injury to conifers in the Sierra Nevada (USA) and Catalonia (Spain)". In: *Remote Sensing of Environment* (2013), p. 11.

[9] Jeremy E. Diem. "Remote Assessment of Forest Health in Southern Arizona, USA: Evidence for Ozone-Induced Foliar Injury". In: *Environmental Management* 29.3 (Mar. 1, 2002), pp. 373–384. DOI: 10.1007/s00267-001-0011-5.

[10] C. Proietti et al. "A multi-sites analysis on the ozone effects on Gross Primary Production of European forests". In: *Science of The Total Environment* 556 (June 2016), pp. 1–11. DOI: 10.1016/j.scitotenv.2016.02.187.

[11] Yo Shimizu et al. "A novel remote sensing-based method of ozone damage assessment effect on Net Primary Productivity of various vegetation types". In: *Atmospheric Environment* 217 (Nov. 15, 2019), p. 116947. DOI: 10.1016/j.atmosenv.2019.116947.

[12] Katherine L Pugsley et al. *Technical report on UK supplementary modelling assessment under the Air Quality Standards Regulations 2010 for 2022*. 2022.

[13] *The Air Quality Standards Regulations 2010*. 2010.

[14] Noel Gorelick et al. "Google earth engine: Planetary-scale geospatial analysis for everyone". In: *Remote Sensing of Environment* (2017). Publisher: Elsevier. DOI: 10.1016/j.rse.2017.06.031.

[15] *Convention on Long-range Transboundary Air Pollution, United Nations Economic Commission for Europe.* In collab. with UNECE. Publisher: Cambridge University Press. 1979.

[16] European Space Agency (ESA). *Copernicus Sentinel-2 (processed by ESA), 2019-2023. Retrieved from GEE (Jan 2025). MSI Level-2A BOA Reflectance Product, Collection 1.* 2024. DOI: https://doi.org/10.5270/S2_-znk9xsj.

[17] C. S. T Daughtry et al. "Estimating Corn Leaf Chlorophyll Concentration from Leaf and Canopy Reflectance". In: *Remote Sensing of Environment* 74.2 (Nov. 1, 2000), pp. 229–239. DOI: 10.1016/S0034-4257(00)00113-9.

[18] J. W. Rouse et al. "Monitoring vegetation systems in the Great Plains with ERTS". In: NASA. Goddard Space Flight Center 3d ERTS-1 Symp., Vol. 1, Sect. A. NTRS Author Affiliations: Texas A&M Univ. NTRS Report/Patent Number: PAPER-A20 NTRS Document ID: 19740022614 NTRS Research Center: Legacy CDMS (CDMS). Jan. 1, 1974.

[19] Ravi Prakash Sripada. "Determining In-Season Nitrogen Requirements for Corn Using Aerial Color-Infrared Photography". In: (Apr. 19, 2005).

[20] Peter Potapov et al. "Mapping global forest canopy height through integration of GEDI and Landsat data". In: *Remote Sensing of Environment* 253 (Feb. 1, 2021), p. 112165. DOI: 10.1016/j.rse.2020.112165.

[21] R Core Team. *R: a language and environment for statistical computing.* manual. Vienna, Austria: R Foundation for Statistical Computing, 2023.

[22] Robert J. Hijmans. *terra: Spatial data analysis.* 2024.

[23] Hadley Wickham. *ggplot2: Elegant graphics for data analysis.* 2016.

[24] Garnier et al. *Viridis - colorblind-friendly color maps for R.* 2024. DOI: 10.5281/zenodo.4679423.

[25] Claus O. Wilke. *cowplot: Streamlined plot theme and plot annotations for 'ggplot2'.* 2024.

[26] Alboukadel Kassambara. *ggpubr: 'ggplot2' based publication ready plots.* 2023.

[27] Christopher Prener, Timo Grossenbacher, and Angelo Zehr. *biscale: Tools and palettes for bivariate thematic mapping.* 2022.

[28] Annemarie Bastrup-Birk et al. "Studying cumulative ozone exposures in Europe during a 7-year period". In: *Journal of Geophysical Research: Atmospheres* 102 (D20 1997), pp. 23917–23935. DOI: 10.1029/97JD01966.

[29] Gina Mills et al. "Evidence of widespread effects of ozone on crops and (semi-)natural vegetation in Europe (1990–2006) in relation to AOT40- and flux-based risk maps". In: *Global Change Biology* 17.1 (2011), pp. 592–613. DOI: 10.1111/j.1365-2486.2010.02217.x.

[30] Chiara Proietti et al. "Trends in tropospheric ozone concentrations and forest impact metrics in Europe over the time period 2000–2014". In: *Journal of Forestry Research* 32.2 (Apr. 2021), pp. 543–551. DOI: 10.1007/s11676-020-01226-3.

[31] Pierre Sicard et al. "An epidemiological assessment of stomatal ozone flux-based critical levels for visible ozone injury in Southern European forests". In: *Science of The Total Environment* 541 (Jan. 15, 2016), pp. 729–741. DOI: 10.1016/j.scitotenv.2015.09.113.

[32] Gina Mills et al. *Chapter 3: Mapping critical levels for vegetation*. ICP Vegetation, 2017.

[33] Jing Wang et al. "Multi-scale integration of satellite remote sensing improves characterization of dry-season green-up in an Amazon tropical evergreen forest". In: *Remote Sensing of Environment* 246.111865 (Sept. 1, 2020). DOI: 10.1016/j.rse.2020.111865.

[34] S. Jacquemoud and F. Baret. "PROSPECT: A model of leaf optical properties spectra". In: *Remote Sensing of Environment* 34.2 (Nov. 1990), pp. 75–91. DOI: 10.1016/0034-4257(90)90100-Z.

[35] J. P. Gastellu-Etchegorry et al. "Modeling radiative transfer in heterogeneous 3-D vegetation canopies". In: *Remote Sensing of Environment* 58.2 (Nov. 1, 1996), pp. 131–156. DOI: 10.1016/0034-4257(95)00253-7.

[36] Stéphane Jacquemoud et al. "PROSPECT+SAIL models: A review of use for vegetation characterization". In: *Remote Sensing of Environment*. Imaging Spectroscopy Special Issue 113 (Sept. 1, 2009), S56–S66. DOI: 10.1016/j.rse.2008.01.026.

[37] Hideki Kobayashi and Hironobu Iwabuchi. "A coupled 1-D atmosphere and 3-D canopy radiative transfer model for canopy reflectance, light environment, and photosynthesis simulation in a heterogeneous landscape". In: *Remote Sensing of Environment* 112.1 (Jan. 15, 2008), pp. 173–185. DOI: 10.1016/j.rse.2007.04.010.

[38] Jing M Chen and Sylvain G Leblanc. "A Four-Scale Bidirectional Reflectance Model Based on Canopy Architecture". In: *IEEE TRANSACTIONS ON GEOSCIENCE AND REMOTE SENSING* 35.5 (Sept. 1997).

[39] Wenge Ni et al. "An analytical hybrid GORT model for bidirectional reflectance over discontinuous plant canopies". In: *IEEE Transactions on Geoscience and Remote Sensing* 37.2 (Mar. 1999). Conference Name: IEEE Transactions on Geoscience and Remote Sensing, pp. 987–999. DOI: 10.1109/36.752217.

[40] Thomas Hilker et al. "Separating physiologically and directionally induced changes in PRI using BRDF models". In: *Remote Sensing of Environment* 112.6 (June 16, 2008), pp. 2777–2788. DOI: 10.1016/j.rse.2008.01.011.

[41] Rebecca J. Oliver et al. "Large but decreasing effect of ozone on the European carbon sink". In: *Biogeosciences* 15.13 (July 13, 2018), pp. 4245–4269. DOI: 10.5194/bg-15-4245-2018.

6
Conclusion

Contents

6.1 Introduction 179
6.2 Key Findings 180
6.3 Discussion 182
6.4 Contribution and Impact 184
6.5 Limitations and Future Directions 185
6.6 Synthesis 188
References 189

6.1 Introduction

In this thesis I sought to address a key knowledge gap in monitoring forest health by establishing the hyperspectral signature of O_3 damage in broadleaf temperate trees. Broadleaf temperate forests are globally important for carbon storage [1], biodiversity [2], and biomass production [3], yet are vulnerable to O_3 damage [4]. Current methods of assessing O_3 damage to broadleaf temperate forests rely on manual leaf inspection, but I have shown that hyperspectral leaf reflectance has exciting potential to be used as a high-throughput, and potentially remote, method of O_3 damage detection.

This concluding chapter summarises the key findings of my thesis; discusses how

these findings relate to each other; explores the impact of this work; reflects on the limitations of my studies; recommends future research; and finally synthesises the thesis as a whole.

6.2 Key Findings

The research objectives set out in Chapter 1 were as follows:

Objectives

1. To experimentally identify the hyperspectral signature of O_3 damage in temperate broadleaf species.

2. To test hyperspectral O_3 damage detection in mature temperate broadleaf trees outside experimental conditions.

3. To compare the effects of elevated CO_2 on leaf reflectance with the effects of O_3, with future monitoring under 2050 atmospheric conditions in mind.

4. To explore the suitability of spectral O_3 damage detection for a remote sensing application.

In relation to Objective 1, I characterised the hyperspectral reflectance response to elevated O_3 across five temperate broadleaf species under controlled conditions in Chapter 2. The high-throughput nature of hyperspectral reflectance measurements allowed a clear signal of O_3 damage to be identified compared to time consuming approaches such as pigment extraction, as demonstrated by the null results in Appendix B. The hyperspectral signature of O_3 damage varied between different sapling species, but a change in the reflectance of the green peak and short wavelength infrared was consistent across species. For every species, supervised machine learning was able to accurately predict the O_3 treatment saplings had been exposed to based on summarised components of the hyperspectral leaf reflectance (PLSDA), indicating a detectable multi-variate spectral change induced by O_3 exposure. To the best of my knowledge, this was the first study to investigate

the effect of O_3 exposure on the hyperspectral leaf reflectance of pedunculate oak, common beech, birch, alder, and crab apple saplings. This was also the first O_3 manipulation experiment on European crab apple in any context.

Chapter 3 fulfils Objective 2, by showing that O_3 induced changes in leaf reflectance can be identified in mature pedunculate oak trees under natural conditions. As found in the sapling experiment, O_3 affected the width and intensity of the green reflectance peak of mature oaks, but in mature trees the red-edge reflectance of leaves was also important in differentiating between levels of O_3 exposure. The short wavelength infrared region did not response to O_3 exposure as strongly in mature oak trees as it had in saplings under experimental conditions. A supervised machine learning model (PLSR) was able to predict the O_3 exposure of trees from hyperspectral leaf reflectance alone. This was the first investigation to examine O_3 induced changes in the leaf reflectance of mature deciduous trees.

Objective 3 was investigated in Chapter 4 using the unique BIFoR FACE CO_2 fertilisation experiment, in a naturally low O_3 exposed environment. Elevated CO_2 (eCO_2) did not have a significant impact on the overall reflectance spectra of mature oak leaves, but did increase the plant senescence reflectance index (PSRI). PSRI did not respond to O_3 exposure in the sapling experiment in Chapter 2 or in mature oak trees in Chapter 3. This bodes well for monitoring O_3 damage in the future under higher CO_2 conditions, because O_3 induced changes in leaf reflectance were much more pronounced than those induced by eCO_2, and affected different parts of the spectrum. However, both PSRI and the shape of the green reflectance peak (which responded to O_3 exposure) are affected by the ratio of carotenes to chlorophyll [5, 6]. In light of this, I argue in favour of whole-spectra analysis to capture the multivariate signal of O_3 stress rather relying on individual vegetation indices.

In Chapter 5 I explored the suitability of leaf reflectance for remotely sensing O_3 damage in forests, addressing Objective 4. Although the open source analysis performed in Chapter 5 did not show correlations between annual O_3 exposure metrics (AOT40) and vegetation indices (MCARI, NDVI or GDVI), this analysis was limited by the coarse spatial and temporal resolution of the public data available.

Chapter 5 discussed different approaches which could be used to scale up leaf level O_3 damage detection to a remote sensing application, such as trialling a proximal remote sensing technique (such as UAV mounted spectrometers) and employing a radiative transfer model. The consistent spectral signature found in Chapter 2 and 3 remains a promising candidate for a remote sensing application, paired with high quality O_3 monitoring.

6.3 Discussion

The spectral signature of O_3 damage I have identified in temperate broadleaf trees has similarities to results from other species. The width of the green reflectance peak was affected by O_3 exposure in my sapling and mature tree studies, similar results have also been found in O_3 treated Ponderosa pine needles [7, 8]. Studies of conifers [9], poplar saplings [10], tomatoes[11], soybeans [12], and clover canopies [13] have used the height of the green reflectance peak, captured by the PRI index, to identify O_3 stress with and without visible injury. PRI was elevated initially under high O_3 treatment in my sapling experiment, but this shift was not maintained under chronic O_3 exposure nor in adult trees.

In one of the few remote sensing studies of O_3 damage to trees, the trough immediately preceding the red-edge (645-655 nm) was specifically sensitive to O_3 damage in pine trees [14]. Shifts in the intensity of the red-edge have also been observed in O_3 exposed vegetation, including a remotely sensed NDVI response in Ponderosa pine [15]. NDVI and PRI characterise the red-edge and green peak (respectively), and did not significantly respond to O_3 exposure in my two studies. However, I did find a significant response in MCARI which is a more complex index combining wavelengths in the green reflectance peak and red-edge. MCARI may therefore capture both the responses previously reported in NDVI and PRI, and by combining them result in a stronger signal. MCARI has not been examined in many previous O_3 studies, as it is a more recent and less well know index. We may also expect different vegetation indices to respond to O_3 exposure in broadleaf temperate trees, compared to the conifers previously studied in the literature.

Although vegetation indices have the advantage of being comparable over different spatial scales and across instruments, because they use ratios of reflectance intensity at different wavelengths, they are limited in the number of spectral features they characterise. Due to their simplicity, the same vegetation index may be associated with many different stressors. Changes in MCARI for example are not unique to O_3 stress, and so would need to be carefully interpreted alongside O_3 exposure data. On the other hand, analyses which utilise the entire spectral signature (such as PLSR and PLSDA) are able to characterise multivariate changes in leaf reflectance which are more specific to a particular stressor, such as O_3. Advances in hyperspectral technology now allow UAV, aircraft, and satellite mounted hyperspectrometers to be deployed, where only banded multi-spectral sensors were previously available.

A different approach to remote-sensing O_3 damage assessment is to use satellite derived estimates of net primary productivity (NPP) alongside cumulative ozone metrics (AOT40) to estimate the linear loss of productivity due to O_3 exposure [16]. While this approach produced significant negative relationships between AOT40 and NPP in the Kanto region of Japan, this correlative approach cannot be attributed solely to O_3 since NPP is affected by many variables. I have shown that there is a specific spectral signature of O_3 damage in temperate broadleaf trees, which alongside the existing literature on conifers and crops, provides a specific detection method for O_3 damage. A more robust damage assessment method could combine NPP reductions with O_3 exposure and the spectral signature of O_3 damage. As CO_2 concentrations increase, NPP is expected to increase via the fertilisation effect, which could decouple the link between O_3 and NPP used by Shmizu et al. Contrastingly, by showing that the signal of O_3 damage is stronger than and distinct from eCO_2 induced changes in leaf reflectance, I have demonstrated that spectral detection of O_3 damage is robust to future conditions.

6.4 Contribution and Impact

This thesis makes a significant contribution to understanding how O_3 affects leaf reflectance, in temperate broadleaf trees which have been understudied compared to conifers and crops. The results of this thesis pave the way for development of a specific remote method of detecting O_3 damage, which would be a quantitive and scalable assessment tool for monitoring the effect of O_3 on temperate forests. A new assessment method is needed to understand the scale of O_3 damage to forests, allowing accurate forecasting of forests' current and future growth, as well as adaptation of reforestation plans to account for areas of O_3 damage. Understanding to what extent temperate broadleaf forests are currently affected by O_3 forests would allows better modelling of their growth and responses to other stressors.

Assessing the extent of O_3 damage to forests is particularly important in light of ambitious reforestation targets [17], many of which are planned for O_3 exposed sites. Projections of carbon sequestration by afforestation, such as the European Commission's 3 Billion Tree Planting Pledge project, do not account for inhibition of productivity and growth by O_3 exposure [18]. A high throughput method for the assessment of O_3 damage to forests over large spatial scales is a crucial component of effective afforestation and accurate carbon sequestration modelling.

Tropospheric O_3 concentrations have plateaued at high levels in UK and Europe, and O_3 background concentrations are predicted to continue to rise until the end of the century [19]. Even if NO_x and VOCs emissions decrease, O_3 may not decrease unless methane emissions are also tackled [20, 21]. In the UK the importance of O_3 as an air pollutant is predicted to increase as other pollutants fall [22]. Despite the high concentrations of tropospheric O_3 and its growing importance, O_3 suffers from a perception problem and has fallen off the radar of many politicians, scientists, and the public. I believe this is largely due to the idea that "we fixed ozone", referring to the stratospheric O_3 hole which received widespread attention around the end of the 20^{th}century and is now the most often cited climate "success story". By contrast, tropospheric O_3 represents a hole in the understanding of many plant scientists and ecologists. By researching the effects of tropospheric O_3 on

trees I have had the opportunity to change academics', students' and the public's perception of O_3 as a contemporary and pressing issue. Indeed, my O_3 monitoring in Wytham Woods was the first time the woodland has been shown to suffer from damaging levels of O_3 exposure, which will be affecting the entire ecosystem. This illustrates how significant a blind spot tropospheric O_3 pollution is, even in one of the most thoroughly studied research woodlands in the world. Further research and assessments of the scale of O_3 damage to forests in the UK would bring tropospheric O_3 into the consciousness of scientists, policy makers, and the public.

6.5 Limitations and Future Directions

Several opportunities remain to extend the research undertaken in this thesis beyond the limitations imposed by the project's resources, scope, and timescale. Over the course of this research, my understanding and scientific skills have also evolved, allowing opportunities to reflect on my development as a researcher.

In the O_3 manipulation experiments detailed in Chapter 2 and Appendix B, I used solvent extractions and spectrophotometry to determine pigment concentrations in leaves. These methods did not show significant differences between O_3 treatments, and the data exhibited substantial variability (Appendix B). Although there may not have been large differences in pigment concentrations between treatments, a more precise method of pigment analysis, high-performance liquid chromatography (HPLC), could have offered more robust results. HPLC separates pigments based on polarity and retention time, providing detailed and precise quantitive measurements. However, access to HPLC facilities and longer processing times were prohibitive in this study. A follow-up investigation utilising HPLC could give insights into the leaf level changes in pigment ratios underpinning the O_3-induced elevation of the MCARI index observed in my research. Future investigations employing HPLC could therefore bridge the gap between detailed leaf biochemistry and spectral responses, thereby contributing to a more robust understanding of tree adaptation mechanisms to O_3 stress and informing improved monitoring strategies.

In Chapter 3, I monitored the O_3 exposure of the two field sites using O_3 diffusion tubes, a passive monitoring technique which measures cumulative O_3 concentrations over several weeks. Diffusion tubes are low-tech, rugged, and can be deployed in most field conditions; however, their temporal resolution is limited. By contrast, UV O_3 analysers provide high-frequency measurements (generally recording at 1-minute intervals) but require a reliable power source and data offloading. UV O_3 analysers require calibration, and are significantly more expensive than diffusion tubes. In my study, a UV O_3 analyser intended to be deployed in the BIFoR forest failed its calibration comparisons at the Birmingham Air Quality Super Site and required lengthy repairs. In field situations where power supply is constrained, budget is limited, or technical issues arise, diffusion tubes provide a reliable and accessible alternative. Employing both methods in long-term field studies could offer a robust solution: using the UV analyser for high temporal resolution analysis to detect O_3 peaks, while relying on diffusion tubes as a fail-safe back up and for cumulative data.

One of the objectives of this thesis was to compare the effects of eCO_2 with O_3 exposure on leaf reflectance and although Chapter 4 addressed this question, only CO_2 was manipulated in the study. As discussed in Chapter 1, eCO_3 may allow plants to avoid O_3 uptake via reduced stomatal conductance and partially offset the negative effects of O_3. While my investigation showed that eCO_2 did not significantly affect leaf reflectance, and did not alter the same regions of leaf reflectance spectra as O_3, I did not have the facilities to investigate the combined effects of CO_2 and O_3 on leaf reflectance. There are a limited number of free-air concentration enrichment experiments which combine CO_2 and O_3, including Tsukuba experiment in Japan which is currently operating, SoyFACE in Illinois, USA and ASPEN FACE in Wisconsin USA which ran until 2010. There are no experiments which combine elevated CO_2 and O_3 in a mature forest, but a future investigation could use temperate broadleaf saplings in a smaller FACE or open top chamber experiment to examine the combined effect of CO_2 and O_3 on leaf reflectance.

As discussed in Chapter 5, the next key step in this research is to scale up spectral O_3 damage detection from leaf reflectance to a remote sensing application.

A prudent next investigation would be to take proximal hyperspectral measurements via UAV from the small scale O_3 FACE experiment on young broadleaf trees which has been set up by CEH in Bangor since my experiments there. Concurrent measurements of leaf reflectance and canopy reflectance within an O_3 exposure experiment would reveal any changes in the signal of O_3 damage in reflectance when sensed at the canopy scale rather than leaf level, which could also be modelled using a radiative transfer model. This investigation would pave the way for a remote method of monitoring O_3 damage to broadleaf trees, although it would need to be followed up by trials in mature trees outside the experimental setting.

In order to further test remote hyperspectral O_3 damage detection, measurements could be taken via UAV in forests identified as experiencing high O_3 stress in the ICP Forests assessment of visible foliar injury and O_3 exposure. Remote monitoring O_3 damage to forests could then be compared to the long record of foliar injury assessments carried out by ICP Forests. Concurrent spectral detection and foliar injury assessment at case study forests would allow comparison of the two methods' accuracy, speed, and sensitivity. Foliar injury assessment would continue to provide a valuable "ground truth" of remote O_3 damage detection.

Additionally, long-term hyperspectral monitoring of a forest for several years would allow analysis of how the O_3 damage signal changes between high and low O_3 years. Where high-resolution spectra are taken by UAV, these measurements could also be aggregated and compared to the resolution of satellite data as discussed in Chapter 5. It would also be important to test the impact of stressors such as drought on the spectral signal of O_3 damage. Additionally, for wider scale applications testing this technique in tropical broadleaf and coniferous forest species would allow my work to be applied beyond its current scope.

Another remote sensing technology with strong potential for monitoring O_3 damage to vegetation is solar induced fluorescence (SIF). SIF is the re-emission of fluorescence from chlorophyll during photosynthesis, and as an optical signal it can be remotely monitored including via satellites [23, 24]. SIF is directly linked to photosynthetic productivity unlike traditional pigment based vegetation indices.

In soybean, reduced SIF has been shown to capture the effects of elevated O_3 on canopy structure and accelerated senescence [25]. Satellite retrievals of regional and global SIF data are now available, and so SIF could be a useful tool in large-scale assessments of O_3 damage to vegetation. The effect of O_3 on temperate broadleaf SIF has not yet been investigated, and unfortunately my attempt to investigate this during the O_3 experiments detailed in Chapter 2 were curtailed due to a technical problems with a proximal SIF spectrometer. Therefore, a poignant further investigation would be to test the effects of different O_3 concentrations on the SIF signal of broadleaf temperate trees, in the hope SIF could act alongside hyperspectral reflectance to inform remote monitoring of O_3 damage in forests as a direct link to photosynthetic productivity.

6.6 Synthesis

In this thesis I have advanced understanding of forest health monitoring by establishing a robust hyperspectral signature of O_3 damage in broadleaf temperate trees, combining detailed experimental analysis with the potential for remote sensing applications. By integrating controlled sapling experiments with field investigations of mature trees, I have was demonstrated that distinct spectral changes, especially in the green peak and red-edge, reliably indicate O_3 stress. This offers a high-throughput, and more sensitive alternative to manual leaf inspection. Moreover, by contrasting the effects of elevated CO_2 on leaf reflectance with O_3, I have shown that the spectral response to O_3 is not only more pronounced but also distinct, thereby underscoring the potential of hyperspectral reflectance for remote sensing applications under future atmospheric conditions. These insights pave the way for deploying remote hyperspectral sensors on UAVs, aircraft, or satellites for wide-scale assessment of the effect of O_3 pollution on forests. This thesis not only fills a critical knowledge gap regarding the spectral signature of O_3 damage in understudied temperate broadleaf trees, but also plots a clear trajectory towards remote O_3 damage detection, thus guiding more effective forest management and reforestation efforts on a global scale.

References

[1] Martin Thurner et al. “Carbon stock and density of northern boreal and temperate forests”. In: *Global Ecology and Biogeography* 23.3 (2014), pp. 297–310. DOI: 10.1111/geb.12125.

[2] Jeňýk Hofmeister et al. “Shared affinity of various forest-dwelling taxa point to the continuity of temperate forests”. In: *Ecological Indicators* 101 (June 1, 2019), pp. 904–912. DOI: 10.1016/j.ecolind.2019.01.018.

[3] Louise Sing et al. “A review of the effects of forest management intensity on ecosystem services for northern European temperate forests with a focus on the UK”. In: *Forestry: An International Journal of Forest Research* 91.2 (Apr. 1, 2018), pp. 151–164. DOI: 10.1093/forestry/cpx042.

[4] Zhaozhong Feng et al. “A unifying explanation for variation in ozone sensitivity among woody plants”. In: *Global Change Biology* 24.1 (2018), pp. 78–84. DOI: 10.1111/gcb.13824.

[5] Mark N. Merzlyak et al. “Non-destructive optical detection of pigment changes during leaf senescence and fruit ripening”. In: *Physiologia Plantarum* 106.1 (1999), pp. 135–141. DOI: 10.1034/j.1399-3054.1999.106119.x.

[6] Daniel A Sims and John A Gamon. “Relationships between leaf pigment content and spectral reflectance across a wide range of species, leaf structures and developmental stages”. In: *Remote Sensing of Environment* 81.2 (Aug. 2002), pp. 337–354. DOI: 10.1016/S0034-4257(02)00010-X.

[7] B. Curtiss and S.L. Ustin. “Parameters Affecting Reflectance Of Coniferous Forests In The Region Of Chlorophyll Pigment Absorption”. In: *12th Canadian Symposium on Remote Sensing Geoscience and Remote Sensing Symposium,* 12th Canadian Symposium on Remote Sensing Geoscience and Remote Sensing Symposium, vol. 4. July 1989, pp. 2633–2636. DOI: 10.1109/IGARSS.1989.577951.

[8] Susan L. Ustin and Brian Curtiss. “Spectral characteristics of ozone-treated conifers”. In: *Environmental and Experimental Botany* 30.3 (July 1, 1990), pp. 293–308. DOI: 10.1016/0098-8472(90)90041-2.

[9] Shawn C Kefauver. “Using topographic and remotely sensed variables to assess ozone injury to conifers in the Sierra Nevada (USA) and Catalonia (Spain)”. In: *Remote Sensing of Environment* (2013), p. 11.

[10] M Meroni et al. “Leaf level early assessment of ozone injuries by passive fluorescence and photochemical reflectance index”. In: *International Journal of Remote Sensing* 29.17 (Mar. 2008), pp. 5409–5422. DOI: 10.1080/01431160802036292.

[11] Schutt J, Rowland R, and Heggestad H. “Identification of injury resulting from atmospheric pollutants using reflectance measurements [Tomatoes, sulfur dioxide].” In: *Journal of Environmental Quality* 13 (1984).

[12] Nichole Gosselin et al. “Using Visual Ozone Damage Scores and Spectroscopy to Quantify Soybean Responses to Background Ozone”. In: *Remote Sensing* 12.1 (Jan. 2020). Number: 1 Publisher: Multidisciplinary Digital Publishing Institute, p. 93. DOI: 10.3390/rs12010093.

[13] M Meroni et al. “Assessing Steady-state Fluorescence and PRI from Hyperspectral Proximal Sensing as Early Indicators of Plant Stress: The Case of Ozone Exposure”. In: *Sensors* 8.3 (Jan. 2008). Number: 3 Publisher: Molecular Diversity Preservation International, pp. 1740–1754. DOI: 10.3390/s8031740.

[14] A. V. Di Vittorio and G. S. Biging. “Spectral identification of ozone-damaged pine needles”. In: *International Journal of Remote Sensing* 30.12 (June 20, 2009), pp. 3041–3073. DOI: 10.1080/01431160802558725.

[15] Jeremy E. Diem. “Remote Assessment of Forest Health in Southern Arizona, USA: Evidence for Ozone-Induced Foliar Injury”. In: *Environmental Management* 29.3 (Mar. 1, 2002), pp. 373–384. DOI: 10.1007/s00267-001-0011-5.

[16] Yo Shimizu et al. “A novel remote sensing-based method of ozone damage assessment effect on Net Primary Productivity of various vegetation types”. In: *Atmospheric Environment* 217 (Nov. 15, 2019), p. 116947. DOI: 10.1016/j.atmosenv.2019.116947.

[17] Thomas Abeli and Andrea Di Giulio. “Risks of massive tree planting in Europe should be considered by the EU Forestry Strategy 2030”. In: *Restoration Ecology* 31.5 (2023), e13834. DOI: 10.1111/rec.13834.

[18] *COMMUNICATION FROM THE COMMISSION TO THE EUROPEAN PARLIAMENT, THE COUNCIL, THE EUROPEAN ECONOMIC AND SOCIAL COMMITTEE AND THE COMMITTEE OF THE REGIONS New EU Forest Strategy for 2030: The 3 Billion Tree Planting Pledge For 2030.* 2021.

[19] Intergovernmental Panel on Climate Change (IPCC). “Short-Lived Climate Forcers”. In: *Climate Change 2021: The Physical Science Basis. Contribution of Working Group I to the Sixth Assessment Report of the Intergovernmental Panel on Climate Change*. Cambridge: Cambridge University Press, 2021, pp. 817–922.

[20] Steven T. Turnock et al. “The impact of future emission policies on tropospheric ozone using a parameterised approach”. In: *Atmospheric Chemistry and Physics* 18.12 (June 28, 2018). Publisher: Copernicus GmbH, pp. 8953–8978. DOI: 10.5194/acp-18-8953-2018.

[21] O. Wild et al. “Modelling future changes in surface ozone: a parameterized approach”. In: *Atmospheric Chemistry and Physics* 12.4 (Feb. 21, 2012). Publisher: Copernicus GmbH, pp. 2037–2054. DOI: 10.5194/acp-12-2037-2012.

[22] Air Quality Expert Group. *Ozone in the UK – recent trends and future projections*. UK Department for Environment, Food and Rural Affairs, 2021.

[23] Gina H. Mohammed et al. “Remote sensing of solar-induced chlorophyll fluorescence (SIF) in vegetation: 50 years of progress”. In: *Remote Sensing of Environment* 231 (Sept. 15, 2019), p. 111177. DOI: 10.1016/j.rse.2019.04.030.

[24] Albert Porcar-Castell et al. “Linking chlorophyll a fluorescence to photosynthesis for remote sensing applications: mechanisms and challenges”. In: *Journal of Experimental Botany* 65.15 (Aug. 1, 2014), pp. 4065–4095. DOI: 10.1093/jxb/eru191.

[25] Genghong Wu et al. “Solar-induced chlorophyll fluorescence captures the effects of elevated ozone on canopy structure and acceleration of senescence in soybean”. In: *Journal of Experimental Botany* 75.1 (Jan. 1, 2024), pp. 350–363. DOI: 10.1093/jxb/erad356.

Appendices

A

Appendix to Chapter 1

A.1 Author Contributions

Chapter 1: ALJ is the sole author.

Chapter 2: ALJ is the first author responsible for conceptualisation, methodology, investigation, project administration, data curation, data analysis, visualisation, software development, writing the original manuscript, and further editing. ANO contributed to software development and reviewing the manuscript. FH contributed to the experimental design, reviewing the manuscript and supervision of the project. ESJ contributed to conceptualisation of the experiment, reviewing the manuscript, and supervision of the project.

Chapter 3: ALJ is the first author responsible for conceptualisation, methodology, investigation, project administration, data curation, data analysis, visualisation, software, writing the original manuscript and further editing. CP and FH contributed to reviewing the manuscript and supervision of the project. ESJ contributed to conceptualisation of the experiment, reviewing the manuscript, and supervision of the project.

Chapter 4: ALJ is the first author responsible for conceptualisation, methodology, investigation, project administration, data curation, data analysis, visualisation, software, writing the original manuscript, and further editing. AG, CP and FH

contributed to reviewing the manuscript and supervision of the project. ESJ contributed to conceptualisation of the experiment, reviewing the manuscript, and supervision of the project.

Chapter 5: ALJ is the sole author.

Chapter 6: ALJ is the sole author.

B

Appendix to Chapter 2

Contents

B.1 Additional Methods 194
B.1.1 O_3 Damage Score Examples 194
B.1.2 Formulae of Vegetation Indices 196
B.1.3 Destructive Harvest 197
B.1.4 Gas Exchange 197
B.1.5 Fluorometry 197
B.1.6 Biochemical Extractions 198
B.2 Additional Results 200
B.2.1 Growth 200
B.2.2 Destructive Harvest 202
B.2.3 Gas Exchange 203
B.2.4 Fluorometry 206
B.2.5 Biochemical Extractions 207
B.2.6 PCA 211
B.2.7 PLSDA 213
B.2.8 Vegetation Indices 216
References 221

B.1 Additional Methods

B.1.1 O_3 Damage Score Examples

Score	Description	Example Photo
1	Healthy green leaves with no visible O_3 damage.	
2	Intervenous stippling or mottles on less than half the leaves, by area or percentage of leaves affected.	
3	Stippling or mottles on half or more of the leaves, by area or percentage of leaves affected.	
4	Stippling or mottles present. Flecks covering less than half the leaves, by area or percentage of leaves affected.	
5	Stippling or mottles present. Flecks of over half the leaves, by area or percentage of leaves affected.	

Table B.1: O_3 damage scoring criteria and examples.

B.1.2 Formulae of Vegetation Indices

Vegetation Index	Equation	Reference
Normalised Difference Vegetation Index	$NDVI = \frac{\rho_{800}-\rho_{670}}{\rho_{800}+\rho_{670}}$	[1]
Modified Chlorophyll Absorption Ratio Index	$MCARI = \Big[(\rho_{700}-\rho_{670}) - 0.2 \times (\rho_{700}-\rho_{550})\Big] \times \frac{\rho_{700}}{\rho_{670}}$	[2]
Red Edge Normalised Difference Vegetation Index	$RENDVI = \frac{\rho_{750}-\rho_{705}}{\rho_{750}+\rho_{705}}$	[3, 4]
Photochemical Reflectance Index	$PRI = \frac{\rho_{570}-\rho_{530}}{\rho_{570}+\rho_{530}}$	[5, 6]
Plant Senescence Reflectance Index	$PSRI = \frac{\rho_{680}-\rho_{500}}{\rho_{750}}$	[3]

Table B.2: Formulae of common vegetation indices used to measure plant health and tested for sensitivity to O_3 damage.

B.1.3 Destructive Harvest

At the end of the experiment, the beech and oak saplings were harvested and separated into roots, stems, and leaves. Stem and leaves were weighed upon harvesting, which was recorded as their fresh weight. Roots were taken back to the laboratory and then carefully washed to remove loose soil while preserving fine roots. The roots stems and leaves were weighed again at the laboratory. The volume of roots and stems was measured using a volumetric water displacement method. The roots, stems, and leaves were then dried at $70 \circ$C until a constant weight was achieved, then their dry weight was recorded. The difference between fresh weight and dried weight was calculated as the water content of the roots and stems.

B.1.4 Gas Exchange

Instantaneous gas exchange was measured in July and August for three replicates of each species from low, medium, and high O_3 treatments using a LI-COR LI-6400 portable photosynthesis system. We concurrently measured the chlorophyll content index on eight locations of the same leaf using a CCM200m, Opti-Sciences, USA chlorometer.

B.1.5 Fluorometry

We assessed the dark and light-adapted leaf fluorescence dynamics of Oak and Beech saplings in June pre-O_3 treatment using a MINI-PAM I, Walz, USA. Saplings were dark adapted for two hours before analysis. We took further Pulse-Amplitude-Modulation (PAM) fluorometry measurements in July and August for three replicates of each species from low, medium, and high O_3 treatments. The following parameters were calculated from the PAM fluorometer results according to the equations derived by Schreiber et al: maximal quantum yield, effective quantum yield (Y), Electron Transport Rate (ETR), and Non-Photochemical Quenching (NPQ)[7].

B.1.6 Biochemical Extractions

One representative leaf was collected per month from each sapling. Each leaf sample was weighed upon harvesting and then dried at room temperature using silica gel packets (Thermo-Fisher) inside sealed polythene bags. Two 6mm diameter leaf discs were taken from each dried leaf sample. Leaf discs from the same species and treatment were pooled and ground to a fine powder using a Mixer Mill for 15 minutes. They were then extracted in 95% acetone (aq) for 15 mins while sonicating. The samples were then centrifuged at 3000 rpm for five minutes. The absorbance spectra of the supernatants were then recorded using a 400-800 nm spectrophotometer in cuvette mode (Ocean View Mini), which was used for all spectrophotometric analyses. The average Chlorophyll A and B concentration of each sapling per leaf area was calculated using the following equations from Sims and Gamon [4]:

1. $Chla \ = \ 0.01373 \cdot A663 - 0.000897 \cdot A537 - \ 0.003046 \cdot A647$
2. $Chlb \ = \ 0.02405 \cdot A647 \ - 0.004305 \cdot A537 - 0.005507 \cdot A663$
3. $Acetone\ Anthocyanins \ = \ 0.8175 \cdot A547 - 0.00697 \cdot A647 - 0.002228 \cdot A663$
4. $Carotenes = \frac{(A470 - ((17.1 \cdot (Chla + Chlb)) - (9.479 \cdot Anthocyanin))}{119.26}$

Following the above method, two ground leaf discs per individual were also extracted in acidified ethanol (1% HCl by volume) to extract anthocyanin pigments more accurately as per Sims and Gamon due to their instability in neutral and basic solutions. The same spectrophotometer set-up was used to analyse anthocyanin absorbance.Total anthocyanin content was then calculated using this corrected absorbance and a molar absorbance coefficient for anthocyanin at 529 nm of 30000 l $\text{mol}^{-1}\text{cm}^{-1}$ [8]:

$Corrected\ Anthocyanin\ Absorbance \ = A529 - (0.288 \cdot A650)$

Total phenols were determined using Ainsworth and Gillepsie's method [9]: Two 6 mm diameter leaf discs per individual were pooled by species and treatment, and then ground in the Mixer Mill. The ground samples were extracted in 95% ethanol while sonicating for 15 min and then incubated at room temperature in the dark for 48 h.

Subsequently, the extract was mixed with 400 ul of 10% Folin-Ciocalteau reagent, 1600 ul of 700 mM Na_2CO_3 and 1600 ul deionised water. Samples were incubated for a further two hours at room temperature and then centrifuged at 3000 rpm for five minutes. Samples absorbance was measured at 765 nm with the spectrophotometer as detailed above. Absorbances were converted to estimated phenolic concentration with a gallic acid standard curve as per Ainsworth and Gillepsie's method.

B.2 Additional Results

B.2.1 Growth

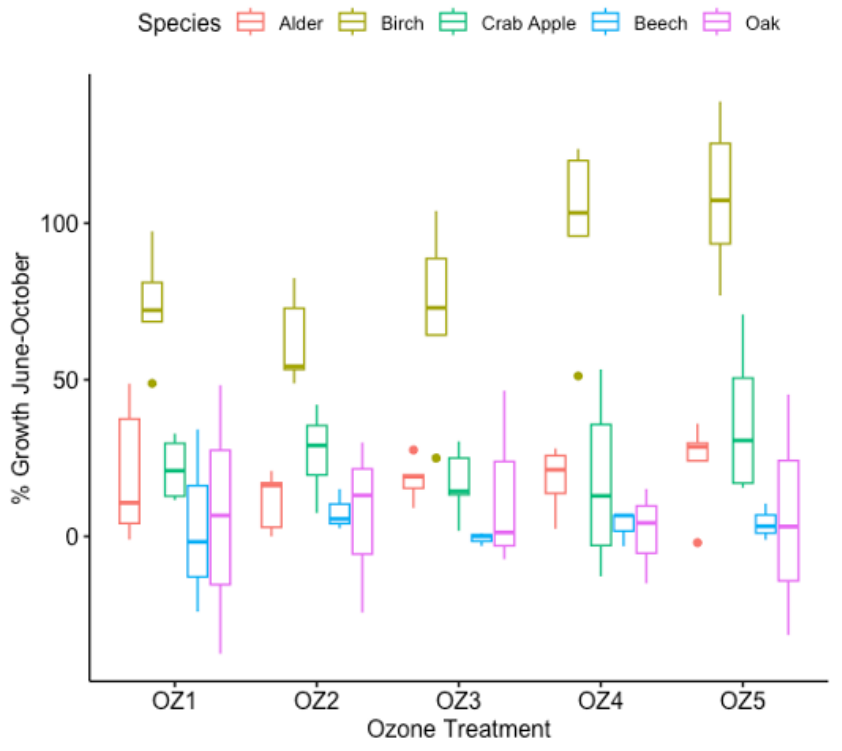


Figure B.1: Percentage growth in height of saplings exposed to different O_3 treatments from June to October 2022 varied significantly between species (Kruskal-Wallis $\chi^2 = 61.5$, d.o.f. $= 4$, $P < 0.001$), but not between O_3 treatments.

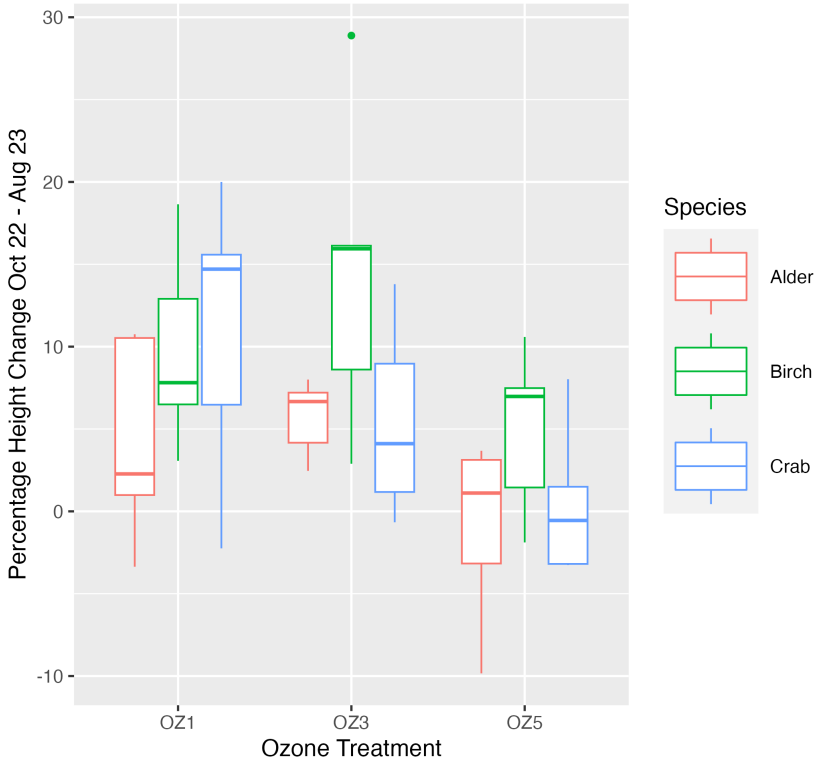


Figure B.2: Percentage growth of saplings between October 2022 and August 2023 in response to O_3 for alder, birch, and crab apple.

B.2.2 Destructive Harvest

Oak sapling stems on average had significantly greater dry mass, volume, and water content than Beech sapling stems (Wilcoxon Test, $W = 72$, $P = 0.004$; $W = 55.5$, $P = 0.002$; and $W = 73, P = 0.009$ respectively). O_3 treatment did not have any significant effect on root dry mass, leaf dry mass, stem dry mass, stem volume, leaf water content or stem water content.

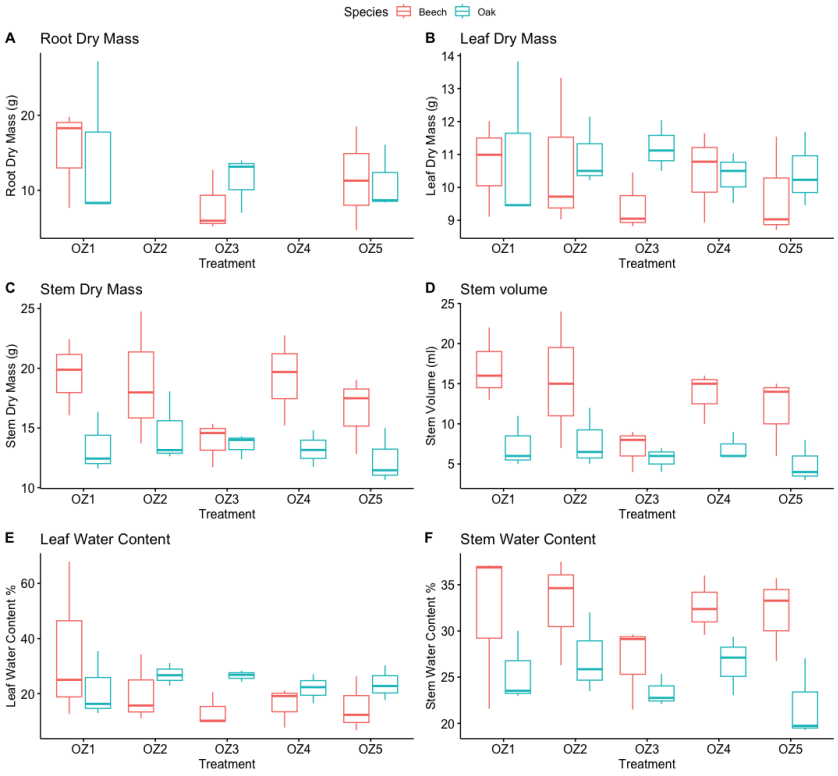


Figure B.3: Destructive harvest results of beech and oak saplings grown in different O_3 treatments from June to October 2022. Oak sapling stems on average had significantly greater dry mass, volume and water content than beech sapling stems (Wilcoxon Test, $W = 72$, $P = 0.004$; $W = 55.5$, $P = 0.002$; and $W = 73$, $P = 0.009$ respectively). O_3 treatment did not have any significant effect on destructively harvested parameters.

B.2.3 Gas Exchange

Instantaneous gas exchange measurements taken alongside relative chlorophyll index in July and August from low, medium, and high O_3 treatments revealed a strong temporal effect. There were no significant differences in gas exchange parameters or chlorophyll index between species when all O_3 treatments and months were averaged.

Figure 8 highlights the differences in instantaneous gas exchange parameters and chlorophyll content between July and August. Photosynthetic rate significantly decreased across all species and O_3 treatments between July and August (Wilcoxon test, $P < 0.001$). The relative chlorophyll content index did not change significantly between July and August, although there was much greater variability in the chlorophyll index of saplings in August compared to July (Standard Deviation August = 49.2, July = 4.85). Conductance to H_2O decreased significantly between July and August (Wilcoxon test, $P < 0.001$), as did intercellular CO_2 concentration (Wilcoxon test, $P < 0.001$). Transpiration rate and leaf temperature-based vapour pressure deficit both increased significantly between July and August (Wilcox Tests, both $P < 0.001$).

Analysis of variance of Aligned Rank Transformed (ART) was used to examine the combined explanatory power of month and O_3 treatment on gas exchange parameters due to the large seasonal effect observed. ART reiterated that the photosynthetic rate was significantly affected by the month of measurement ($P < 0.001$), but O_3 treatment did not have a significant simple main effect ($P = 0.178$). There was however a significant interaction between the effects of the month of measurement and O_3 treatment ($P = 0.0138$). Similarly, chlorophyll index and conductance were significantly affected by the month of measurement (both $P<0.001$), with a significant interaction between the effects of the month of measurement and O_3 treatment ($P = 0.0113$ and $P = 0.0268$ respectively). O_3 treatment also had a significant main effect on conductance ($P = 0.011$). Simple main effects analysis showed transpiration rate was significantly affected by the month of measurement ($P < 0.001$). O_3 treatment also had a significant simple main effect on transpiration rate ($P < 0.001$). There was not a significant

interaction between the effects month of measurement and O_3 treatment in the case of transpiration rate (P=0.0815). ART was not appropriate for analysing intercellular CO/2 concentration and vapour pressure deficit due to F values on aligned responses exceeding zero. However, there was a significant difference in vapour pressure deficit between low, medium and high O_3 treatments when averaged across all species and months (Kruskal-Wallis $\chi^2 = 20.5,\ df = 2,\ P < 0.001$).

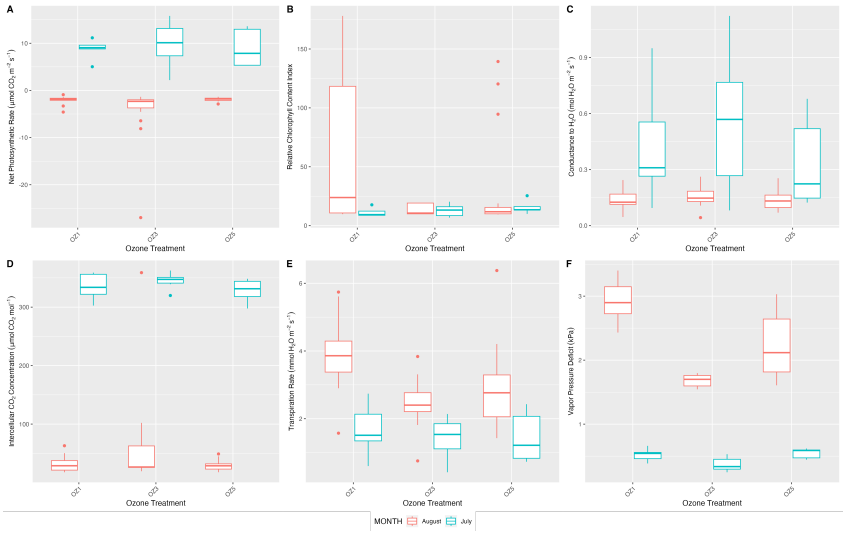


Figure B.4: Average instantaneous Gas Exchange and chlorophyll measurements from Alder, Beech, Birch, Crab Apple and Oak saplings exposed to low (OZ1, daytime target maxima 30 ppb), medium (OZ3, daytime target maxima 65 ppb) and high (OZ5, daytime target maxima 110 ppb) O_3 regimes in July and August 2022. Saplings in higher O_3 treatments had significantly faster rates of transpiration (Kruskal-Wallis $\chi^2 = 10.691$, $df = 2$, $P = 0.0048$). The Vapour Pressure Deficit was significantly greater in saplings exposed to the lowest O_3 treatment (Kruskal-Wallis $\chi^2 = 20.452,\ df = 2,\ P > 0.001$).

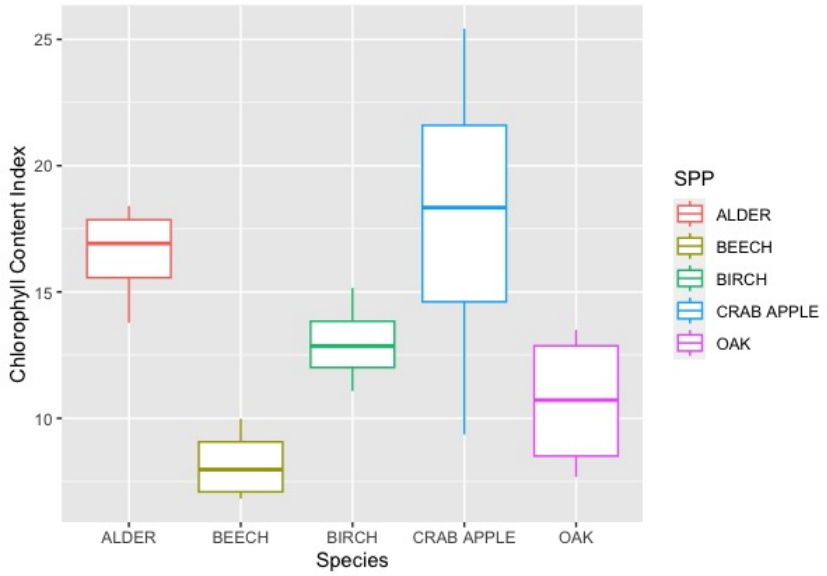


Figure B.5: Chlorophyll content index of saplings across all O_3 treatments measured in July 2022. Chlorophyll content differs significantly between species (Kruskal-Wallis $\chi^2 = 12.4$, d.o.f. $= 4$, $P = 0.0149$). Dunn post hoc testing revealed alder and crab apple had a significantly higher chlorophyll index on average than beech ($Z = 2.93$, $P_{\text{adjusted}} = 0.0341$; $Z = -2809$, $P_{\text{adjusted}} = 0.0497$, respectively). The chlorophyll content index agrees closely with the interspecific differences seen in chlorophyll A extractions in Acetone.

B.2.4 Fluorometry

Fluorescence dynamics analysed via PAM fluorometry did not show any significant differences between low, medium, and high O_3-exposed saplings. Some trends can be seen however, such as reduced ETR in all species in the highest O_3 exposure regime compared to the lowest. Trends were visible between species, for example on average Alder saplings had a faster electron transport rate than Beech saplings, but the overall effect of species on fluorescence parameters was not significant.

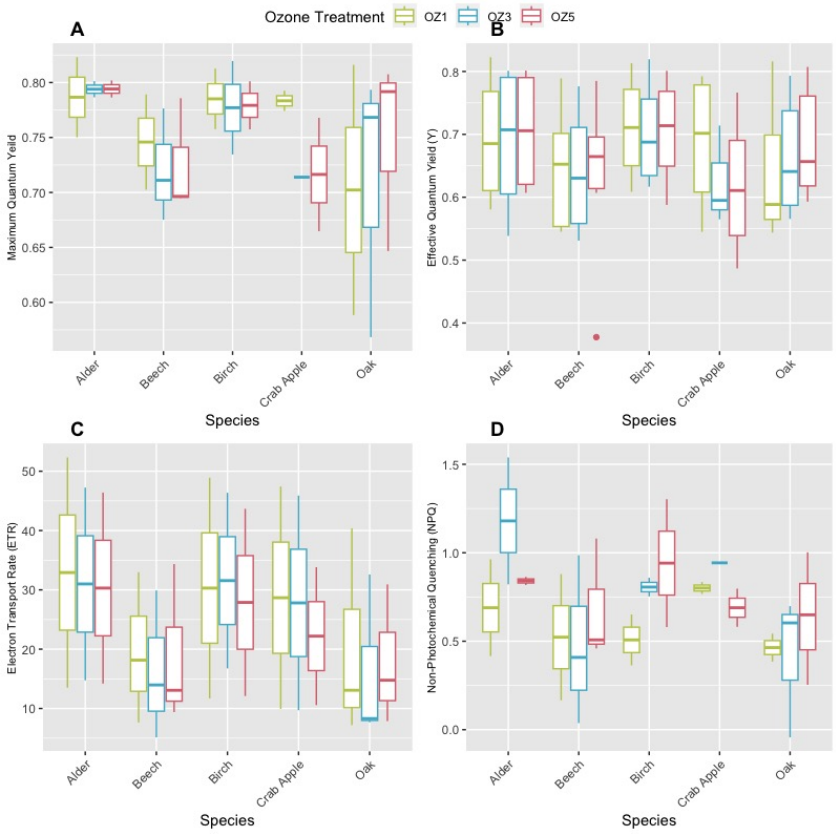


Figure B.6: Pulse Amplitude Modulated fluorescence analysis of Alder, Beech, Birch, Crab Apple and Oak saplings exposed to low (OZ1, daytime target maxima 30 ppb), medium (OZ3, daytime target maxima 65 ppb) and high (OZ5, daytime target maxima 110 ppb) O_3 regimes. No significant differences in maximum quantum yield (A), effective quantum yield (B) electron transport rate (C), or non-photochemical quenching (D) were found between the different O_3 treatments.

B.2.5 Biochemical Extractions

Species had a strong impact on the concentrations of chlorophyll A, chlorophyll B, carotenoids and xanthophyll (Kruskal Wallis $\chi^2 = 69.1$ $P < 0.001$, $\chi^2 = 25.8$ $P < 0.001$, $\chi^2 = 26.5$ $P < 0.001$, $\chi^2 = 27.4$ $P < 0.001$, respectively). Due to this strong species effect, the impact of O_3 treatment on pigment concentrations was analysed separately for each species. However, no significant effect of O_3 treatment was found for any species' concentration of chlorophyll A, chlorophyll B, carotenoids, xanthophyll or phenols.

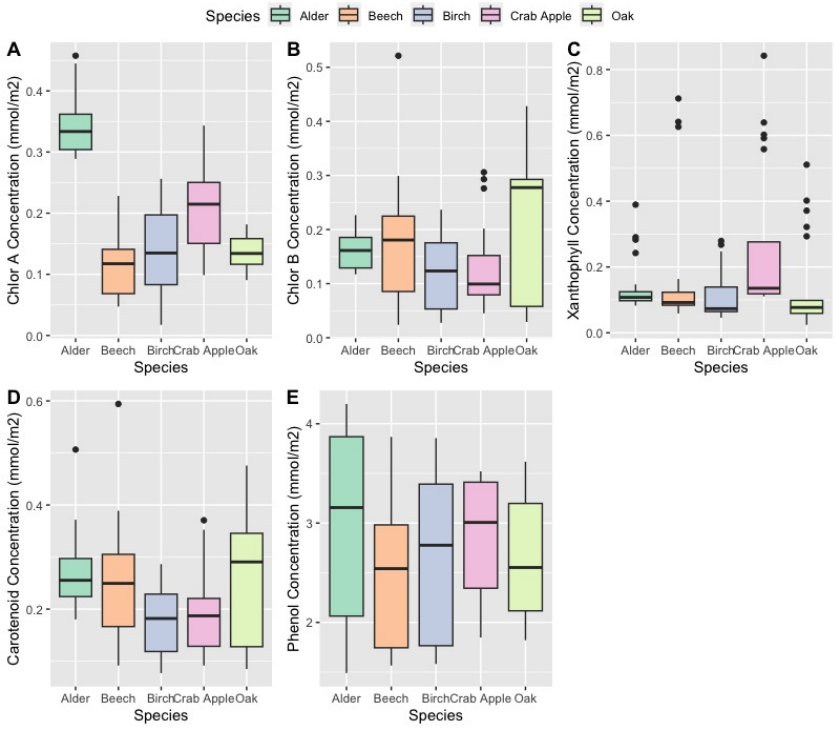


Figure B.7: Pigment extractions averaged from June to October 2022 across all O_3 treatments show variation in pigment content between the test species. Chlorophyll A, chlorophyll B, carotenoid and xanthophyll content all differed significantly between species (Kruskal-Wallis $\chi^2 = 69.1$ $P < 0.001$, $\chi^2 = 25.8$ $P < 0.001$, $\chi^2 = 26.5$ $P < 0.001$, $\chi^2 = 27.4$ $P < 0.001$, respectively). Phenol concentration did not differ significantly between species (Kruskal-Wallis $\chi^2 = 3.65$ $P = 0.455$).

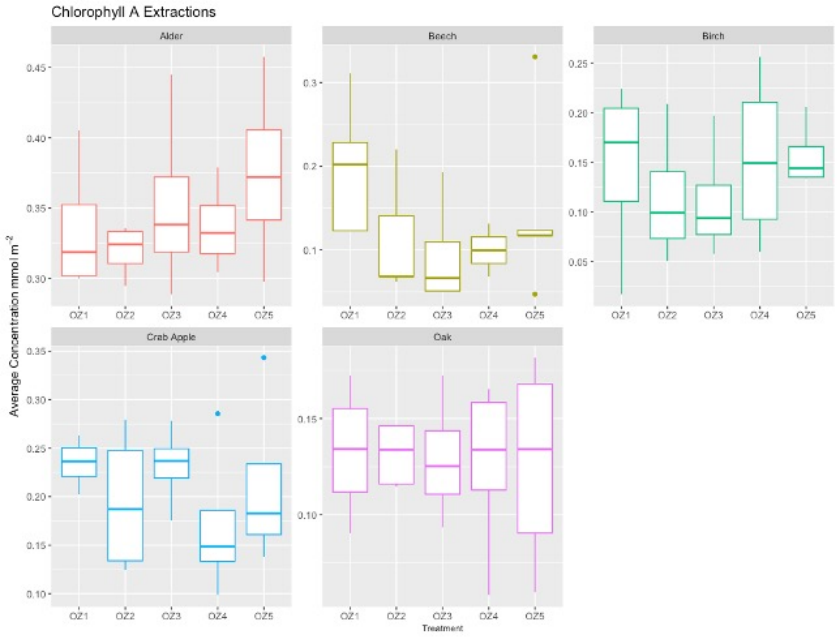


Figure B.8: Average chlorophyll A concentrations derived via spectrophotometry of ground dried leaves extracted in acetone each month from June to October 2022. Species are separated due to high interspecific variation. No significant O_3 treatment effect was found for any species although trends are visible in alder and beech. In alder, Chlorophyll A shows an increasing trend with O_3 concentration, the opposite is seen in beech which is a more O_3-sensitive species.

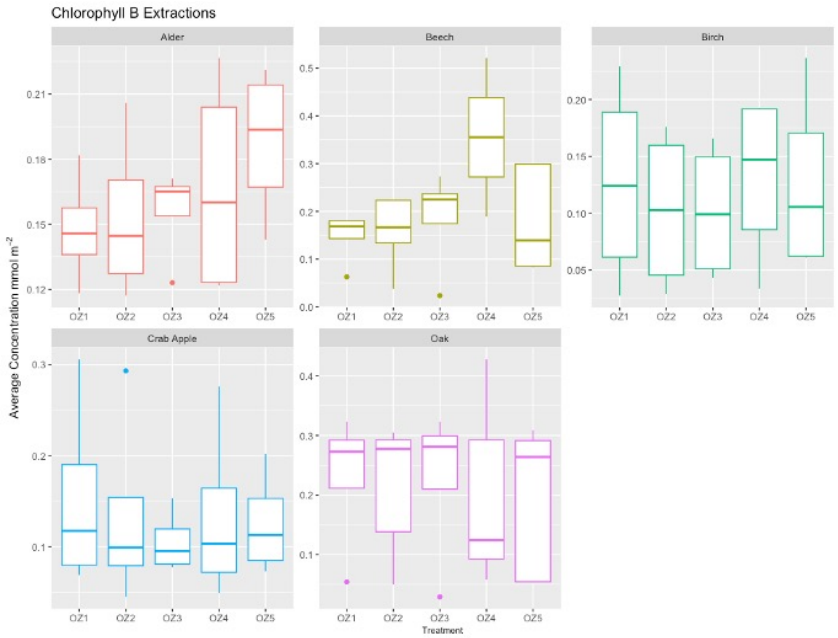


Figure B.9: Average chlorophyll B concentrations derived via spectrophotometry of ground dried leaves extracted in acetone each month from June to October 2022. Species are separated due to high interspecific variation. No significant O_3 treatment effect was found for any species. In alder Chlorophyll B shows an increasing trend with O_3 concentration.

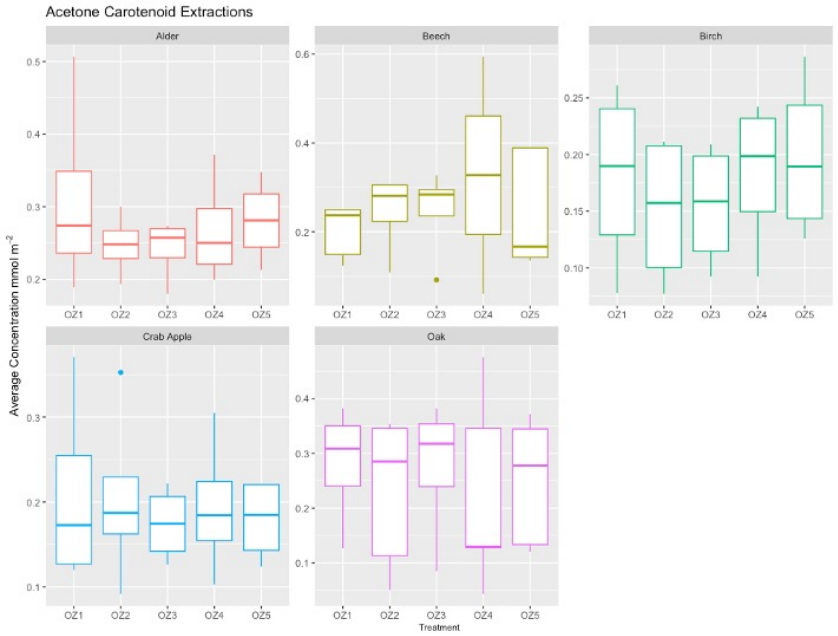


Figure B.10: Average carotenoid concentrations derived via spectrophotometry of ground dried leaves extracted in acetone each month from June to October 2022. Species are separated due to high interspecific variation. No significant O_3 treatment effect was found for any species.

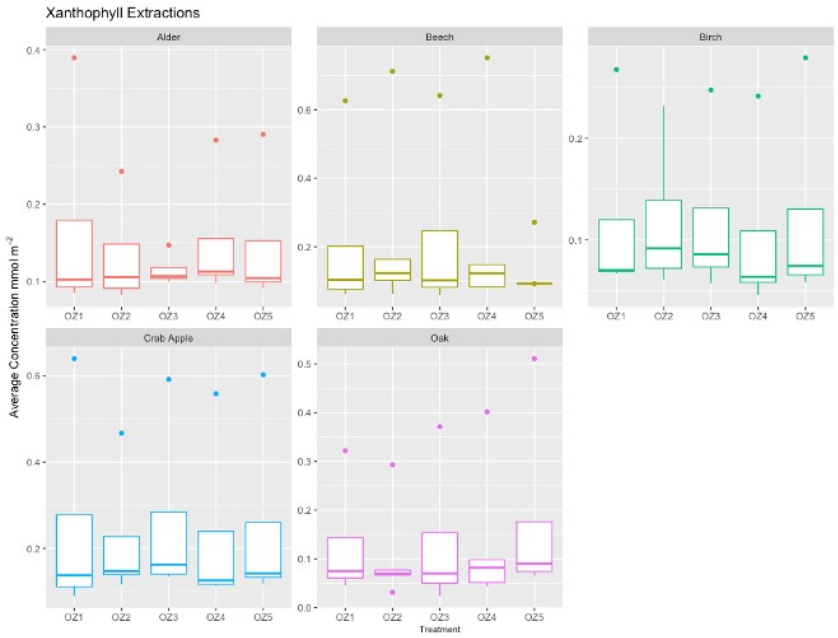


Figure B.11: Average Xanthophyll concentrations derived via spectrophotometry of ground dried leaves extracted in acidified ethanol each month from June to October 2022. Species are separated due to high interspecific variation. No significant O_3 treatment effect was found for any species. The outliers are caused by the large increase in xanthophyll content in leaves collected in October compared to all other months.

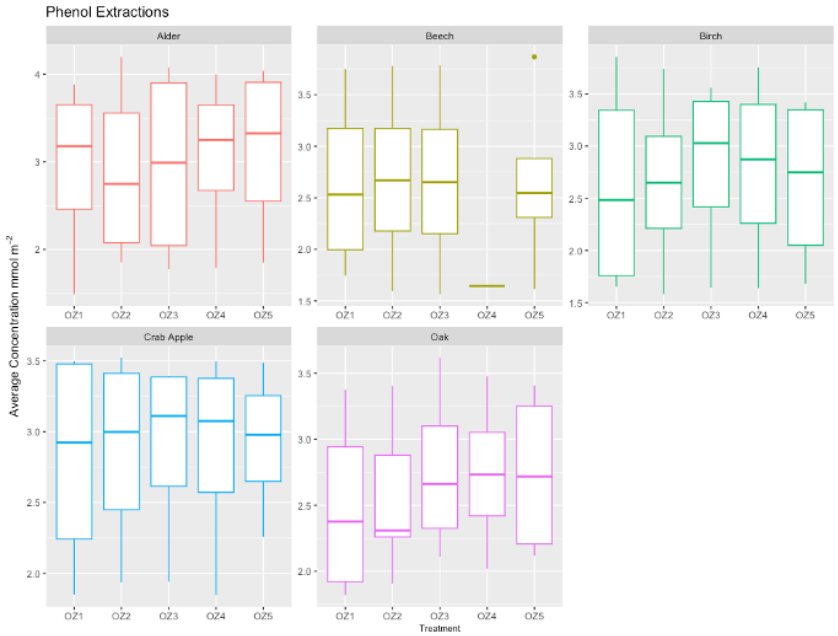


Figure B.12: Average phenol concentrations of leaves collected each month from June to October 2022 derived via the Folin-Ciocalteau method. Species are separated due to high interspecific variation. No significant O_3 treatment effect was found for any species.

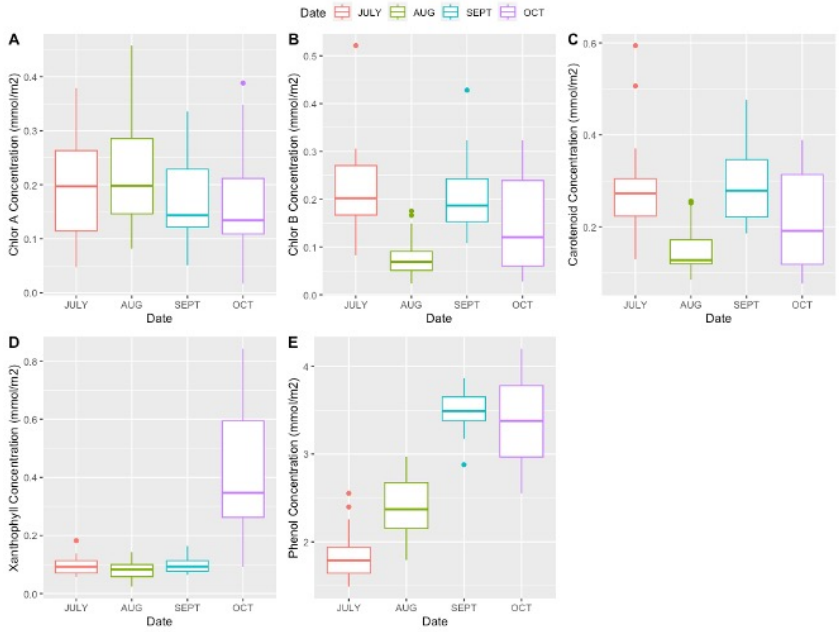


Figure B.13: Several pigments showed seasonal variation throughout the experimental period. Xanthophyll content varied significantly between months of leaf collection (Kruskal-Wallis $\chi^2 = 55.8$, d.o.f. $= 4$, $P < 0.001$). Post-hoc testing shows Xanthophyll concentration was significantly higher in October than in all other months ($P < 0.001$). Phenol concentration differed significantly between all months except September and October (Kruskal-Wallis $\chi^2 = 85.202$, d.o.f. $= 4$, $P < 0.001$, Wilcoxon post hoc $P < 0.001$ for all month pairwise comparisons except September and October where $P = 0.32$).

B.2.6 PCA

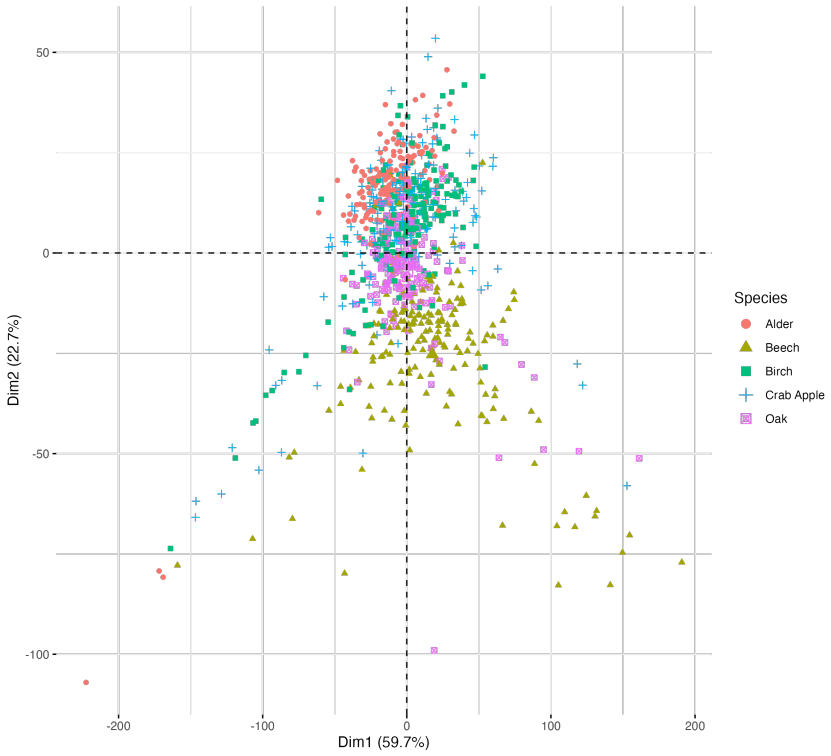


Figure B.14: Principal component plot of leaf reflectance spectra, coloured by species.

Effect	d.o.f.	F-statistic	P-value
Species	5	24.3299	<0.001***
O3 Treatment	4	5.7377	<0.001***
Month	3	25.9126	<0.001***
Species x O3 Treatment	16	3.6983	<0.001***
Species x Month	12	2.2111	0.003**
O3 Treatment x Month	12	2.9678	<0.001***
Species ×O3Treatment ×Month	46	1.3329	0.040*

Table B.3: Results from PERMANOVA of leaf reflectance by species, O_3 treatments and their interaction.

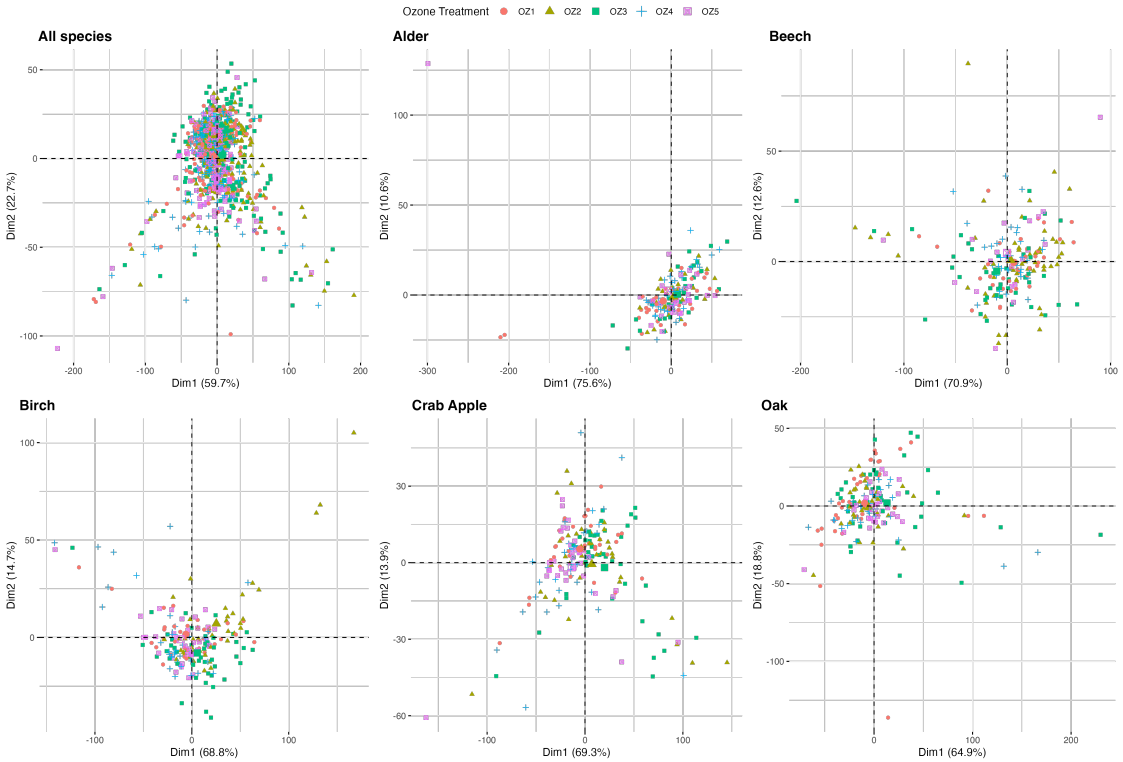


Figure B.15: Principal component plots of leaf reflectance spectra separated by species and coloured by O_3 treatment.

B.2.7 PLSDA

PLSDA results per species are presented below.

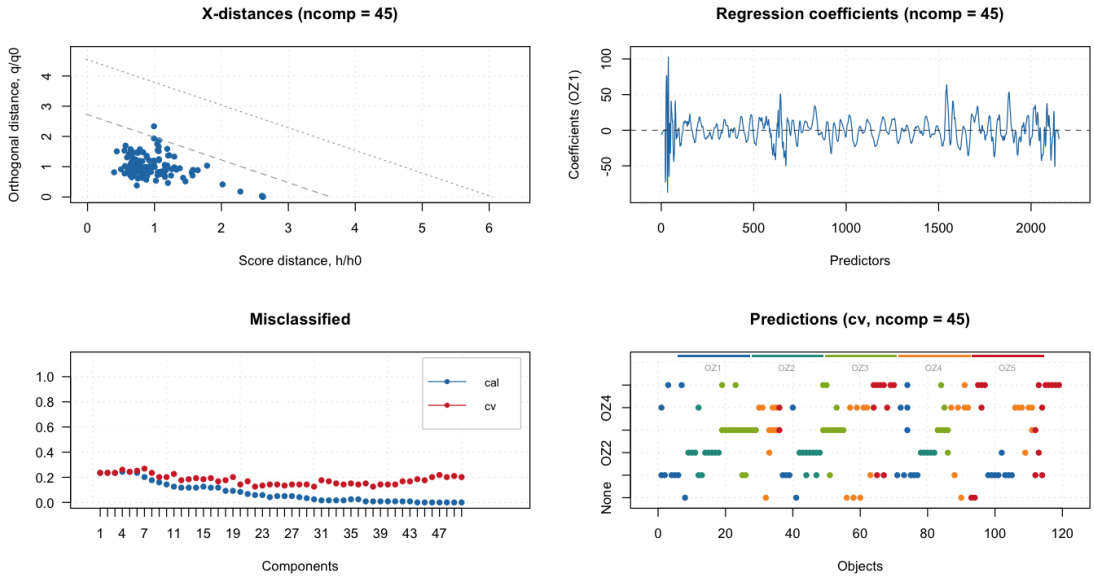


Figure B.16: Partial Least Squares Discriminant Analysis model plots for alder saplings exposed to five O_3 treatments, 45 components.

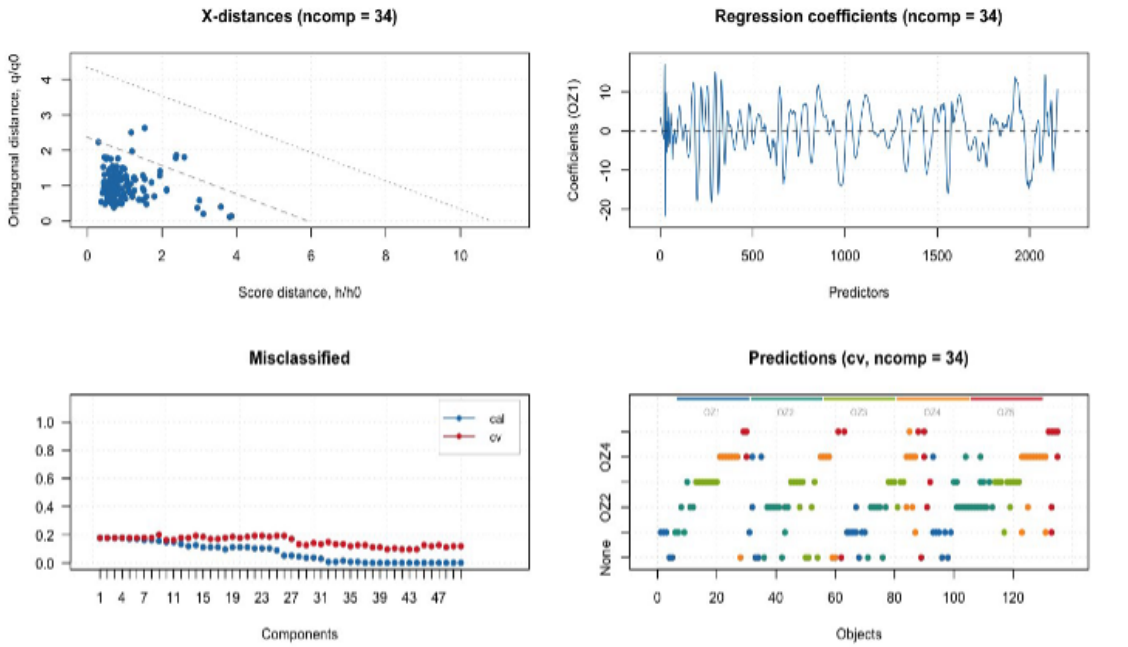


Figure B.17: Partial Least Squares Discriminant Analysis model plots for beech saplings exposed to five O_3 treatments, 45 components.

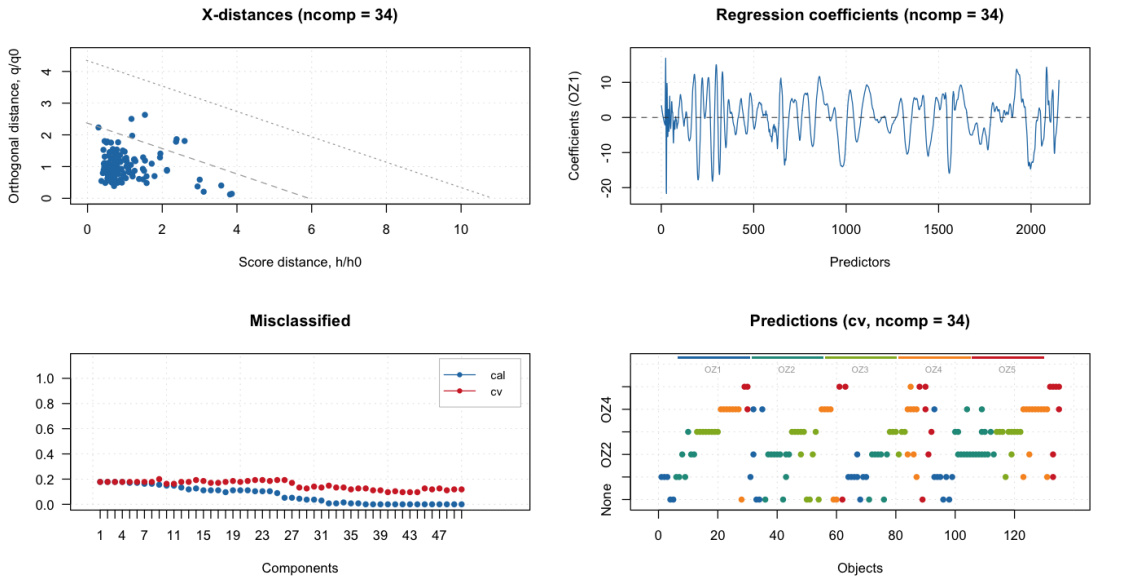


Figure B.18: Partial Least Squares Discriminant Analysis model plots for birch saplings exposed to five O_3 treatments, 45 components.

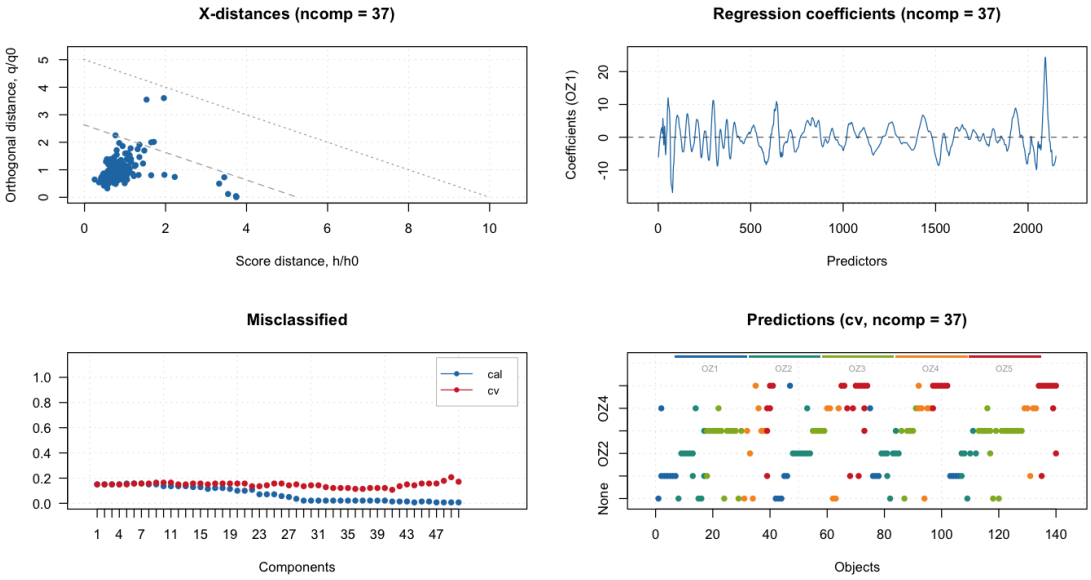


Figure B.19: Partial Least Squares Discriminant Analysis model plots for crab apple saplings exposed to five O_3 treatments, 45 components.

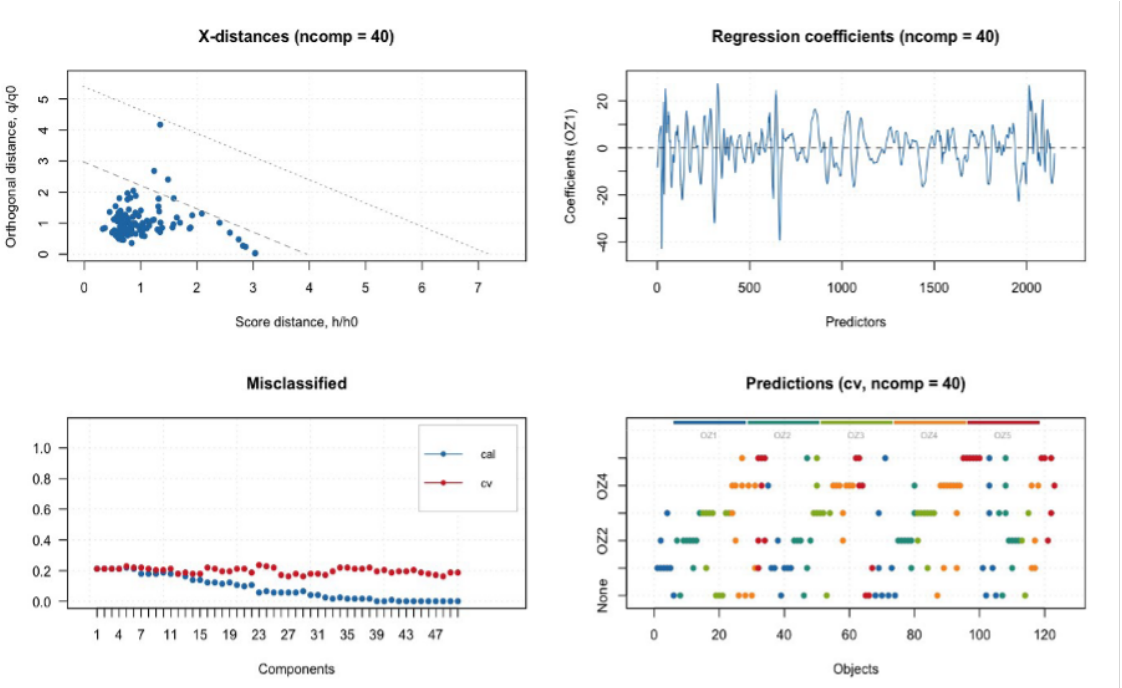


Figure B.20: Partial Least Squares Discriminant Analysis model plots for oak saplings exposed to five O_3 treatments, 45 components.

B.2.8 Vegetation Indices

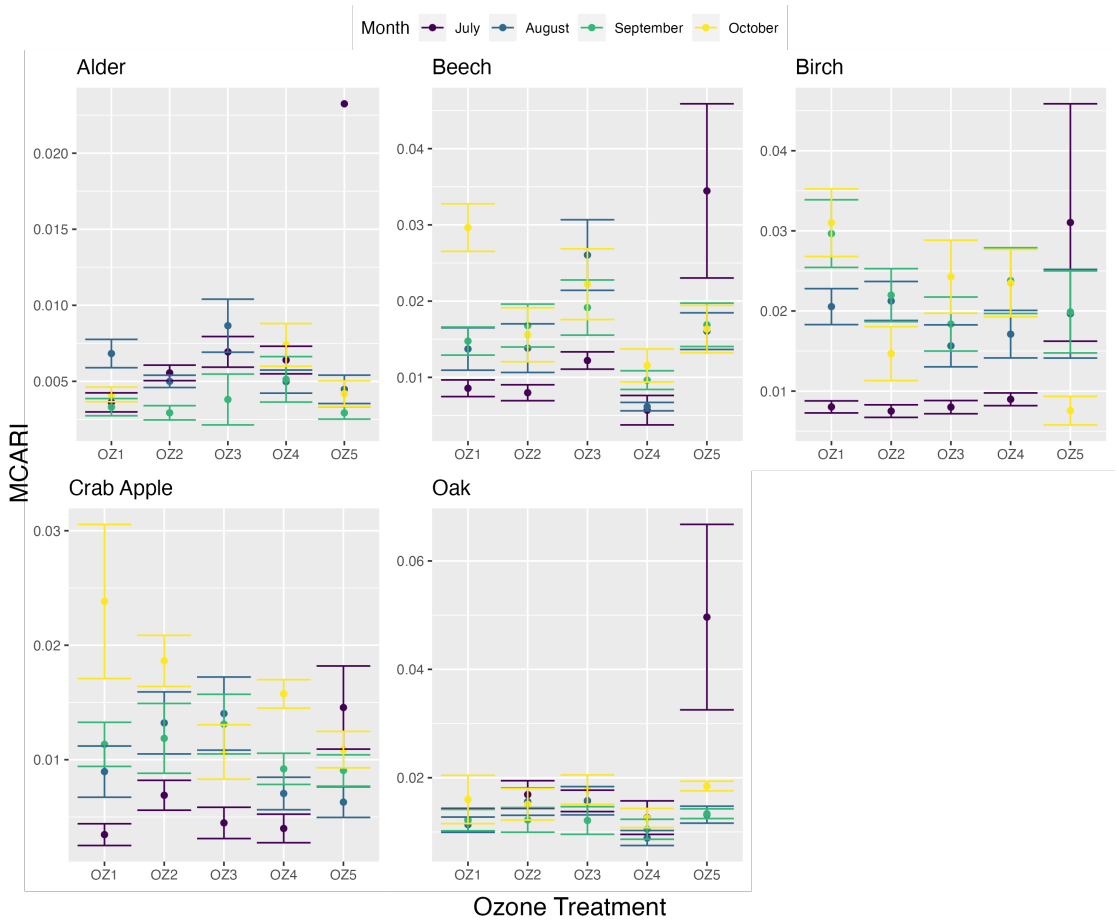


Figure B.21: MCARI split by species in different O_3 treatments, coloured by month of measurement.

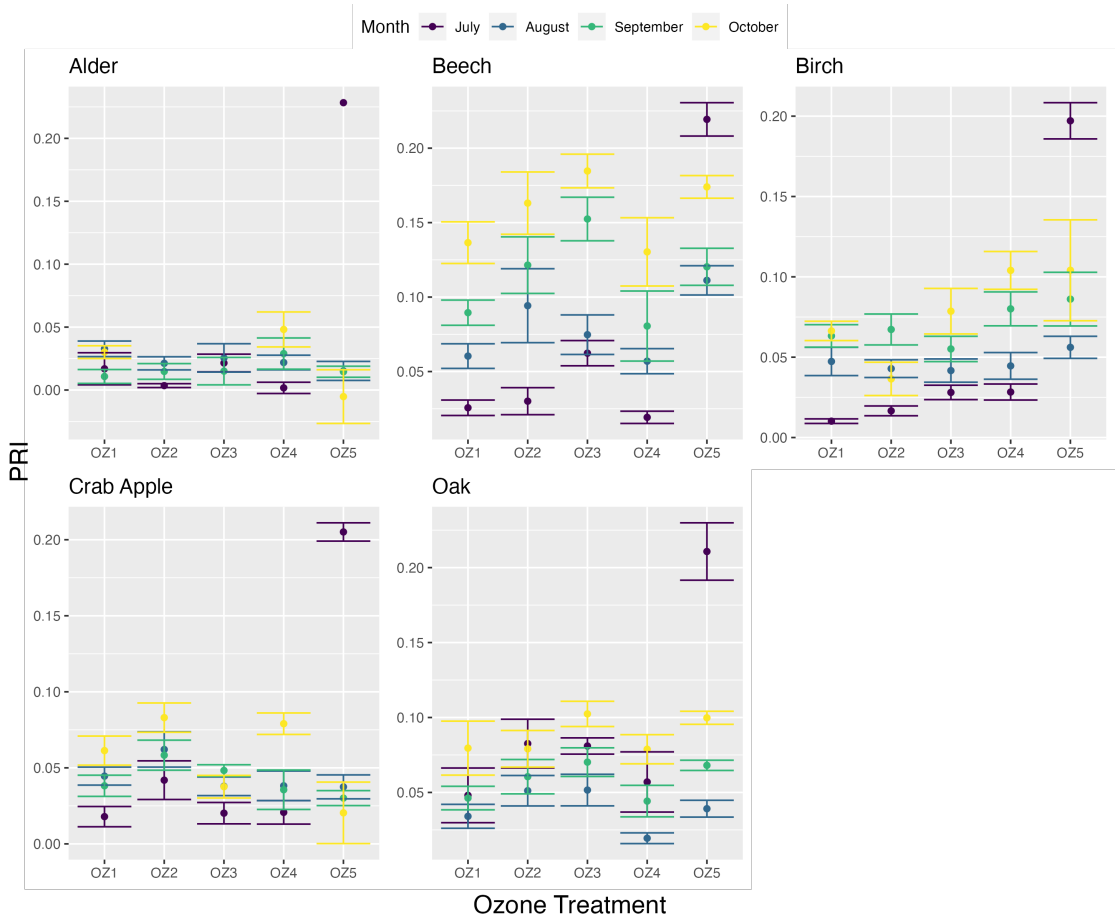


Figure B.22: PRI split by species in different O_3 treatments, coloured by month of measurement.

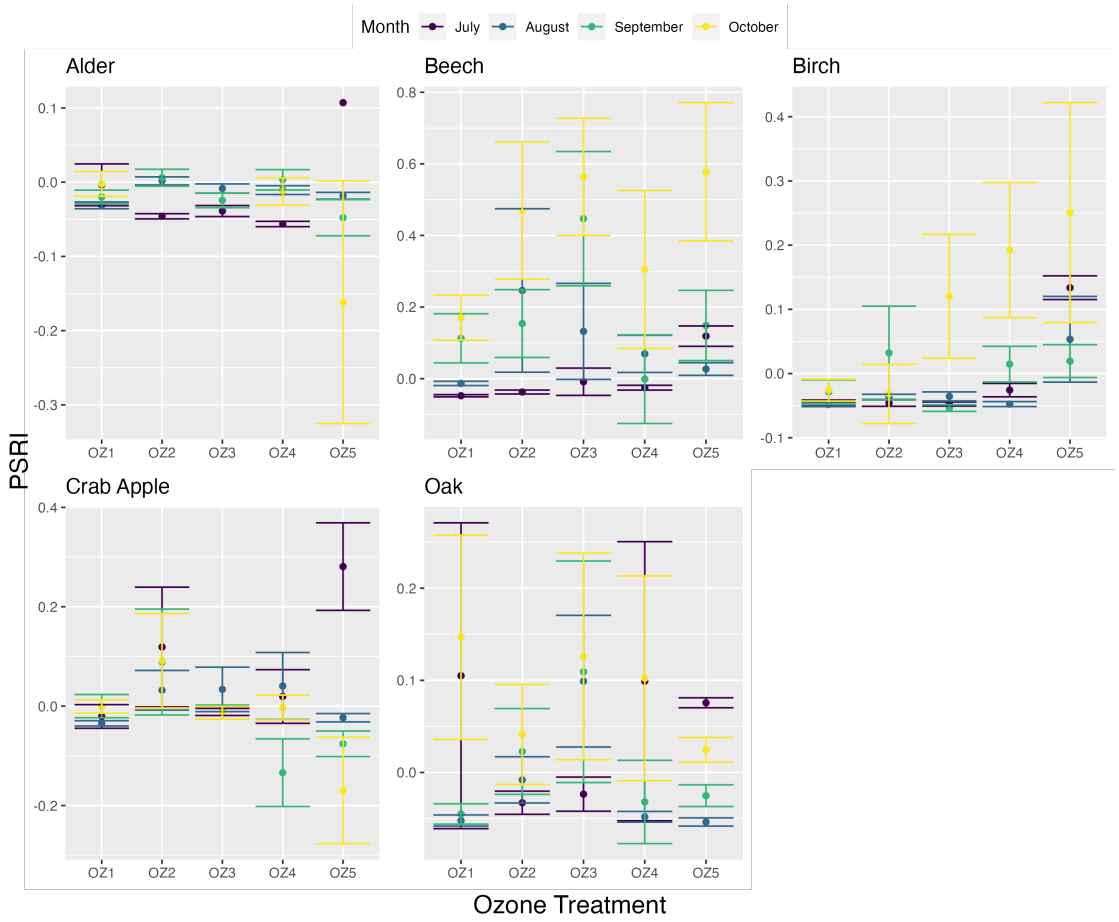


Figure B.23: PSRI split by species in different O_3 treatments, coloured by month of measurement.

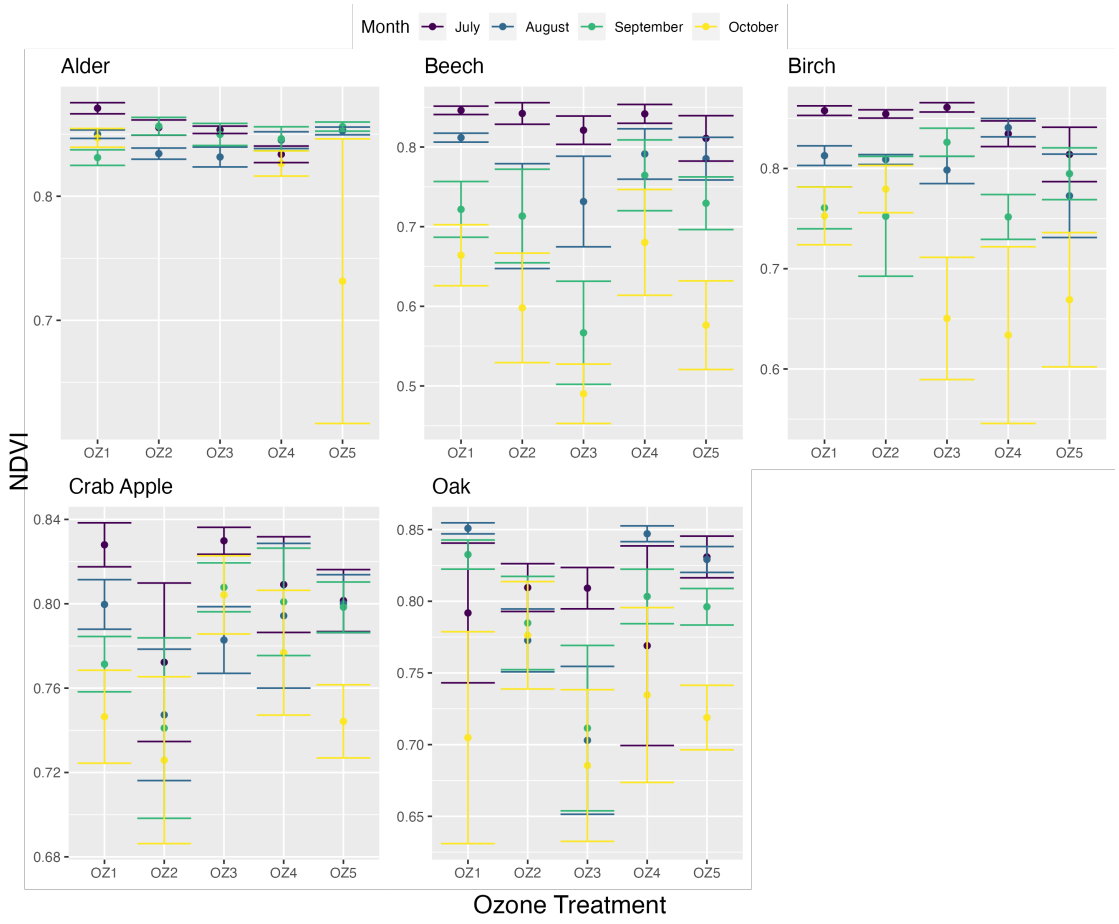


Figure B.24: NDVI split by species in different O_3 treatments, coloured by month of measurement.

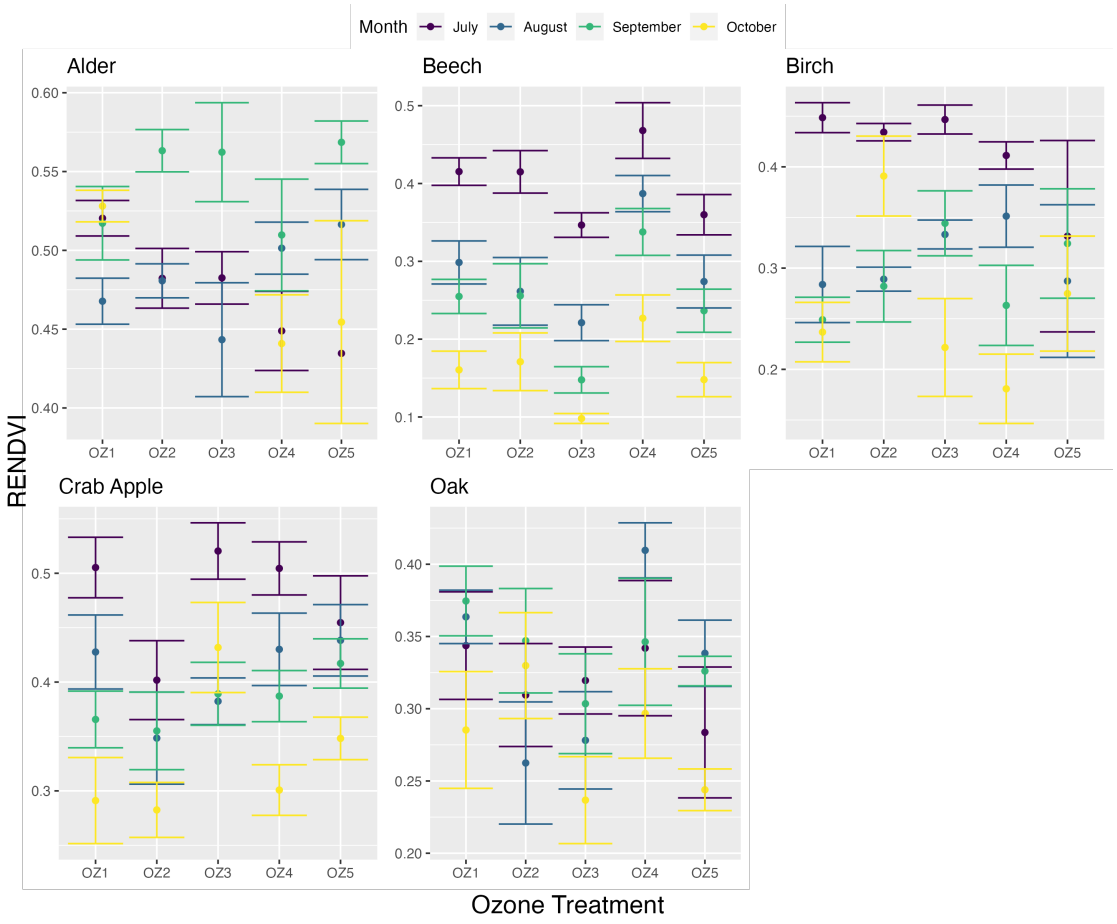


Figure B.25: RENDVI split by species in different O_3 treatments, coloured by month of measurement.

References

[1] J. W. Rouse et al. “Monitoring vegetation systems in the Great Plains with ERTS”. In: NASA. Goddard Space Flight Center 3d ERTS-1 Symp., Vol. 1, Sect. A. NTRS Author Affiliations: Texas A&M Univ. NTRS Report/Patent Number: PAPER-A20 NTRS Document ID: 19740022614 NTRS Research Center: Legacy CDMS (CDMS). Jan. 1, 1974.

[2] C. S. T Daughtry et al. “Estimating Corn Leaf Chlorophyll Concentration from Leaf and Canopy Reflectance”. In: *Remote Sensing of Environment* 74.2 (Nov. 1, 2000), pp. 229–239. DOI: 10.1016/S0034-4257(00)00113-9.

[3] Mark N. Merzlyak et al. “Non-destructive optical detection of pigment changes during leaf senescence and fruit ripening”. In: *Physiologia Plantarum* 106.1 (1999), pp. 135–141. DOI: 10.1034/j.1399-3054.1999.106119.x.

[4] Daniel A Sims and John A Gamon. “Relationships between leaf pigment content and spectral reflectance across a wide range of species, leaf structures and developmental stages”. In: *Remote Sensing of Environment* 81.2 (Aug. 2002), pp. 337–354. DOI: 10.1016/S0034-4257(02)00010-X.

[5] J. A. Gamon, L. Serrano, and J. S. Surfus. “The photochemical reflectance index: an optical indicator of photosynthetic radiation use efficiency across species, functional types, and nutrient levels”. In: *Oecologia* 112.4 (Nov. 1, 1997), pp. 492–501. DOI: 10.1007/s004420050337.

[6] Josep Peñuelas, Iolanda Filella, and John A. Gamon. “Assessment of photosynthetic radiation-use efficiency with spectral reflectance”. In: *New Phytologist* 131.3 (1995), pp. 291–296. DOI: 10.1111/j.1469-8137.1995.tb03064.x.

[7] U. Schreiber. “Detection of rapid induction kinetics with a new type of high-frequency modulated chlorophyll fluorometer”. In: *Current topics in photosynthesis: Dedicated to Professor L.N.M. Duysens on the occasion of his retirement*. Ed. by J. Amesz, A. J. Hoff, and H. J. Van Gorkum. Dordrecht: Springer Netherlands, 1986, pp. 259–270. DOI: 10.1007/978-94-009-4412-1_24.

[8] John R Murray and Wesley P Hackett. “Dihydroflavonol Reductase Activity in Relation to Differential Anthocyanin Accumulation in Juvenile and Mature Phase Hedera helix L.V”. In: 97 (1991), p. 9.

[9] Elizabeth A Ainsworth and Kelly M Gillespie. “Estimation of total phenolic content and other oxidation substrates in plant tissues using Folin–Ciocalteu reagent”. In: *Nature Protocols* 2.4 (Apr. 2007), pp. 875–877. DOI: 10.1038/nprot.2007.102.

C
Appendix to Chapter 3

BIFoR		Wytham	
Measurement Date	O_3 monitoring period (hrs)	Measurement Date	O_3 monitoring period (hrs)
22/06/23	NA	27/06/23	477
05/07/23	310	12/07/23	360
25/07/23	482	01/08/23	476
10/08/23	384	09/08/23	NA
24/08/23	334	04/09/23	817
13/09/23	480	22/09/23	434
06/10/23	552	12/10/23	482

Table C.1: Leaf reflectance sampling dates for BIFoR FACE and Wytham Woods, O_3 diffusion tubes were also changed on these dates. O_3 diffusion tubes measure cumulative O_3 exposure during the monitoring period, which is then divided by exposure hours to produce average O_3 concentration values.



Figure C.1: Examples of stippling of oak leaves in Wytham Woods.

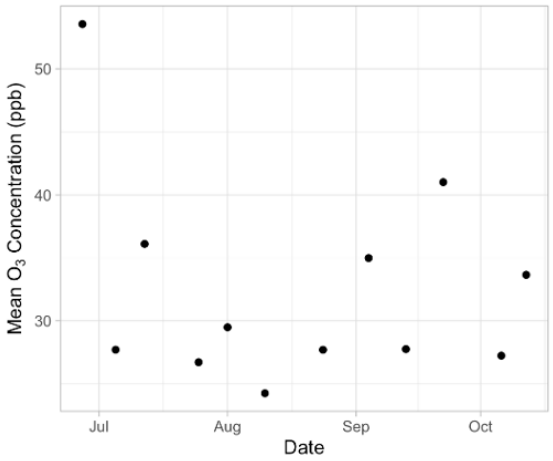


Figure C.2: Mean O_3 concentration against date, data from both sites

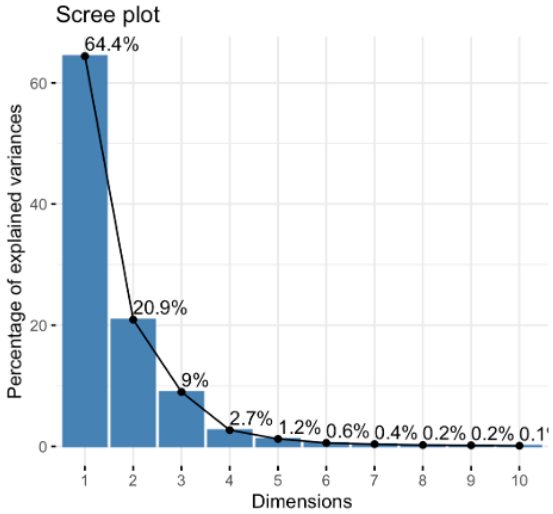


Figure C.3: Scree plot of principal components calculated from the hyperspectral leaf reflectance dataset.

Vegetation Index	Correlation	Degrees of Freedom	T Value	*P* Value
NDVI	0.52	10	1.92	0.0832
MCARI	0.826	10	4.63	0.000933 ***
PRI	0.0273	10	0.0864	0.933
PSRI	-0.563	10	-2.15	0.0569
Max NDSI	0.839	10	4.88	0.000639 ***
OzDI	-0.301	10	-0.997	0.342

Table C.2: Results of Pearson Correlation analysis of different vegetation indices against cumulative O_3 concentration. * indicates $P\ value < 0.05$, ** indicates $P\ value < 0.01$, *** indicates $P\ value < 0.001$.

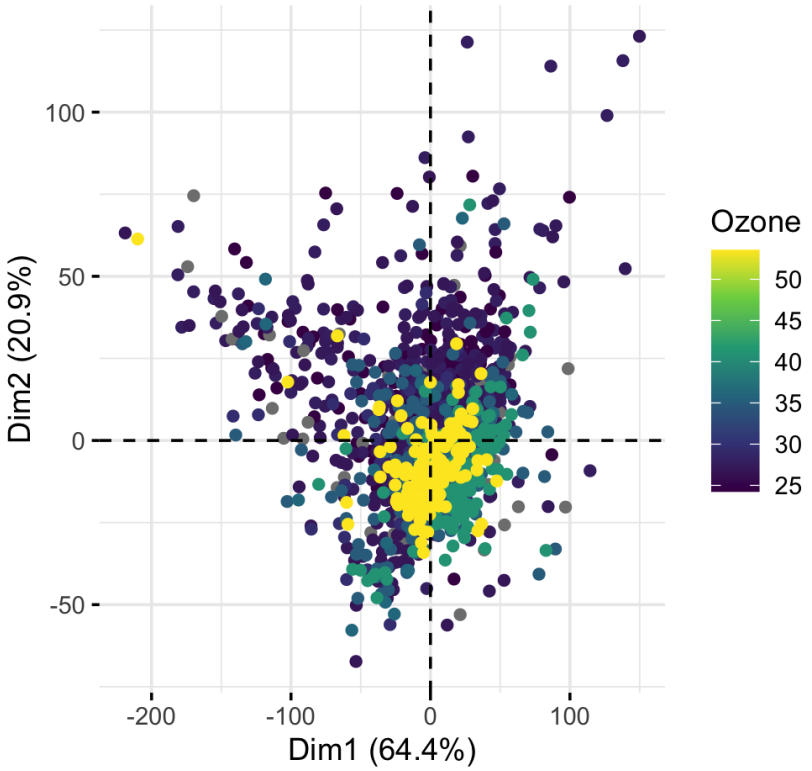


Figure C.4: PCA plot of leaf spectra coloured by average ozone concentration (ppb), against the first two principal components.

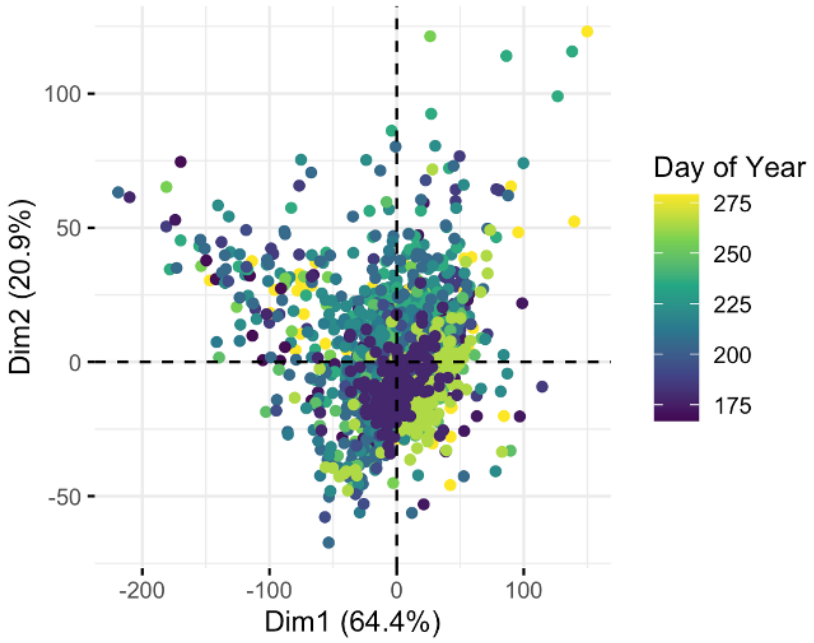


Figure C.5: PCA plot of leaf spectra coloured by date of measurement (as day of year) against the first two principal components.

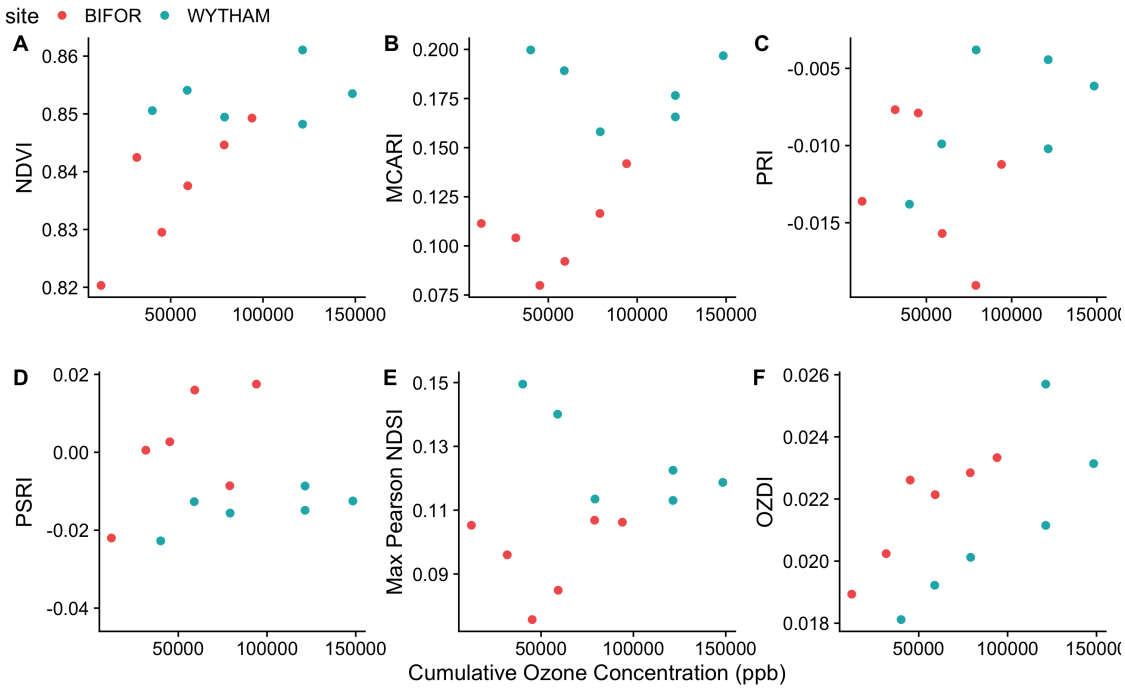


Figure C.6: Vegetation indices plotted against cumulative ozone concentration, coloured by site of measurement (BIFoR in red, Wytham Woods in blue).

D

Appendix to Chapter 5

Contents

D.1 GRVI 227
D.2 NDVI 230

The same analysis as presented in Chapter 5 for MCARI was also carried out for NDVI and GRVI. Neither showed an annual correlation with O_3 damage in forested areas of the UK at 1 km resolution. The results of NDVI and GRVI analyses are presented in this appendix.

D.1 GRVI

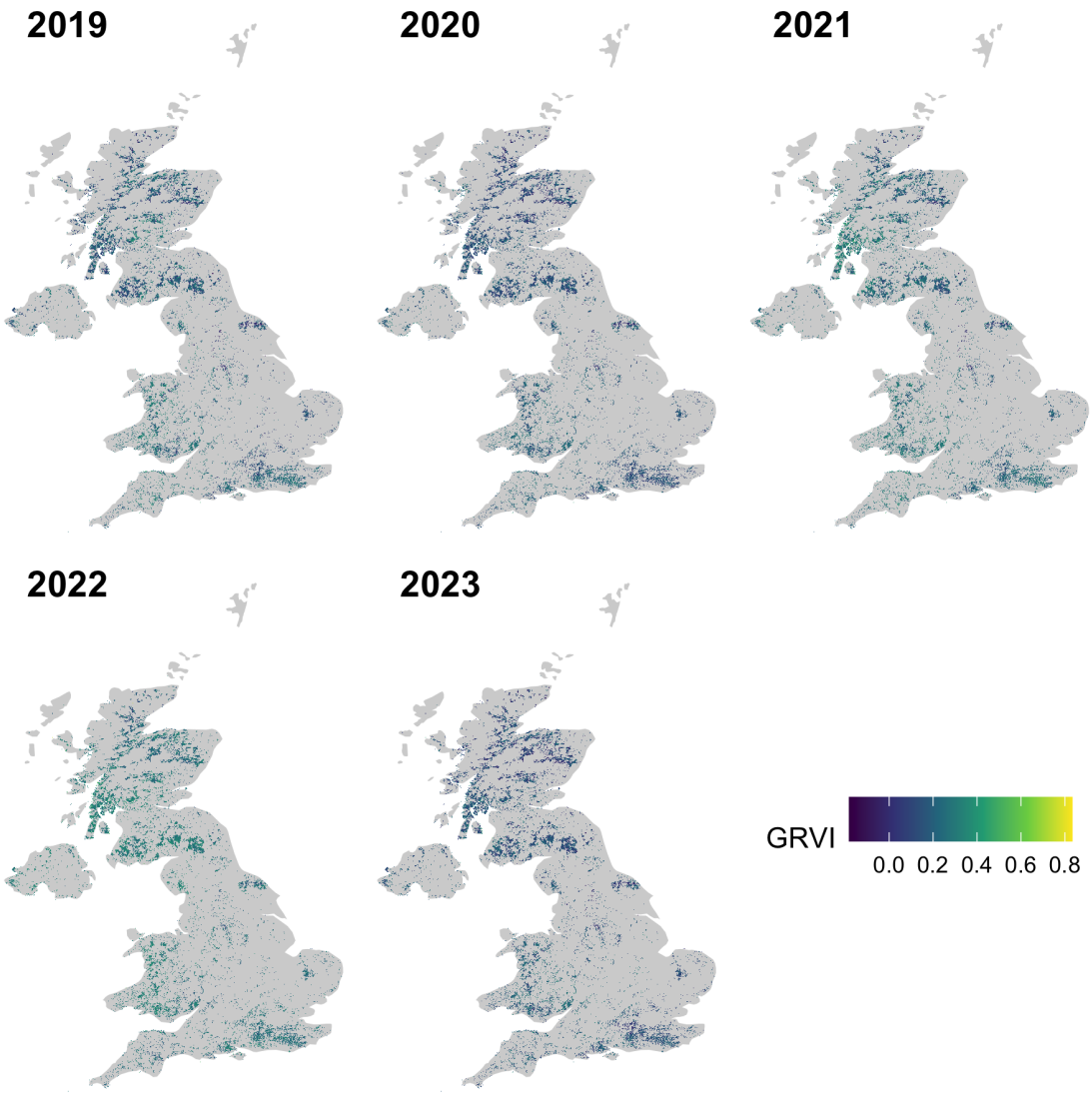


Figure D.1: Maps of median annual GRVI of forested areas of the UK, calculated from Sentinel 2 data down sampled to 1 km spatial resolution, 2019 to 2023.

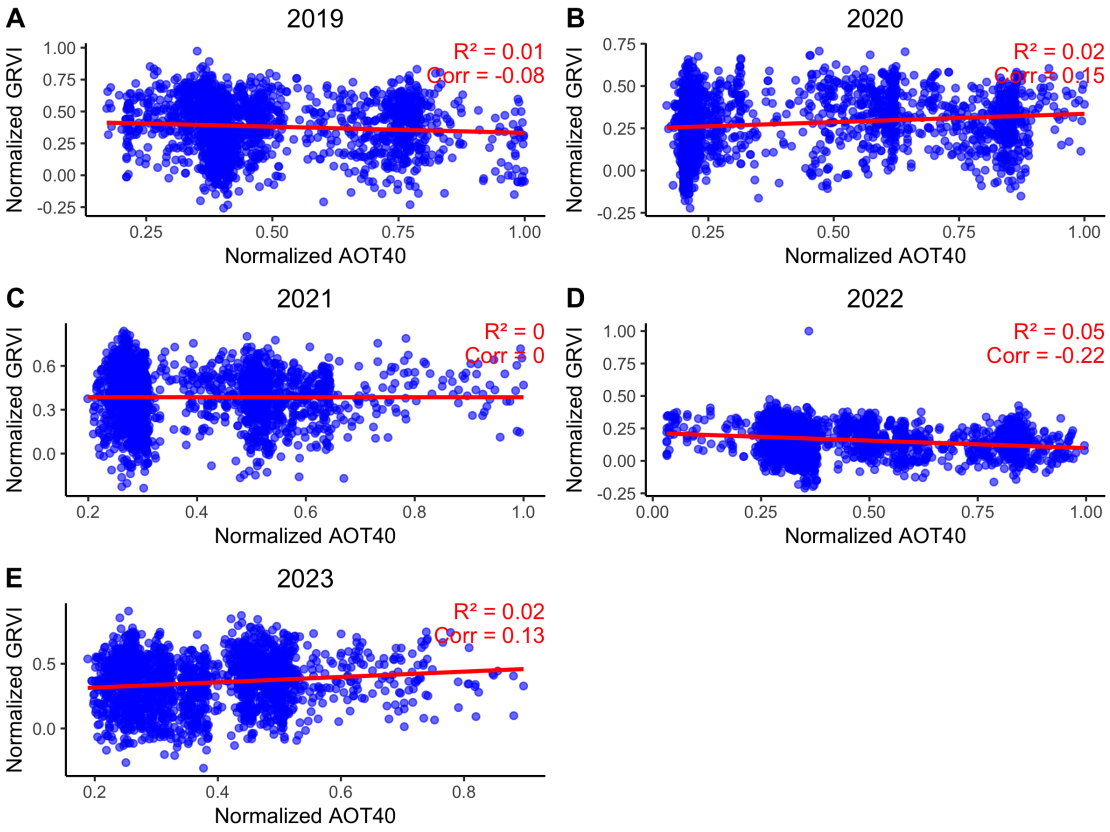


Figure D.2: The correlative relationship between annual GRVI and AOT40 for 20,000 forested 1 km cells in the UK plotted in blue, fitted with linear models in red. The R^2 and correlation coefficient (*Corr*) are shown red text. Analyses for the years 2019-2023 are shown in panels A-E.

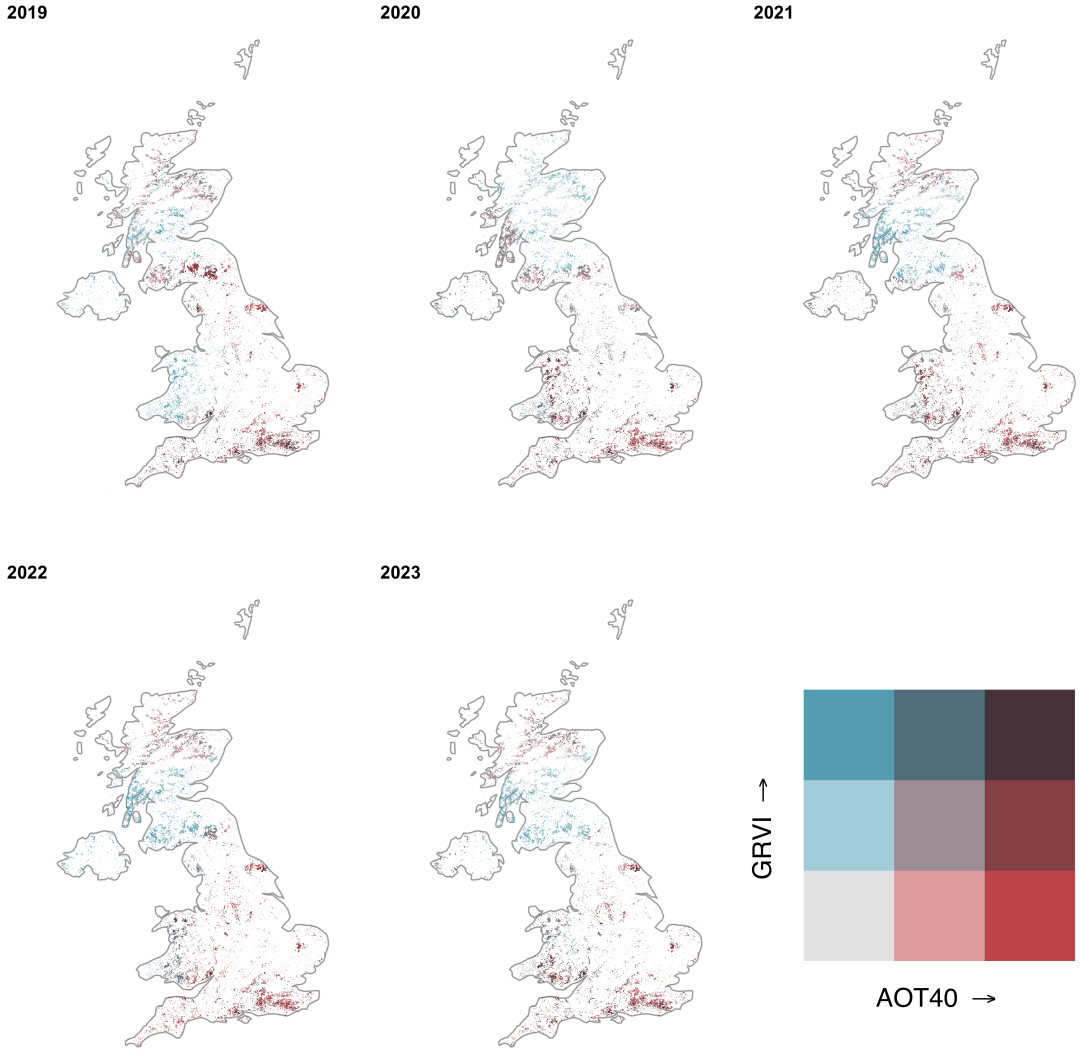


Figure D.3: Bivariate maps of annual median GRVI against annual AOT40 for forested areas of the UK, at 1 km spatial resolution. Areas with high GRVI and low AOT40 are shown in bright blue, areas with high AOT40 and low GRVI are shown in bright red. Areas with both high AOT40 and GRVI are coloured dark purple, areas with both low AOT40 and GRVI are coloured in grey, as per the bivariate legend. The years 2019-2023 are presented.

D.2 NDVI

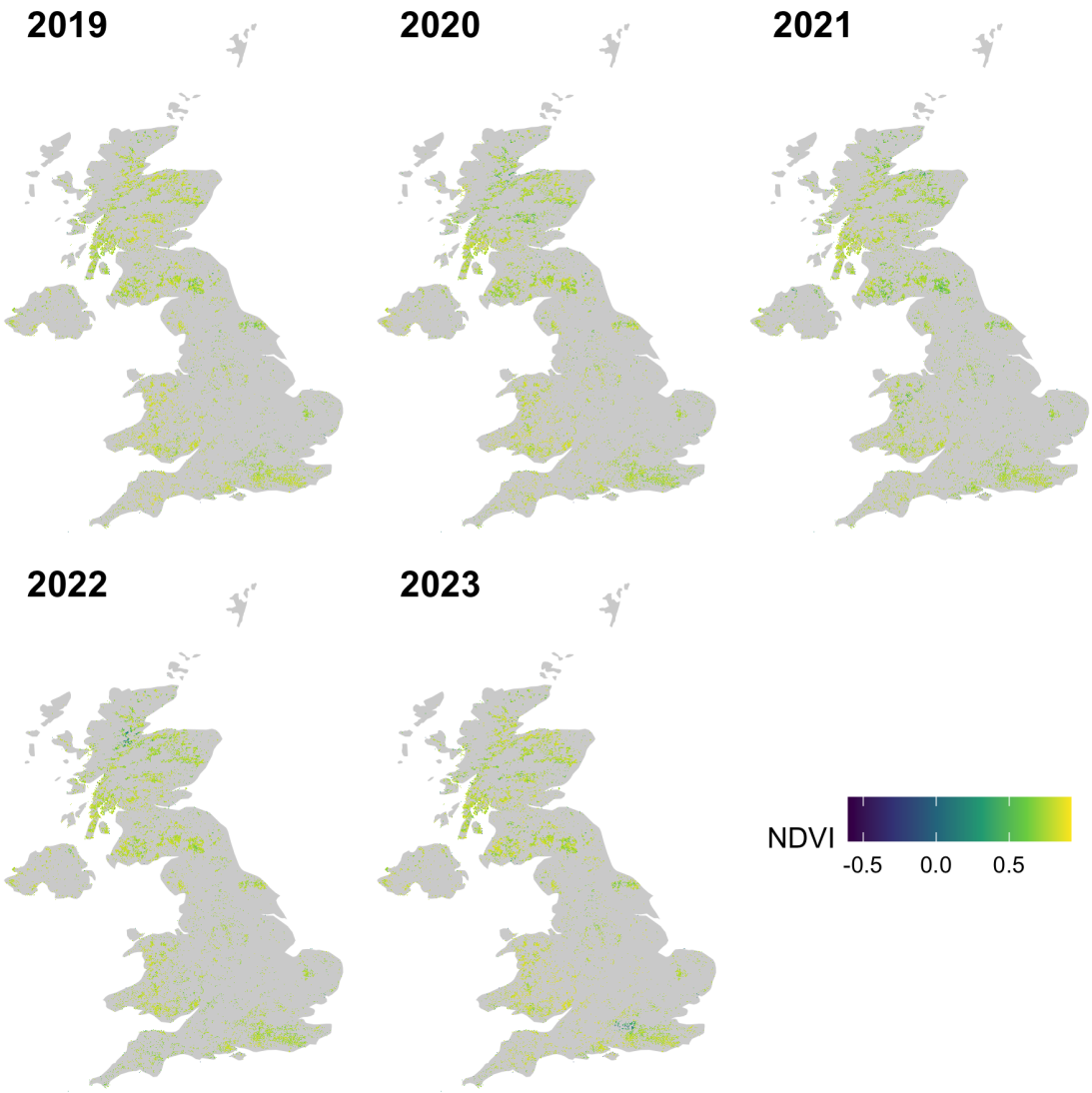


Figure D.4: Maps of median annual NDVI of forested areas of the UK, calculated from Sentinel 2 data down sampled to 1 km spatial resolution, 2019 to 2023.

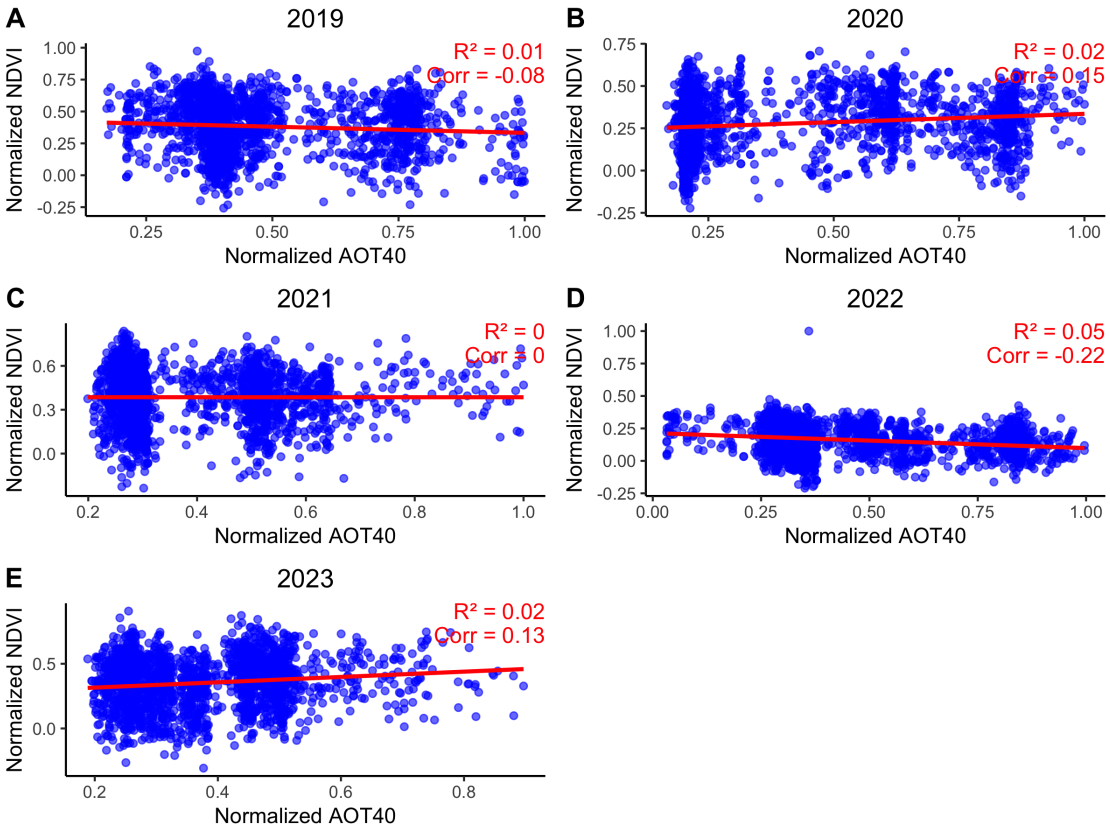


Figure D.5: The correlative relationship between annual NDVI and AOT40 for 20,000 forested 1 km cells in the UK plotted in blue, fitted with linear models in red. The R^2 and correlation coefficient (*Corr*) are shown red text. Analyses for the years 2019-2023 are shown in panels A-E.

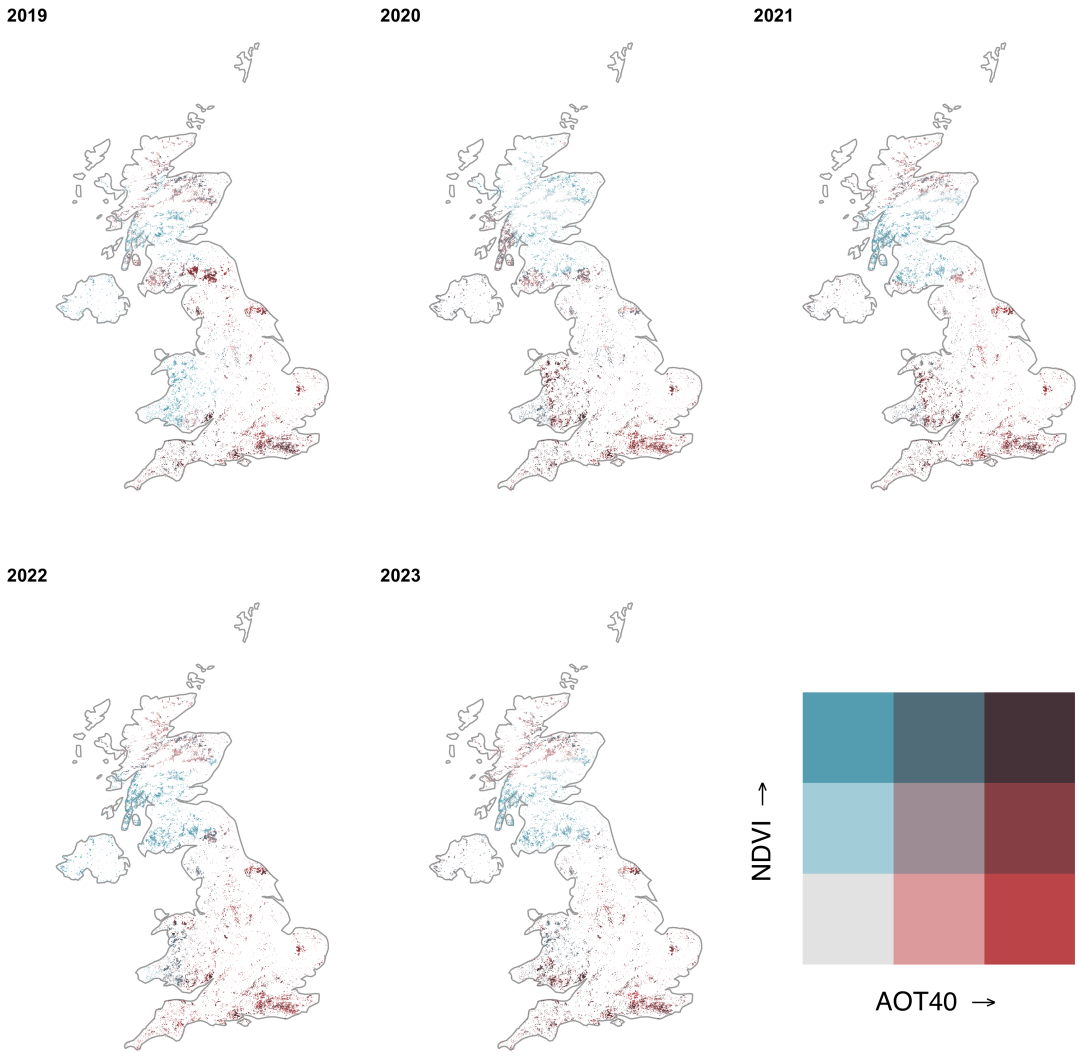


Figure D.6: Bivariate maps of annual median NDVI against annual AOT40 for forested areas of the UK, at 1 km spatial resolution. Areas with high NDVI and low AOT40 are shown in bright blue, areas with high AOT40 and low NDVI are shown in bright red. Areas with both high AOT40 and NDVI are coloured dark purple, areas with both low AOT40 and NDVI are coloured in grey, as per the bivariate legend. The years 2019-2023 are presented.